THE MORPHOLOGY OF SPRAY-DRIED PARTICLES

DAVID EDWARD WALTON

Doctor of Philosophy

THE UNIVERSITY OF ASTON IN BIRMINGHAM

AUGUST 1994

THE UNIVERSITY OF ASTON IN BIRMINGHAM

THE MORPHOLOGY OF SPRAY-DRIED PARTICLES

DAVID EDWARD WALTON

Doctor of Philosophy

1994

ABSTRACT

Samples of various industrial or pilot plant spray-dried materials were obtained from manufacturers together with details of drying conditions and feed concentrations. The samples were subjected to qualitative and semi-quantitative examination to identify structural and morphological features. The results were related to measured bulk physical properties and to drying conditions.

Single particles were produced in a convective drying process analogous to spray drying, in which different solids or mixtures of solids were dried from solutions, slurries or pastes as single suspended droplets. The localized chemical and physical structures were analysed and in some cases the retention of volatiles monitored. The results were related to experimental conditions, viz.; air temperature, initial solids concentration and the degree of feed aeration.

Three distinct categories of particle morphology were identified, i.e.; crystalline, skin-forming and agglomerate. Each category is evidence of a characteristic drying behaviour which is dependent on initial solids concentration, the degree of feed aeration, and drying temperature. Powder flowability, particle and bulk density, particle-size, particle friability, and the retention of volatiles bear a direct relationship to morphological structure.

Morphologies of multicomponent mixtures were complex, but the respective migration rates of the solutes were dependent on drying temperature.

Gas-film heat and mass transfer coefficients of single pure liquid droplets were also measured over a temperature range of 50°C to 200°C under forced convection. Enhanced transfer rates were obtained, attributed to droplet instability or oscillation within the airflow, demonstrated in associated work with single free-flight droplets.

The results are of relevance to drier optimization and to the optimization of product characteristics, e.g.; particle strength and essential volatiles-retention, in convective drying.

KEY PHRASES

Spray Drying, Particle Morphology, Single Droplet Drying Behaviour

ACKNOWLEDGEMENTS

I would like to thank Dr C.J.Mumford for his help and guidance in the preparation of this thesis, to past and present Heads of Department, Dr E.L.Smith and Professor B.J.Tighe, to Mr S.Ludlow, and to the following companies for supplying samples of spray-dried material,

Niro Atomizer Ltd.

Dairy Crest Foods

Drytec Ltd.

THE MORPHOLOGY OF

SPRAY-DRIED PARTICLES

CONTENTS

CHAPTER THREE - HEAT AND MASS TRANSFER CORRELATIONS FOR THE EVAPORATION OF PURE LIQUID DROPLETS AND SPHERES UNDER NATURAL AND FORCED CONVECTION

CHAPTER FOUR - PARTICLE MORPHOLOGY : THE DRYING OF SINGLE DROPLETS AND SPRAYS CONTAINING DISSOLVED OR SUSPENDED SOLIDS

CHAPTER FIVE - EXPERIMENTAL APPARATUS AND PROCEDURE

CHAPTER SIX - EXPERIMENTAL RESULTS

QUALITATIVE AND SEMI-QUANTITATIVE EXAMINATION OF COMMERCIALLY SPRAY-DRIED SAMPLES

THE EVAPORATION OF PURE LIQUID DROPLETS

SINGLE DROPLET DRYING STUDIES

APPENDICES

FIGURES

CHAPTER SIX - EXPERIMENTAL RESULTS

TABLES

CHAPTER ONE - SPRAY DRYING FUNDAMENTALS Page

CHAPTER FOUR - PARTICLE MORPHOLOGY : THE DRYING OF SINGLE DROPLETS AND SPRAYS CONTAINING DISSOLVED OR SUSPENDED SOLIDS

CHAPTER SIX - EXPERIMENTAL RESULTS

CHAPTER ONE

SPRAY DRYING FUNDAMENTALS

1.0) Introduction

Most manufacturing operations entail one or more stages in which drying is carried out. In fact, as a unit operation drying has probably the widest application in industry. The term drying is generally understood to cover the removal of a liquid from a solid usually in the form of a solution, suspension, slurry, paste or a solid matrix such as wood, clays, vegetables etc. In most cases this involves the vaporization of the liquid and its subsequent diffusion away from the surface. Since the vaporization is associated with a change in heat content, in convective drying the process must also involve a transfer of heat from the bulk gas to the liquid. The rate of this process will depend upon the resistances to heat and mass transfer within the system. The mode of heat transfer depends on drier design but is predominantly by convection or by direct contact (conduction), although nearly all driers transfer some heat by radiation. Heat supplied by radiation alone is exceptional and is usually restricted to infra-red drying. In convection drying hot air is blown over the surface of the wet solid and

provides both the source of heat and the means for removal of the vapour. In conduction drying the wet solid is for example, placed in a vessel which is heated from the outside or on a static or moving heated surface and the vapour is discharged via a vent.

Examples of convective driers include, direct rotary, pneumatic, fluid bed and spray driers, whereas, indirect rotary, drum, agitated and freeze driers are conductive. Some types, e.g.; band and tray driers, can be either convective or conductive. Whatever the type of drier, product quality and product performance characteristics, e.g.; moisture content, density, colour, aroma retention, particle-size distribution etc., all of which are affected by the drying operation, are a significant factor in drier selection.

The large number of drier types available commercially, either conductive, convective or radiant in nature, renders it impracticable to study all the associated drying mechanisms in any detail. It may not however, be unrealistic to extend the drying mechanisms of one particular type of drier to another, similar or analogous method of drying. For example, the drying mechanisms associated with spray drying may be similar to those found in fluidised bed and possibly pneumatic drying.

In the present study the morphology of spray-dried particles has been investigated. Information has been obtained from the qualitative and semi-quantitative examination of industrial spray-dried material and from experiments performed with a single droplet drying apparatus - a process analogous

to spray drying. The main aim of the work was to reproduce and predict the morphology of production dried formulations without recourse to expensive plant trials. This would assist spray drying technology in,

- The comparison of drying rates between products and different formulations.

- The assessment of particle morphology.

- Spray drier optimization.

Because of the difficulties associated with investigating spray drying in situ, research has in general tended to be divided into four main areas,

1.) Atomization studies, which attempt to correlate droplet-size distribution with feed characteristics, atomizer design, pressure (or rotational speed) and throughput.

2.) Studies of gas flow patterns and residence times.

3.) Single droplet drying studies.

4.) Mathematical models, which bring together the data from 1 to 3 to simulate drier performance, and to predict droplet drying rates and drying behaviour.

The majority of this research has been concerned with studies of atomization and gas flow patterns, with single droplet drying studies receiving relatively little attention. However, in the past 10 to 15 years this has begun to change (cf. page 26).

All three areas of research employ mathematical models to explain the complex interactions between droplet-size distribution, temperature, rate and direction of airflow, droplet drying behaviour, the resulting residence time and product temperature. They are particularly useful in the food industry where users claim the accurate modelling of droplet formation during atomization allows the prediction of aroma loss without recourse to expensive pilot plant trials.

However, this approach requires caution since many of the models are being developed more rapidly than the available experimental techniques or data used to validate them. Indeed, the majority of drier manufacturers regard computer modelling as being far less important than experience (1). This is understandable since few of the models predict the production of a final hollow particle, which is commonly encountered, or droplet / particle expansion during drying.

1.1) Spray Drying

Spray drying, an example of convective drying, is probably the most widely used dried particle formation process in industry. It is applicable to a wide range of products and industries

(see Table 1), e.g.; for the continuous production of dry solids in powder, granulate or agglomerate form from liquid feedstocks as solutions, emulsions and pumpable suspensions. Although regarded as a relatively new technique, Masters (2), who extensively chronologs the historical development of spray drying up to 1949, reports the first acknowledgement of the process to be in 1865. However, because of practical problems, such as the inability to achieve continuous feed atomization and the frequency of shutdown necessary to remove deposit formation, the first successful commercial spray driers did not appear until the 1920's. A notable exception was the Merril-Soul milk drier in 1905. Various attempts were made to improve the available atomization systems but most designs met with limited success. In 1911 however, a patent by Meisters (3) clearly describes what appears to be the forerunner of the modern rotary or centrifugal atomizer with a more novel form appearing in 1921 by Akermann. By the 1930's spray drying had become firmly established as a successful drying operation, although it was not until the mid 1940's that information started to appear concerning the fundamentals of spray drying. This has been primarily attributed to the faulty design of equipment covered by many early patents (4), i.e. pre 1930's, most of which failed to operate when constructed. Post war re-evaluation of all drying methods however, began to change this and from the late 1940's onwards a substantial increase in the

Table 1. Industrial Applications of Spray Drying

Chemical Industry

- Catalysts
- Dyestuffs / pigments
- Detergents
- Tannins
- Fine organic / inorganic grades
- Fungicides
- Insecticides
- Herbicides
- Fertilizers
- Chelates

Polymer Industry

- PVC-emulsion & suspension type
- Rubber latex
- Urea, Melamine and Phenol-formaldehyde resins
- Poly(methyl methacrylate)
- Poly(vinyl butyrate)
- Poly(vinyl acetate)
- Poly(acrylonitrile)
- Poly(ethylene)
- Polycarbonate
- Poly(vinyltoluene)

Food and Dairy Industry

- Milk
- Spices / herb extracts
- Cheese / whey products
- Coffee / coffee substitutes
- Eggs
- Tomatoes
- Baby food
- Soup mixes
- Coconut milk
- Coffee whiteners
- Flavours
- Soya-based food

Ceramic Industry

- Carbides
- Ferrites
- Nitrides
- Oxides
- Wall tile material
- Silicates
- Steatites
- Titanates
- Enamels
- Kaolin

Pharmaceutical Industry

- Analgesics
- Antibiotics
- Enzymes
- Plasma / plasma substitutes
- Hormones
- Vaccines
- Vitamins
- Yeasts
- Amino acids
- Dextran

number of fundamental studies concerning all drying processes is reported (5-11).

The modern spray drying process, shown schematically in Figure 1, involves the atomization of a liquid feedstock into a spray of droplets which are contacted with hot gas in a drying chamber, generally in a co-current or counter-current flow. Evaporation of moisture from the droplets and formation of dry particles (see Figure 2) proceed under controlled temperature and airflow conditions, the powder being discharged continuously from the bottom of the drying chamber.

Operating conditions and drier design are selected according to the drying characteristics of the product and powder specification. Hence it is an ideal process when the end-product must comply to precise quality standards regarding particle-size distribution, bulk and particle density, strength, dustiness, absorbency, dispersibility, flavour and aroma retention, in addition to residual moisture content.

The ability to control such product characteristics is a major advantage of the spray drying process over other drying methods, especially when dealing with high performance (high cost, low volume) and consumer products. This is particularly true in the food and dairy industries where the relatively large loss of volatile flavour and aroma substances during drying or evaporative concentration of liquid foods, reduces product quality, i.e.; all processing reduces quality, so the aim is to keep the processing times short and temperatures as low as possible.

Figure 1. The Process Stages Involved in Spray Drying

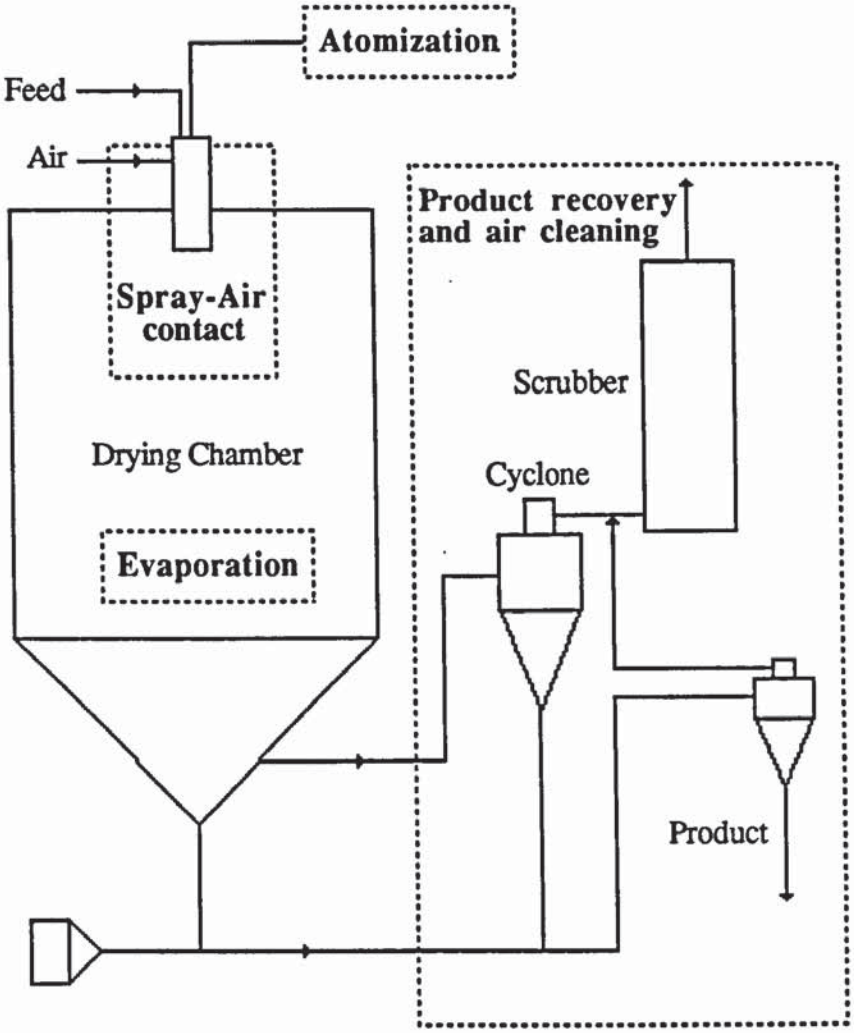

Numerous different process layouts are possible. The above design is typical of an open-cycle, co-current flow drier.

Figure 2. Examples of a Spray-Dried Product

dyestuffs (mag. x 16), In. conc. 30% to 40 % w/w, Temp. in 350°C

out 110°C

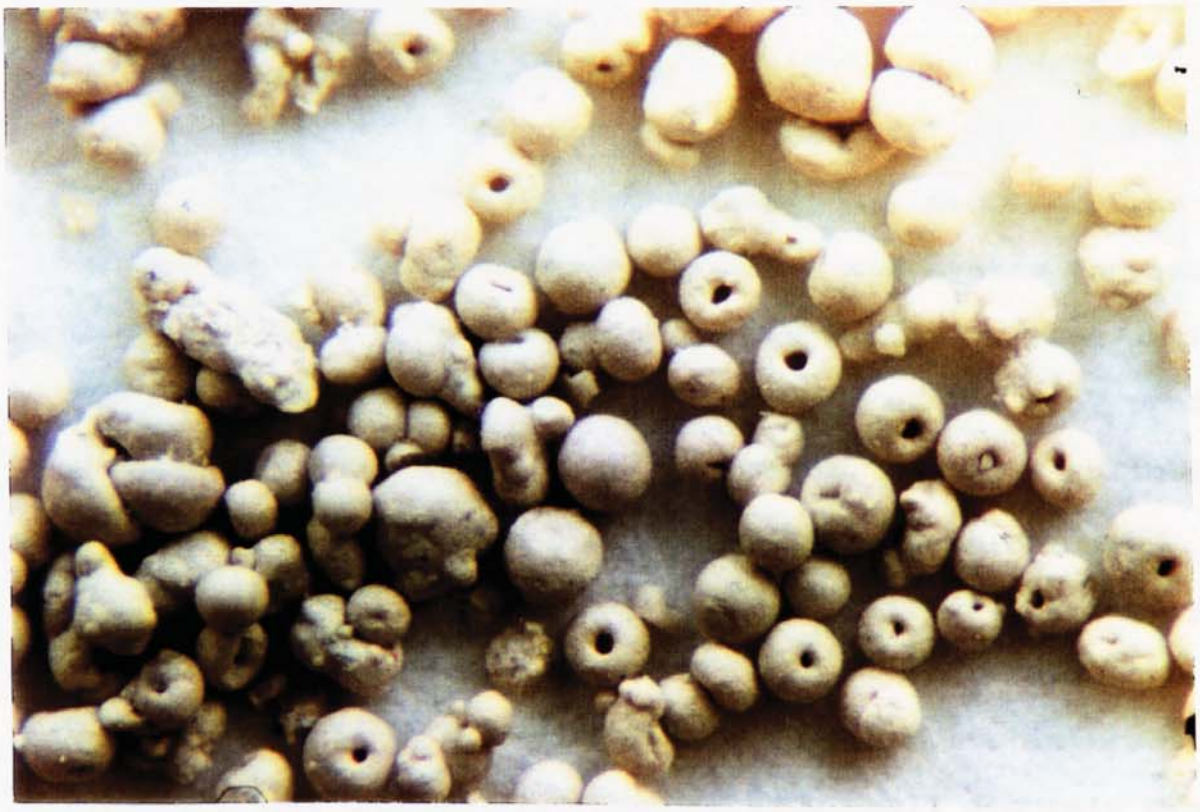

wall tile clay (mag. x 16) In. conc. -- , Temp. in 550°C

out 90°C

Hence, in recent years the focus of drying technology in general, has tended to move away from minimizing the capital cost of equipment, energy usage and operating costs, to delivering specific product performance characteristics. Although these costs are still important, they are less so when drying high performance and consumer products since up to 80 % to 90 % of the total cost of manufacture can be due to product raw materials (12).

From a research point of view, this has resulted in greater interest being focused upon understanding the microscale (particle down to molecular level) rather than mesoscale considerations such as spray drier design options. Consequently, the development and use of new analytical methods and tools has been necessary.

1.2) Spray Drying Fundamentals

Every spray drier consists of a feed pump, atomizer, gas heater, air disperser, drying chamber, and system for exhaust gas cleaning and powder recovery. The widely varying drying characteristics and quality requirements of the many products determine the selection of the atomizer, the most suitable airflow pattern, and the drying chamber design.

Within the atomizer the feed is accelerated to a very high velocity, normally between 100 m/s and 200 m/s, and then dispersed into a thin liquid film. The film, on interacting with the drying gas, is broken-up into small discrete droplets

which are forced into a drying chamber at high speed where they dry to form powder particles. Correct atomization and the formation of a spray which has the required droplet-size distribution is vital to the successful operation of any spray drier.

Relatively uniform particle sizes are required because oversize droplets tend not to dry adequately before reaching the chamber wall or base. Undersize droplets produce excessive fines which are generally undesirable, and also experience extended residence times which may result in thermal degradation.

The mean particle-size and particle-size distribution for a spray-dried powder is determined initially by the method of atomization. Therefore, the atomization system is selected and designed individually to meet the specific demands of the industry (see Tables 2 and 3). Factors such as bulk density, dispersibility, colour, powder handling properties and dust characteristics are very dependent on particle-size distribution.

Three main methods of atomization are used in commercial spray drying,

1.) Centrifugal atomization, where the liquid feed is accelerated and atomized by means of centrifugal force in a rapidly rotating disc.

Table 2. Atomization Systems used in the Food and Chemical Industries (13)

Product	Atomizer	Moisture Content	
		Inlet %	Outlet %
full-fat milk	rotary wheel pressure nozzle	50-60	2.5
consumer milk	rotary wheel pressure nozzle	50-60	4
skim milk	rotary wheel pressure nozzle	48-55	4
instant coffee $D_{3,2}$ = 300 µm	pressure nozzle	75-85	3.5
instant tea	pressure nozzle	60	2
PVC emulsion			
90 % particles > 80 µm	pressure nozzle	40-70	0.01
90 % particles > 60 µm	pneumatic nozzle		
detergents	pneumatic nozzle	36-50	8-13
95 % particles > 60 µm			
kaolin	rotary wheel pneumatic nozzle	35-40	1
superphosphate	pneumatic nozzles		

(moisture content expressed on dry basis)

Table 3. Atomization Systems
in Relation to Mean Particle-Size

Atomizing System	Operating Parameters	Mean Particle-Size
• Spinning Disc:	(peripheral speed)	
- high speed	200 m/s	25-100 µm
- medium speed	150 m/s	50-200 µm
- low speed	100 m/s	100-300 µm
• Pressure nozzle:		
- high pressure	4000 psig	25-100 µm
- medium pressure	2000 psig	50-200 µm
- low pressure	1000 psig	100-300 µm
- very low pressure	400 psig	200-600 µm
• Two-fluid nozzle:		
- high pressure	90 psig	10-50 µm
- medium pressure	45 psig	25-100 µm
- low pressure	12 psig	50-200 µm

The mean particle-size range for a rewet agglomerated powder from a fluid bed is typically 0.5 mm to 5 mm.

Table 3 shows the type of atomization systems and parameters recommended by APV (14) to produce a powder with a given mean particle-size. The limits apply to an average non-agglomerated product although finer and coarser powders can be produced under special circumstances. The operating parameters quoted can only be regarded as approximate, actual values are dependent on, e.g.; the type of material being spray-dried, feed viscosity, feed concentration etc..

2.) Pressure atomization (single-fluid nozzle), where the liquid feed is atomized upon being forced under high pressure through a narrow orifice.

3.) Pneumatic atomization (two-fluid nozzle), where compressed air supplies the necessary energy for atomization and the liquid is fed to the nozzle without pressure.

Spray drying plants with centrifugal atomization are designed for co-current flow only, i.e.; the product spray pattern is flat and horizontal, whereas nozzle atomization allows co-current, mixed and counter-current drying as the product spray angle and direction are selectable.

In co-current operation (see Figure 3) the drying air and particles move through the drying chamber in the same direction. Product temperatures on discharge from the drier are lower than the exhaust air temperature; hence, this is an ideal mode for drying heat-sensitive products. When operating with a rotary atomizer, the air disperser creates a high degree of air rotation promoting uniform temperatures throughout the drying chamber. However, an alternative non-rotating airflow is often used in tower-type spray driers using nozzle atomizers.

In counter-current operation the drying air and particles move through the drying chamber in opposite directions. This mode is suitable for products which require a degree of heat

Figure 3. Modes of Spray-Air Contact used in Spray Drying

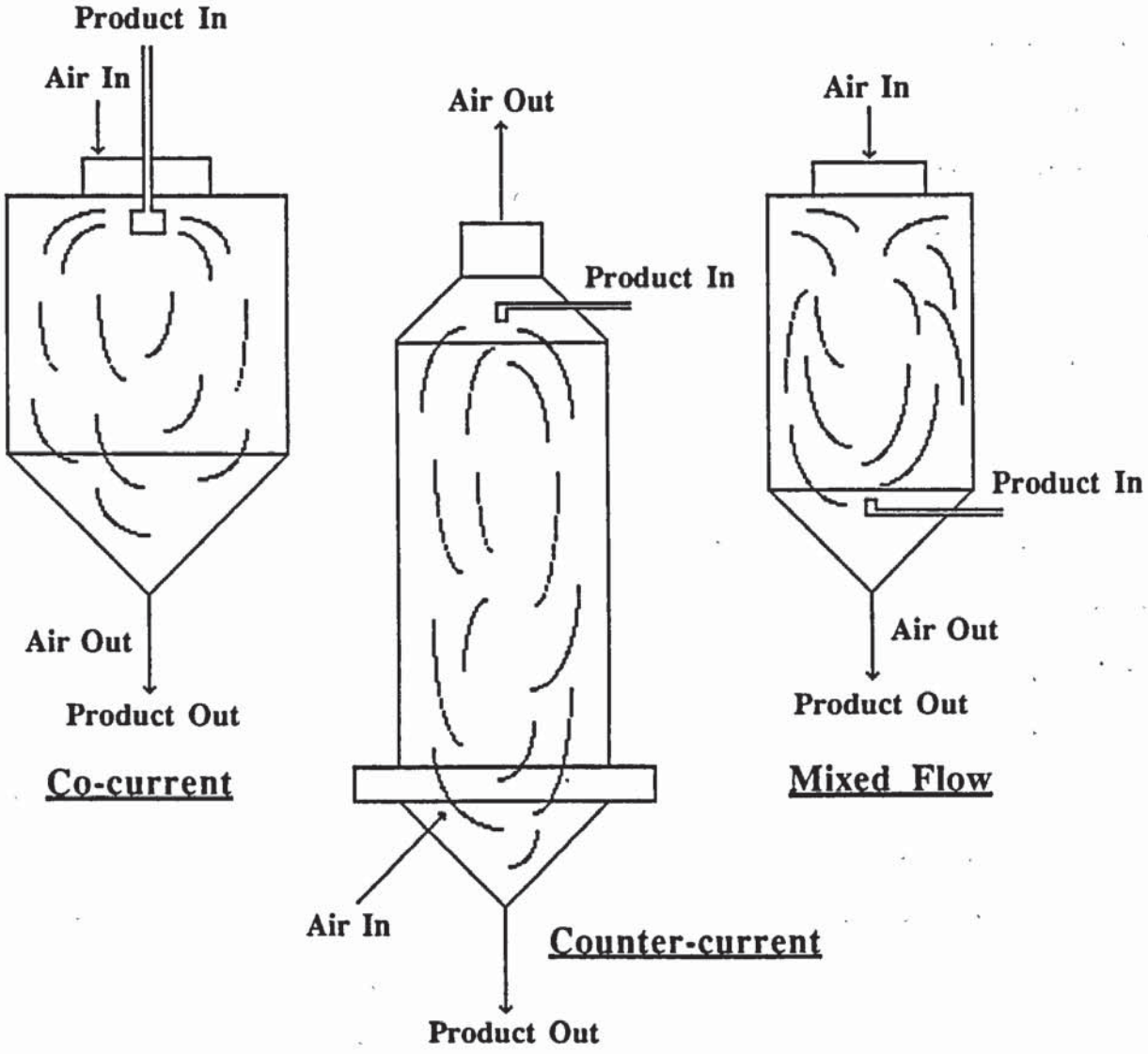

Co-current flow - Widely used, especially if heat sensitive products are involved.

Counter-current flow - Offers drier performance with excellent heat utilization, but subjects the driest powder to the hottest airstream.

Mixed flow - Allows coarse free-flowing powders to be produced in drying chambers of relatively small size, but the powder is subjected to higher particle temperatures.

treatment during drying. The temperature of the powder leaving the drier is usually higher than the exhaust air temperature.

In mixed flow driers particle movement through the chamber experiences both co-current and counter-current phases. This mode is suitable for heat-stable products where coarse powder requirements necessitate the use of nozzle atomizers, spraying upwards into an incoming airflow.

Dried or semi-dried powder is discharged from the drying chamber for either powder separation or after-treatment, before storage and packing.

Most plants are equipped with cyclone filters for primary separation of powder from the drying air. Cyclone systems have a high separation efficiency, normally more than 99.5 %, which for most products is sufficient to ensure a satisfactory low powder loss and to comply with local environmental protection regulations. If further cleaning is required, either a bag collector, electrostatic precipitator or a wet scrubber system is used for secondary powder separation after the cyclone battery. A bag collector may be applied as an alternative to cyclones.

A wide diversity of materials are now spray-dried. For example, Masters (2) lists over 400 which have been either successfully spray-dried on an industrial basis or been involved in spray cooling, spray reaction, spray absorption or spray concentration. This has resulted in a wide variety of drier designs for spray drying and related operations. The type of system selected depends upon the properties of the

material being spray-dried together with safety and emission requirements (see Figure 4).

Open cycle systems, used mainly with aqueous feedstocks, are the most common. In these drying air is drawn in from the atmosphere and, after passing through the drying chamber and air cleaning equipment, discharged to atmosphere. Emission standards require the appropriate choice of air cleaning equipment; hence cyclone / bag / filter / scrubber combinations are selected depending upon the maximum permitted particulate emission levels.

Closed cycle systems involve drying in an inert gas atmosphere recycled within the drier. This system must be used for the spray drying of feedstocks which contain organic solvents or where the product must not come into contact with oxygen during drying. Closed cycle plants are gas and powder-tight, and must be designed to the strictest safety standards. The flammable solvent vapours are subsequently recovered by a scrubber-condenser system.

Semi-closed cycle systems operate in either a partial recycle mode, recycling up to 60 % of the exhaust air as inlet air to the drier for effective waste heat utilization, or in a self-inert mode, where direct air heating and a minimal air bleed creates the low atmosphere necessary for drying aqueous feedstocks that form flammable powder - air mixtures. If odour is generated during drying, the small volumes of air vented from the system can be effectively and economically incinerated.

For specialized applications, aseptic systems are available featuring sterile feed atomization and air filtering systems. These driers have found extensive use in the pharmaceutical industry where any form of powder contamination by foreign particulate matter or bacteria, must be avoided, e.g.; the drying of streptomycin sulphate for direct injection purposes. They are fabricated to special standards of finish and operate under a slight pressure with fully automated cleaning-in-place and sterilization facilities.

Figure 4. Spray Drying Systems

Closed cycle

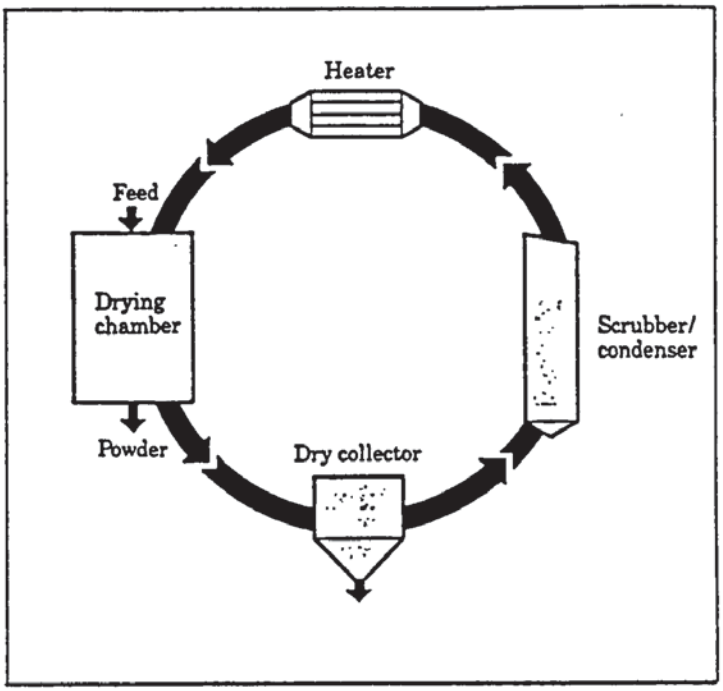

Open

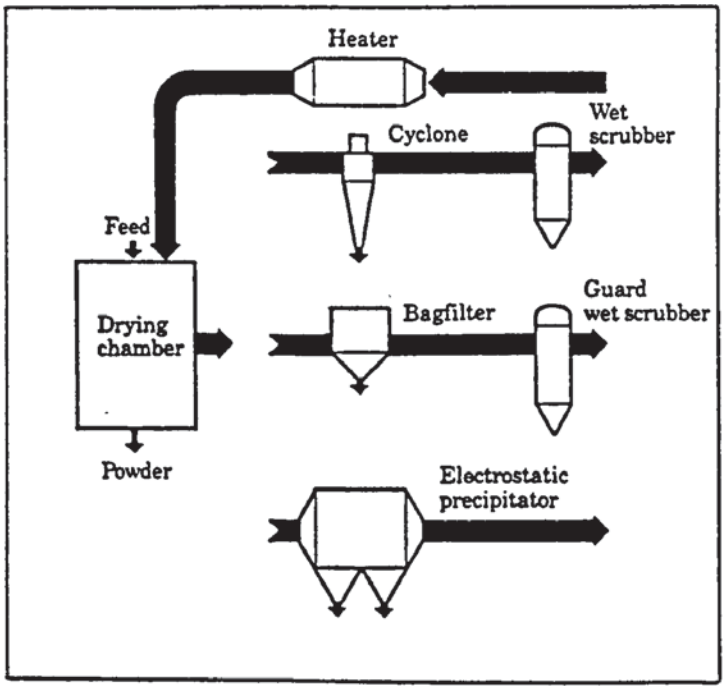

Semi-closed cycle

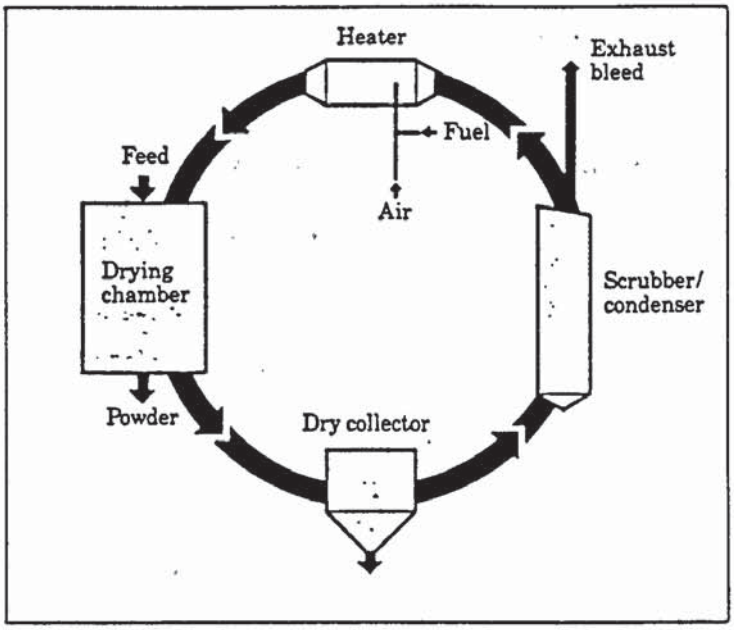

Aseptic

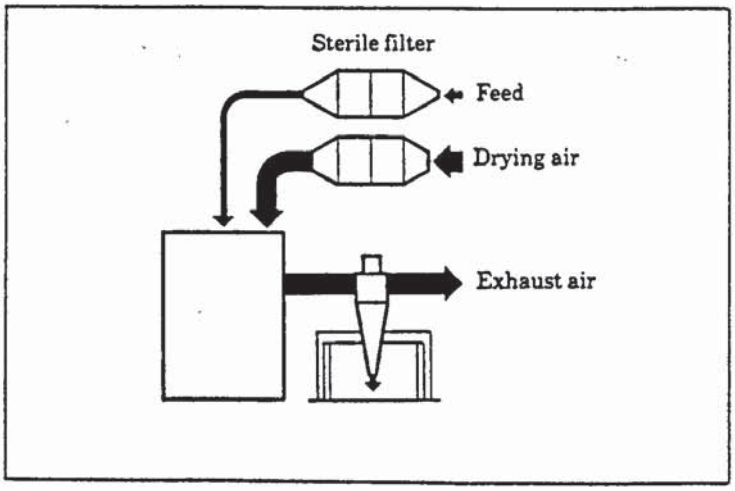

Fluidized Spray Drying

In recent years, there has been a growing demand in many industries for powders which are dust-free, agglomerated, easily dispersible and free-flowing. The purpose is to facilitate powder handling for both the producer and the end user of powders. The Fluidized Spray Drier or FSD has been specifically designed to meet this demand, i.e.,

- Improved heat economy (higher inlet drying temperatures and lower outlet drying temperatures).

- Improved drying of heat sensitive products, e.g.; typically many food and dairy products - milk, spices, flavours etc.

- Troublefree drying of many thermoplastic products, e.g.; polycarbonates, polyethylene, polyvinylchloride, and / or hygroscopic products, e.g.; potassium carbonate, calcium nitrate.

- A dustless, free-flowing product with good redispersability.

The FSD is essentially a new concept in spray drying, the first plant being commissioned in 1981 and differs significantly from the conventional spray drier design.

A stationary fluid bed is placed within the drying chamber base and the product to be dried is sprayed downwards onto the bed. Vigorous fluidization of the bed plus recycle of fines from the attached powder collector is claimed to result in spray drying taking place in a powder-laden atmosphere to produce porous and dustless agglomerates. Particles of higher moisture content can be handled in the drying chamber due to the resulting ' powdering effect ' overcoming problems of product stickiness. This effect enables the use of reduced outlet air temperatures, thereby lowering powder temperature and increasing thermal efficiency. Moisture content and product form are controlled in the stationary fluid bed.

Flexibility in operation is claimed to enable different powder forms to be produced with varying degrees of agglomeration and hence particle-size distribution, which can be varied by changing the operating conditions and therefore the residual moisture content of the spray particles within the drying chamber.

Rewet Agglomeration (Instantizing)

Rewet agglomeration or instantizing can also be used for the production of coarse and stable agglomerates, and for the addition of liquid components to a powder mixture. An atomized wetting agent is sprayed onto an external fluidized powder bed to agglomerate the particles. The agglomeration is often followed by drying and cooling before packaging.

CHAPTER TWO

THE DRYING OF DROPLETS AND SPRAYS

2.0) Droplet Formation During Atomization

The majority of atomizers in spray drying are designed to discharge the feed in the form of a thin liquid sheet or film, usually in the shape of a hollow cone, flat sheet or flattened ellipse, depending on the design. Break-up of the liquid sheet into a spray of droplets is generally regarded as a highly chaotic and poorly-understood process, although in most cases disintegration initially occurs by the formation of ligaments which then break-up to form droplets.

Work by Dombrowski and Fraser (15) essentially established four possible mechanisms for sheet disintegration (see Figure 5), namely,

1.) Rim disintegration.

2.) Wave disintegration.

3.) Perforated-sheet disintegration.

4.) Thick-sheet disintegration.

Figure 5. Possible Mechanisms for Sheet Break-up (16)

a.) Rim disintegration

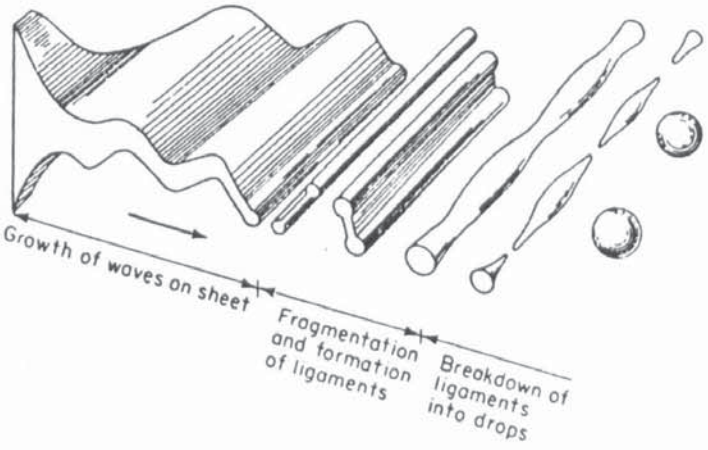

b.) Wave disintegration (17)

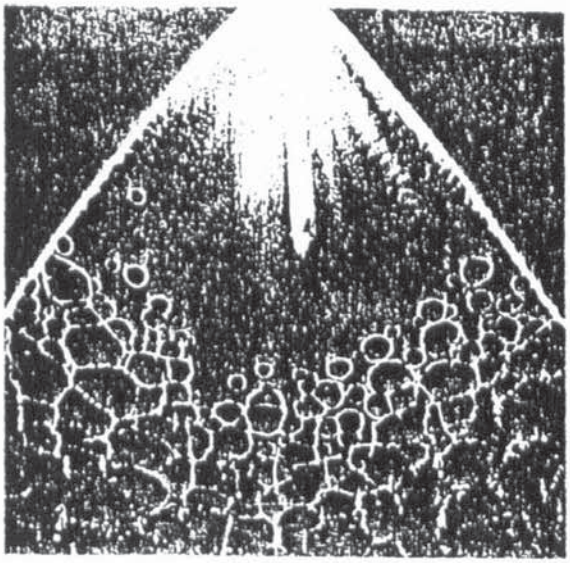

c.) Perforated-sheet disintegration

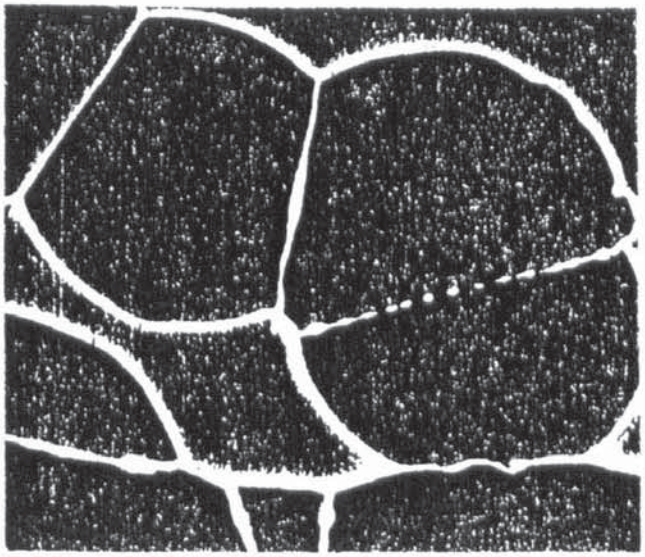

d.) Collapsing network of threads and droplets

The type of sheet break-up occurring within a spray drier is difficult to determine, mainly because little is known about the characteristics of sheet formation when atomization takes place in a hot swirling gas stream. However, work carried out by Garner et al (18), Fraser et al (19), Addison (20) and particularly Dombrowski and Hooper (21), suggests sheet formation, sheet break-up and therefore droplet-size, are strongly influenced by a relatively large number of parameters, e.g.; nozzle design, liquid / gas velocities, gas density, gas flow patterns within the drying chamber, and the physical condition and properties of the feed.

In most types of sheet disintegration, break-up of the ligaments into droplets occurs by the Rayleigh-Weber mechanism (22,23).

Because of the complex nature of the break-up process, and since the droplets once formed can disintegrate into smaller droplets, no simple criteria exists for the prediction of ultimate droplet-size. Equations provide a useful guide but fall short of a complete description, so that specific correlations apply to individual atomizer designs (24-26). In reality a range of droplet-sizes are produced during atomization. It is usual therefore, to consider the evaporation process in relation to single droplets and to then estimate the effects of mutual interaction within a spray.

2.1) Mass Transfer Across a Phase Boundary

A number of theories have been proposed to describe the mechanism of mass transfer across a phase boundary. In 1923 Whitman's Two-Film Theory (27) was the first serious attempt to represent the conditions which occur when material is transferred from one fluid stream to another. It proposed that the resistance to transfer in each phase could be regarded as residing in a thin film or ' hypothetical laminar layer ' of finite thickness near the interface. Transfer across the film is considered to be a steady state process of molecular diffusion with turbulence in the bulk fluid dying out at the interface.

The Penetration Theory, introduced by Higbie (28) in 1935, suggests the transfer process is mainly due to fresh material being brought to the interface by eddies within the bulk fluid. A process of unsteady state transfer then takes place for a short, fixed period of time at the freshly exposed surface.

A modification to this theory by Danckwerts (29) however, postulated that the surface at the interface is continuously replaced by fresh fluid in a random fashion rather than the fluid being exposed for a fixed period of time.

A more general approach, the Film Penetration Theory (30), incorporates principles from both the Two-Film and the Penetration Theory, in that, the resistance to transfer is

regarded as lying within a laminar film at the interface, as in the Two-Film Theory, with mass transfer being regarded as an unsteady state process. It is assumed that fresh surface is being formed at intervals from fluid brought to the interface by eddy currents within the bulk fluid. Mass transfer then takes place as in the Penetration Theory but with the resistance confined to the finite film, so that material which traverses this film is immediately and completely mixed within the bulk fluid.

The Boundary-Layer Theory, first postulated by Prandtl in 1904 (31), has become widely used in spray drying to describe the heat and mass transfer processes which occur during atomization, namely, the evaporation of droplets. Equations of motion, continuity and energy can be solved approximately to obtain the velocity, concentration and temperature profiles which exist within the thin boundary layer at the droplet-gas interface.

2.2) Heat and Mass Transfer - Boundary-Layer Theory

Consider the liquid-vapour interface illustrated in Figure 6 (16). It is assumed that the vapour concentration Ci in the gas phase at the interface is that of the saturated vapour at the temperature Ti of the surface, whereas the bulk concentration is at some lower value, Cb. The difference in concentration constitutes a driving force for the transfer of vapour. Similarly, the temperature difference Tb - Ti, where

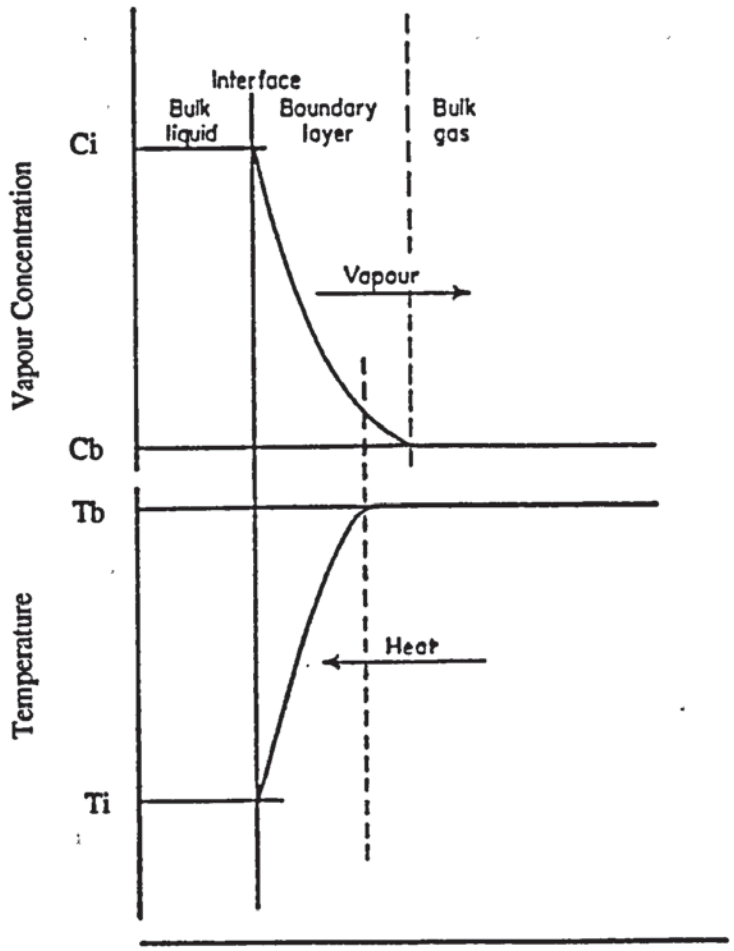

Figure 6. Interface Conditions

Tb is the bulk temperature, constitutes a driving force for the transfer of heat to the liquid.

Normally, turbulence or eddy diffusion rapidly produces a uniform concentration throughout the gas except in a boundary layer near the interface where viscous forces are greatest. The thickness of this layer will be controlled by flow conditions and it is assumed that the resistance to transfer occurs across this layer.

If the concentration gradients are assumed constant in this region, the vapour flux is given by,

$$\frac{dMv}{dt} = \frac{Dv}{z}(Ci-Cb) \quad \ldots\ldots\ldots\ldots\ldots\ldots (1)$$

where Mv = molar diffusivity per unit area
z = boundary layer thickness
Dv = diffusivity
t = time

similarly, the heat flux is given by,

$$\frac{dq}{dt} = -\frac{Kd}{z}(Ti-Tb) \quad \ldots\ldots\ldots\ldots\ldots\ldots (2)$$

where q = heat transferred per unit area
Kd = thermal conductivity of air / vapour mixture

However, the boundary layer thickness is not usually known and these equations are rewritten,

$$\frac{dW}{dt} = A.\frac{dMv}{dt} = k.A(Ci-Cb) \quad \ldots\ldots\ldots\ldots\ldots\ldots (3)$$

and

$$\frac{dQ}{dt} = A.\frac{dq}{dt} = h_T.A(Tb-Ti) \quad \ldots\ldots\ldots\ldots\ldots\ldots (4)$$

where W = moles of vapour transferred
Q = heat transferred
A = transfer surface area

k and h_T are the mass and heat transfer coefficients respectively and are dependent upon the fluid properties and

flow conditions. They are usually established by experimental techniques.

Under steady-state conditions the sensible heat transferred to the liquid surface must balance the latent heat required to evaporate the quantity ' W ' of liquid, i.e.;

$$Q = W \lambda_M \quad \ldots\ldots\ldots\ldots\ldots\ldots\ldots (5)$$

where λ_M = molar latent heat of vaporization

combining equations 3, 4 and 5,

$$h_T(Tb-Ti) = k(Ci-Cb)\lambda_M \quad \ldots\ldots\ldots\ldots\ldots\ldots (6)$$

A knowledge of the ratio h_T / k and the latent heat of vaporization is sufficient to calculate the interfacial conditions for a given bulk concentration and temperature. This ratio can be calculated from,

$$\frac{h_T}{k} = Cp.\rho_a(Le)^{0.67} \quad \ldots\ldots\ldots\ldots\ldots\ldots (7)$$

where Cp = specific heat capacity of the gas phase
ρ_a = density of the gas phase
Le = Lewis Number, Kd / DvCpρ_a

The Lewis number is unique in being unity for air-water vapour systems, which results in the adiabatic cooling line and wet bulb line coinciding on the psychrometric chart. This greatly simplifies drier calculations for solids containing water dried in air.

A resistance to the heat and mass transfer processes exists on the liquid side of the interface, which implies the temperature and concentration of the bulk liquid are different from that of the interface. In most cases this resistance is small and the interfacial conditions can be regarded as being equal to those of the bulk liquid.

To calculate the transfer rates on which the rate of drying depends, both individual gas-film transfer coefficients must be known.

In the case of spray drying, the effects of the flow conditions surrounding a droplet and of the physical properties of the droplet liquid upon the gas-film transfer coefficients, are usually correlated in the form of certain dimensionless groups, e.g.; the Sherwood number, Nusselt number, Reynolds number, Prandtl number and Schmidt number.

2.3) The Evaporation of Droplets

The drying of droplets during spray drying involves simultaneous heat and mass transfer in which heat for evaporation is transferred, predominantly by convection, from a hot gas to the droplet surface. The vapour is then transferred by diffusion and convection back into the gas stream.

The overall rate of drying is a function of,

- The temperature, humidity and transport properties of the gas.

- The droplet diameter and temperature, and the relative velocity between the droplet and its surroundings.

- The nature of the solid material dissolved or suspended in the liquid.

When a droplet leaves an atomizer its velocity is usually high relative to the surrounding air, but is rapidly retarded to the terminal velocity due to frictional forces acting upon the droplet surface. Once the droplet has reached its terminal velocity it falls through the drier at an approximately constant speed (32).

Predictions by the Boundary-Layer Theory and experimental investigations (33,34,35) have shown that, except at low velocities, transfer rates are at a maximum on the side of the droplet facing the oncoming air stream and decrease to a minimum near the boundary-layer separation point (see Figure 7). Beyond this point the transfer rates start to increase again owing to a reversed flow produced by the formation of vortices (36). These effects are due to skin friction and form drag, the former caused by the viscous resistance of the gas

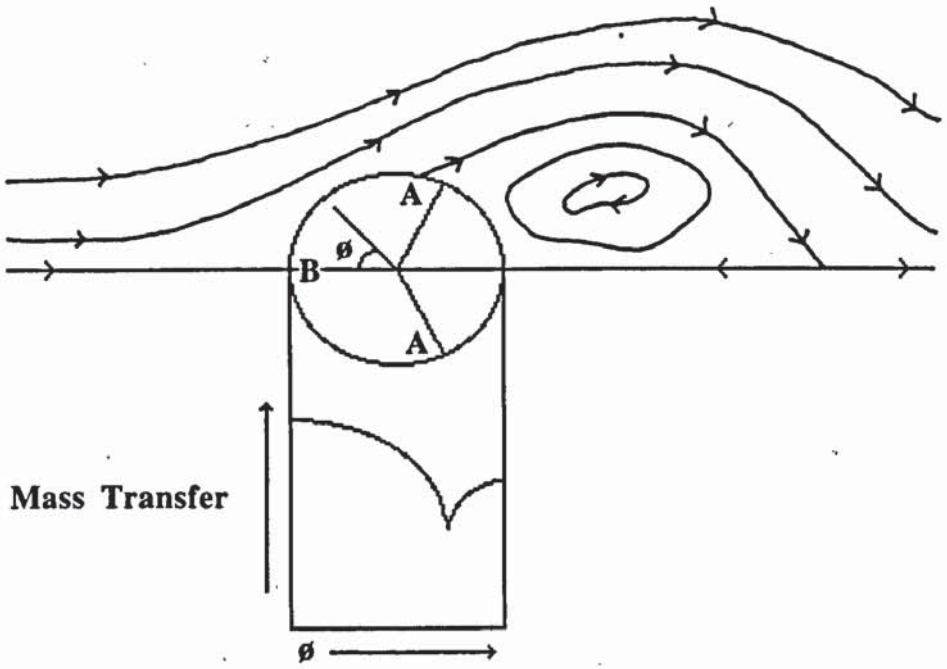

Figure 7. Flow Past a Single Sphere Showing Separation and Wake Formation (33)

A.) Separation point.

B.) Maximum transfer rate.

For laminar flow in the boundary layer, ø approximately equals 85°, and for turbulent flow, ø approximately equals 140°.

at the droplet surface, and the latter by the shape of the droplet, which produces back eddies on the trailing side (37).

To date, no practical design method has incorporated such detail and the droplet evaporation is assumed to take place uniformly over the surface.

As a droplet forms during atomization it undergoes distortion due to oscillations. This causes the drag coefficient Cd to vary as the droplet shape varies. Cd also changes with the droplet velocity.

A number of experimental investigations have been made to determine how Cd varies with the droplet Reynolds number. Figure 8 shows the type of correlation usually reported for spheres (37). The region up to Re = 1.0 is generally designated as the Stoke's Law region, whereas the region from Re = 1.0 to 1000 is termed the intermediate or transition region. Beyond this, Cd is virtually constant and this portion has been termed the Newton's Law region. The motion of particles in a spray drier is generally confined to the first two regions. However, when droplets are first formed at the atomizer they are almost certainly well into the intermediate region, although the time period is very short as a result of rapid deceleration. Furthermore, the initially-formed droplets are not rigid spheres but oscillate violently, thereby producing an even more variable condition of drag.

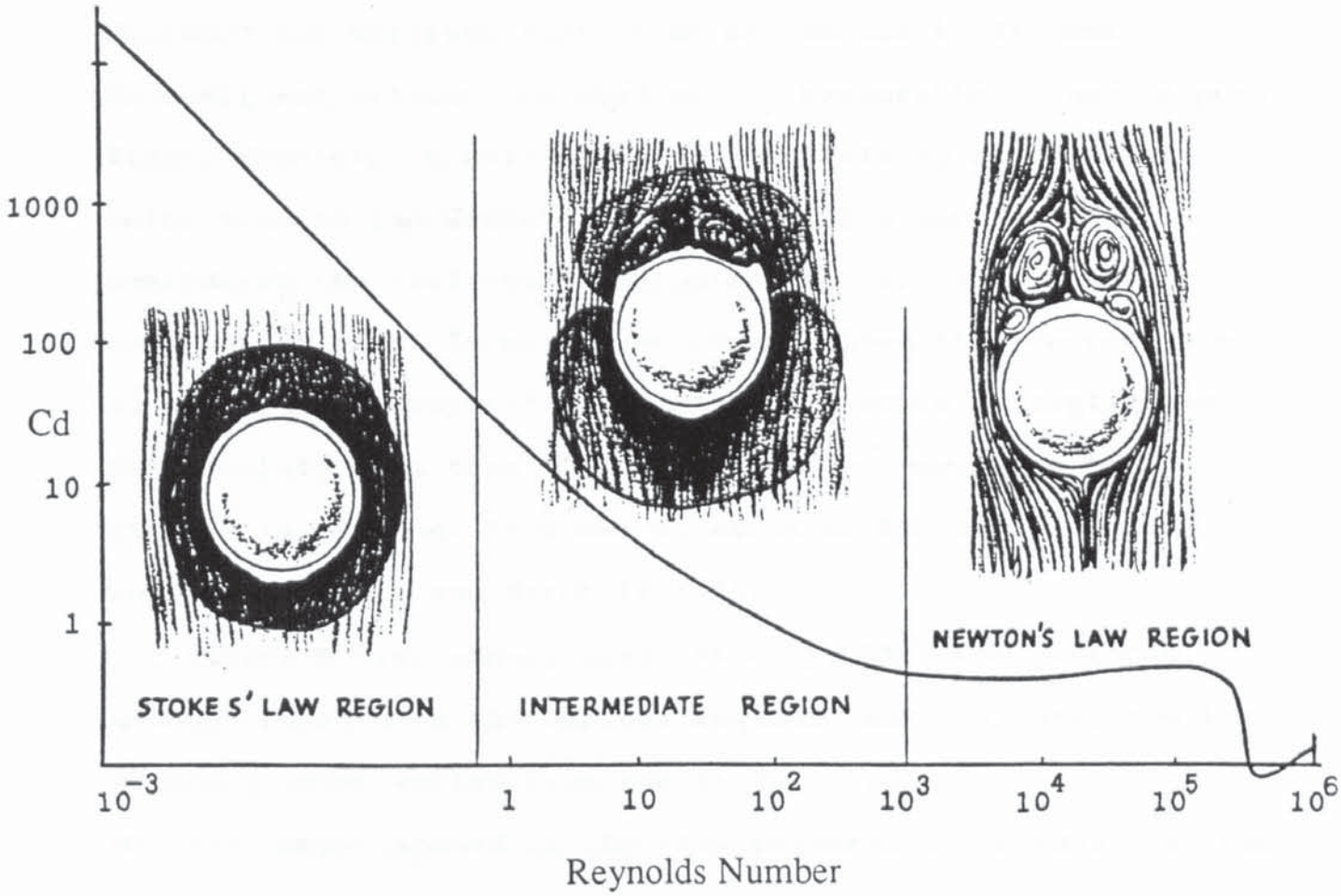

Figure 8. Non-uniformity of Heat and Mass Transfer Around an Evaporating Droplet (37).

The flow patterns set up around the droplet in each region create variations in the mass and heat transfer rates over the droplet surface.

Sherwood and Williams (38), Ranz and Marshall (39) and Marshall and Seltzer (4) studied the evaporation times of pure liquid droplets in still air and when falling at terminal velocities in the Stoke's Law region. Sjentzer (40) also considered the influence of droplet deceleration on evaporation time. In all cases it was shown that corrections to the time of evaporation in still air would be negligible for droplets less than 100 μm in diameter moving in the Stoke's Law region. This was extended to the Newton's Law region by Duffie and Marshall (41).

Figure 8 also shows, qualitatively, the flow patterns around droplets in the various regions, and indicates how the boundary layer varies from the front to the rear of the droplet. Superimposed on the flow patterns are shaded portions representing the magnitude of the Nusselt number, that is, the transport coefficients at various positions around the droplet. This gives some idea, albeit in two dimensions, of the variability of evaporation around a droplet in relative motion and the averaging included in most correlations for heat and mass transfer coefficients.

2.4) General Heat and Mass Transfer Considerations for Evaporating Pure Droplets

The basic theory of evaporation for liquid droplets was proposed by Maxwell (42) in 1877. For a spherical droplet stationary relative to an infinite gaseous medium the rate of evaporation was shown to be given by,

$$-\frac{dm}{dt} = 4\pi r Dv(Ci-C\infty) \quad \ldots\ldots\ldots\ldots\ldots\ldots (8)$$

where m = droplet mass
r = droplet radius
C∞ = vapour concentration at an infinite distance

This equation is based upon the assumptions of isothermal conditions and the attainment of a steady state at each infinitesimal stage in the evaporation process.

From equation 3, the rate of evaporation for a spherical droplet can be expressed as,

$$-\frac{dm}{dt} = k4\pi r^2 (Ci-Cb) \quad \ldots\ldots\ldots\ldots\ldots\ldots (9)$$

Therefore, a gas phase mass transfer coefficient under natural convection, i.e.; Re = 0, can be defined as.

$$k = Dv/r \quad \ldots\ldots\ldots\ldots\ldots\ldots (10)$$

Under similar conditions the Sherwood number, Sh, for a spherical droplet is given by,

$$Sh = \frac{k2r}{Dv} = 2 \quad \ldots\ldots\ldots\ldots\ldots\ldots (11)$$

Following the heat and mass transfer analogy (43), the Nusselt number, Nu, for a spherical droplet becomes,

$$Nu = \frac{h_T 2r}{Kd} = 2 \quad \ldots\ldots\ldots\ldots\ldots\ldots (12)$$

This represents the contribution from molecular diffusion alone. The transfer coefficients are then inversely proportional to the droplet diameter, which has been confirmed experimentally (44). As a consequence the smallest droplets in the distribution generated in a spray drier will dry very rapidly; since their residence times will be greatest they may therefore be prone to thermal degradation, e.g.; charring.

Equations 11 and 12 describe the mass and heat transfer processes of an isolated droplet under natural convection, but Gauvin et al (45) demonstrated they can also apply to fine droplets (i.e.; of 12 μm to 39 μm diameter) entrained in turbulent air. Whenever the droplet-size is much smaller than the scale of turbulence, the relative velocity between the droplet and the gas stream is negligible and therefore, they closely follow the motion of the continuous phase (46). Moreover, the atomized droplets are swiftly dispersed,

occupying less than 0.1 % of the available space - the reported threshold for significant droplet interaction (47,48).

Commercial atomizers usually produce droplets within the size range of 10 μm to 1000 μm in diameter (49), where most, if not all fines are recycled. Clearly close process control is therefore required to maintain product quality. Droplets larger than 100 μm fall with significant slip velocities and droplet Reynolds numbers up to 100 are not uncommon.

For all practical purposes, droplet evaporation takes place under forced convection where evaporation rates increase with increasing relative velocity between the droplet and air. This is due to the additional evaporation caused by convection in the boundary layer around the droplet.

Frossling (34,35) considered the solution to the simultaneous equations of continuity and heat and mass balances across the boundary layer of an evaporating droplet and derived an expression to account for the contribution of forced convection. Frossling and subsequently other authors, e.g.; Kramers (50), Maisel and Sherwood (51), Ranz and Marshall (52), have obtained experimental data at Reynolds numbers in the range of 0 to at least 10,000 and proposed equations of the form,

$$Sh = 2 + \alpha_1 Re_D^{n} Sc^{m} \quad \ldots\ldots\ldots\ldots\ldots\ldots (13)$$

$$Nu = 2 + \alpha_2 Re_D^{q} Pr^{p} \quad \text{.....(14)}$$

where Re_D = Reynolds number (droplet), $vD\rho_G / \mu_G$
Sc = Schmidt number, $\mu_G / D v \rho_G$
Pr = Prandtl number, $C_p \mu_G / K_d$
v = velocity
D = droplet diameter
μG = viscosity of gas phase

The most widely accepted values of α_1, α_2 and the exponents m, n, p and q, are those obtained by Rowe et al (53) and Ranz and Marshall, i.e.; $\alpha_1 = \alpha_2 = 0.6$ and, $n = q = 0.50$, $m = p = 0.33$.

Heat and mass transfer coefficients can be predicted from these equations if the properties of the system, the droplet diameter and velocity are known. There are however, certain limitations and a number of assumptions must be taken into account (54), namely,

- Steady-state drag coefficients apply. It is convenient to apply the drag equations at steady state to the case of accelerating or decelerating droplets. In reality, the drag coefficients for accelerated motion can be 20 % to 60 % higher than values at constant velocity.

- Sensible heat transfer to evaporated moisture is neglected. For drying conditions at high temperatures, a considerable amount of heat is taken up in heating the vapour as it is transported outwards from the droplet surface.

- The equations only apply at low evaporation rates. At higher rates the diffusing vapour leaving the droplet surface changes the temperature gradient in the gas-film surrounding the droplet and use of a correction factor is therefore necessary (55,56,57).

- The droplets are dimensionally stable within the airflow. Any oscillation or surface distortion of the droplet will increase the rate of heat and mass transfer due to variations in the thickness of the boundary layer and increases in droplet surface area. Distortions occur during atomization and when the droplets are subjected to a swirling airflow inside the drying chamber.

2.5) The Evaporation of Sprays

The evaporation characteristics of droplets within a spray differ from those of single droplets. Although basic evaporation theory is unaffected, it is difficult to apply in the case of a large number of droplets evaporating in close proximity to each other and to the atomizer.

Any analysis of spray evaporation depends upon defining the spray in terms of a representative mean droplet diameter and droplet-size distribution, the relative velocity between the droplet and surrounding air, droplet trajectory, and the number of droplets present at any given time per given volume of drying air. Consideration must also be given to droplet

impingement or agglomeration resulting in larger droplets, and any shielding effects, i.e.; where a droplet does not experience the local velocity environment; for example, in a back-spray. Furthermore, because of the practical difficulties in determining these factors, particularly in the vicinity of the atomizer, they are seldom quantifiable with any accuracy. Consequently, there have been few attempts at analysing the problem (44,45,58-68).

2.6) Droplets Containing Dissolved or Suspended Solids

The heat and mass transfer considerations for pure liquid droplets must be modified for droplets containing dissolved or suspended solids. When a droplet contains dissolved materials which lower the normal vapour pressure of the liquid, the temperature and vapour pressure differences causing heat and mass transfer are also lowered and the rate of evaporation is less than for pure liquid droplets. For droplets of solutions with a negligible vapour pressure lowering effect, and for suspensions of inert solids, the evaporation rates in the initial stages of drying can be treated in the same manner as for pure liquid droplets of the same size. However, once a solid starts to precipitate or deposit on the droplet surface, and to eventually cover the whole droplet surface trapping liquid inside, heat and mass transfer processes become impaired (69). The reduction in mass transfer depends upon the

nature of the solid crust or skin formed (206), i.e.; whether it is porous, non-porous, rigid, flexible etc..

Thus the evaporation and drying of droplets in spray drying generally involves a period of surface evaporation comparable to the evaporation of pure liquid droplets at a constant temperature, termed the constant-rate period. Because of the high feed concentrations often used for economic reasons, and the rapid mass transfer, this period would normally be very short. This is followed by a period in which the rate decreases rapidly, the droplet temperature increases continuously and the temperature driving force decreases. This is termed the falling-rate period (see Figure 9).

Ranz and Marshall (52) have shown that a droplet containing solids will evaporate as though it were saturated, even though its average concentration is well below saturation. This was explained on the basis that the rate of diffusion of the dissolved material back into the droplet was slow compared with the rate of evaporation; hence, solid build-up occurs on the surface of the droplet. At high air temperatures, around 250°C (37), the effect of solids in solution becomes less pronounced as the temperature driving force for saturated solutions and pure water become almost equal.

When the heat of crystallization is significant the droplet temperature shows a marked rise when crystallization occurs. A detailed analysis is given by Williams and

Figure 9. Theoretical Drying Rate Curve

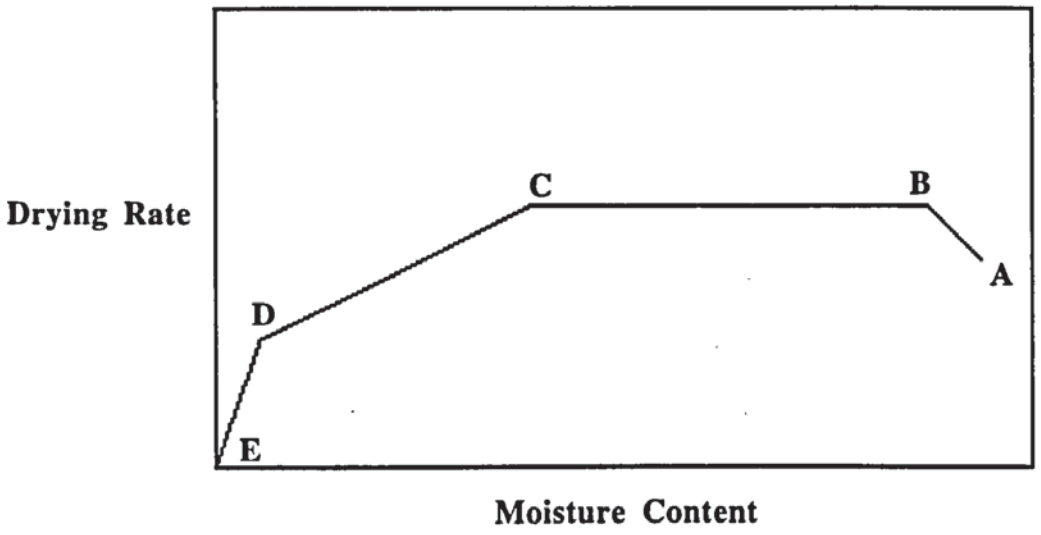

ABC - First period of drying. Includes evaporation during both the retarded flight and free-fall at the terminal velocity.

AB - Approach to the dynamic equilibrium temperature.

BC - Constant-rate peroid. Analogous to the evaporation of pure liquid droplets, i.e.; saturated surface drying.

C - Critical moisture content.

CDE - Second period of drying. Skin or crust formation; the falling-rate period.

Drying curves in reality have no sharply defined points. Some of the drying zones shown above may not even occur.

Schmidt (70). In some spray drying applications where the amount of water to be evaporated is small, the drying air may actually experience a temperature rise caused by the heat generated from crystallization. At low air temperatures, when crystals or a non-liquid surface (skin) forms, the droplet diameter may no longer decrease and may eventually become constant. At higher temperatures the diameter may actually increase if the droplet / particle inflates.

The first period of drying ends when solid begins to form on the droplet surface. This may occur before conditions of uniform saturation throughout the droplet are reached. To estimate the time of this period some method must be established to predict the critical moisture content of various materials, that is, the moisture content corresponding to the end of the first drying period.

Estimation of drying rates during crust formation should take into account the increased resistance to transfer across the solid shell. A method for assessing the effect has been suggested by Charlesworth and Marshall (71), and Dlouhy and Gauvin (45).

The drying time for the second period of drying, or the falling-rate period, depends upon the nature of the solid phase. Ranz and Marshall (52) however, proposed a relationship in terms of the critical moisture content,

$$t_F = \frac{\lambda(Wc - Wf)\rho_P Dm^2}{12Kd\Delta T} \quad \ldots\ldots\ldots\ldots\ldots\ldots (15)$$

where t_F = drying time for falling-rate period
Wc = critical moisture content
Wf = final moisture content
ρ_P = particle density
Dm = droplet diameter at critical moisture content

They also proposed an expression for the total drying time of a droplet drying at a low Reynolds number and for conditions of negligible vapour pressure lowering, although a knowledge of the relationship between moisture content and droplet temperature is necessary.

$$t = \frac{\lambda\rho_L(Do^2 - Dm^2)}{8Kd(Ta-Td)} + \frac{\lambda(Wc - Wf)\rho_P Dm^2}{12Kd\Delta T} \quad \ldots\ldots\ldots (16)$$

where ρ_L = liquid density
Do = initial droplet diameter
Ta = air temperature
Td = droplet temperature
λ = latent heat of vaporization
ΔT = temperature difference driving force

The evaporation time of droplets containing solids with negligible vapour pressure lowering effect is usually greater than for pure liquid droplets; the actual increase in time is dependent on the moisture content of the droplet / particle. In cases where vapour pressure lowering is encountered, the temperature driving force is less, which tends to further increase the drying time.

Droplet-size must also be taken into account when evaluating drying times. For all droplets the fraction evaporated during the retardation period is approximately constant and usually small in comparison to that occurring during free-fall at the terminal velocity. However, in free-fall, small droplets evaporate rapidly, whereas both the drying times and the terminal velocities of larger droplets are greater. Hence, large drying chambers may be required in spray drying to dry a product satisfactory.

When volatile components other than water are present, e.g.; flavours and aromas in the spray drying of coffee, their loss will be related to their relative volatilities prior to crust or skin formation. Little work has been carried out on such systems, although there is evidence to suggest that the overall loss depends upon the relative diffusivity of the volatiles through the solid phase. This appears to be independent of their relative volatilities (72).

2.7) The Migration of Moisture in Solids

The rate of mass transfer during the drying of a solid by forced convection is controlled by two mechanisms,

1.) The removal of water vapour from the solid surface due to external conditions, e.g.; gas temperature, humidity and velocity, and the exposed surface area.

2.) The movement of moisture internally, which for a static bed or rigid solid is a function of the internal physical nature of the solid and its moisture content.

Either of these two mechanisms may be the limiting factor on the rate but both proceed simultaneously throughout drying. With some materials, the rate of surface evaporation may be the controlling factor during the initial stage of drying, i.e.; the constant-rate period. Later in the drying process, the rate of moisture movement to the solid surface tends to be the controlling factor, i.e.; the falling-rate period.

External Conditions

An understanding of the manner in which external conditions affect moisture loss from a solid surface is of major importance when investigating the drying characteristics of a material, e.g.; to select the correct type of drier and its

operating conditions. Some materials of a fibrous or porous nature possess properties promoting rapid capillary and diffusive movement of moisture to the surface. The controlling factor in drying is then the rate at which surface evaporation can be maintained.

Surface evaporation is essentially the diffusion of vapour from the solid into the surrounding atmosphere through a relatively stationary film of air or other drying gas in contact with its surface. This film represents a resistance to the vapour flow and is a heat insulant (see Figure 6). The thickness of the film rapidly decreases with an increase in the velocity of the gas in contact with it but never actually disappears. The film of gas in contact with the wet solid remains saturated with vapour so long as the solid surface has free or unbound moisture present, i.e.; moisture which is not adsorbed at the solid surface or chemically combined with the solid - water of crystallization. This results in a vapour pressure gradient through the film from the wetted solid surface to the outer gas and, with large gas movements, the rate of moisture diffusion through the gas-film will be considerable. Therefore, a large exposed solid surface area, high gas velocity relative to the solid surface, and a low relative humidity for the drying medium all promote a high rate of surface evaporation.

Internal Conditions

As a result of heat transfer to a wet solid a temperature gradient develops from the heated surface inwards whilst evaporation occurs at the surface. A quite different situation arises in direct conductive drying where the highest temperature is experienced by solid in contact with the walls of the heating vessel. This promotes migration of moisture from within the solid to the surface through one or more mechanisms, namely,

1.) Diffusion of vapour and / or liquid.

2.) Capillary flow.

3.) Repeated evaporation and condensation.

4.) Flow caused by shrinkage and pressure gradients - This results in a complex situation when drying droplets since they can inflate, rupture, disintegrate etc..

5.) Flow caused by gravity. This mechanism is not applicable to spray drying since droplets rotate during travel. It has however, been a factor in some single droplet research with large slurry droplets of low viscosity (200).

The first three mechanisms may be illustrated by considering a porous solid as it dries. Four phases of moisture movement are distinguishable. In the first, moisture flows as liquid under a hydraulic gradient. Initially the pores are full but gradually air pockets appear to replace the moisture lost. In the second phase, moisture withdraws to the neck of the pores and migrates either by creeping along the capillary walls or by successive evaporation and condensation between liquid bridges, a process termed ' liquid-assisted vapour transfer '. On further drying these liquid bridges evaporate entirely leaving only adsorbed moisture behind which moves by unhindered diffusion of vapour. The final phase is one of desorption-adsorption during which any moisture that vaporizes is condensed, the solid being in hygrothermal equilibrium with its environment.

Moisture flow brought about by morphological changes and pressure gradients during drying (see Figure 15) is particularly relevant when considering material which forms a non-liquid surface or skin during drying. A non-porous skin, which is flexible or pliable in nature, may result in the particle inflating due to internal moisture vaporization. The particle may remain inflated, or, if the internal pressure is too great, rupture to release the moisture causing the particle to collapse and shrivel. Alternatively, if the skin is non-porous and rigid, the particle may crack or even explode to release the internal pressure. Thus, moisture

movement and particle morphology in the final stages of drying are very dependent on the nature of the solid being dried.

All of the above mechanisms may occur simultaneously with one or more being predominant at different stages in the drying process. The net result will generally be a moisture gradient through the thickness of material. For a solid exposed to the heat transfer medium on more than one side, for example a spherical particle, identical gradients should exist more or less from the centre outwards to the surface, although in practice this may not occur (see Figure 7). These moisture gradients, determined experimentally, are due to the flow of liquid from within the solid to replace moisture evaporated from the surface.

Understanding the internal moisture movement of a drying solid becomes important once the critical moisture content has been reached, i.e.; it becomes the factor controlling the residence time required, especially when drying to very low moisture contents. Variables such as gas flowrate, which normally enhance the rate of surface evaporation, become decreasingly important, except insofar as they promote higher rates of heat transfer. Longer residence times and, when practicable, higher temperatures become necessary. Similarly, with some materials, excessive surface evaporation sets up high moisture gradients from the interior towards the surface. This can cause overdrying and possibly thermal degradation. In such cases it is necessary to avoid too-high moisture gradients by retarding surface evaporation, through lower air

temperatures or higher humidities, whilst maintaining an optimum rate of internal moisture movement.

CHAPTER THREE

HEAT AND MASS TRANSFER CORRELATIONS FOR THE EVAPORATION OF PURE LIQUID DROPLETS AND SPHERES UNDER NATURAL AND FORCED CONVECTION

3.0) Evaporation under Natural Convection

One of the first to study the evaporation of pure liquids under natural convection was Sreznevskii (73) in 1882. By monitoring the decrease with time in the height of a liquid meniscus formed at the upper end of a thin capillary tube or on the top of a vertical cylindrical rod, the rate of evaporation of a liquid was determined; the outline of the meniscus was observed through a cathetometer. Evaporation rates were determined for water, carbon disulphide, chloroform, ether and benzene.

By varying the tube or rod diameter, the following relationship was established,

$$r_T \frac{dh}{dt} = \text{constant} \quad \ldots\ldots\ldots\ldots\ldots\ldots (17)$$

where h = height of meniscus
r_T = radius of the tube or rod

Some thirty years later, Morse (74) studied the evaporation of iodine spheres in air by recording their weight loss using a quartz microbalance. The rate of evaporation was found to be proportional to the radii of the spheres. Langmuir (75) subsequently used these results to derive a modified version of Maxwell's equation (42), based on partial pressures, to account for this proportionality. In 1934, Whytlaw-Gray and Patterson (76) used the same technique to monitor the evaporation of 2 mm to 4 mm droplets of water, aniline, p-cresol, quinoline and methyl salicate. The surface area of a droplet was found to decrease linearly with time, over a volume decrease by a factor of almost a hundred.

The technique of placing a sphere or droplet on the pan of a microbalance to study evaporation phenomena, was gradually superseded by filament or capillary suspension methods. This produced conditions more closely resembling evaporation in free-flight, in that, suspension from the end of a filament exposed virtually all the surface area of the material, particularly in the case of a liquid where the droplet remains approximately spherical. The heat gain from the support was also reduced.

Topley et al (77), fused a sphere of iodine 2 mm in diameter to a quartz fibre. The sphere was placed in a cylindrical vessel 40 mm in diameter and left to evaporate. The walls and base of the cylinder were coated in a thin film of potassium hydroxide to absorb the iodine vapour. The

results provided the first real quantitative support for Maxwell's equation.

Houghton (78) measured the rate of evaporation from single water droplets suspended from a glass fibre using a horizontal microscope to monitor the decrease in droplet size. Different sized fibres, varying from approximately 2 μm to 240 μm in diameter, enabled droplets of 100 μm to 200 μm in diameter to be studied. The fibres were coated with a thin layer of paraffin to reduce droplet distortion and to prevent wetting of the fibre stem. Experiments were performed at ambient temperature and with droplet temperatures being estimated indirectly, on the assumption that they corresponded to the wet bulb temperature. Actually however, equality of the adiabatic saturation temperature and wet bulb temperature, i.e.; for the psychrometric ratio $h_T / k'c_s = 1$, where k' is the unit humidity difference and c_s is the humid heat, normally requires a gas velocity > 4.5 m/s. No details are given regarding the dimensions of the experimental apparatus.

Direct measurements of individual droplet temperature were first made by Frossling (34,35) and later by Kiriukhin (79) by using the junction of a thermocouple as the suspension device.

Langstroth et al (80) studied the evaporation of liquid droplets 1 mm to 2 mm in diameter at room temperature. Sample liquids were graded according to their relative volatility and ranged from toluene and aniline, to water. A glass fibre 100 μm in diameter, or a copper-constantan thermocouple, was used to suspend the droplets at the centre of a glass flask of

20 mm internal diameter. The inside of the flask was coated in a thin layer of active charcoal to absorb the organic vapours, or a mixture of charcoal and phosphorous pentoxide to absorb water vapour. The pressure inside the flask was equalized with that of the atmosphere (≈ 690 mm Hg) via a small opening. Droplet diameters were viewed horizontally through a small plane window and measured by means of a microscope fitted with an ocular micrometer. Although radiation effects were accounted for, heat transfer through the glass fibre was ignored. The experimental results obtained agreed with calculations based on diffusion and heat transfer theory.

Ranz and Marshall (52) constructed a special drier in which to study the evaporation of a number of pure liquids, e.g.; water, benzene, and aniline. Individual droplets were suspended from either a glass filament or a thermocouple, or from the tip of a capillary burette. Rates of evaporation were determined by monitoring the decrease in droplet diameter with time, or by measuring the decrease in liquid level within the burette whilst keeping the droplet diameter constant. Droplets of 0.6 mm to 1.1 mm in diameter were dried at temperatures ranging from ambient up to 220°C. The results were correlated by,

$$Nu = 2 + 0.6\ Pr^{0.33}\ Gr^{0.25} \quad \ldots\ldots\ldots\ldots (18)$$

$$Sh = 2 + 0.6\ Sc^{0.33}\ Gr^{0.25} \quad \ldots\ldots\ldots\ldots (19)$$

where Gr is the Grashof number, $D^3\rho_a g\beta\Delta T/\mu_a^2$

Mathers et al (81) were the first to solve the simultaneous heat and mass transfer equations numerically for natural convection. In experiments using internally heated brass spheres coated with naphthalene, the correlations obtained were,

$$Nu = 2 + 0.282(GrPr)^{0.37} \quad \ldots\ldots\ldots\ldots\ldots (20)$$

$$Sh = 2 + 0.282(GrSc)^{0.37} \quad \ldots\ldots\ldots\ldots\ldots (21)$$

when GrPr and GrSc < 100, and,

$$Nu = 2 + 0.5(GrPr)^{0.25} \quad \ldots\ldots\ldots\ldots\ldots (22)$$

$$Sh = 2 + 0.5(GrSc)^{0.25} \quad \ldots\ldots\ldots\ldots\ldots (23)$$

when GrPr and GrSc > 100 and < 10^6

Steinberger and Treybal (82) studied the rates of solvation of benzoic acid spheres 12.7 mm, 19.1 mm and 25.4 mm in diameter at room temperature. The spheres were immersed in Dewar flasks full of water and left undisturbed for a period of 8 hours. They were then removed and the resulting solutions titrated to determine the benzoic acid content.

After correcting for the heat of solution, the data was divided according to whether GrSc was less or greater than 10^8 due to the onset of turbulence within the boundary layer at the higher range. The correlations were,

$$Sh = 2 + 0.569(GrSc)^{0.25} \quad \ldots\ldots\ldots\ldots\ldots (24)$$

when $GrSc < 10^8$,

$$Sh = 2 + 0.025(GrSc)^{0.33} \, Sc^{0.24} \quad \ldots\ldots\ldots\ldots (25)$$

when $GrSc > 10^8$,

Clearly however, the analogy with evaporation is imprecise since no convective heat transfer was required.

Yuge (83) investigated heat transfer under natural convection from internally heated carbon-chrome steel and brass spheres suspended from two sides by thermocouple wires. The data were correlated by the equation,

$$Nu = 2 + 0.392 \, Gr^{0.25} \quad \ldots\ldots\ldots\ldots\ldots\ldots (26)$$

when $Gr > 1$ but $< 10^8$

The evaporation of unsupported droplets under natural and forced convection has also been studied using electrostatic fields (84-86), and more recently ultrasonic fields (87), as a

means of suspension. Although it is possible to produce and study very small droplets using these techniques, i.e.; in the region of 1 μm to 6 μm in diameter, the results are reported to be far less reliable than those derived from physical suspension techniques. Droplet oscillation, which tends to increase the rate of mass transfer (117,119,199), must be taken into account, as well as any possible effects the electrostatic field has upon the physical properties of the droplet, e.g.; surface tension.

3.1) Evaporation under Forced Convection

The evaporation of pure liquid droplets and spheres under natural convection can be expressed in terms of the rate of mass transfer by the simple relationship shown in equation 9. A similar analogy applies to heat transfer. Under natural convection, the values of the mass and heat transfer coefficients, k and h_T respectively, are simply related to the transport properties shown in equations 11 and 12. However, when relative motion occurs between the droplet and its surroundings, correlations for k and h_T must take into account the relative velocity.

Mass Transfer Experiments

Majama (88) was among the first to measure the rates of evaporation of droplets in a gas stream. Individual droplets

of water approximately 0.2 mm in diameter, or of a number of organic liquids, were supported on a horizontal glass fibre 5 μm in diameter within an air stream travelling at up to 18 m/s. The results demonstrated that the rate of change of droplet diameter squared, was constant.

Frossling's pioneering work (34,35) provided the first accurate measurements of droplet evaporation under forced convection. Using a glass fibre or thermocouple assembly, accurate measurements were made of the rates of evaporation of droplets of water, aniline, nitrobenzene and spheres of naphthalene at room temperature. Individual droplets, 0.2 mm to 1.88 mm in diameter, were suspended 20 cm above the exit of a vertical wind tunnel. The air velocity was varied from 0.2 m/s to 7 m/s and the rate of evaporation was determined by periodically photographing the droplet. The results were correlated according to equations 13 and 14 over a Reynolds number range of 2 to 1280.

Ranz and Marshall (52) extended their work on the evaporation of droplets under natural convection to evaporation under forced convection. Using the same apparatus, and experimental techniques, individual droplets were evaporated in an air stream with Reynolds numbers in the range 0 to 200. Their results generally confirmed those of Frossling - but differed in the values of the coefficients α_1 and α_2.

Hsu et al (89) studied the evaporation of n-heptane droplets with particular emphasis on the influence of droplet

size and shape. A method of steady-state measurement was developed similar to that used by Ranz and Marshall. Evaporation rates were measured at 38°C in air stream velocities of 0.6 m/s, 1.3 m/s, 1.8 m/s and 2.4 m/s. Data were collected for 26 different droplet configurations varying in shape from pendant to oblate spheroids.

The rate of evaporation was found to increase rapidly with deviations from sphericity, the oblate spheroids yielding higher evaporation rates than the pendant droplets. The following correlation was proposed,

$$Sh = (1 + 0.178\ Re_D^{0.56}\ Sc^{0.37}) \rightarrow$$

$$\rightarrow [1 + 2.292\ (1-\phi)][1 - 0.257\ (1-h/Dh)] \quad \ldots\ldots\ldots (27)$$

where ϕ = $6Vd / As((Dh+h)/2)$
Vd = volume of droplet
As = surface area of droplet
Dh = maximum horizontal diameter of droplet
h = maximum vertical diameter of droplet

Tverskaia (90-92) used a travelling microscope to determine the rate of evaporation of water droplets 0.4 mm to 1.6 mm in diameter. He suspended individual droplets from a thermocouple within a wind tunnel, and varied the air temperature and humidity. The results, correlated in the form of Frossling's equations, showed an increase in the value of the coefficient α_1 with an increase in the Reynolds number, i.e.; at Re_a = 10, 20, 100, 200 and 300 to 500, α_1 = 0.10, 0.15, 0.18, 0.24 and 0.26 respectively.

Sokolskii and Timofeyeva (93) obtained similar results using droplets of water 1 mm to 2 mm in diameter. Their results, measured over a Reynolds number range of 0.7 to 200, were correlated by,

$$Sh = 2 \left(1 + 0.08\ Re_D^{0.66} \right) \quad \ldots\ldots\ldots\ldots (28)$$

and for $Re_D > 200$,

$$Sh = 0.52\ Re_D^{0.50} \quad \ldots\ldots\ldots\ldots\ldots\ldots (29)$$

The rates of evaporation and heat transfer of wet marl particles (a clay-type soil) were measured by Van Krevelen and Hoftijzer (94) at room temperature. Individual particles of 5.5 mm to 14.5 mm in diameter, were suspended by a thin wire from the beam of a torsion balance and dried in an air stream with a constant velocity of 1.4 m/s. The data for the first stage of drying, i.e.; the constant-rate period, was expressed as,

$$Sh = 0.5\ Re_D^{0.50}\ Sc^{0.33} \quad \ldots\ldots\ldots\ldots\ldots (30)$$

Ingebo (95) measured the rate of evaporation of water and a number of organic liquids, e.g.; nitrobenzene, methanol, acetone, benzene and ethanol, from the surface of cork spheres approximately 5 mm in diameter. Measurements were made over a temperature range of 20°C to 500°C and a Reynolds number range

of 1000 to 1600. The results were correlated in the form,

$$Sh = 2 + 0.3\ (Re_D Sc)^{0.6}\ (Kd/Kv)^{0.5} \quad \ldots\ldots\ldots (31)$$

where Kd and Kv are the thermal conductivities of the air and organic vapour respectively.

Maisel and Sherwood (51) experimented with spheres of calcium silicate wetted with water and benzene, and showed that within a Reynolds number range of 2000 to 50000, the Sherwood number was proportional to $Re_D^{0.56}$. However, benzene was found to evaporate so quickly, i.e.; some 5 to 10 times faster than water especially at high values of Re_D, that the surface of the spheres were not always completely wetted. Such data, with a varying surface area, cannot therefore be considered reliable.

Garner and Grafton (96) studied the solvation of benzoic acid spheres into a moving stream of water. Experiments were performed at room temperature over a range of Reynolds number of 20 to 1000. The correlation proposed was,

$$Sh = 44 + 0.48\ Re_D^{0.5}\ Sc^{0.5} \quad \ldots\ldots\ldots\ldots (32)$$

In a similar experiment (97), the rates of solvation of adipic acid and benzoic acid spheres ranging from 9.5 mm to 19.0 mm in diameter, were measured over a range of Reynolds number of 100 to 700. The spheres were supported on a brass rod 1.6 mm

in diameter and the rate of solvation followed photographically. The results were correlated by,

$$Sh = 2 + 0.95\ Re_D^{0.5}\ Sc^{0.33} \quad \ldots\ldots\ldots\ldots (33)$$

Garner and Keey (98) used a low-speed water tunnel to measure the rates of solvation of benzoic acid spheres 19 mm in diameter at 30°C. Measurements were taken over a Reynolds number range of approximately 2 to 255, although comparison with similar data enabled the upper limit to be extended to 900. The results of the investigation show that free convection effects were not entirely absent until a Reynolds number of approximately 750. Over the range of 250 to 900, the overall mass transfer results were in approximate agreement with,

$$Sh = 0.94\ Re_D^{0.5}\ Sc^{0.33} \quad \ldots\ldots\ldots\ldots\ldots (34)$$

Subsequently, Garner and Hoffman (99) used a similar technique and experimental conditions and concluded that free convection effects did not disappear entirely until the Reynolds number reached 250. Although smaller benzoic acid spheres were used in the investigation, i.e.; 9.5 mm in diameter, this should not have effected the results if the experimental technique and dimensional analysis were correct.

All data obtained by Garner et al (96-99) using benzoic or adipic acid were corrected for heat of solution.

Pasternak and Gauvin (100) measured the rate of evaporation of water from the surface of Celite ® (a silica based material) particles of various shapes and sizes (see Figure 11). The particles, measuring between 5 mm and 64 mm in characteristic length, comprised spheres, cylinders, prisms, cubes and hemispheres. The particles were suspended from an aluminium rod, and positioned inside a vertical glass column 38 mm in diameter through which turbulent air was passed under controlled conditions of temperature (21°C to 121°C), humidity and velocity (1.2 m/s to 7.6 m/s). The results, for a Reynolds number of between 500 and 5000, were correlated by,

$$Sh = 0.692\ Re_D^{0.514}\ Sc^{0.33} \quad \ldots\ldots\ldots\ldots (35)$$

In later experiments (101), conducted in free-fall, equation 35 was confirmed using Celite spheres impregnated with radioactively-labelled acetone. Particle velocities were accurately determined using a radioactive tracer technique.

Fuchs (102) suggested that the rate of heat and mass transfer to and from a droplet may be doubled by internal circulation. In a later theoretical analysis concerned with the influence of internal circulation on the mass transfer rate from spherical droplets, Bowman et al (103) postulated that the external flow pattern is affected by internal circulation thereby decreasing the resistance to transfer in the external fluid. Ward et al (104) verified this using mass

Figure 10. Test Section used by Steinberger and Treybal (82) for Experiments Carried out under Forced Convection

Figure 11. Apparatus used by Pasternak and Gauvin (100)

transfer data taken from water droplets travelling through, and suspended in cyclohexanol, and droplets of cyclohexanol, iso-butanol and o-toluidine in water (see Figures 12a and 12b). Sherwood numbers were found to be in good agreement with the theoretical predictions and the results show a 4 to 6 fold enhancement of mass transfer due to internal circulation for water droplets falling in cyclohexanol. This effect was shown to depend on the ratio of the continuous to dispersed phase viscosity of the system. Hence, for a system such as water droplets in cyclohexanol (with a viscosity ratio of the continuous phase to the dispersed of approximately 68), the rates were as expected, several times greater than those for solid spheres. The reverse was found for cyclohexanol droplets in water (the viscosity ratio being approximatley 0.01), i.e.; very little enhancement was found due to circulation.

Consequently, for liquid droplets in air, where the viscosity ratio is generally far less than 0.1, e.g.; the ratio for water droplets in air at 20°C is < 0.02, it is reasonable to assume that negligible enhancement in mass transfer will result from internal circulation.

Results obtained by Steinberger and Treybal (82) on the solvation of benzoic acid spheres in water or in aqueous solutions of propylene glycol under laminar and turbulent flow conditions (see Figure 10), showed that mass transfer by natural and forced convection were additive. Their data however, showed a marked dependence on the ratio of the sphere

Figure 12a. Droplets allowed to fall through the continuous phase.

Figure 12. Extraction Apparatus used by Ward et al (104)

Figure 12b. Droplets suspended in the continuous phase.

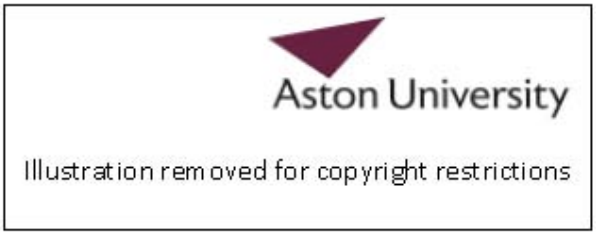

to-water tunnel diameter,

$$Sh = 2 + 0.347 \left(Re_D Sc^{0.5} \right)^{0.62} \quad \ldots\ldots\ldots\ldots (36)$$

Kinard et al (105) reviewed the theoretical approaches for the estimation of mass transfer rate from single spheres. It was considered that the Boundary-Layer Theory cannot accurately predict the overall mass transfer rate because it neglects transfer from the rear surface of the sphere. A semi-theoretical equation was proposed based on the linear addition contributions from forced convection in front of, and behind, the separation zone of the boundary layer. The data, correlated in the form of equation 35, was tested using selected data from Ranz and Marshall (52), Garner and Suckling (97) and Steinberger and Treybal (82).

$$Sh = 2.0 + 0.45\, Re_D^{0.5}\, Sc^{0.33} + 0.00484 \left(Re_D Sc \right)^{0.33} \quad \ldots\ldots\ldots\ldots (37)$$

Audu (106) suspended hemispherical droplets of water from a rotating nozzle placed inside a horizontal wind tunnel. Rotation of the nozzle ensured that all sides of the droplet were exposed to the impinging air. For ambient conditions, the correlation obtained was,

$$Sh = 2.0 + 0.473\, Re_D^{0.5}\, Sc^{0.33} \quad \ldots\ldots\ldots\ldots (38)$$

At temperatures greater than ambient, i.e.; up to 118.5°C, the results were correlated by,

$$Sh = 2 + 0.44 \left(Ta - Td / Tamb \right)^{-0.008} Re_D^{0.5} Sc^{0.33} \quad ..(39)$$

where Tamb = ambient air temperature

A number of inaccuracies may have arisen however, due to the method of monitoring droplet evaporation, i.e.; via an inlet / outlet humidity balance, and because of interference by the nozzle (which had a similar diameter to the droplet) on the airflow pattern around the droplet. This resulted in profiles different from those of a spherical droplet. In addition, heat transfer by conduction along the suspension nozzle and by radiation were not taken into account. Details of the apparatus are given elsewhere (cf. page 129).

Using the same apparatus as Audu, Ali and Bains et al (207) measured the heat and mass transfer rates of water droplets over a temperature range of 21°C to 120°C. The results were correlated by,

$$Sh = 2 + 0.501 \left(Ta - Td / Tamb \right)^{-0.03} Re_D^{0.5} Sc^{0.33} \quad ..(40)$$

$$Nu = 2 + 0.228 \left(1 / B \right)^{0.2} Re_D^{0.5} Pr^{0.33} \quad .....(41)$$

where B = transfer number, $Cp(\Delta T/\lambda)$

The exponent on the temperature correction term in equations 39 and 40 had only a marginal effect over the range of temperatures covered.

Hassan et al (200,210) obtained similar correlations for water droplets over a temperature range of 23°C to 80°C after modifying Audu's apparatus by replacing the steel droplet support with a glass support to minimize heat transfer (cf. page 131). The rate of evaporation was calculated from measurements of droplet weight rather than from a humidity balance over the droplet surface. Data was correlated by,

$$Sh = 2 + 0.575 \left(Ta - Td / Tamb \right)^{-0.04} Re_D^{0.5} Sc^{0.33} \quad .(42)$$

$$Nu = 2 + 0.270 \left(1 / B \right)^{0.18} Re_D^{0.5} Pr^{0.33} \quad .....(43)$$

Virtually identical heat transfer correlations to Hassan et al were obtained by Cheong (180,194) in an earlier, independent study carried out over the same temperature range. Data for water droplets was correlated by $0.19(1/B)^{0.24}$ with respect to equation 43. Experimental details are reported elsewhere (cf. page 156).

Sandoval-Robles et al (107) investigated mass transfer around a sphere using electrolysis. The electrodes, brass spheres 5 mm, 7 mm, 9 mm and 10 mm in diameter, coated in gold 5 μm thick, were rotated at a constant velocity, ranging from

2×10^{-3} m/s to 2.5 m/s, around a circular channel containing a stationary electrolytic solution of 2×10^{-6} M ferrocyanide in 0.5 M sodium hydroxide. The data obtained showed a significant dependency on the Reynolds number,

$$Sh = 1.032\ Re_D^{0.385}\ Sc^{0.33} \quad \text{for } Re_s > 2 \text{ but } < 20 \quad \ldots\ldots\ldots (44)$$

$$Sh = 0.803\ Re_D^{0.475}\ Sc^{0.33} \quad \text{for } Re_s > 20 \text{ but } < 2000 \quad \ldots\ldots (45)$$

$$Sh = 0.300\ Re_D^{0.593}\ Sc^{0.33} \quad \text{for } Re_s > 2000 \text{ but } < 23000 \quad \ldots (46)$$

One major disadvantage however, was that after one single revolution the probe no longer rotated in a stagnant liquid but in its own wake; consequently, this added to the overall rate of mass transfer.

In a similar experiment (108) mass transfer rates were measured around single spheres in a highly turbulent liquid. The results were correlated by,

$$Sh = 6.82\ Re_D^{0.559}\ Tu^{0.069} \quad \text{for } Re_s > 330 \text{ but } < 1720 \quad \ldots\ldots (47)$$

where Tu = turbulence intensity

At low values of Tu, the results were in good agreement with published data for laminar conditions (100).

Heat Transfer Experiments

Heat transfer to a suspended droplet takes place by some combination of convection, radiation and conduction. However, in spray drying, with gas temperatures typically in the range of 250°C to 550°C, only convection is regarded as significant.

Kramers (47) developed an empirical equation for the heat transfer film coefficient of a fluid flowing past a steel sphere. The spheres ranged from 7.0 mm to 12.7 mm in diameter and were heated by a high frequency induction current to maintain them at a constant, uniform temperature, and they were suspended vertically by a pair of fine thermocouple wires in a vertical stream of air, water or oil. The results, covering a Reynolds number range of up to 10^5 and Prandtl numbers between 0.7 to 400, were correlated by,

$$Nu = 2.0 + 1.3\ Pr^{0.15} + 0.66\ Pr^{0.31}\ Re_D^{0.5} \quad \ldots\ldots (48)$$

The second term on the right side of this equation is necessary to bring together data for air, water and oil. However, the physical properties of these liquids are likely to have been affected by temperature gradients at the surface of the spheres. Hence, film coefficients calculated from equation 48 are probably only applicable to heat transfer between a continuous fluid and a stagnant droplet. In the case of oscillating or circulating droplets, e.g.; a droplet in

free-fall as in practical driers, such a coefficient would serve only as an approximation.

In a novel experiment, Tsubouchi and Sato (109) investigated the steady state heat transfer between single particles and a fluid. Thermistor spheres 0.3 mm to 2.0 mm in diameter, were suspended in two types of wind tunnel. The first consisted of a revolving arm providing a velocity range of 0.01 m/s to 0.5 m/s, and the second, of the Eiffel type with a velocity range of 1 m/s to 20 m/s. By monitoring the current and voltage supplied to the spheres, and the resistance, the temperature and the amount of heat dissipated were calculated. The results, for Reynolds numbers > 0.3 but < 3000, were correlated by,

$$Nu = 2.0 + 0.5\ Re_D^{0.5} \quad \ldots\ldots\ldots\ldots\ldots\ldots (49)$$

Yuge (83) studied heat transfer from carbon-chrome steel and brass spheres and compared the effects of counter-current and co-current airflows on the rate of transfer. Metal spheres less than 6 mm in diameter, were preheated in an electric furnace prior to being inserted into the air flowstream. Larger spheres, 6 mm to 60 mm in diameter, were heated internally.

The experimental results were expressed in terms of,

$$Nu = 2.0 + 0.493\ Re_D^{0.5} \quad \ldots\ldots\ldots\ldots\ldots (50)$$

for $Re_a > 10$ but < 1800

$$Nu = 2.0 + 0.300\ Re_D^{0.57} \quad \ldots\ldots\ldots\ldots\ldots (51)$$

for $Re_a > 1800$ but $< 1.5 \times 10^5$

Following a review of the literature on heat and mass transfer, Rowe et al (53) presented new data concerning the heat transfer of internally-heated copper spheres in air and water, the sublimation of naphthalene in air, and the solvation of benzoic acid spheres in water. For heat and mass transfer in air, the results were correlated by,

$$Nu\ (Sh) = 2.0 + 0.69\ Re_D^{0.5}\ Pr\ (Sc)^{0.33} \quad \ldots\ldots\ldots (52)$$

and for water,

$$Nu\ (Sh) = 2.0 + 0.79\ Re_D^{0.5}\ Pr\ (Sc)^{0.33} \quad \ldots\ldots\ldots (53)$$

A dilatometric method combined with cinematography, was used by Adams and Pinter (110) to obtain an average heat transfer coefficient for the evaporation of cyclopentane and isopentane in continuous phases of 0 %, 56 %, 73 % or 77 % w/w glycerol-

water solutions. Different size air bubbles were injected into droplets of the solution and, as evaporation occurred, the increases in volume of the air bubbles were monitored using a dilatometric tube. The data were correlated by,

$$Nu = 7550\ Pr^{-0.75}\ [\mu_c/(\mu_c + \mu_o)]^{4.3}\ Bo^{0.33} \quad .....(54)$$

where μ_c = viscosity of continuous phase
μ_o = viscosity of dispersed phase
Bo = Bond number, $(\rho_c - \rho_M)\ D^2 g/\sigma_L$

3.2) Evaporation from Unsupported Single Droplets

The earliest reported work concerning the evaporation of unsupported droplets was by Gudris and Kulikova (84) in 1924. They retained charged droplets in an electrostatic field by continuously varying their potential so that the electrostatic and gravitational fields exactly balanced causing the droplets to float. The rates of evaporation of water droplets 1.2 μm to 2.5 μm in diameter were measured in various gaseous atmospheres at ambient temperature. In carbon dioxide, the rate of evaporation was found to be negligible, and in air, only very slow. In a mixture of 70 % hydrogen and 30 % air, the rate of evaporation was reported to be several times greater than in air. Other workers (82,111,112) used a similar technique, and studied systems such as benzophenone, benzil, dibutyl tartrate, mercury and diamyl sebacate.

The majority of heat and mass transfer experiments carried out using an electrostatic field are strictly related to droplets moving freely with respect to the medium, but with such small diameters (in the region of 2 μm to 4 μm), and correspondingly small Reynolds numbers (between 10^{-5} and 10^{-4}), the effect of movement on the rate of evaporation is extremely small.

Measurements of the rates of evaporation of larger unsupported droplets were first made in 1949 by Vyrubov (113). Water droplets of 2 mm diameter were allowed to fall freely through a vertical tube 1 m long. The drying air, at between 40°C and 100°C, and with a velocity of 1 m/s, was passed down the tube and the droplets were finally collected on a weighing pan. The results were correlated by,

$$Sh = 0.52\ Re_D^{0.5} \qquad \text{.....(55)}$$

for $Re_D > 100$ but < 500

Kinzer and Gunn (114) studied the evaporation of water droplets ranging from 10 μm to 3 mm in diameter at temperatures between 0°C to 40°C. The smaller sized droplets, i.e.; 10 μm to 140 μm, were charged electrostatically and allowed to fall freely through detector rings. Droplets in excess of 1 mm were supported by inversion of a gas velocity profile. A similar relationship to Frossling's was obtained for droplets in the range of 0.6 mm to 3.0 mm in diameter,

with an α_1 coefficient value of 0.23 over a Reynolds number range > 100 but < 1600. For a Reynolds number < 0.9, the ' wind factor ' was found to be unity, i.e; $\alpha_1 = 0$. As the Reynolds number was increased to 4, α_1 rose to a value of 0.46 and then gradually fell to a value of 0.23 at a Reynolds number of 100.

The rates of evaporation of freely-suspended benzoic acid, camphor and naphthalene spheres were measured by Jones and Smith (115) using a high velocity air stream passing through rotameter tubes. Despite the fact that the spheres spun erratically, mass transfer coefficients showed no significant difference when compared to those for stationary spheres. One possible reason for this is that when one side of the spinning sphere is stationary relative to the gas, the other side meets the flow at twice its linear velocity. Relationships were proposed which take into account the Reynolds number of the gas - Re_G, i.e.; for the laminar region,

$$Sh = 2.0 + 25 \left(Re_D Sc \, Re_G^{0.5} \right)^{0.33} \quad \ldots\ldots\ldots (56)$$

and for the turbulent region,

$$Sh = 2.0 + 0.055 \left(Re_D Sc \, Re_G^{0.5} \right)^{0.5} \quad \ldots\ldots\ldots (57)$$

Several workers (116-118) have studied the shapes, and oscillations of, and internal circulations within, droplets suspended at their terminal velocity. Of particular interest

is the work of Finlay (117) who suspended droplets of water, iso-butanol, n-heptane and iso-octane in an air stream within a wind tunnel. After a given time period, the droplets were collected, weighed and their Sherwood values calculated for droplet diameters ranging from 1 mm to 5 mm. By comparison with the results of Ranz and Marshall, Finlay found a marked discrepancy in rates of mass transfer from droplets with diameters greater than 3 mm. This was attributed to enhanced droplet oscillations later confirmed by Ahmadzadeh and Harker (119) who studied the evaporation of acetone-water droplets in free-fall. They also found that the nozzle diameter constituted an additional parameter. For the acetone-water system, mass transfer data were correlated by,

$$Sh = 3.0 \left(0.345\ D - 0.744 \right) Re_D \quad \ldots\ldots\ldots (58)$$

During a number of experiments concerned with the absorption of carbon dioxide into droplets of water and various hydrocarbons, and with the absorption of water into glycols and amines, Garner and Lane (120) noticed that the droplets oscillated in three characteristic ways,

i.) Prolate / oblate oscillations about an equilibrium spheroidal shape.

ii.) Oscillations about axes 90° apart in the horizontal plane.

iii.) Eccentric rotation about the vertical axis whilst the horizontal axis remains constant.

They also found that the droplets absorbed at very high rates during the first few seconds of formation due to the high initial internal turbulence. When damped down, internally stagnant droplets absorbed at rates commensurate with molecular diffusion. For example, water droplets were found to absorb at 60 to 80 times the molecular rate of diffusion due to internal turbulence.

Yao and Schrock (121) studied the rates of heat and mass transfer of water droplets 3 mm to 6 mm in diameter at temperatures below ambient. The experiments were designed to provide accurate data concerning the relationship between the mean droplet temperature and its position in free-fall, initial temperature and the temperature / humidity of the air through which it fell. The apparatus comprised a droplet generator and a vertical plastic column 3 m high through which conditioned air was passed. A calorimeter could be positioned at any point on the tube to catch a droplet and measure the mean temperature. Droplet sizes and oscillations were observed and recorded photographically. The results demonstrated far less cooling than predicted, suggesting that deformation and vibration of the droplets had an important effect on boundary layer conditions. To bring existing model predictions into agreement with the data, a correction factor was obtained for

the Ranz and Marshall equation. This was in effect a transient correction factor that allowed for the effects of droplet vibration and distortion during fall. The modified Ranz and Marshall equation is thus,

$$Nu = 2.0 + 15.0\ Re_D^{0.5}\ Pr^{0.33}\ (x/D)^{-0.7} \quad .....(59)$$

$$Sh = 2.0 + 15.0\ Re_D^{0.5}\ Sc^{0.33}\ (x/D)^{-0.7} \quad .....(60)$$

for D > 3 mm but < 6 mm, and x/D > 10 but < 600, where x is the distance of fall measured from rest.

Miura et al (122) used a similar apparatus to Garner and Kendrick (123) and Lihou (212), shown in Figure 13, to measure the rates of heat and mass transfer of individual floating droplets in an ascending air current. Water droplets 2.9 mm to 3.3 mm in diameter, were dried at temperatures of 53°C and 75°C. Their experimental data were well represented by the Ranz and Marshall equation over a Reynolds number range of 2 to 1600. Akbar (198) however, performed similar experiments (after Lihou) using water droplets 1 mm to 5 mm in diameter, and found a marked increase in the rates of mass transfer during the initial stages of evaporation, similar to those reported earlier (116-121). Droplets were evaporated at temperatures ranging from ambient up to 180°C and a Reynolds number range of 500 to 1000. Experimental data were correlated by,

$$Sh = -105 + 3.9\ (\ Ta - Td\ /\ Tamb\ )^{0.18}\ Re_D^{0.5}\ Sc^{0.33} \quad ..(61)$$

Figure 13. Air Circulating System used by Garner and Kendrick (123)

Oteng-Attakora et al (199) measured the rates of heat and mass transfer of individual droplets of water, ethanol, propan-1-ol, butan-2-ol, phenol, heptane, monoethanolamine, and solid spheres of naphthalene. Studies were performed independently using a modified version of Lihou's (212) apparatus and a horizontal wind tunnel (206,211). Droplets and spheres 1 mm to

5 mm in diameter, were dried over a temperature range of 50°C to 200°C and a Reynolds number range of 500 to 1000.

The results showed enhanced rates of heat and mass transfer which decreased exponentially with $Re_D^{0.5}$ $Sc(Pr)^{0.33}$. This was in contrast to the linear relationship predicted by Ranz and Marshall (52). Experimental data were correlated by,

$$Sh\ (Nu) = A\ e^{-N} \cdot 10\ \hat{}\ (\ B\ Re_D^{0.5}\ Sc\ (Pr)^{0.33}\ ) \quad \ldots(62)$$

Results for naphthalene spheres however, and the highly viscous liquid monoethanolamine, exhibited almost linear transfer rates with respect to $Re_D^{0.5}$ $Sc(Pr)^{0.33}$.

The enhanced heat and mass transfer rates observed by Akbar (198) and Oteng-Attakora et al were attributed to droplet oscillation (cf. page 283). Consequently, the transfer rates of solid spheres and of droplets with deliberately inhibited surface behaviour approximated to straight lines.

3.3) Evaporation of Single Droplets at High Temperatures

Sensible heat transfer to a droplet occurs by convective transfer directly from the drying medium and to a lesser extent by radiation from the surrounding enclosure, e.g.; the walls of the drying chamber. The radiative contribution from the gas Qr, is normally assumed to be negligible.

The overall convective heat transfer Qc, is therefore,

$$Qc = Q - Qr \quad \ldots\ldots\ldots\ldots\ldots\ldots (63)$$

The contribution due to natural convection, i.e.; for a Reynolds number of approximately 200, has been estimated (124) to be negligible,

$$\frac{Q \text{ free convection}}{Q \text{ forced convection}} \propto 0 \; (\; 0.01 \;)$$

consequently, Qc in equation 63 actually represents the heat transferred by forced convection only.

It has previously been assumed that all the sensible heat transferred to a droplet surface provides the latent heat of vaporization. However, when the gas temperature is high, i.e.; > 300°C (37) - much greater than the wet bulb temperature - consideration must be given to the heat transferred to the vapour which diffuses away from the droplet surface. A considerable amount of the heat conducted inwards is used to heat the vapour diffusing outwards, which consequently reduces the heat transfer rate. Ranz (56) has shown that in the case of an evaporating droplet, the actual heat available for vaporization may be as little as 25 % of the total heat transferred.

Colburn and Drew (125) considered the problem in connection with the condensation of mixed vapours, and

Godsave (126) analysed the problem in relation to burning droplets of liquid fuel. The following expression was derived for the temperature gradient in a gas-film surrounding a droplet in the latter case,

$$T = \frac{Tb - Td}{e^{-E/rI} - e^{-E/r}}\, e^{-E/r} + \frac{Td\, e^{-E/rI} - Tb\, e^{-E/r}}{e^{-E/rI} - e^{-E/r}} \quad \ldots (64)$$

where rI = outer radius of gas-film
E = wCp / 4πKd
w = rate of evaporation (mass flowrate)

Variations in the heat capacity and thermal conductivity of the gas-film caused by temperature and concentration gradients were neglected.

Using equation 64 to substitute for h_T / Kd in the Nusselt number, Godsave showed that,

$$Nu = \frac{2}{r}\left[\frac{1}{\left[\frac{1}{r} - \frac{1}{rI}\right] + \frac{E}{2}\left[\frac{1}{r} - \frac{1}{rI}\right]^2 + \ldots}\right] \quad \ldots\ldots (65)$$

which reduces to the usual form when E → 0. When rI → ∞, Nu = 2.

Ranz (56) derived a similar expression but included an additional term for radiant heat transfer effects. Yuen and Chen (124) and Eisenklam et al (127), have also studied the

effects of high temperatures on the evaporation of liquid droplets.

In the case of burning fuel droplets, Godsave (126) showed that the value of the Nusselt number when evaporation occurred was about a quarter of the value for heat transfer to a non-volatile sphere. Thus, when simultaneous evaporation occurs the value of the Nusselt number can fall below the theoretical minimum value of 2, which means the effective heat transfer coefficient calculated from equation 12 is too high when the evaporation rate is high.

Hoffman and Gauvin (128) measured the evaporation rates of individual droplets of water and various hydrocarbon liquids suspended from a thin glass fibre inside an electrically-heated stainless steel sphere 0.23 m in diameter (see Figure 14). Air temperatures ranged from 100°C to 550°C and droplet diameters from 0.4 mm to 1.4 mm. The rate of evaporation was monitored and recorded photographically. It was reported that the rate of evaporation was not controlled by the rate of heat transfer due to natural convection, but depended on the transfer number B, i.e.; Cp ($\Delta T/\lambda$). The results were correlated by,

$$B' \, Nu \, (Pr)^{-0.33} = 3.2 \, B^{0.97} \qquad \ldots\ldots\ldots\ldots (66)$$

where B' is the Spalding transfer number, $Cp\Delta T/(\lambda - Qr/w)$.

Figure 14. Apparatus used by Hoffman and Gauvin (128)

However, equation 66 is only valid when the gas, and the experimental chamber walls containing the gas, are at the same temperature.

In a later experiment, Pei and Gauvin (129), using essentially the same apparatus as Hoffman and Gauvin, studied the evaporation of similar materials absorbed onto stationary porous spheres 6.4 mm to 12.7 mm in diameter at temperatures of 130°C to 700°C. The relationship obtained was,

$$(Nu/Re_D)^{0.5} (B'/Pr)^{0.33} = 3.32\ (Gr/Re_D^2)^{0.007} \quad .....(67)$$

However, within the limits of experimental error an exponent as small as 0.007 is of dubious value.

Further investigation by Pei et al (130) into the effects of natural and forced convection upon the evaporation of droplets, showed the effects to be non-additive and the transition from one to the other to be gradual. They concluded that when $Gr/Re_D^2 < 0.2$, the effects of natural convection were negligible, and for values greater > 10, forced convection had little or no influence. No correlation was proposed.

Downing (131) made extensive measurements concerning the rate of evaporation of water, acetone, benzene and n-hexane droplets, approximately 1 mm in diameter. The droplets were suspended in a laminar airflow at temperatures ranging from 27°C to 340°C, with a Reynolds number of between 24 and 325. The transfer number B, ranged from 0 to 2. Data was correlated according to,

$$Nu = MN \frac{\ln(1+B)}{B} (2.0 + 0.6\, Re_D^{0.5}\, Pr^{0.33}) \quad \ldots\ldots (68)$$

and,

$$Sh = M\,(2.0 + 0.6\, Re_D^{0.5}\, Sc^{0.33}) \quad \ldots\ldots\ldots\ldots (69)$$

where,

$$M = 1 - 0.4\,[1 - (Td/Ta)] \text{ and, } N = 1 - 0.4\,\left(1 - \frac{\ln(1+B)}{B}\right)$$

The average physical / transport properties were calculated at an average film temperature Tf, defined as,

$$(Tf - Td)/(Ta - Td) = 0.6$$

Narashimhan and Gauvin (132) measured the rate of evaporation of water absorbed onto 6 mm, 10 mm and 13 mm Celite spheres, in superheated steam at temperatures ranging from approximately 200°C to 700°C and at pressures up to 50 atmospheres. They used a similar experimental apparatus to that of Hoffman and Gauvin (128). The results were correlated by,

$$Nu\ (1 + B)^{0.66} = 0.68\ Re_D^{0.5} \quad \ldots\ldots\ldots\ldots (70)$$

In similar experiments, Lee and Ryley (133), used superheated steam at a Reynolds number of 64 to 250, and followed the rate of evaporation of water droplets suspended from a 50 μm glass fibre positioned inside a horizontal test section. Correlations were obtained similar to those of Ranz and Marshall with typical α_1 values of 0.74. The results were not however, corrected for radiation.

In a study by Frazier and Hellier (134), the rate of evaporation of Freon droplets of approximately 440 μm diameter, were measured by injecting a stream of the droplets into an air jet at a temperature of 669°C. A photographic

technique was used to monitor changes in the droplet size, thus enabling the rate of evaporation to be calculated. In applying the Ranz and Marshall equation to the data, it was found that the mass transfer coefficient was underestimated by a factor of 4. However, using corrections for the net flow through the interface, based on the Film Theory, Crosby and Stewart (135) recalculated the results and found a much smaller deviation of 33 % between the experimental and predicted values.

Trommelen and Crosby (136) measured the rate of evaporation of water droplets approximately 1.6 mm in diameter in superheated steam at temperatures of 150°C to 250°C travelling at velocities of 1.5 m/s to 2.1 m/s. The experimental procedure was similar to that followed by Sano and Nishikawa (137), which in turn was based on a method developed by Charlesworth and Marshall (71). Single droplets were suspended at the junction of a Chromel-Constantan thermocouple attached to the end of a horizontally mounted fine glass fibre. This allowed simultaneous measurement of droplet temperature and droplet weight. Heat transferred by direct radiation and conduction through the thermocouple wires was taken into account, although the cross-sectional area of the wires rather than the bead at the junction of the wires, was used in the calculations. This led to an underestimation of the area by at least a factor of 4. The results show that under identical test conditions, the rate of evaporation was greater in air than in superheated steam. However, as the

temperature of the drying medium increased the difference in the rates decreased, i.e.; at higher temperatures the thermal driving forces of the two media become similar. It was further concluded that the correlations developed for the heat transfer coefficients of small droplets in air, also apply to superheated steam.

Kadota and Hiroyasu (138) derived a mathematical model for single droplets evaporating at high pressures and temperatures. The quasi-steady state model allowed for natural convection, non-ideal behaviour, the effect of high mass transfer rates on temperature and concentration profiles, and the thickness of the boundary layer. Results from an earlier study (139) involving the evaporation of droplets of water and a number of organic liquids, e.g.; ethanol, n-heptane and benzene, were found to be in good agreement with the proposed model.

Yuen and Chen (124) simulated liquid droplet behaviour by using a porous sphere continuously-saturated in liquid. The heat transfer rates of water and methanol were measured under forced convection in air at velocities of 2.1 m/s to 11.4 m/s, covering a Reynolds number of 200 to 2000. Temperatures ranged from 150°C to 960°C. The data were correlated according to,

$$Nu\ (1 + B) = 2 + 0.6\ Re_D^{0.5}\ Pr^{0.33} \qquad \ldots\ldots\ldots (71)$$

Although the study was limited in extent, the experimental data does suggest that evaporation at high temperatures reduces heat transfer film coefficients by a factor of (1 + B).

Recently, Renksizbulut and Yuen (140), used a similar technique to measure the rates of heat transfer to single droplets of water, methanol, and heptane, and presented the equation,

$$Nu\ (1 + B)^{0.7} = 2 + 0.57\ Re_D^{0.5}\ Pr^{0.33} \quad \ldots\ldots\ldots (72)$$

where Re_D ranges from 25 to 2000, and B from 0.07 to 2.79.

In summary, information concerning the rates of heat and mass transfer for single, pure liquid droplets and solid spheres evaporating under natural and forced convection has been well-documented. The most significant contribution to the data was almost certainly the introduction of the Ranz and Marshall (52) equation in 1952; the majority of transfer data relating to droplets and solid spheres are correlated by this equation. Although a number of these correlations may be no more than artefacts of the experimental apparatus or experimental technique, the majority provide a useful reference for heat and mass transfer data. For example, individual gas-film transfer coefficients can be calculated and therefore, the rate at which drying depends. They also allow the effects of flow conditions and fluid properties upon

the transfer rates to be studied, which is of particular relevance to drying processes such as spray drying. A particularly good example is the enhancement of heat and mass transfer rates by oscillating droplets (116-121,199), where the Reynolds number alone is clearly insufficient to characterize droplet oscillating behaviour.

CHAPTER FOUR

PARTICLE MORPHOLOGY

THE DRYING OF SPRAYS AND SINGLE DROPLETS CONTAINING DISSOLVED OR SUSPENDED SOLIDS

4.0) Methods used to Study Particle Morphology

Several different experimental approaches have been used to study particle morphology. Marshall and co-workers (41,71,141) carried out many of the early important phenomenological studies on particle morphology by simply collecting dried powders directly from a spray drier and examining them under a microscope at magnifications ranging from x 10 to x 300. Buma and Henstra (142) analysed morphological changes in milk and milk constituents in a similar manner, work later extended by Verhey (143).

Single droplet drying studies, originally developed to study the evaporation of pure liquid droplets by Fuchs (144), Frossling (34,35) and Langstroth et al (80), have been extended, particularly by Ranz and Marshall (52), to solutions, suspensions and pastes. This allowed direct observation of the formation of particle morphologies produced

under controlled conditions similar to those found in a spray drier. The techniques involve suspending a single droplet or stream of droplets in free-flight, or by physical suspension, in an oven or wind tunnel in which air temperature, velocity and humidity are carefully controlled and monitored. Alternatively, droplets are allowed to free-fall.

Free-flight studies achieve droplet suspension in a number of ways. For example, Miura et al (122), Akbar (198) and Oteng-Attakora et al (199) used the inversion of a gas velocity profile to keep a single droplet floating in an ascending air current by matching the air current velocity with the terminal velocity of the droplet. Other methods include the use of electrostatic, or more recently ultrasonic, fields (87) for suspending droplets 1.5 mm to 2.0 mm in diameter.

Alternatively, King (145) and co-workers developed a device which formed a single stream of droplets of uniform size which were allowed to free-fall through a heated column 2.3 m in length. They reported a uniform and controllable temperature profile during drying, albeit of very limited residence time, i.e.; approximately 0.2 s to 0.3 s. Under these conditions the degree of drying is not comparable to that in a practical drier.

Physical suspension techniques, typically those used by Charlesworth and Marshall (71) and subsequently Crosby et al (146,147), have been used extensively to investigate the evaporation rates of single droplets and the phenomena

associated with the evaporation process. Although there are a number of variations, the method generally involved suspending a single droplet in a controlled air stream from the end of a vertical, or in the centre of a horizontal, fine glass filament or filament-thermocouple. These were usually in the region of 200 μm to 600 μm in diameter and some were rotated depending on the design. Droplet sizes were initially in the range of 0.2 mm to 2.0 mm in diameter.

Glass nozzles (200), hypodermic syringes (168,207) and microburettes (52) have also been used as suspension devices. Once in place, measurements of droplet weight, size and temperature are possible, as well as visual observations of drying behaviour.

Both free-flight, free-fall and the physical suspension methods are subject to certain limitations. In particular droplet sizes can be twice the size of those produced by spray drying, i.e.; spray-dried droplets can range from 10 μm to 1000 μm in diameter. The physical support may act as a restraint and in some cases allow an additional heat transfer path. Large droplets may also oscillate, resulting initially in increased mass transfer (116-119). However, these single droplet studies avoid many of the complex interactions encountered in production and pilot plant scale spray driers. Although for this reason alone they have been criticized as being unrealistic, particularly by Toei (87), they offer at present the only practical and direct means of observing spray drying phenomena at the droplet or particulate level and

they have found increasing use in industrial development laboratories during the last 10 years. The importance of single droplet drying techniques was emphasized by Genskow (12) who, in reviewing the problems associated with the spray drying of consumer products, particularly in terms of product quality and performance, outlined the need for new analytical methods and tools to provide a better insight into the fundamentals of drying. Drying kinetics, sorption isotherms and the determination of specific surface areas were discussed, as well as individual techniques such as Scanning Electron Microscopy (SEM), Transmission Electron Microscopy (TEM), laser particle sizing, and Electron Spectroscopy for Chemical Analysis (ESCA). Transport phenomena and mechanisms were reviewed in terms of shrinkage, biochemical degradation and product stickiness.

4.1) Spray-Dried Particles

Marshall and Seltzer (4) provided a brief description of the various particle morphologies produced by spray drying, in relation to feed concentrations and methods of atomization. Materials studied included lemon juice, pectin, milk, sodium chloride, coffee and gelatine. Photomicrographs of the particles show most to be spherical with a large proportion of agglomerates, although gelatine appears to yield elongated, egg-shaped particles. Spray-dried sodium chloride shows particles composed of individual cemented crystals, whereas a

number of other materials appear to have their morphology dominated by the formation of hollow particles. Size distributions vary from being uniform, e.g.; 25 μm to 67 μm in diameter for milk, to relatively wide-ranged, e.g.; 8 μm to 108 μm in diameter for coffee.

A possible mechanism was proposed for the formation of hollow particles dried from skin-forming materials. Marshall and Seltzer suggested that once a skin has formed over the droplet surface, entrapping liquid inside, it casehardens as it dries. The entrapped liquid then starts to exert a pressure as it vaporizes which causes the casehardened surface to stretch and / or rupture to produce a hollow particle which may or may not have blowholes. The term caseharden however, implies an element of rigidity or inflexibility in the skin. This surely cannot be the case as the particle would tend to explode rather than deform or rupture via a blowhole. If casehardening does take place it is more likely to occur when most of the internal liquid has been vaporized, i.e.; in the final stages of drying. The importance of certain morphological features were also discussed in terms of drier design and operating conditions, i.e.; the nature of the dried product (whether hollow or solid particles), particle-size, particle-size distribution, bulk density, feed concentration, drying temperature, mechanical degradation of the product, particle strength, and flow characteristics.

Chu et al (148) studied the effects of operating variables on the bulk density and moisture content of a synthetic detergent using a co-current spray drier 1.2 m in diameter and 3.2 m high. Various operating characteristics were investigated including the addition of organic solvents to the feed prior to spray drying, feed temperature (20°C to 82°C), feed concentration (5 % to 35 % w/w), atomization pressure (10 psig to 60 psig), and drying air temperature (177°C to 566°C). They concluded that,

- Both moisture content and bulk density decreased with increasing drying temperature, approaching a constant value at high temperatures, i.e.; 500°C.

- Bulk density decreased with an increase in atomization pressure, whereas moisture content showed a slight increase.

- Bulk density increased with an increase in feed concentration, with moisture content showing a slight decrease. Bulk density decreased with an increase in feed temperature.

- The addition of 5 % w/w organic solvent (i.e.; acetone or methanol) to the feed produced no generalized correlation with bulk density or moisture content.

Photomicrographs of the spray-dried particles reveal little about the morphology, since the dried product was passed through a centrifugal fan between the drying chamber and the cyclone separator which mechanically ground the particles into a fine powder. This post-drying operation also raises some doubt as to the reliability of observations regarding bulk density and moisture content. However, the presence of hollow particles and a mixture of spherical particles with irregular fragments and agglomerates was reported. A compressed gas was used to transfer the feed from a feed tank to the atomizer; this may have promoted the formation of hollow particles by the desorption of absorbed gas within the droplets during drying (173).

Buckham and Moulton (151) spray-dried aqueous ammonium sulphate solutions covering a concentration range of 0.1 g/cm^3 to 0.7 g/cm^3, using a co-current drier 1.2 m in diameter and 3.8 m high with a unique product collection system consisting of both a gravity and cyclone separator. Inclined protecting trays inside the drying chamber 50 cm long were however, used to protect temperature and humidity sensors. These may have seriously affected airflow patterns within the drying chamber. Drying air temperatures ranged from 216°C to 232°C with droplet and particle diameters in the range 65 μm to 120 μm and 60 μm to 195 μm respectively. Hence, particle fragmentation or shrinkage and expansion phenomena must have been present. As with Chu et al (148), transfer of the feed from the feed tank to the atomizer was by compressed gas. Only

parameters which they thought directly affected the drying operation were monitored, namely droplet-size and droplet-size distribution, drying air temperature and feed concentration. The principal product property determined was the ratio of the final particle diameter to the original droplet diameter, termed the particle expansion ratio. This ratio was found to increase with both feed concentration and original particle diameter.

Generally, their results show that under the same drying conditions the larger particles dried to a less dense product than the smaller particles, which indicates a greater tendency on the part of large particles to form porous or hollow spheres. This was substantiated by bulk density measurements, particle settling rates and microscopic observations. Photomicrographs of the samples show mainly spherical particles with a high proportion of agglomerates. Buckham and Moulton suggested that agglomeration may have occurred due to static electrical effects. No drying rate equations were proposed, although some qualitative factors regarding the drying mechanism of ammonium sulphate were suggested from measurements of final particle diameters, i.e.; many of the particles expanded on drying forming porous or hollow particles. Particle expansion was found to increase with particle-size as well as feed concentration.

Crosby and Marshall (141) spray-dried sodium sulphate solution, coffee extract and a clay slip which when in liquid form, represented a true solution, a colloidal suspension and

a fine slurry or suspension respectively. The liquid feeds (7 % to 22 % w/w) were atomized into a drying chamber 0.6 m in diameter and 6.1 m high using a grooved-cone pressure nozzle with a narrow cone angle. This produced droplets in the range 50 μm to 300 μm in diameter. Air temperatures ranged from 160°C to 280°C with feed temperatures of 35°C to 80°C. The final spray-dried product was oven dried and the particle-size distribution, bulk and particle densities determined; photomicrographs were taken of several narrow-sized fractions, i.e.; sieve mesh diameters ranged from 53 μm up to 250 μm. There is a strong possibility however, that the particle parameters measured would have been considerably altered by oven drying. Bulk and particle density values may have been further altered since particle aggregates were deagglomerated using a series of baffles.

General considerations included, the drying cycle of a droplet and the predition of particle properties using equations developed by Charlesworth and Marshall (71).

The results of their experiments, including photomicrographs of dried particles of all three materials, show that the effects of operating variables on the properties of the spray-dried particles depended upon the type of material being spray-dried, classified as, crystalline (sodium sulphate), amorphous (coffee extract), and agglomerates (clay slip). For sodium sulphate, the effect of inlet air temperature on particle density and hence the final particle diameter, was not found to be significant at low

solid concentrations, i.e.; 10 % w/w, or at concentrations near to saturation. However, for coffee extract, a skin forming material, the inlet air temperature had a very pronounced effect over a wide range of feed concentrations, i.e.; 7 % to 22 % w/w. Feed concentration had a marked influence on the particle properties of sodium sulphate over a range of air temperatures, whereas for coffee, the effects were relatively unpronounced. Feed temperature had little or no effect upon the particle properties of sodium sulphate, except at a feed concentration of 15 % w/w, at which particle density was reported to increase and particle diameter to decrease as feed temperature was increased. For feed concentrations of 10 % and 20 % w/w, this tendency was found to be negligible.

These results indicate that, depending on the material being dried, the particle properties of spray-dried materials can be varied within a limited range by changing air temperature, feed concentration, and in some cases feed temperature. Regardless of the type of material being spray-dried, the final particle diameter rarely equalled the initial droplet diameter. Only in the case of the skin-forming material when dried from sufficiently high feed concentrations at high air temperatures, did particle diameters tend to equal or exceed initial droplet diameters. Particle densities were found to vary over a three to four fold range with bulk density being determined primarily by the density of the larger diameter particles.

For spray-dried materials in general, the bulk density seldom approaches 50 % of the true density of the solid being spray-dried. Crosby and Marshall's results clearly bear this out, i.e.; for sodium sulphate the density of the salt is 2.7 g/cm^3, whereas the highest bulk density they recorded was only 0.5 g/cm^3. Similar results were obtained by Riera et al (211) as demonstrated, in part, by the study described in Appendix A 6.0 i.

Photomicrographs of the sodium sulphate particles show hollow structures composed of multiple crystals concentrated at the crust surface. The effective wall thickness of the larger particles, estimated using a refractive index technique, was found to be comparable to that of the smaller ones, although the internal crystalline structure of the smaller particles was reported to be denser, resulting in a higher average particle density.

Crosby and Marshall concluded from the overall structure of the particles that once a solid wall had formed, no further change in particle diameter occurs throughout the drying process. The general sphericity and uniform wall thickness shown in the photomicrographs also suggests that the droplets have dried symmetrically with the crystalline nature of sodium sulphate being evident from the characteristic ' furry ' appearance of the particles, i.e.; variations in crystal mass on the surface - dendritic growth, cracks, fissures etc..

The coffee extract particles appeared to be hollow and exceptionally thin-walled with the smaller particles having a

slightly thicker wall structure resulting in a higher average density. The shape of the larger particles confirms expansion and contraction during drying, although no particle collapse toward the end of the drying cycle was reported. Using cinephotography, Crosby and Marshall also found that expansion of the particles occurred towards the end of the drying cycle after most of the moisture had evaporated. By far the most interesting particle morphologies have been produced by the spray-dried clay particles. Photomicrographs reveal shrivelled mushroom cap-shaped particles indicative of collapse or deformation of the wall structure in some way. Crosby and Marshall proposed that this may have been caused by capillary action of the dried surfaces drawing liquid and solids outwards uniformly around the droplet, thus creating a vacuum inside the particle and resulting in eventual collapes of the wall structure.

Dlouhy and Gauvin (45) studied the evaporation and drying rates of calcium lignosulphonate solutions (18 % w/w) using an experimental co-current spray drier 0.2 m in diameter and 5 m high. Drying air temperatures ranged from 40°C to 215°C with droplet diameters in the region of 100 μm, produced by pneumatic nozzle atomization. Photomicrographs of the spray-dried material show mainly discrete particles with clear, smooth outer skins. Drying the material at different air temperatures produced considerable differences in particle size and shape. At air temperatures of 52°C to 64°C, the particles appeared to be smaller and more regular-shaped than

those dried at 192°C to 215°C. A greater proportion of hollow particles was also produced at the higher temperature although, as previously reported for Chu et al (148) and Buckham et al (151), a gas pressurized feed tank was used to transfer the feed to the atomizer which would tend to promote particle vacuolation. Dlouhy and Gauvin reported no significant falling-rate period when drying the lignosulphonate and suggested that this was due to the concentration at which a skin was formed, i.e.; skin formation did not occur until the very last stages of drying, with no evidence of skin formation below a solids content of 85 % w/w.

To increase the overall economy of the spray drying operation, most manufacturers find it necessary to pre-concentrate the feed prior to atomization. However, in the concentration range of commercial interest, usually between 40 % to 50 % total solids, the viscosity of many materials increases exponentially, making filtration, heating and atomization of the feed difficult. Hayashi and Kudo (184) have studied the effects of viscosity on the spray drying of milk. A commercial co-current spray drier 8 m in diameter and 22.2 m high with pressure nozzle atomization, was used to dry feed concentrations ranging from 44 % to 50 % total solids at temperatures of 165°C and 187°C. Their results demonstrated that the viscosity of milk increased exponentially with an increase in feed concentration. Values of 70 mPa/s at 47 % total solids, rising to 140 mPa/s at 50 % total solids, were quoted. Particle-size was also found to increase with

increasing viscosity, but to decrease with increasing atomization pressure.

Yan (185) discussed the difficulties of spray drying animal glue (gelatine) due to incomplete atomization of the feed. Photomicrographs of the spray-dried product reveal excessive ligament formation. Atomization was found to be improved by using feed concentrations of 15 % w/w to 17 % w/w, by decreasing the feed viscosity by increasing the feed temperature, and by spray drying at air temperatures of < 150°C.

Leong (169) studied the morphology of particles dried from aqueous solutions of lithium carbonate and manganese hypophosphite at ambient temperatures ranging from 22°C to 25°C and with relative humidities of 23 % to 95 %. A vibrating orifice aerosol generator was used to generate a cloud of monodispersed droplets 20 µm to 30 µm in diameter. This produced dry particle diameters in the region of 0.8 µm to 6 µm. Solution concentrations ranged from 0.5 g/l to 60 g/l.

Photomicrographs of both the lithium carbonate and the manganese hypophosphite particles demonstrated contrasting morphologies. Lithium carbonate formed spherical, hollow particles with single crater-like blowholes. The exterior wall structures were highly porous and composed of a composite structure of small spheriods, agglomerates or polycrystalline material. The degree of porosity was found to decrease with increasing humidity which was considered to be due to higher rates of evaporation. The interior structure of the particles

appears to be very irregular; no solid particles were produced. Manganese hypophosphite formed solid spheroids with smooth, pliable outer skins. The exterior surfaces of the particles were greatly distorted by shrinkage, shrivelling and folding. No blowholes are shown or reported.

From these results and information obtained from the literature (see Table 4), the following conclusions were drawn,

- The rate of evaporation depends upon the air temperature and humidity.

- High rates of evaporation tend to produce porous particles from solutions that do not form impermeable shells.

- Supersaturation occurs in the absence of nuclei, which results in the formation of smaller particles.

- Conditions found favourable for the formation of solid spherical particles include, a nuclei-free environment, a highly soluble solute, and low drying rates at a low enough humidity to form dry particles.

Leong also considered both the theoretical and experimental aspects of morphological control in aerosol particles (170,171) via controlled homogeneous nucleation and crystal growth. The controlling parameters investigated included, air

Table 4. The Various Morphologies of Particles Generated by Nebulizer (N),Spinning Disk (SD) and Vibrating Orifice (VO) Atomization (169)

Solute	Solvent	Generator	Thermal Condition	Relative Humidity	Particle Diameter (μm) († Particle Volume)	Morphology
methylene blue	1:1 water-alcohol	VO	ambient	low	3.7	smooth solid sphere
			ambient	low	3.3	hollow, rough surface spheroid with hole
			heated	10-80%	6.0	dented solid spheroid
			ambient	-	2.5-4.0	smooth spheroid
		SD	ambient	low	< 2	sponge balls
					> 15	hollow smooth spheroids with hole
methylene blue	water-alcohol	VO	ambient	low	-	hollow smooth spheroid
nigrosin dye	water	VO	ambient	low	3.56	smooth solid sphere
uranine	water	N	ambient	47%	2.4-8.0	porous spheroid
		VO	heated	low	6	spheroid
		VO	ambient	low	3.5, 5	smooth spheres with hole
					8.0	spheroidal
					11.8	polycrystaline spheroid with crystal outgrowths
	1:1 water-alcohol	VO	heated	20-60%	5.5	smooth sphere with hole
acetyl cellulose	acetone	VO	high	low	22	shrivelled spheroid

m.methacrylate	chloroform	VO	high	low	20	shrivelled
chelate solutions		N	1150 °C	low	0.1-10	solid or hollow sphere
of metals						
cupric acetate	water	VO	high	low	12	shrivelled spheroid
lithium	water	VO	ambient	92%	4	smooth cenosphere with small hole
carbonate				60%	5.52 †	various polymorphic structures
				26%	2	porous spherical shell
manganese	water	VO	ambient	30%	1.2-6.3	spheroids with dented or shrivelled
hypophosphite						surface
manganous	water	VO	boiling	low	-	smooth thin spherical shell
chloride						
potassium	1:1 water-alcohol	VO	ambient	-	3.5-5.0	hollow smooth sphere
biphthalate						
sodium chloride	water	VO	355 °C	low	1-40	polycrystalline spherical shells
	water-alcohol	VO	ambient	low	27 †	polycrystalline solid
					125 †	hollow spheroid with porous wall of
	1:1 water-alcohol	VO		high	6	single crystals
	water	VO	ambient	low	3.1-5.0	
	water	VO	ambient	low	5.7	single crystals
	1:1 water-alcohol	VO	ambient	-	1.5-5	crystalline structure
sodium sulphate	water	VO	355°C	low	1-40	polycrystalline spheroid

temperature, solvent evaporation rate and the solubility and concentration of the solute.

Qualitative aspects of the particle morphologies obtained were found to be consistent with model predictions, demonstrating that for a given compound a limited amount of control over particle-size, density and shape is possible by controlling the temperature and humidity of the drying air, or in this case the aerosol carrier gas.

4.2) Particles Produced from Single Droplet Drying Experiments

Ranz and Marshall (52), used the same experimental apparatus and conditions described to study the evaporation of pure liquid droplets, to investigate the various factors which influence the rate of evaporation of aqueous droplets containing dissolved or suspended solids. As with previous experiments, the rate of evaporation for droplets under forced convection was followed by measuring the decrease in the liquid level within a microburette used to support individual droplets whilst the droplet diameter was kept constant. This must have been technically difficult, and possibly a source of error. Heat transfer to the droplet via the burette and a thermocouple used to monitor the droplet temperature was found to be negligible. The study was restricted to a Reynolds number range of 0 to 200, the range usually encountered during spray drying. Drying temperatures ranged from 85°C to 220°C with droplet diameters in the region of 0.6 mm to 1.1 mm. From

their results they considered that a droplet evaporates initially as though it were saturated throughout until a skin or crust has formed, even though the average concentration is far less than saturation. Charlesworth and Marshall (71) however, disputed this.

A convenient method has also been proposed (71) for estimating the temperature and evaporation rates of single droplets of aqueous ammonium nitrate and sodium chloride solutions. For droplets containing insoluble materials, initial evaporation rates were found to correspond to that of pure water. General observations of drying behaviour suggested that when a droplet formed a solid structure and its diameter became constant, the falling-rate period followed, during which time the droplet temperature continually rose. In the case of solutions, this temperature rise was due to both the heat of crystallization and sensible heat transfer, whereas for suspensions the temperature rise was due to sensible heat transfer only.

The drying of single droplets of water, aqueous solutions and slurries of sodium sulphate, and detergent slurries were studied by Audu and Jeffreys (168) by suspending 1 mm, 3 mm and 5 mm droplets inside a wind tunnel and estimating the drying rate at different air flowrates (0.3-1.5 x 10^{-3} kg/s) and temperatures (26.5°C to 118.5°C). The droplets were suspended from a 9.5 mm O.D. stainless steel tube which was rotated at 20 rpm to ensure uniform drying of the droplet or particle. The droplets were not however spherical but

hemispherical with the same diameter as the stainless steel tube. Heat transfer from the steel tube to the droplet would have been significantly greater than with other suspension techniques, although this was taken into account in drying rate calculations. Crust thicknesses were measured by SEM and crust porosities estimated from the pressure drop through the crust. No values of porosity were given but from the description of the techniques, porosity values could have been affected by physical damage to the crust. The nature of pores was not discussed, but presumably they were assumed to be cylindrically symmetrical. Measured drying rates however, i.e.; moisture content versus time, were reported to show a good general agreement with those predicted from theory.

Using essentially the same apparatus as Audu and Jeffreys, Ali et al (207) dried solution and slurried droplets of sodium sulphate (50 % to 60 % w/w), proprietary organic dyes (12 % to 18 % w/w) and a number of chelating agents (25 % to 70 % w/w). The effects of air temperature (20°C to 200°C), air velocity (0.1 m/s to 2.1 m/s) and solute concentration were evaluated in terms of evaporation rate, crust thickness, overall and crust mass transfer coefficients, and crust porosity.

Plots of droplet evaporation rate versus time revealed three distinct periods of drying. The first was characterized by a sharp increase in the drying rate which corresponded to evaporation from the free liquid surface, the second by partial crust formation followed by a rise in droplet

temperature, and the third by a rapid decrease in the evaporation rate due to complete crust formation. Crust structure, thickness and porosity had a marked effect upon the rate in the final stages of drying. Particle morphologies were reported to be hollow with either a crystalline porous, rough non-crystalline, or very smooth and ' less porous ' crust structure. Consequently, the drying rate after crust formation was dependent on the type of material being dried. At temperatures approaching 200°C particles had a greater tendency to deform and even explode, although crust thicknesses were reported to increase with an increase in the drying temperature. Increasing the solids concentration reduced the drying rate whereas an increase in air velocity promoted crust formation. The addition of a commercial surfactant Dispersol ® or sodium chloride (13 % w/w) to the organic dyes resulted in both additives migrating to the surface of the particle during drying. This increased particle porosity, particularly the addition of sodium chloride.

A good general agreement between experimental and predicted (168) mass transfer rates was also reported.

Hassan and Mumford (200,210) studied the skin-forming properties of single droplets of 20 % w/w and 40 % w/w custard, rice starch, gelatine, skimmed milk and fructose at temperatures ranging from 19°C to 175°C. The droplets, 3 mm to 8 mm in diameter, were dried in a horizontal wind tunnel (after Audu (168) and Ali (207)) at an air velocity of approximately 0.5 m/s and 1.0 m/s. Droplet weight and droplet

core temperature were recorded versus time. Droplet weights were obtained by detaching the suspension nozzle plus droplet from the main working section of the apparatus and suspending both from beneath an analytical balance. By subtracting the known weight of the nozzle (50 g) from the combined weight of the nozzle plus droplet, the weight of the droplet was obtained. The accuracy of the technique however, may be questionable due to, the large difference in weight between the nozzle and droplet (the nozzle had a mass approximately 5000 times greater than the droplet, typically 10^{-2} g), the relatively small weight loss of the droplet during drying, and vibration of the nozzle / droplet within the wind tunnel.

The results of their investigation revealed three different types of drying behaviour. With type 1 (custard and rice starch), a skin formed over the droplet surface due to solute granule swelling or gelatinisation; this only occurred at high temperatures, i.e.; > 150°C. At temperatures below this, no granule swelling occurred and the droplet formed a porous crust. Variations in solute concentration had little or no effect upon the droplet drying rate, doubling the air velocity however produced a two-fold increase in the drying rate. With type 2 (gelatine), the droplet formed a skin almost immediately. Increasing the drying temperature and air velocity produced a decrease in the overall droplet drying rate due to an increase in the rate of skin formation. The rate of skin formation was also affected by solute concentration, i.e.; the greater the concentration the greater

the rate of skin formation. With type 3 (skimmed milk and fructose), the droplet formed a skin at a certain stage in the drying process depending on the drying conditions and solute concentration. The effects of air temperature, velocity and solute concentration on the droplet drying rate were identical to those of a type 2 material.

A mathematical model was also developed to predict the time ' ts ' at which skin formation first appeared on the surface of a droplet containing a type 1 material,

$$ts = \frac{Cp_D / 2 \pi r^2 \Delta T_d}{h_T (Ta - Td) - k (p_s - p_A) \lambda} \quad \ldots\ldots\ldots (73)$$

where Cp_D = specific heat capacity of droplet
Td = droplet temperature
Ta = air temperature
p_s = vapour pressure at the droplet surface
p_A = partial pressure of water vapour in air

Duffie and Marshall (41) used a vertical cylinder co-current spray drier, 0.20 m in diameter and 7 m high, to dry a number of materials. Droplets > 200 μm in diameter were produced by forcing the feed through small-bore capillary tubes 80 μm to 200 μm in diameter. Drying temperatures ranged from 300°C to 500°C, below which only partially dried particles were formed. Bulk densities were studied as a function of air temperature, feed temperature (30°C to 130°C), feed concentration (4 %

to 60 % w/w) and material properties. In summary, the bulk density of some of the materials, namely the organic dyestuff and sodium silicate, were found to decrease with an increase in drying air temperature due to an increase in dried particle-size. Similarly, the bulk densities of the dyestuff, sodium silicate and sodium chloride tended to decrease slightly with an increase in feed temperature. This was thought to be the result of changes in atomization conditions. Increasing feed concentration also produced a decrease in the bulk density of the dyestuff due to an increase in dried particle-size. However, with some of the materials it was noted that the effects of feed concentration and temperature could produce the opposite effect.

Although obtained in an experimental laboratory drier, the above trends are comparable with other published data. The data of Willman and Blyth (149) are, for example, probably the most reliable, as a good experimental procedure was adopted throughout, i.e.; spray-dried samples of sodium silicate were taken directly from the drier without further processing and only after the drier had reached equilibrium, a small scale industrial drier 2.3 m in diameter was used as opposed to a laboratory scale drier, drying temperatures were relatively high for experimental work ranging from 200°C to 360°C, and bulk densities showed good reproducibility with four runs per drying temperature. There were however, two possible sources of error. Bulk and particle density calculations were based only on 90 % of the spray-dried product as 10 % was lost as

fines < 10 μm in diameter, and, hollow particles did not give true results in sedimentation tests. In hindsight, the latter may have arisen because of the tendency of spray-dried sodium silicate particles to inflate during drying.

The data of Chu et al (148) are questionable, for the reasons mentioned earlier, although there is general agreement that bulk density decreases with increasing drying air temperature. The effect of increasing feed temperature has, in most reported instances, been to produce a slight reduction in bulk density. Lamont's (150) data for soaps are an exception, whilst Marshall and Seltzer (4) reported that an increase in feed temperature can result in an increase in bulk density for some materials. These apparently conflicting results are in accord with those of Duffie and Marshall (41).

The effects of concentration appear to be more difficult to generalize. Much of the available information indicates a decrease in bulk density as the solid concentration increases. Marshall and Seltzer (4) reported that hydrophilic materials such as soaps and detergents exhibited a decrease in bulk density with increasing concentration; the reverse was found to be true for materials such as inorganic salts, pigments, dyes etc., materials which they termed non-hydrophilic.

In all, Duffie and Marshall (41) spray-dried thirteen materials, including ammonium nitrate, sodium sulphate, potassium sulphate, milk, gelatine, coffee and corn syrup. Photomicrographs of the particles show a number of interesting

morphological features such as ' ballooning ', e.g.; potassium nitrate particles 1.8 mm to 2.0 mm in diameter, ' mushroom cap-shaped ' particles, e.g.; sodium silicate, and shrivelling, e.g.; gelatine. Hollow particles appear to be a relatively common feature, although corn syrup produced solid spherical particles. A detailed description was provided of the drying conditions and final particle morphologies of all the samples. They noted the skin-forming properties of sodium silicate, mentioned earlier by Willman and Blyth (149), along with its tendency to form hollow particles. Various operating parameters affecting the properties of spray-dried materials were listed, viz., the physical and chemical nature of the feed material, feed concentration, feed temperature, drying air temperature, and the type and conditions of atomization. The principal product properties of concern in spray drying were identified as, bulk and particle density, bulk appearance, particle-size and distribution, particle friability or resistance to fracture, moisture content, dispersibility or tendency to agglomerate, and the retention of desirable product qualities, such as flavour, aroma, colour, reconstitutability, etc..

By means of a specially-designed sensitive balance, Charlesworth and Marshall (71) investigated the evaporation of single droplets containing mainly crystalline solids (5.3 % to 50 % w/w), i.e.; aqueous solutions of sodium sulphate, potassium sulphate, copper sulphate, ammonium nitrate, calcium chloride, sodium acetate, ammonium sulphate, ammonium

chloride, sodium chloride, potassium nitrate, lithium hypochlorite, coffee extract, sucrose, dispersible dyes, milk and PVA. The droplets, approximately 1.3 mm to 1.8 mm in diameter, were suspended on a fine glass filament 43 cm long inside a vertical wind tunnel in an air stream with a velocity of 0.4 m/s to 1.6 m/s. Inlet air temperatures ranged from 31°C to 160°C. Droplet drying behaviour was observed and recorded; weight changes were measured during evaporation by recording the vertical deflection of the droplet. Accurate readings must have been difficult to obtain however, due to droplet / filament oscillation, particularly at higher air velocities.

Experimental data were presented on the time of appearance of the first solid phase and the formation of a solid crust for a wide range of drying conditions. A theory was advanced for predicting the time to formation of a solid phase of a drying droplet containing dissolved solids. The results show a reasonable agreement with experimental data and a proposal was made for the application of the data to spray drier performance.

The drying behaviour of the droplets was expressed in the form of a generalized sequence of morphological events, leading to a classification of the final particle morphology (see Figure 15). There was however, no mention of the enantiomorphic changes for sodium sulphate characterized by Cheong et al (180). Numerical data were expressed in graphical form, i.e.; weight loss or temperature versus time.

Observed examples of their morphological classifications include, by reference to Figure 15,

sodium chloride, copper sulphate - sequence (Va),
ammonium sulphate - (Vb),
lithium hypochlorite, sucrose, ammonium sulphate - (VIa),
potassium nitrate, milk, polyvinyl acetate - (VIb),
coffee extract - (VIc).

In virtually all cases, the final particle morphology of these materials was reported to be similar, consisting of a hollow, thin, nearly spherical crust with an outer surface which was usually quite smooth, and an inner surface which was rough and uneven. No photomicrographs were shown of dried particles.

Charlesworth and Marshall's interpretation of data from the weight loss and temperature versus time curves, suggested that at the start of drying the temperature of a solution droplet was slightly above that of pure water evaporating under the same conditions. The extent of the difference was dependent upon the relative lowering of the vapour pressure by the dissolved salt. As evaporation continued and the surface layer of solution became more concentrated, the droplet temperature rose slowly. The rate of temperature rise increased with the first appearance of the solid phase and increased rapidly as the crust neared completion. An exception to this drying behaviour was shown by droplets of potassium sulphate, particularly from a weight loss point of view, i.e.; completion of the crust did not cause the evaporation rate to drop off too sharply. In fact, relatively fast rates of

(a) The temperature of the drying air below the boiling point of the liquid

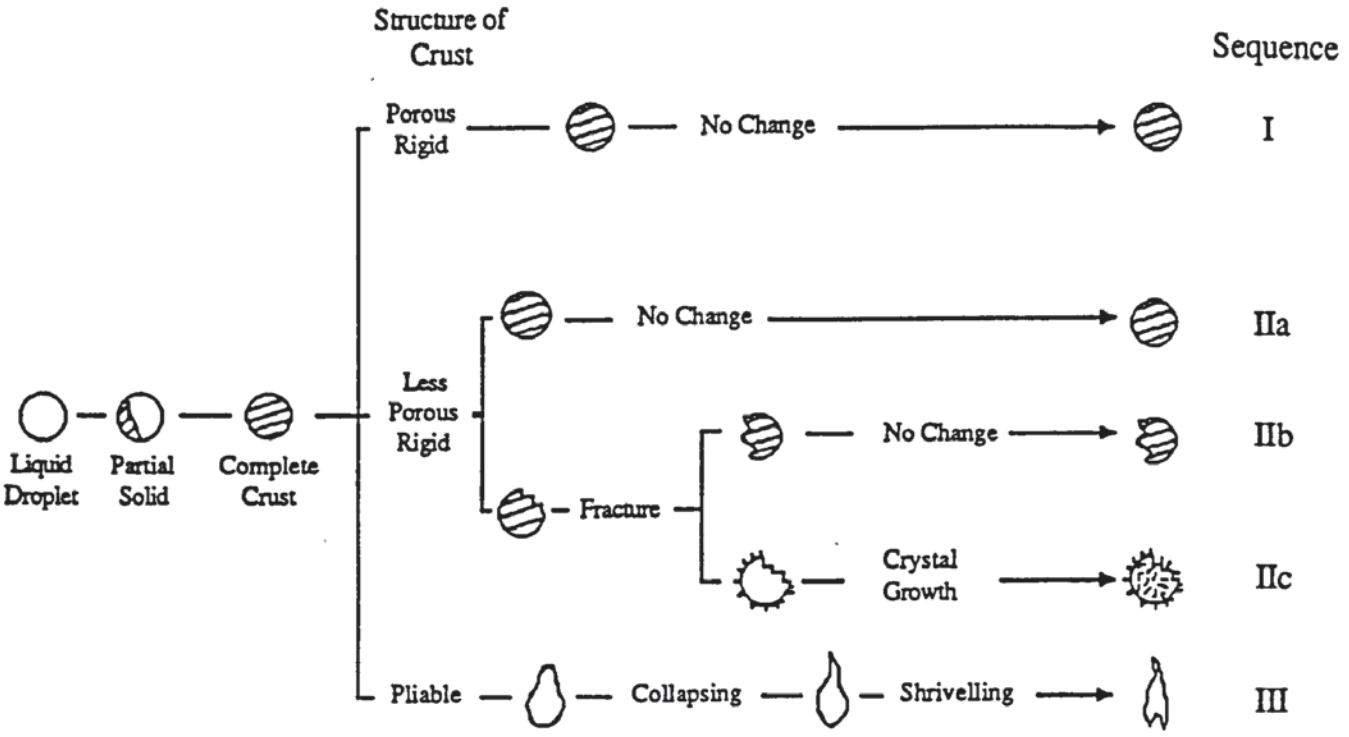

(b) The temperature of the drying air above the boiling point of the liquid

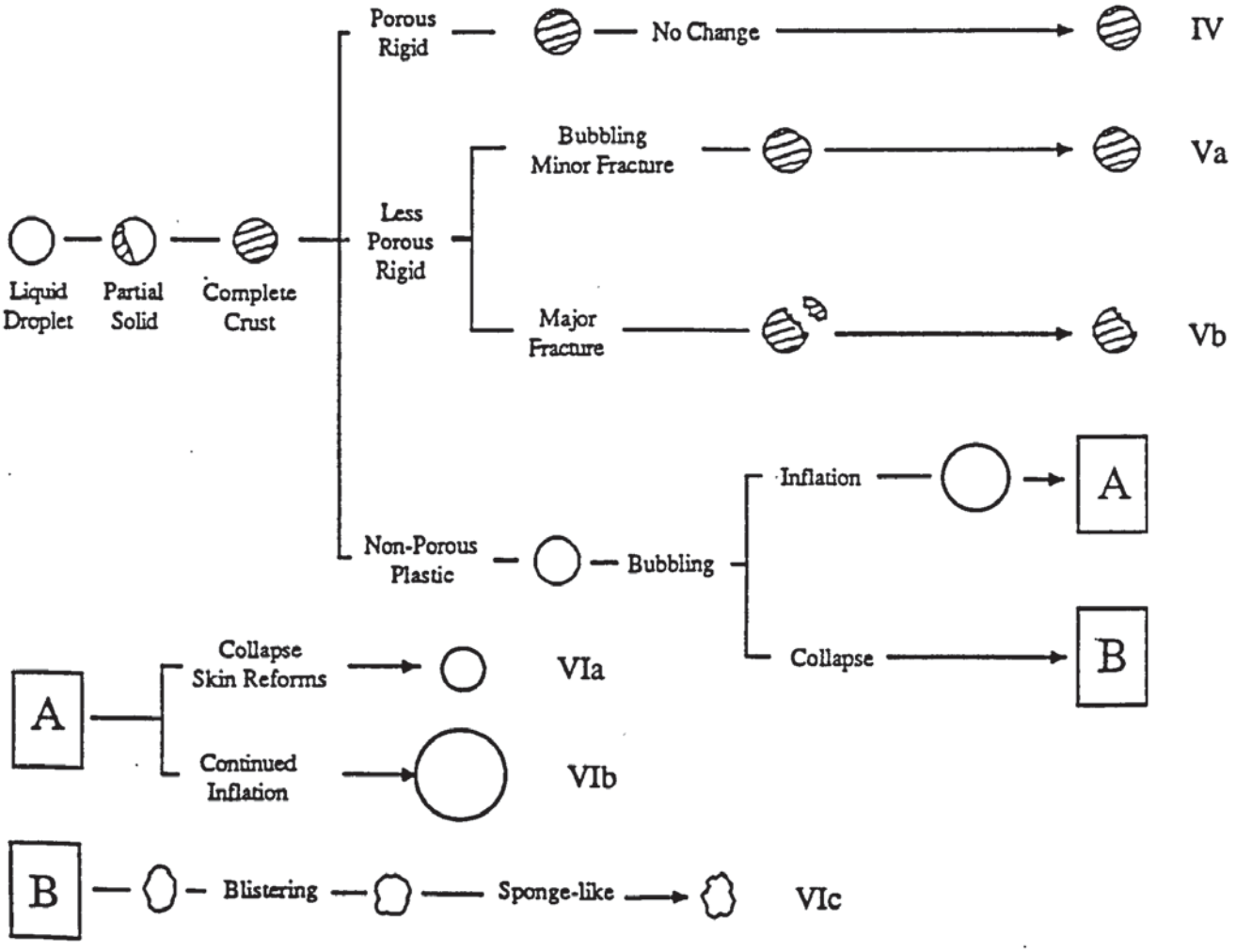

Figure 15. Charlesworth and Marshall's Classification of Drying Behaviour and Particle Morphology

evaporation were found to persist until the particle was completely dry. This was thought to be due to the open structure of the crust allowing the liquid from the interior to flow freely to the outer surface. So rapid was the flow that the crust did not have time to completely cover the droplet. As the crust neared completion, the liquid was drawn away from the open area, leaving a crater in the crust.

The previous claim by Ranz and Marshall (52) that solution droplets prior to crust formation evaporate at all times as if they were saturated, was disproved by Charlesworth and Marshall. They measured droplet temperatures and the weight loss of calcium chloride solutions at four different initial concentrations and noted pronounced differences in droplet temperature and the rate of evaporation. It is therefore apparent that droplets of all aqueous solutions of any concentration do not necessarily evaporate as if they were saturated. Final particle diameters were not always spherical making volume determinations difficult to estimate. In many cases the final particle was found to be larger than the original droplet due to inflation caused by internal vaporization. The degree of inflation varied from particle to particle even though drying conditions remained the same. For some materials, e.g.; sodium sulphate, relatively little expansion occurred under any circumstances. Circulation of liquid within the droplet parallel to its surface was predominantly due to droplet rotation.

Using a similar apparatus to King et al (173,178), Flick et al (182) studied the drying behaviour of single droplets of reconstituted milk powder at concentrations of 24 % and 45 % w/w. The effects of air temperature (80°C to 180°C), droplet-size (200 μm to 400 μm) and feed concentration on the moisture content of partially dried particles were examined. A drying column 0.16 m in diameter and 2 m high was used with a co-current air velocity of 0.35 m/s. The experimental results were compared with values obtained from a model proposed by Sano and Keey (172) and exhibited a reasonably good correlation. Although photomicrographs of the dried particles were not clear, particles derived from a feed concentration of 24 % w/w were reported to be irregular and shrivelled in shape, whereas those dried from a higher feed concentration of 45 % w/w were almost spherical with only a limited amount of folding. This is in direct contrast to the findings of Alexander and King (178). These morphological observations must however be treated with some scepticism, since after falling through the column the partially dried particles were collected on a type of aluminium conveyor belt, which would be expected to seriously damage the morphology of the soft particles. Possible differences in morphology may however have arisen due to a number of factors. Particles formed from higher feed concentrations for example, would tend to dry quicker; their surface structures would hence be less likely to flow due to greater viscosities, and the overall mechanical strength of the particles could have been greater

preventing both internal and external distortion. Differences in feed concentration and drying temperatures may also have been relevant.

Further models were proposed by Nesid (183) to describe the drying behaviour of silica, sodium sulphate and skimmed milk, i.e.; materials which form porous and non-porous particle structures. Experimentally, single droplets were dried at temperatures ranging from 20°C to 200°C from feed concentrations of 4 % to 40 % w/w. A similar experimental apparatus to Charlesworth and Marshall (71) was used; air velocities ranged from 0.1 m/s to 2.0 m/s.

From their results they suggested that particles of sodium sulphate form impermeable crust structures. This is in contrast to the findings of Audu and Jeffreys (168). Furthermore, there was also no mention of the enantiomophic changes observed by Cheong et al (180). Skimmed milk particles were reported to be relatively porous with a skin diffusivity twice that of silica and 15 times that of sodium sulphate. This seems highly unlikely owing to the very porous nature of silica particles and the particle inflation experienced by most skin forming materials (71,206). Surprisingly however, no mention was made of particle inflation with any of the three materials.

El-Sayed et al (186) studied the effects of composition, drying conditions and drying rate on the particle morphology of carbohydrate solutions and food liquids dried as single droplets. Both suspended (71) and free-fall (173,178) drying

techniques were used. Drying temperatures ranged from 88°C to 280°C and solution concentrations from 20 % to 40 % w/w. General observations of the drying behaviour of these materials using the suspended droplet technique revealed three distinct regions or periods of drying. The first essentially involved a constant-rate period in which the droplet diameter gradually decreased uniformly until a skin had formed. At this point, the surface started to exhibit shallow wrinkles and folds as the surface layer was less able to flow; however, the droplet still remained relatively spherical. According to El-Sayed, over 50 % of the droplet volume was lost during this period. In the second period of drying, the temperature of the droplet started to rise and remained near the boiling point of the solution. This promoted internal bubble nucleation. Bubbles grew and eventually burst through the surface of the droplet ejecting wet material from the core. This was followed by rapid inflation and deflation cycles, which were a manifestation of the phenomenon observed by Greenwald and King (173), i.e.; the internal bubbles develop high partial pressures and hence high mole fractions and high volumes of water vapour as the temperature rises and the vapour pressure of the water approaches atmospheric.

The third and final period of drying involved the loss of most of the droplet moisture. The inflation-deflation cycles ceased and the particle started to ' balloon ', encapsulating residual vapour. The temperature of the droplet also started to rise rapidly from the boiling point of the solution toward

the drying air temperature as the final, solidified particle morphology was formed.

Similar observations were reported by Charlesworth and Marshall (71) when drying coffee extract.

The effects of air temperature, solute composition and solute concentration on the above drying behaviour are summarized below for solutions of sucrose, maltodextrin and coffee extract. The effects of dissolved gas are reported elsewhere (cf. page 151).

Air Temperature : The higher the drying air temperature the greater the evaporative driving forces involved. Initiation of the inflation-deflation cycle and the final drying period occurred more rapidly, as expected, at the higher temperatures. At temperatures below the boiling point of the solution, i.e.; 88°C, no bubble nucleation, and consequently no inflation-deflation cycle, were observed. It was also noted that the degree of expansion of the dried particle was greater at higher temperatures. El-Sayed suggested that this was due to the higher internal pressures and / or lower viscosity of the surface material.

Solute Composition : The drying behaviour of all the solutes was reported to be similar during the first and second periods of drying, although solutes of lower molecular weight, i.e.; sucrose, exhibited a longer first period due to greater water diffusivity at a given dissolved solids concentration. Droplets of maltodextrin and coffee extract entered the falling-rate period much quicker than sucrose; similarly,

droplet temperatures rose quicker. This led to earlier bubble nucleation, growth and droplet / particle expansion.

The main differences in drying behaviour arose during the final stages of drying. Droplets of sucrose slowly collapsed forming relatively smooth, solid particles. Diffusivities were probably still high enough for water vapour to diffuse through the particle surface, and the viscosity low enough to permit flow which enabled full collapse and smoothing of the surface (177). Droplets of maltodextrin and coffee extract however, remained expanded when fully dried, forming hollow particles with a high degree of surface folding.

Solute Concentration : Increasing the solute concentration decreased the overall drying time of the droplets. This would be expected since the amount of water to be removed was less. At higher concentrations, larger final particle volumes were produced with the volume of expanded particles being approximately proportional to the initial solute content.

Blowholes : Appart from qualitative observations, El-Sayed rationalized the tendency for the sealing or closure of ruptures that occurs during the drying of a droplet in terms of a competition between a sealing flow due to a surface tension driving force and a viscous resistance to that flow. The concept was similar to those employed by King et al (178,188) to describe the extent of smoothing of surface folds in spray-dried carbohydrates and stickiness and agglomeration tendencies in amorphous powders. The relationship between

surface tension, viscosity, rupture diameter and the time required for the closure of a rupture through viscous flow driven by surface tension has been expressed numerically by Bellows and King (179),

$$t_T = \frac{\mu_L Di}{\sigma_L} \quad \ldots\ldots\ldots\ldots\ldots\ldots\ldots\ldots (74)$$

where t_T = time required for total closure of rupture
Di = initial rupture diameter
μ_L = viscosity of liquid

Measurements of the surface tension and viscosity of various carbohydrate materials, including sucrose, maltodextrin and coffee extract (187,188), indicated that the viscosity of these materials changes over a much wider range than does the surface tension, suggesting that viscosity is the dominant property determining the time for rupture closure.

The Predictive Model : Using a model proposed by Frey and King (189), El-Sayed predicted the average water content of a droplet versus time for sucrose, maltodextrin and coffee extract at a concentration of 30 % w/w. Drying temperatures ranged from 120°C to 280°C and droplet diameters from approximately 0.2 mm to 0.3 mm. Although no equations were given, the model postulated the drying of a sphere with no internal voidage and allowed diffusion coefficients within the sphere to vary sharply with solute concentration and temperature. Because the model did not allow for non-

sphericity, surface ruptures, residual blowholes, surface folds and / or wrinkles, it provided a good basis for determining to what extent these factors affect the drying rate of a droplet. As expected, the best correlation between the predicted and experimental results were in the order of sucrose, maltodextrin and coffee extract, i.e.; the greater the molecular weight of the carbohydrate the greater the tendency to form surface morphological features and develop internal voidage (178). Correspondingly, deviations from the model were greatest when the air temperature was highest.

Comparison of Suspended and Free-fall Drying Techniques : Both suspended and free-fall droplets showed qualitatively similar drying behaviour with the effects of air temperature, solute concentration and dissolved gas content for the free-fall droplets, comparable with those observed for suspended droplets. Differences did however arise in that suspended droplets tended to dry quicker and have more expanded particle morphologies. El-Sayed attributed this to the filament promoting both heat transfer and bubble nucleation. Another difference appeared to be the uneven distribution of surface features on the suspended droplets, compared to a more even distribution over the surface of the free-fall droplets. This was presumably due to free rotation and the absence of a support filament.

4.3) Particle Inflation and Vacuolation

Most of the theoretical models developed for predicting the drying behaviour of solution droplets have assumed that water transport within a drying droplet occurs by a process of binary diffusion within a homogenous liquid. However, work carried out by Thijssen (72), Van der Lijn (174), Kerkhof and Schoeber (175) and Vijlhuizen et al (176), suggests diffusivity decreases sharply with increasing concentration. Therefore a droplet will approach the drying air temperature very early-on in the drying process, when a substantial fraction of the initial liquid is still present. Particle inflation may then occur if air bubbles are formed and the particle surface has not ruptured. This contradicts the work of Verhey (143) who assumed that a droplet will only start to heat-up when most of the moisture has evaporated, i.e.; late-on in the drying process.

Sano and Keey (172) have modelled the drying of an initially-voidless, spherical particle which subsequently inflates and bursts to yield a hollow sphere. It was assumed that only a single inflation and rupture takes place, afterwhich, the hollow particle can deform and conserve mass in only one of two ways (see Figure 16), i.e.; when the maximum radius does not change but the void radius, R4, increases due to the moisture loss, or, when the void radius, R4, remains the same but the outer radius, R2, shrinks from R3.

Figure 16. Modelled Process of Inflation and Rupture of a Droplet During Drying (172)

To test the model, single droplets of skimmed milk 1 mm to 3 mm in diameter were dried at temperatures of 100°C and 200°C using the same techniques described by Charlesworth and Marshall (71). A solution / suspension concentration of 30 % w/w was used for all experiments. There was a good correlation between the predicted values and those obtained experimentally. No photomicrographs were published of the dried particles, although particle inflation was reported to have occurred in over 75 % of the droplets dried. An increase in the rate of drying due to particle inflation was also reported owing to the decreasing distance for internal moisture movement and the increase in drying surface area.

Greenwald and King (173) considered the mechanisms by which internal void formation and / or particle expansion occurs during spray drying. Single droplets of reconstituted spray-dried coffee, from a 20 % w/w feedstock saturated with air, were dried at temperatures ranging from 70°C to 160°C. Their experimental apparatus consisted of a heated column 0.08 m in diameter and 2.3 m high with a unique droplet generation device, i.e.; a vibrating reed which produced a stream of uniform droplets 180 μm to 240 μm in diameter by impinging on the liquid feed surface. The droplets were allowed to free-fall through the column and samples were collected at various points along the column which corresponded to different drying times. The particles and partially dried droplets were then examined using both optical

microscopy and SEM. Magnifications ranged from x 20 to x 50000.

Whilst reconstitution does not simulate coffee extract drying, their results demonstrated that bubble nucleation within the droplets occurred by internal desorption of dissolved air. The bubbles, including those from mechanical entrainment, were found to grow by further desorption of air due to an increase in droplet temperature and / or solute concentration, volume shrinkage during drying, expansion due to increases in droplet temperature, and the internal evaporation of water. Theoretical predictions of bubble-size showed quantitative agreement with experimental values. General observations suggested that the bubbles did not substantially contribute to the particle volume until the internal evaporation of water became predominant. This required droplet temperatures in the region of 100°C. Trends in particle-size with changes in air temperature and initial droplet-size were found to support the concept of expansion through vaporization of water into air bubbles. However, the final degree of expansion depended upon the rheological properties of the crust which are unlikely to be predictable by theoretical modelling.

Based on the work of Verhey (143) and Greenwald and King (173), El-Sayed et al (186) dried single droplets of maltodextrin solution (20 % w/w) saturated with air or carbon dioxide. The droplets were dried at a temperature of 150°C using a suspended droplet technique (71) and ranged from

1.4 mm to 2.0 mm in diameter. The droplets exhibited virtually identical drying behaviour to those reported by Crosby and Weyl (147) with gas bubble nucleation and growth occurring earlier in the carbon dioxide saturated droplets due to the greater solubility of the gas. Droplets dried from degassed solutions (acheived by boiling) showed retarded bubble nucleation, confirming the importance of bubble nucleation through the desorption of gases other than water vapour (173). Although the degassed droplets boiled more violently than the air saturated droplets, probably due to the higher droplet temperatures achieved before bubble nucleation, the final particle morphologies were typical of those formed from air saturated droplets.

4.4) Particle Stickiness

Some material feedstocks are so sticky they cannot be spray-dried by conventional means. Particles stick to the walls of the drying chamber and degrade or clump together to become non-free-flowing. Fruit juices, particularly those containing high proportions of monosaccharides, are for example notoriously difficult to spray-dry. Conversely, many products such as milk and instant coffee are agglomerated to form larger particle aggregates with a more attractive appearance and better handling and reconstitution properties. Agglomeration is usually accomplished through a controlled stickiness (often assessed through a sticky-point

test (12)), created through heat and / or humidity. For example, with coffee steam may be blown into a fluid bed of coffee particles.

Downton et al (177) postulated a mechanism of sticking and agglomeration through viscous flow driven by surface tension and the formation of bridges between particles. The size of a bridge needed to cause particle sticking has been estimated at 0.1 % to 1.0 % of the particle diameter, which yields a predicted critical viscosity of 10^{9} mPa/s to 10^{11} mPa/s. For amorphous particles with concentrate viscosities greater than this value, there will be insufficient flow to cause sticking during short contacts, i.e.; 1 s to 10 s. For viscosities below this critical value, flow and stickiness will occur.

Based on this mechanism it is possible to explain why certain processing approaches help resolve the problem of stickiness. These include, the addition of small amounts of high molecular weight material and the introduction of cool air along the walls of the drier, both of which can increase viscosity by orders of magnitude.

4.5) Surface Folding

Using essentially the same experimental apparatus as Greenwald and King (173), Alexander and King (178) monitored the changes in particle morphology of a number of food and food-related materials. Qualitative observations were reported for the drying of aqueous solutions of lactose, maltodextrin, skimmed

milk and coffee extract. Feed concentrations ranged from 30 % to 40 % w/w and drying air temperatures from 189°C to 225°C. Modifications to Greenwald and King's apparatus included, the replacement of the vibrating reed with a pulsed-orifice droplet generator which gave a greater degree of control over the number and size of droplets produced, i.e; diameters ranged from 180 μm to 230 μm, the use of a co-current airflow with a velocity of 0.07 m/s with respect to the droplets, and the incorporation of heated sampling ports, since Greenwald and King had temperature minima at their sampling ports. However, even with these modifications droplet residence time must have remained a problem, particularly with co-current operation, i.e.; in the region of 0.2 s to 0.3 s.

Particular emphasis was placed upon a mechanistic model, originally developed by Bellows and King (179) and Downton et al (177), describing the phenomenon of surface folding, i.e.; the tendency of a particle to develop surface irregularities such as ridges, dimples, and / or wrinkles during drying, in relation to the rate of viscous flow of the surface material in response to a surface tension driving force.

A folding parameter Γ was defined which compares the relative rates of fold formation and fold smoothing,

$$\Gamma = \frac{v_F}{v_s} = \frac{(-dr/dt)\mu_L}{\sigma_L} \qquad \text{.....(75)}$$

where Γ = folding parameter
v_F = velocity for fold development
v_s = velocity for smoothing
μ_L = viscosity of liquid
σ_L = surface tension of liquid

A simple folding criterion was then expressed as,

if $\Gamma \gg 1$, there is a large tendency to fold,

if $\Gamma \ll 1$, there is little or no tendency to fold,

The model provided semi-quantitative agreement with observations of particles dried from solutes of different molecular weights and feed concentrations. Deviations from the model were thought to be the result of assuming a constant value for the surface tension of the solutes during drying.

Photomicrographs of dried lactose particles revealed highly spherical particles with no surface folding. They have a solid internal structure with little or no void or bubble formation. Alexander and King considered the lack of surface folding to be due to the low molecular weight of the sugar, although there is a positive deviation between the theoretical and measured particle diameters indicating some internal voidage.

By contrast, the skimmed milk particles exhibited a high degree of surface folding and particle distortion. The average width and depth of the surface folds were reported to increase with solids concentration. Examination of the internal structure revealed no void or bubble formation.

The effects of feed concentration on particles formed from droplets of maltodextrin, sucrose and fructose solution were also studied by altering the ratio of maltodextrin to a constant 7:1 mixture of sucrose and fructose. It is evident

from the photomicrographs of the dried particles that as the maltodextrin concentration was increased in relation to the sucrose and fructose, i.e.; a change from low molecular weight sugars to a high molecular weight sugar, the degree of surface folding increased. This can be attributed to the higher viscosity associated with solutes of higher molecular weight resisting flow sufficiently to preclude smoothing of surface irregularities under the surface tension driving force.

The phenomenon of surface folding may have a number of explanations. Buma and Henstra (142) and Verhey (143) postulated that the folds are due to insoluble materials near the droplet surface impeding uniform movement of the highly viscous surface layer, whereas Van der Lijn (174) considered them to be caused by uneven heat and mass transfer. Calculations have shown that variations in heat and mass transfer around a drying droplet (see Figure 8) can lead to serious deviations from the radial symmetry of concentration gradients within the droplet.

4.6) Receding Interface Model

Cheong et al (180) and Bains (181) developed a receding interface model to describe the drying of single droplets of sodium sulphate decahydrate in the form of a slurry (40 % w/w). The model predicts the drying behaviour of the material and allows estimation of drying rates for particulate slurries in general. Simultaneous heat and mass transfer rate

equations have been solved numerically and the results compared with those obtained experimentally.

A novel suspension device has also been developed based on a flexible glass filament incorporating a thermocouple (after Charlesworth and Marshall (71)). This gave simultaneous readings of both droplet weight, by deflection, and droplet temperature. Droplets 1.0 mm to 1.5 mm in diameter were suspended in a vertical wind tunnel and dried at temperatures of 40.7°C, 59.3°C and 78.3°C. A constant air velocity of 2 m/s was used.

The results, i.e.; graphs depicting droplet weight and temperature versus time, demonstrated two distinct drying periods for sodium sulphate, an initial constant-rate period, followed by a falling-rate period once a crust had formed. However, initial experiments showed the drying process to be complicated by enantiomorphic changes taking place at 33°C. This led to discrepancies between the predicted and experimental results until the heats of solution of the different hydrates, and heats of transition of the various crystal forms, were taken into account. There was then a good general agreement between the two, even though various morphological considerations such as the formation of hollow particles, crust porosity, blowholes and crust fracture were largely ignored due to the difficulties in quantifying such parameters. No photomicrographs were presented of the dried particles.

4.7) Selective Diffusion

Menting and Hoogstad (152) monitored the retention of model or pseudo volatiles individually, i.e.; acetone, benzene, ethanol and ethyl acetate at concentrations of 10 ppm in single droplets of 10 % w/w maltodextrin solution. The droplets were suspended from a horizontally-secured thermocouple wire in an ascending air current at a velocity of 2.8 m/s and a temperature of 55°C. This type of suspension device had a tendency to spread the droplets out into a semicircle. Radioactive labelling with C^{14} was used to accurately determine the concentration of volatiles within the droplet as it dried. The film or skin-forming properties of maltodextrin and two distinct drying periods were identified, i.e.; period I, in which the volatiles escaped very rapidly, and period II, in which skin formation was complete and volatile loss was minimized. The period during skin formation was termed the transition period. No photomicrographs were produced of dried particles and there were no descriptions of particle morphology. A tendency was however, reported for droplets of higher initial carbohydrate concentration to form films more rapidly than those of lower concentration.

From their results Menting and Hoogstad concluded that the film surrounding the droplets was permeable to water, but impermeable to volatiles. They considered that adsorption was not involved and could give no satisfactory explanation for

their results. At this time, Thijssen's selective diffusion concept (72) had not been fully established.

In the mid 1960's and early 70's, Thijssen (72) proposed a selective diffusion mechanism which led to a greater understanding of the factors affecting the loss and retention of volatile flavour and aroma substances during the drying of foodstuffs. The concept was based on the fact that the diffusivity of water in concentrated solutions behaves differently to that of other substances, i.e.; whilst the diffusivity of water and other solutes decreases substantially as the water concentration decreases in aqueous solutions of carbohydrates and other food related substances, the diffusivity of water does not decrease to the same extent as those of other component solutes (see Figure 17). This behaviour is general and applies to numerous different organic solutes and mixtures of dissolved solids. For example, the diffusivity of oxygen in sucrose solutions decreases much more rapidly with increasing sucrose concentration than the diffusivity of water (153).

As a result, above a given dissolved solids content, the diffusivity of other substances become far less than the diffusivity of water. Therefore, if it is possible to reach a high enough concentration of dissolved solids at the surface of the material being dried before there has been a major loss of volatile flavour and aroma, the remainder of the volatiles should become trapped because the surface becomes relatively impermeable to them. Hence, there is generally a good

Figure 17. The Effect of Water Concentration on the Diffusion Coefficients of Water and Acetone in Coffee Extract and Maltodextrin at 25°C (153)

retention of volatiles in freeze drying due to the concentrating effect of the freezing process. Similarly, the retention of volatiles in spray drying can be improved if a high concentration of dissolved solids has built-up on the surface of the droplets early enough in the drying process. Preconcentration of the feedstock prior to spray drying may be necessary.

The phenomenon of selective diffusion has been verified experimentally in a number of ways. For example, using a co-current spray drier 2.5 m in diameter and 4 m high with nozzle atomization, Rulkens and Thijssen (154) measured the retention of model volatiles, acetone, methanol, propan-1-ol and pentan-1-ol at 0.1 % concentration in spray-dried solutions of maltodextrin (partially hydrolysed starch, 20 % w/w). The spray-dried powders were reconstituted and the volatiles quantified by gas liquid chromatography. Drying air temperatures ranged from approximately 200°C to 300°C.

They concluded that,

- Retention of volatiles in the spray drying of carbohydrate solutions appeared to be independent of their relative volatilities.

- Retention was found to increase with an increase in the molecular size of the volatile.

- At low volatile concentrations, similar to the level found in liquid foods, volatile retention appeared to be independent of initial volatile concentration. Volatile retention, expressed as a percentage, was calculated from the mass ratio of the amount of volatile in the spray-dried powder to that in the feed.

- Retention strongly increased with an increase in the dissolved solids concentration of the feed and with an increase in feed viscosity. A prerequisite is however, that the viscosity remains low enough for proper atomization. Therefore, maximum retention is obtained from combinations of high feed concentration and high feed temperature. Low concentration feeds have to be atomized at low feed temperatures.

- At high feed temperatures and high feed concentrations, an increase in air inlet temperature above 210°C caused a decrease in volatile retention.

- The observed trends indicated that volatile retentions higher than 90 % are feasible, provided the process conditions are fully optimized.

The bulk densities of the spray-dried powders were measured after vibrating the samples for 4 minutes. This could have

resulted in particle damage, e.g.; fractures, deagglomeration. Values ranged from 0.10 g/cm^3 to 0.46 g/cm^3.

Menting et al (155) carried out slab drying experiments with aqueous solutions of maltodextrin covering an initial concentration range of 10 % to 70 % w/w. The maltodextrin solutions contained 1 g/cm^3 of acetone labelled with C^{14} to act as a pseudo-volatile. The solutions were gelled with agar and formed into slabs of 11 cm x 3.3 cm x 0.4 cm. Each slab was supported by a p.t.f.e. frame (which may have affected heat and mass transfer) and placed inside a humidity-controlled, horizontal wind tunnel with an air velocity of 3 m/s and a temperature of 21.5°C. Volatile loss was measured as a function of time using a liquid scintillation counter and found to occur almost exclusively during the constant-rate period. At high moisture contents the rate of volatile loss was mainly dependent upon component volatility, whereas at low moisture contents the diffusivity of the component became the determining factor.

Thijssen (72), using similar drying conditions but a slightly smaller spray drier than Rulkens and Thijssen (154), i.e.; 1.5 m in diameter, spray-dried coffee extract which had previously been stripped of aroma compounds and model aromas added, i.e.; methanol, acetone, pinacol and ethylene, in ppm concentrations. These were quantified by gas chromatography before and after spray drying. The results of the investigation showed that the dissolved solids concentration of the feed had a strong influence on flavour retention, and

confirmed the insensitivity of the retention to the relative volatility of the model aroma compounds. A theoretical approach was postulated to quantify the volatile loss. Thijssen concluded that provided droplets remain rigid and do not expand, very high aroma retentions are possible. However, relatively low aroma retention may arise from,

- Balloon-like expansion of the droplets.

- A low temperature and high relative humidity near the spray nozzle, i.e.; conditions which would extend the drying time of the droplets. Droplet concentration in the vicinity of the nozzle is very high and the droplets contact only a small fraction of the hot air. Consequently, the use of co-current spray drying would be an advantage when drying aroma / flavour products due to high air temperatures and low relative humidities within the nozzle region.

- Internal circulation. It is assumed in the calculations that the droplets remain rigid throughout. In fact, droplet formation can induce strong circulations within the droplet. The addition of thickeners to the feed such as gums or carboxymethylcellulose, produces a significant improvement in aroma retention. Droplet oscillation can also increase mass transfer (199).

Further experimental evidence for the selective diffusion mechanism comes from,

- Measurements of diffusivity under carefully controlled conditions have demonstrated that the trend in the ratio of diffusivities, as shown in Figure 16, does indeed occur (156,157).

- Volatile retention in spray drying (158) and freeze drying (159) vary with changing operating conditions in the direction predicted by selective diffusion.

- It is possible to model the loss of volatiles from suspended droplets under controlled conditions on the basis of measured diffusivities (152).

- The retention of volatiles as a function of axial distance from the atomizer has been measured (160), and, for high feed concentrations, volatile retention approaches a non-zero asymptotic value at large distances from the atomizer.

Volatile flavour and aroma compounds were modelled experimentally by Verderber and King (208) using the highly volatile compound, sulphur hexafluoride (SF_6). Single droplets of 20 % w/w glucose, sucrose, maltodextrin and 5 % w/w coffee extract (saturated with SF_6) were dried at a temperature of 150°C inside a vertical wind tunnel 4 cm in

diameter and 61 cm high. The droplets, typically 1.0 mm to 2.5 mm in diameter, were suspended from a glass fibre filament 0.36 mm in diameter. The SF_6 was detected continuously in a nitrogen gas stream (travelling with a velocity of approximately 0.02 m/s) downstream of the drying droplet by means of an electron-capture detector, an extremely sensitive detector to electronegative atoms such as fluorine, i.e.; the detection level is less than 10^{-12} g. The technique was coupled with in situ video recording of the droplet, thereby enabling the loss of SF_6 to be correlated with any morphological changes which occurred during drying. The results revealed substantial volatile loss during rapid cycles of droplet expansion, bursting and cratering for glucose, sucrose and maltodextrin. Droplets of coffee extract did not show the same rapid expansion and bursting cycles but formed protrusions which also resulted in substantial volatile loss. Increased volatile retention due to the onset of selective diffusion was noted for all solutes. Similar results were obtained by Sunkel and King (209) who modified the apparatus to allow operation at higher temperatures, i.e.; single droplets of 30 % w/w maltodextrin, coffee extract, skimmed milk, and mixtures of coffee and skimmed milk were dried at temperatures ranging from 115°C up to 220°C.

4.8) Foamed Droplets

One method of altering the specification of a spray-dried product is to inject an inert gas into the concentrated feedstock to form an emulsion or foam. Although most of the relevant literature is covered in patents, Heath and Washburn (161) dissolved carbon dioxide in concentrated milk before drying to destroy bacteria and produced a better product. Reich and Johnston (162) showed that bulk density, colour and the free-flowing characteristics of coffee and tea powders could be controlled and improved by the injection of air, carbon dioxide, or nitrogen into the feed concentrate under pressure. Carbonation in instant coffee manufacture was patented by Chase and Lawsen (163). Oakes et al (164) described a similar process for instant non-fat dry milk, whereby the concentrate was whipped under pressure with nitrogen or nitrous oxide to form a stable foam. Cottage cheese whey is difficult to dry conventionally, but can be dried to a free-flowing powder by foam spray drying. Moreover, spray-dried foams of whole milk (165), non-fat dry milk (166) and Cheddar cheese (167) have been successfully produced. The rated capacity of spray driers can be exceeded if the feedstock is foamed (165). Increased drier capacity was attributed to particle buoyancy and enhanced drying rates.

Abdul-Rahman et al (146), the source of the above literature, dried single droplets 1 mg and 2 mg in weight of foamed and non-foamed sodium caseinate solutions at a

concentration of 15 % w/w. The droplets were dried at air temperatures of 100°C and 200°C. Droplet weight and temperature were obtained using the techniques developed by Charlesworth and Marshall (71) and Trommelen and Crosby (136) respectively. Their results demonstrated that foaming markedly increased the rate of droplet drying when compared to non-foamed droplets of equal mass. Droplets foamed with insoluble gases dried as fast as those foamed with soluble gases. From these observations, and on the bases of the two main mechanisms responsible for food degradation, namely, undesirable chemical reactions between the different chemical species present and / or direct pyrolysis, they concluded that any improvement in products dried as foams results from a reduction in the time required for drying. Consequently, any improvement of product quality is a result of less thermal degradation with little or no change in the evaporative losses of volatile constituents under identical drying conditions. Droplets foamed with soluble gases experience lower temperatures during drying than droplets foamed with insoluble gases at equivalent moisture contents. Hence, the spray drying of feedstocks foamed with soluble gases should yield products slightly less degraded than those foamed with insoluble gases.

Crosby and Weyl (147) continued the work of Abdul-Rahman et al (146) on foam spray drying with a general discussion concerning the principles, methods of foam generation, and the physical nature of foamed droplets. Photomicrographs of the

drying histories of single, foamed droplets were presented as well as limiting models for the description of drying mechanisms. The effects of foam spray drying on particle properties and the foaming conditions used for a number of materials were reported (see Tables 5 and 6). The relationship between the volume-fraction of gas in a foam and the volume-ratio of gas to feedstock was discussed in terms of pressure, temperature and gas solubility.

In practice, aeration of feed solutions such as in the production of detergent is actively discouraged (to the extent that application of vacuum to the feed tank has been considered) because of its undesirable effect on product bulk density. However, briefly summarizing the main points of their discussion,

Formation of Foamed Droplets : There are three basic ways of forming dispersions of gases in liquids,

1.) Direct mixing - mechanical blending.
2.) Desorption from solution - supersaturation of a liquid containing a dissolved gas with subsequent bubble formation and growth either by reduction of pressure, or an increase in temperature.
3.) Chemical generation - gas production by a chemical reaction within the droplet.

All three methods have been used in spray drying.

Table 5. The Effects of Promoted Foaming in Spray Drying

1.) Properties of Products*

- Bulk density reduction and control.
- Particle-size and porosity increase.
- Colour density control.
- Moisture content reduction.
- Dispersion / dissolution improvement.

2.) Characteristics of Drying

- Improves ' dryability '.
- Enhances the retention of highly volatile substances**
- Minimizes thermal degradation of solids.

3.) Influence on Operation and Processing

- Increases capacity of an existing drier.
- Allows the direct introduction of inert gases inside dried particles.
- Increases thermal efficiency of drying gases.

*The main objectives in foamed spray drying.
**Foaming introduces a perforation mechanism that causes the liquid sheet to break-up sooner, thereby reducing the loss of volatiles. However, this may produce smaller droplets initially if the sheet disrupts randomly. Therefore, in terms of volatile loss these two phenomena act in opposition.

Table 6. Foaming Conditions for Certain Spray-Dried Materials

Type of Feed	Feed Concentration (Wt. % solids)	Foaming Gas	Operational Gas-Liquid Ratio	Maximum Vol. % of Gas*
Whole milk	50	N_2	6-28 cm^3/g feed	87-97
Skimmed milk	50-60	Air	4-15 cm^3/cm^3 feed	79-94
Cheddar cheese	42.5	N_2	15 cm^3/cm^3 feed	94
Tea	30-35	CO_2	.05-.06 g/cm^3 water	96-97

* 25°C at 1 atm.

Foam generation within the feed can either be before or after atomization. Generation after atomization can be achieved by the use of highly soluble gases dissolved at or below atmospheric pressure by the use of highly volatile and miscible liquids, or, through thermally initiated chemical reactions.

Physical Characteristics of Foamed Droplets : Single droplet drying studies have shown that particles produced from foamed feedstocks may contain, small uniformly dispersed voids, resemble thin or thick shelled hollow spheres, or, contain a large number of small voids with a smaller number of large voids. Crosby and Weyl report no direct comparisons with industrial or pilot plant scale spray-dried particles, although from experiments carried out on the spray drying of milk foamed with nitrogen under a pressure of 1800 psig to 2000 psig, Hanrahan et al (165) observed two types of bubble present in the spray-dried particles. One type was extremely small, numerous and distributed throughout the milk solid, and the other was relatively large, fewer in number and only occupied the interior of the particles. It was suggested the former arose from dissolved gas, and the latter from non-dissolved gas dispersed in the milk by the mixing device.

These general observations are based upon the drying of skin-forming materials, e.g.; sodium casienate, milk etc.. Feedstocks of crystalline or slurried materials are not readily foamable unless a film-forming phase is added. Little or no work has been done in this area.

Limiting Mechanistic Models : The diffusivity of moisture in the liquid portions of a foamed droplet is at least 5 to 6 times less than the diffusivity in the gaseous portions, because the dispersed gas offers negligible resistance to drying. Crosby and Weyl therefore postulated that there are two limiting configurations for a foamed droplet from which an upper and lower boundary for the drying time can be estimated. Collection of all the liquid feedstock into a central reduced sphere, which is equivalent to a non-foamed droplet of equal mass, will give the maximum drying time, and, collection of all the liquid feedstock into an outer spherical shell, will give the minimum drying time (see Figure 18).

Based on these two models, the calculated theoretical and experimental values of moisture diffusivity, and hence drying times, correlated reasonably well. The spherical shell model tends to overestimate the effective diffusivity slightly more than the reduced sphere model underestimates it. Crosby and Weyl considered this to be mainly due to uneven particle expansion.

In summary, new data, theory and information concerning the spray drying process began to emerge during the 1950's. This is reflected in drying reviews of the period, particularly those by Friedman (5), Calus (6), Gluckert (7), Bagnoli (8), and McCormick (9), who reported an increasing interest in spray drying by the process industries. Belcher (10) suggested this was largely due to the overall economy of operation and the desirable characteristics of the spray-dried

Figure 18. Limiting Configurations for Drying Models of Foamed Droplets (147)

product. Few studies involved particle morphology however; those that did, were mainly concerned with the effects of drier operation and feed specifications (temperature, concentration etc.) on product properties, e.g.; bulk and particle density, particle-size distribution, particle friability, and moisture content. The most significant contribution to these early studies was the work of Marshall et al (4,41,52,71,141). The introduction of Thijssen's (72) selective diffusion concept in 1970 focused attention on maximizing volatile retention during spray drying. The effects of particle morphology on the retention of volatile flavours and aromas however, has only recently been investigated (206,208,209).

As far back as 1951, Marshall (11) noted a lack of papers concerning the use of spray drying in the chemical industry. He attributed this to the need for commercial confidentiality, or, because developments within the field were not significantly worth reporting. The continued lack of published data from the process industries concerning all aspects of the spray drying process, particularly experimental data relating to, e.g.; heat and mass transfer coefficients, diffusivities, drying mechanisms, particle morphology etc., would tend to suggest the former is more likely, although the impracticalities of investigating the spray drying process in situ is also a contributory factor. As a result, spray drying is still regarded as more of an art than a science.

CHAPTER FIVE

EXPERIMENTAL APPARATUS AND PROCEDURE

A single droplet drying technique was used to investigate the rate of evaporation of pure liquid droplets, and the drying behaviour of droplets containing dissolved or suspended solids. Individual droplets were suspended in a controlled air stream and their moisture loss recorded. Visual observations were made of the appearance and size of the droplets or particles.

The experimental apparatus shown in Figure 19 and illustrated schematically in Figure 20, was modelled after the drying apparatus of Ali (190,207) but used a filament suspension device rather than a nozzle. It comprised two sections,

1.) A horizontal wind tunnel in which air temperature, humidity and velocity were controlled and monitored.

2.) A working section consisting of a droplet suspension / rotation device (see Figure 21).

Figure 19. The Single Droplet Drying Apparatus - Wind Tunnel plus Working Section

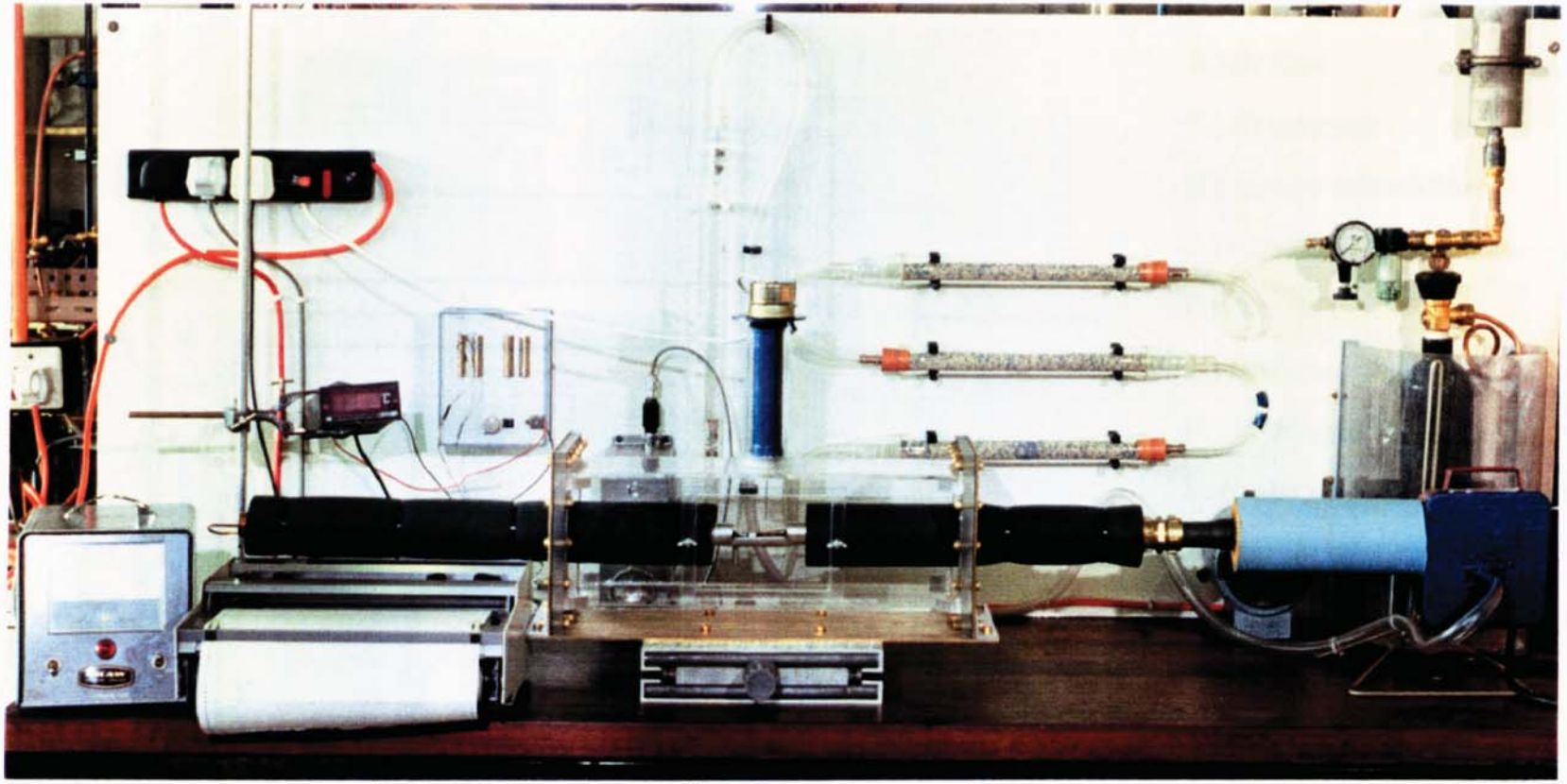

Figure 20. Single Droplet Drying Apparatus

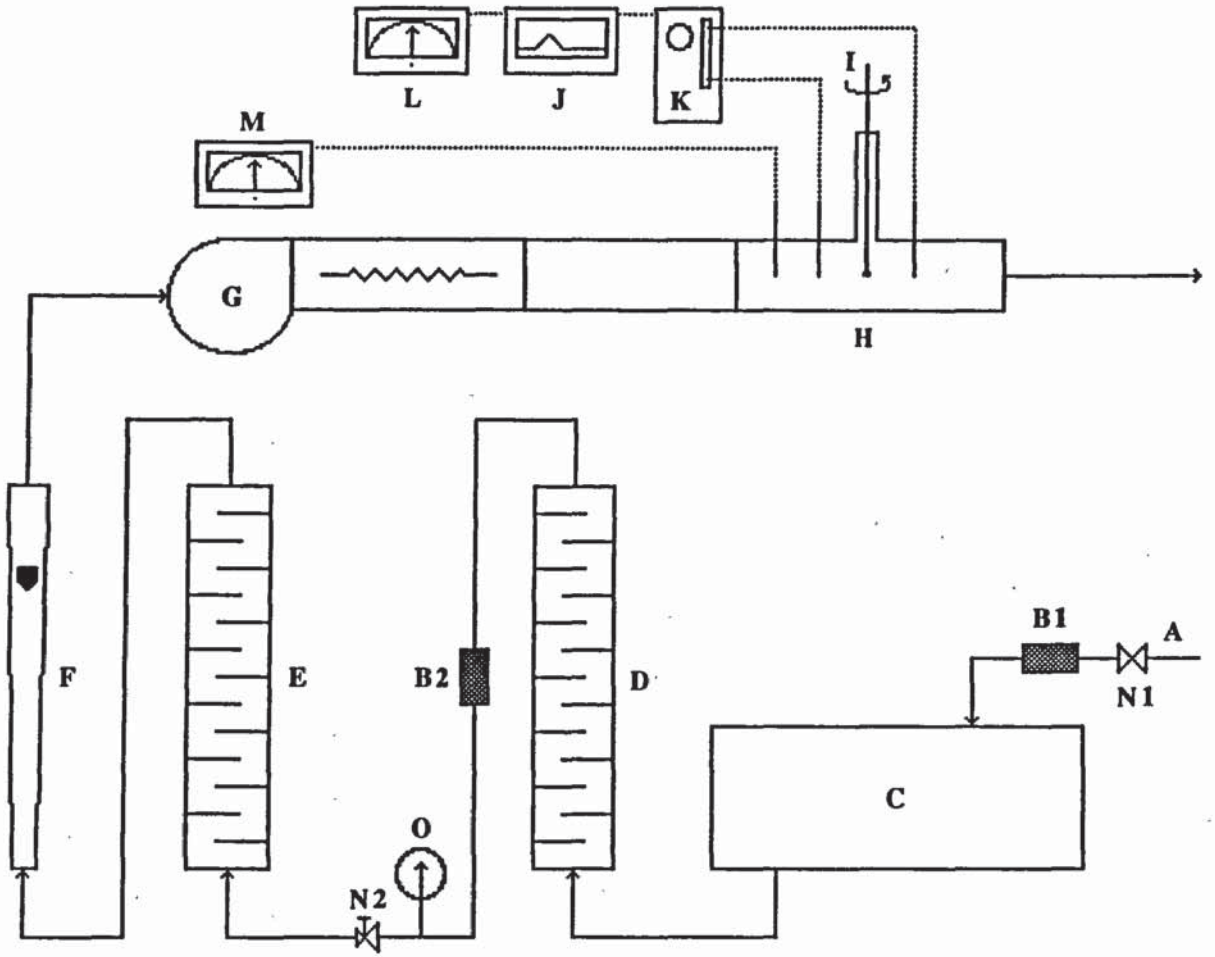

A.) air inlet - 80 psig

B.) air filter

C.) air reservoir

D.) primary dehumidifier

E.) secondary dehumidifier

F.) rotameter

G.) fan blower / heater

H.) working section

I.) droplet suspension / rotation device

J.) chart recorder

K.) thermocouple switching unit •

L.) temperature unit

M.) electronic anemometer

N.) valve

O.) pressure gauge

• The tip of the one thermocouple was wrapped in a muslin cloth and saturated with water to give the wet bulb temperature.

5.0) Wind Tunnel Design

The wind tunnel was constructed from a length of copper tubing 1 m long and 0.025 m internal diameter. A 0.01 m hemispherical section was cut from the centre to allow access to the air stream, one end of the section being slightly tapered (0.020 m internal diameter) to produce a flat air velocity profile (71). The tube was mounted horizontally inside a 0.47 m x 0.15 m x 0.15 m rectangular box and supported at either end by flanges made from 3 mm brass plate. Contact between the flange plates and the tube was made via p.t.f.e. inserts, thus insulating the copper tube from the brass and allowing horizontal movement of the tube for alignment, cleaning, and maintenance purposes. The entire length of the tube was insulated with a heat-resistant foam rubber.

The sides of the box were constructed from 6 mm perspex to facilitate all-round observation of the working section, access to which was gained through a 0.15 m x 0.10 m sealable inspection hatch positioned centrally on the front side of the box. When sealed, the box provided a thermally-insulated, almost airtight environment for the working section, excluding draughts, dust and moisture from the surrounding atmosphere.

Once assembled, the box was mounted on a 0.52 m x 0.20 m section of 3 mm brass plate. This produced a robust, heavy construction to minimize vibration from the surroundings. To reduce vibration further the whole assembly rested on 5 mm thick rubber matting.

5.1) Control and Measurement of Air Stream Conditions

The air stream, supplied from mains compressed air at 80 psig, was fed to a reservoir, filtered to remove particles down to 5 μm and dehumidified using molecular sieve type 4A (2 mm pellets) in accordance with Figure 20.

Metering and control was achieved by passing the air through a reducing regulator to obtain a working pressure of between 3 psig to 8 psig depending on the flowrate, and a rotameter previously calibrated by monitoring the airflow at the working section of the tunnel using a hot wire anemometer. Flowrates up to 2.2 m/s were obtained giving maximum Reynolds numbers of 1278 at 200°C and 2481 at 50°C.

After metering, the air passed into a fan blower housing a 1.5 kW heating coil. This was closed to atmosphere and connected directly to the wind tunnel by compression fittings, the exposed areas being lagged with glass fibre insulation. Air temperature was controlled by connecting the coil to a 240 V, 13 A Variac. This produced temperatures in excess of 250°C. To ensure an even temperature profile, a 2 mm mesh wire gauze was placed directly after the coil.

Dry and approximate wet bulb temperatures inside the wind tunnel were measured to an accuracy of ± 0.01°C by means of platinum resistance thermocouples (Type Pt 100 - RS) placed in close proximity to, but not interfering with, the suspended droplet. Temperature profiles were recorded using a Tarkan V + V 600 chart recorder.

5.2) Construction and Description of the Droplet Suspension / Rotation Device

The droplet suspension device, shown in Figures 21 and 22, allowed rotation of the droplet at 3 rpm during drying. This ensured uniform evaporation and / or drying of the droplets and particles. It was constructed from two concentric stainless steel tubes and enabled the use of relatively high air stream velocities, since movement and vibration of the suspension filament was minimized.

The inner tube, 0.27 m in length with an internal diameter of 1.0 mm and external diameter of 1.8 mm, was connected to a 240 V electric motor (held in position by a locking nut) which rotated via a gearing system at a constant 3 rpm. The outer tube, 0.20 m in length with an internal diameter of 2 mm and an external diameter of 3 mm, was incorporated into the main body of the suspension device. This consisted of an inner and outer casing separated by an airspace for insulation, the outer concentric tube being housed in the inner casing. For assembly, the inner tube was inserted into the outer tube with the electric motor attached to the top of the outer casing. Contact between the two tubes was made using a high viscosity silicone fluid to ensure smooth rotation. The whole assembly was then inserted into a centrally-positioned perspex tube extending from the topside of the wind tunnel. O-rings ensured an airtight fit but allowed movement for centralization of the inner tube within the tunnel.

Figure 21. The Droplet Suspension / Rotation Device

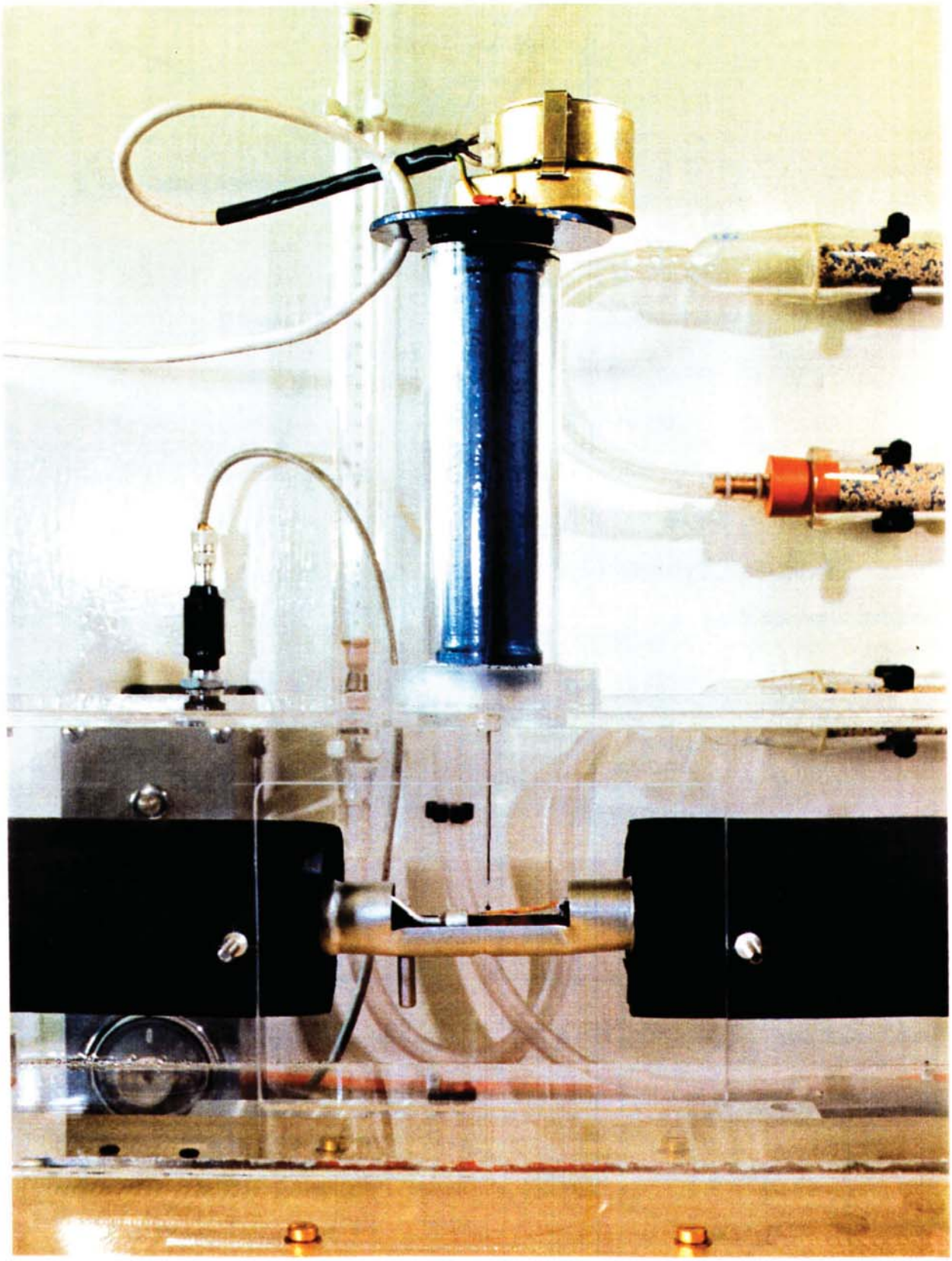

Figure 22. Droplet Suspension / Rotation Device

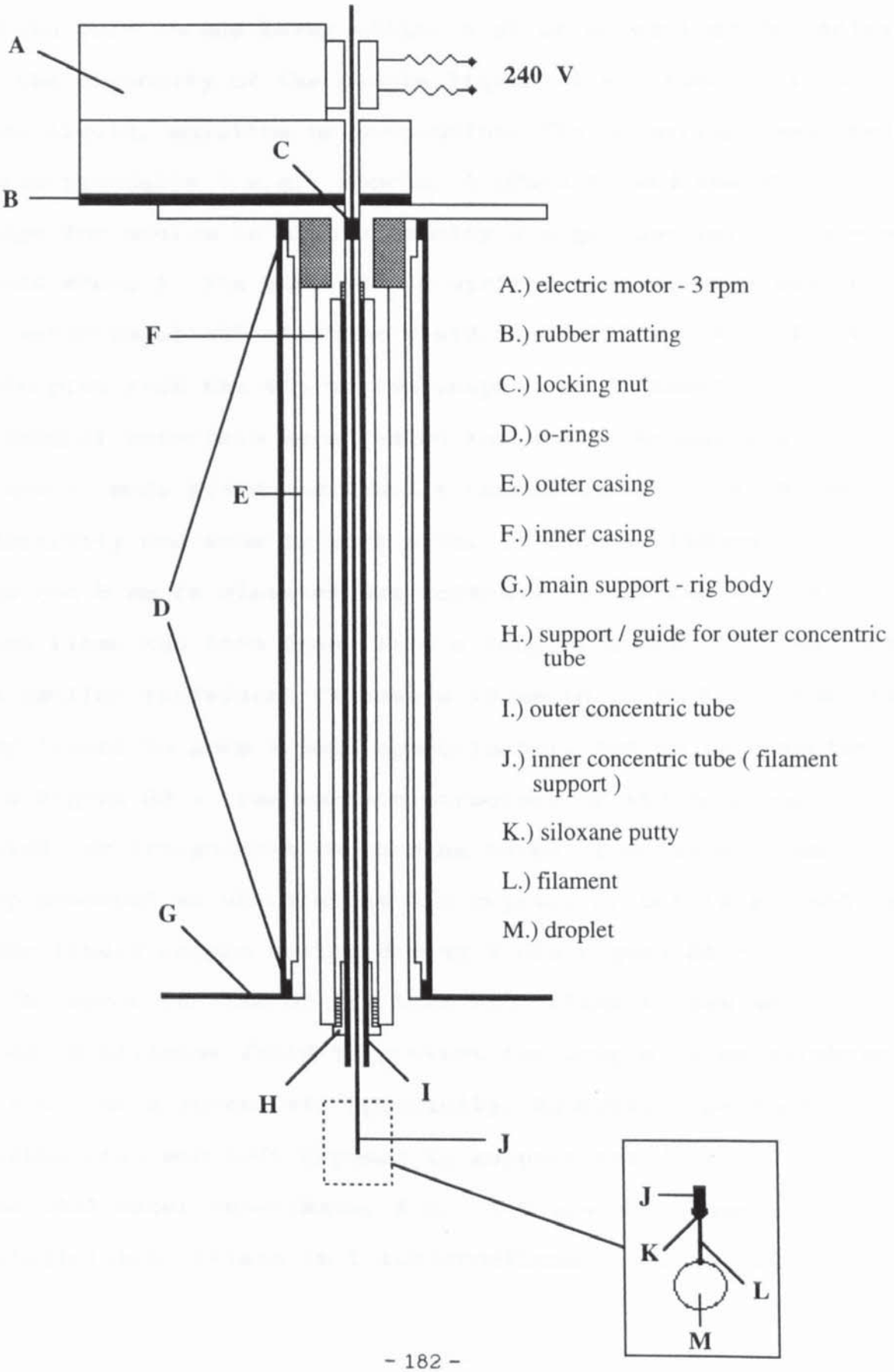

5.3) Droplet Formation and Suspension

Droplets were formed using either a µl or ml syringe depending upon the viscosity of the sample liquid, i.e.; whether it was a pure liquid, solution or suspension. The µl syringe was used for low viscosity (e.g.; approx. 1 mPa/s), and the ml syringe for medium to high viscosity (e.g.; approx. 500 mPa/s to 3000 mPa/s). The tips of the syringe needles were coated in a water-repellent silicone fluid to facilitate transfer of the droplet from the tip to the suspension filament.

Several materials were tested for use as suspension filaments; soda glass was finally chosen for its low thermal conductivity and ease to work with. To form a filament, a glass rod 5 mm in diameter was softened by heating over a Bunsen flame and then drawn into a long filament. This was cut into smaller individual filaments 10 mm to 15 mm long, one end being flamed to form a bead approximately 300 µm in diameter (see Figure 23). The surface structure of the bead was checked for irregularities such as holes, fractures or any sharp protrusions which might aid crystal or bubble nucleation of the liquid sample during drying (see Figure 24).

The upper portion of the bead and filament stem were coated in silicone fluid to prevent the droplet from climbing the stem, thus losing its sphericity. However, a sufficiently wettable area was left exposed to support the droplet. Commercial water repellents, i.e.; 2 % w/w solutions of dimethyldichlorosilane in trichloroethane, were not used

because evaporation of the solvent was found to leave an irregular surface which, like defects in the filament bead surface structure, could act as nucleation sites for bubble or crystal growth.

The unbeaded end of the support filament was inserted into the inner concentric tube of the suspension device using tweezers and held in place by Siloxane putty. This insulated the glass filament from the stainless steel support and allowed easy removal of the filament plus dried particle after drying.

Transfer of a droplet from the tip of the syringe needle to the suspension filament was accomplished by gently stroking the tip on the bead end of the suspension filament. This allowed the droplet to slide-off one and be left clinging to the other (see Figure 25). Depending on the size, the surface of a droplet suspended from a filament intersected the filament bead at approximately the bead equator. For a droplet 1 mm in diameter, the intrusion of the bead constituted approximately 0.4 % of the droplet's total volume. For larger droplets this was considerably less since the increase in weight pulled the droplet further down the bead.

Where possible, depending upon the surface tension of the droplet liquid, the whole of the bead was coated in silicone fluid, although this made suspension difficult. When achieved, a droplet would stand almost proud of the bead making only a small indentation in the surface.

Figure 23. Droplet Suspension Filament

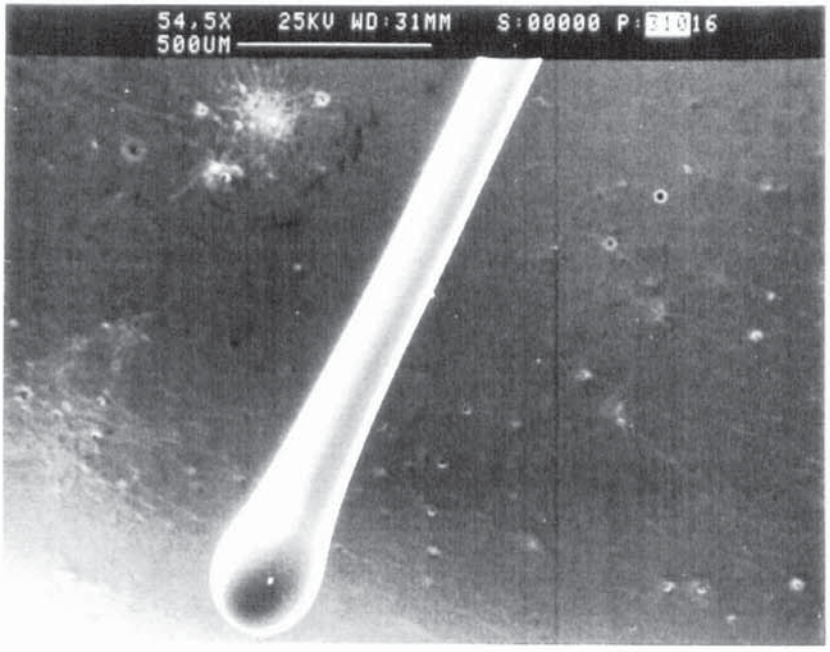

Figure 24. Suspension Filament Showing Surface Defect (Top Left)

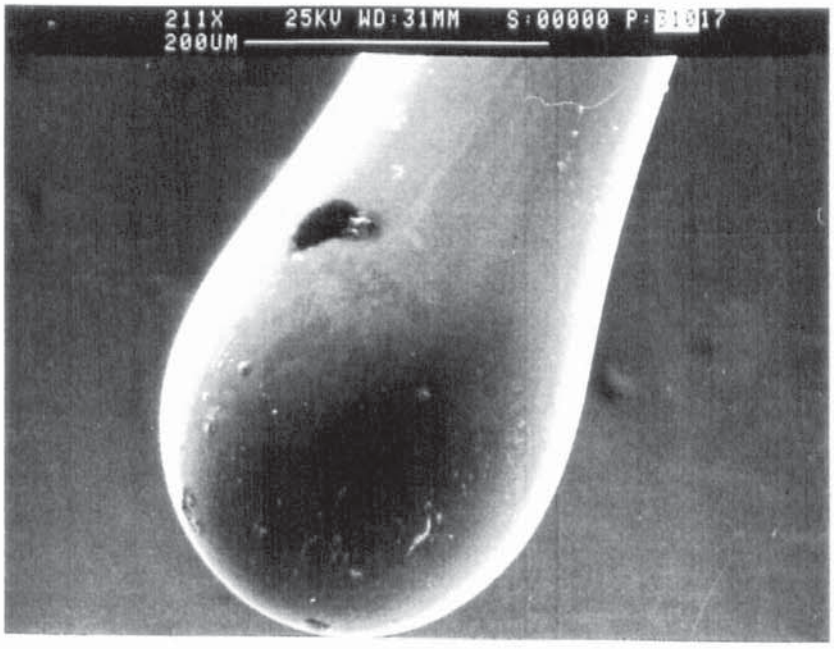

Figure 25. Suspended Droplet

(The filament has been extended for photographic purposes)

The droplet-size most frequently used ranged from 1 mm to 2 mm in diameter, although a size range of 500 μm to 2.5 mm was possible.

5.4) Experimental Procedure - Single Droplet

Before transferring the droplet to the suspension filament the wind tunnel was left in operation for approximately one hour to reach steady state. On transference, the air stream was momentarily diverted to allow placement of the droplet and to minimize evaporation. This took approximately 6 to 7 seconds. When a droplet was in position, the air temperature (dry bulb and approx. wet bulb) were constantly monitored and recorded. On average, droplets took between 3 to 4 minutes to completely dry (see Figure 26) depending on the material being dried, the droplet-size, initial concentration and conditions.

All the experimental runs were observed and recorded using a colour video camera with a macro lens attachment. With the aid of a x 3 magnifying objective lens placed in front of the camera, a total magnification of x 30 was possible. This produced droplet images with diameters ranging from 40 mm to 80 mm when viewed on a 70 cm television screen.

A background scale was place behind the droplet and filmed during all runs. This allowed any distortion of the magnified droplet image to be corrected.

Illumination of the droplet with incident and transmitted light (i.e.; the droplet was in silhouette) allowed detailed

observation of both the surface and internal structure. This provided valuable information concerning the development of particle morphology, the first appearance of crystals within the droplet, and the time taken for crust completion.

Frame by frame advancement of the video tape, in conjunction with the video's integral stopwatch, allowed the determination of the rate of evaporation of pure liquids, the constant-rate period of solutions etc., and assisted in understanding other experimental data.

On completion of the drying experiment, the air stream was momentarily diverted and the sample or particle (unless drying a pure liquid) carefully removed from the suspension device and wind tunnel using tweezers. The particle was then stored in a desiccator until required for examination by optical or / and Scanning Electron Microscopy.

Figure 26. Estimation of Droplet Drying Time for a Procion Dye at Various Concentrations

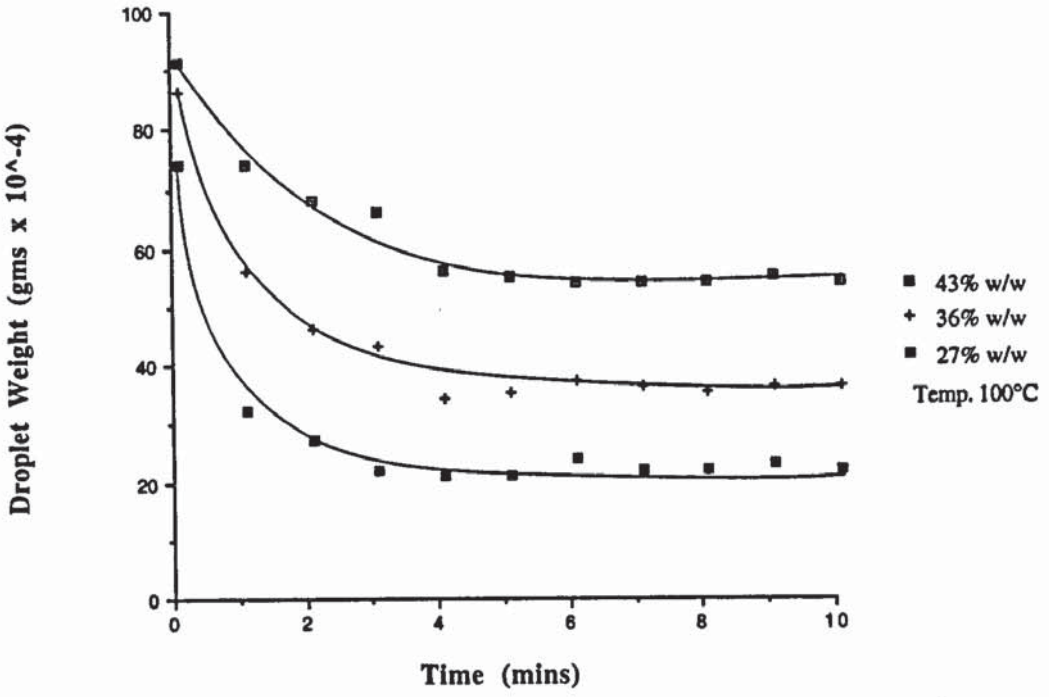

(Data represents an average of 3 plots)

Figure 26 shows the drying curves (weight-loss versus time) of three Procion dyes in aqueous solution dried as 2 mm droplets at 100°C.

To obtain the weight-loss, individual droplets were suspended from a filament attached to the weighing arm of a balance accurate to four decimal places. Temperature controlled air at a velocity of 1.1 m/s was channelled over the droplet and its weight recorded every minute.

Because weight-losses were so small i.e.; in the region of 0.005g to 0.006g, excessive vibration due to droplet movement and the loss of solid material from particle fractures, explosions etc., the results could only be regarded as approximate. The method does however, provide a useful way of estimating droplet drying times and moisture content.

5.5) Examination of Samples by Optical and Scanning Electron Microscopy (S.E.M.) - A Protocol

Both Optical and Scanning Electron Microscopy (SEM) were used to examine sample particles, whether commercially spray-dried or dried from single droplets.

Optical microscopy was used for preliminary examination of the samples prior to examination by SEM, to identify any obvious surface features such as blowholes and shell fractures, or to determine the location of the support filament relative to the crust structure in single droplet drying experiments. For powders, examination by optical microscopy enabled a check to be made that the chosen sample was representative of the bulk product, since only a small amount of powder was required for SEM work.

Electron microscopy was used to examine and photograph the samples in more detail, paying particular attention to the surface and internal structures. Consequently, an examination protocol (191) was adhered to as closely as possible (see Figures 27 and 28).

Because of the relatively small amount of sample required for SEM work, i.e.; between 0.1g and 0.2g, it was difficult to obtain a representative sample from a bulk product due to classification of the particles in the container. This was overcome by initially cone and quartering the sample, care being taken not to physically damage any of the particles, and then placing the remaining fraction into a glass bottle. The

bottle was rotated in a horizontal plane for 30 seconds and then gently turned upright and a sample taken. The representative sample was scattered onto an adhesive SEM examination stub to obtain an even or monolayer covering of particles. Excess sample was blown-off. The retained sample was examined under an optical microscope and compared with a few grams of the bulk product placed in a petrie dish to check that the size distribution was similar. If it was not, another stub was prepared.

In the case of single droplet studies, all the sample material was placed onto a stub. For a powder sample, once a representative sample stub was obtained, a number of the particles were broken open in a restricted area of the stub (making location of the particles easier when inside the SEM) by applying light pressure with a needle.

Safe storage of the stubs / samples, i.e.; protection from moisture, dust and physical damage, was achieved by placing them in a numbered holder inside a desiccator until required for use.

Before examination under the SEM, the stubs were ' sputter ' coated with gold to render the particles conductive (care being taken to retain identities) and loaded into the SEM in such a way as to allow a long working distance for magnifications as low as x 20.

The following examination protocol was then adopted,

1.) Examine the whole stub sample at x 20 magnification. Find a representative area and photograph at x 20.

2.) Identify a smaller representative area with a good size distribution and photograph at x 100.

3.) Find the broken particles. Check for any differences in wall thickness / structure. If none, take a single photograph at x 300. If there are differences, take a sufficient number of photographs at x 300 to show the differences, noting which photographs represent the bulk of particles and which represent the minority.

4.) Examine the outer surface of the particles at x 1000. Take at least two photographs at x 1000 showing,

a.) The surface detail of the skin, plus any differences.

b.) The cross-sectional structure of the wall, plus any differences.

Figure 27. Example of Examination Protocol (191)

Sample - aqueous soluble proprietary dye

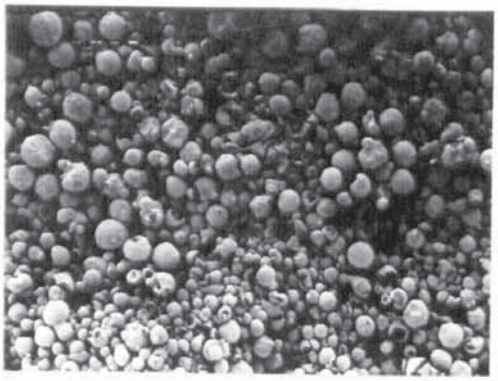

general view (mag. x 20)

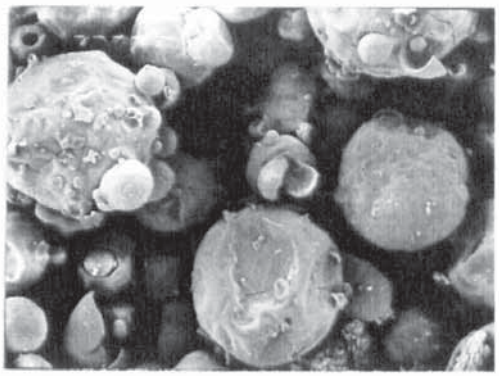

general view (mag. x 100)

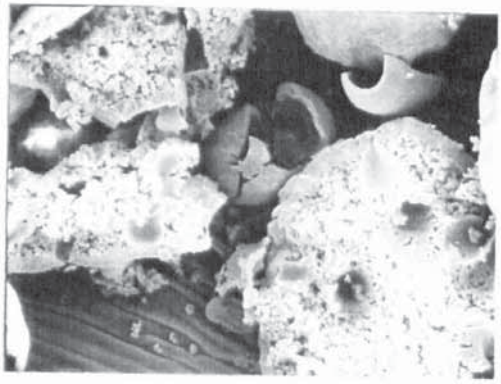

broken grain (mag. x 300)
(interior detail)

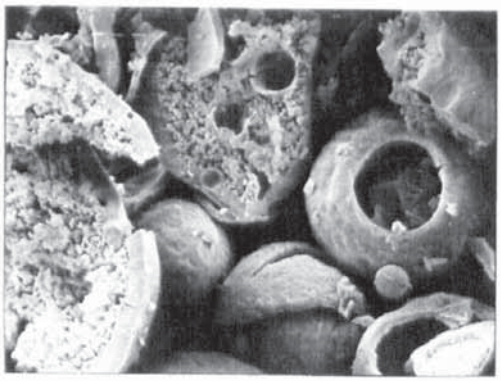

broken grain (mag. x 300)

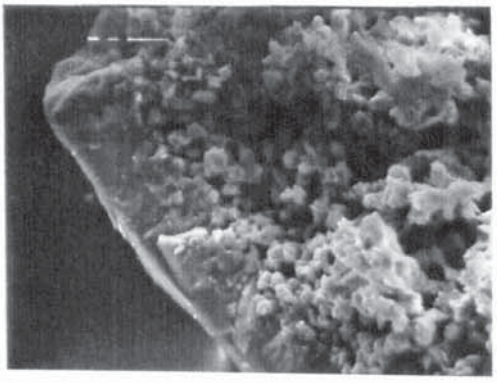

wall plus interior (mag. x 1000)

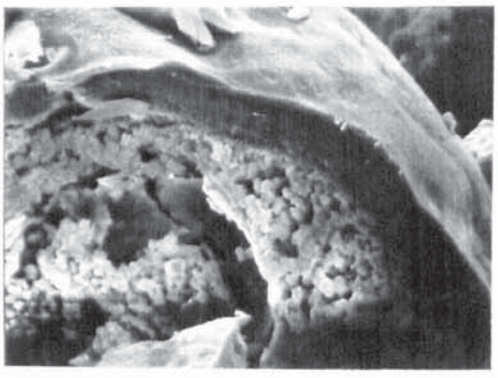

wall detail (mag. x 1000)

Figure 28. Outline of Examination Protocol

OBJECTIVES

To obtain information and representative photographs showing,

1.) The qualitative measure of size distribution.

2.) The overall general shape of the particles, e.g.; regular spheres, distorted spheres - shrivelling,' ballooning '.

3.) Surface features, e.g.; incidence of blowholes, surface deposit s.

4.) Nature of small particles (fines) e.g.; very small spheres, fragmented spheres - large and small.

5.) Internal and wall morphology of medium sized particles, e.g.; hollow or solid, degree of porosity, casehardening, double-skinned.

6.) Wall thickness.

7.) Nature of the outer skin, e.g.; crystalline, amorphous, clean or dusty.

PROCEDURE

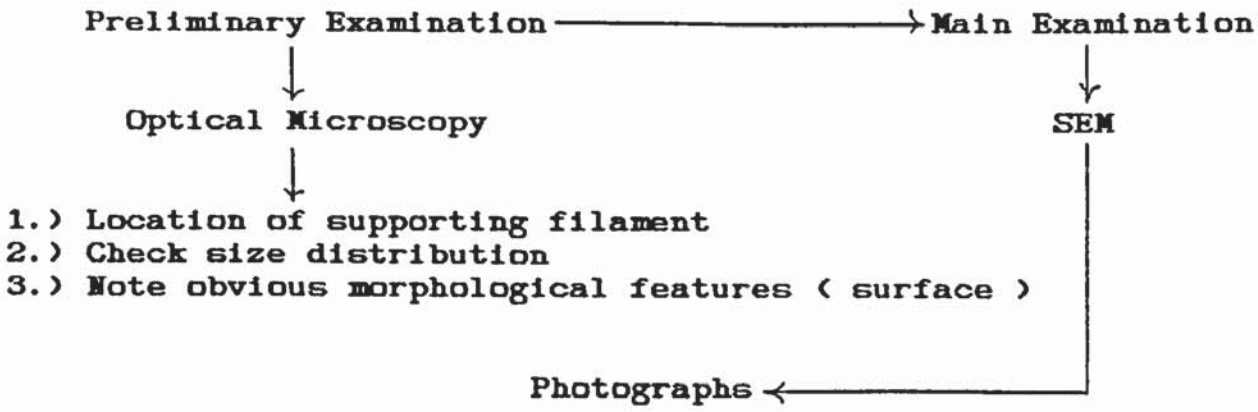

1.) Representative view - x 20, Qualitative particle-size distribution
2.) Representative view - x 100, Qualitative particle-size distribution
3.) Fragmented particles - x 300, Morphology of particles
4.) Wall surface, cross-section - x 1000, Morphology of skin, walls

5.6) Qualitative and Semi-Quantitative Examination of Spray-Dried Materials

Technical details concerning qualitative observations and semi-quantitative measurements, i.e.; bulk density, particle-size and flowability, are reported in Chapter 6.

5.7) Grade of Materials Used

Unless otherwise stated, all the chemicals used, i.e.; both inorganic and organic, were of analytical grade, and obtained from the following suppliers,

BDH (Merck Ltd) - AnalaR ●	Fisons Scientific Equipment - A.R.●
Hunter Boulevard	Bishop Meadow Road
Magna Park	Loughborough
Lutterworth	Leicestershire LE11 ORG
Leicestershire LE17 4XN	England (UK)
England (UK)	

All aqueous solutions were prepared using distilled water. Similarly, the measurement of gas-film heat and mass transfer coefficients for water were carried out using distilled water.

The proprietary materials were of commercial grade. Details are given below.

Semi - instant skimmed milk - ' Quickmix Dried Skimmed Milk '

Gateway Foodmarkets Ltd.,

PO Box 197, Bristol.

Stated Ingredients

Dried Skimmed Milk, Vitamins A and D.
Protein = 36.2 % w/w
Carbohydrate = 52.5 % w/w
Fat = 1.5 % w/w

Detergent (anionic) - ' Ariel Automatic '

Procter and Gamble Ltd., PO Box 1EL,

Newcastle upon Tyne, NE99 1EL.

Stated Ingredients

Polycarboxylate	= < 5 % w/w
Phosphonate	= < 5 % w/w
Anionic Surfactants	= 5 % - 15 % w/w
Nonionic Surfactant	= 5 % - 15 % w/w
Oxygen based bleaching agent	= 5 % - 15 % w/w
Phosphate	= 15 % - 30 % w/w

(Enzyme, Brightening Agent)

Colloidal carbon - ' Black Indian Drawing Ink '

George Rowney and Company Ltd.,

Bracknell, Berkshire.

Co-dried egg and skimmed milk - Sample No. 24 reconstituted †.

† see Table 7

CHAPTER SIX

EXPERIMENTAL RESULTS

QUALITATIVE AND SEMI-QUANTITATIVE EXAMINATION OF COMMERCIALLY SPRAY-DRIED SAMPLES

6.0) Introduction

A range of commercially spray-dried materials, thirtynine in all, were obtained from various manufacturers with details of drying conditions and feed specifications (see Table 7). They covered inorganic materials, e.g.; aluminium silicate, tungsten carbide, lead chromate, organic materials, e.g.; glucose, dichloropropanoic acid, gum acacia, and a number of proprietary materials, e.g.; detergent, semi-instant skimmed milk and yogurt powder. All samples were obtained directly from the manufacturer's spray drier without any further processing, e.g.; grinding and / or re-agglomeration.

The samples were subjected to qualitative and semi-quantitative examination to identify structural and morphological features. The results have been interpreted in terms of bulk physical properties, and where possible, related to drying conditions.

Table 7. Drying Specifications of Commercially Spray-Dried Samples

Sam.No.	Material	Feed Conc. (w/w)	Air Temperature In	Air Temperature Out	Drying Details
1	Aluminium hydroxide	30 % to 50 %	350°C	90°C	Co-current rotary atomization, dried in a small capacity drier.
2	Aluminium silicate	30 % to 50 %	350°C	90°C	Mixed flow nozzle atomization.
3	Dyestuffs	30 % to 40 %	350°C	110°C	Co-current nozzle atomization, dried in a tall-form drier (18 m high).
4	Tungsten carbide	60 %	200°C	80°C	Mixed flow nozzle atomization, dried with binders using a non-aqueous solvent, e.g.; ethanol, hexane.
5	Aluminium oxide	60 %	350°C	115°C	Mixed flow nozzle atomization.
6	Titanium dioxide (Niro)	40 % to 50 %	550°C	200°C	Co-current rotary atomization, dried in a conical based drying chamber.
7	Ferrite	40 %	350°C	120°C	Mixed flow nozzle atomization, dried with binders and lubricant.
8	Kaolin	60 %	550°C	120°C	Co-current rotary atomization,dried in a conical based drying chamber.
9	Barium titanate	50 %	350°C	120°C	Mixed flow nozzle atomization, dried with binders in a small capacity drier.

10	tri - sodium ortho-phosphate	--	400°C	100°C	Co-current rotary atomization, dried in a conical based drying chamber.
11	Copper oxychloride	--	400°C	100°C	Co-current rotary atomization, dried in a conical based drying chamber.
12	Lead chromate	--	350°C	100°C	Co-current rotary atomization, dried with binders in a small capacity drier with a conical based drying chamber.
13	2,3 - dichloro-propanoic acid	--	200°C	< 50°C	Co-current rotary atomization, dried in a small capacity drier with a conical base.
14	Copper ore	--	550°C	100°C	Co-current rotary atomization, dried in a conical based drying chamber.
15	Coffee	30 % to 50 %	230°C	115°C	Co-current nozzle atomization, dried in a tall-form spray drier.
16	Magnesium hydroxide	----------			Co-current rotary atomization, dried in a conical based drying chamber.
17	Dextran	40 %	250°C	100°C	Co-current nozzle atomization, dried in a tall-form spray drier.
18	Clay (tile material)	--	550°C	100°C	Mixed flow nozzle atomization.
19	Clay (tile material)	--	550°C	90°C	Co-current rotary atomization, dried in a conical based drying chamber.
20	Glucose	--	--	--	Co-current rotary atomization, dried in a conical based drying chamber.

21	Detergent	--	300°C	70°C	Co-current nozzle atomization, dried in a 7.3 m diameter spray tower. Slurry sprayed through a 4.4 mm hollow-cone swirl nozzle at 80 bar.
22	Semi - instant skimmed milk	----------			
23	Yogurt powder	----------			
24	Co - dried egg and skimmed milk	----------			
25	Titanium dioxide (Drytec - A)	----------			
26	Polymer (Drytec - A)	----------			
27	Instant drink powder	----------			
28	Encapsulated flavour	----------			
29	Polymer (sodium salt)	----------			Two - fluid nozzle atomization.
30	Organic U.V. brightner	----------			
31	Soluble titanium salt	----------			Two - fluid nozzle atomization.

32	Soluble titanium salt	Pressure nozzle atomization.
33	Soluble titanium salt	Rotary atomization.
34	Polymer (Drytec - B)	
35	Calcium stearate	
36	Titanium dioxide (Drytec - B)	
37	Gum acacia	
38	Skimmed milk (high density powder)	
39	Skimmed milk analogue	

Samples **1** to **20**. Obtained from **Niro Atomizer Ltd**. 30 Clarendon Rd., Watford, Herts., WD1 1JJ.

Sample **21**. Confidentiality requested on manufacturer's identity and feed specifications.

Samples **22** to **24, 38** and **39**. Obtained from **Dairy Crest Foods**. Development Centre, Crudgington, Telford, Shropshire, TF6 6HY.

Confidentiality requested on details of drying conditions and feed specifications.

Samples **25** to **37**. Obtained from **Drytec Ltd**. Morley Road, Tonbridge, Kent, TN9 1RA.

Confidentiality requested on sample details, drying conditions and feed specifications.

6.1) General Remarks

The majority of the samples had been dried from initial feed concentrations ranging from 30 % to 60 % solids; therefore most would have been of slurry or a slurry type consistency. This range of concentration is typical for most industrial spray-dried materials, although lower and certainly higher concentrations are used. For example, detergent slurries can have a solids content of up to 70 %. In most cases manufacturers tend to use the highest possible feed concentration for thermal economy, although as discussed later it may also offer the advantage of improved ' volatiles-retention '. The pumpability of the feed and the ability to atomize it effectively are the main limiting factors.

Drier inlet and outlet temperatures varied from 200°C to 550°C, and from 50°C to 120°C, respectively. With the exception of tungsten carbide which had been suspended in an organic medium rather than an aqueous one, in order to carry a binder, the inorganic materials had been dried at a much higher inlet temperature than either the organic or proprietary materials. This was practicable because they are thermally more stable. As with increased feed concentration, the greater the inlet drying temperature the greater the thermal efficiency of the drying process, i.e.; the evaporative capacity of the drier increases with increasing inlet temperature. However this must be balanced against the

thermal stability of the product; the effect of inlet temperature on bulk density must also be taken into account.

Outlet temperatures do not generally vary to any great extent, mainly because the moisture content of the product has to be carefully-controlled. Powder packing, powder flowability, bulk density and particle agglomeration are all affected by moisture content.

Atomization and drier details are incomplete due to commercial confidentiallity, although from the details given both co-current and mixed flow drier designs (tall form and conical based) had been used with either nozzle or rotary atomization. Mixed flow driers provide higher drying rates and longer particle trajectories than the equivalent co-current drier.

Binders and lubricants were used in a number of samples, i.e.; tungsten carbide, ferrite, barium titanate and lead chromate. Binders are usually used where particle attrition or friability is a problem, to prevent particle inflation which increases bulk density, to control the rate of dissolution, or to simply bind the constituents of a multicomponent particle together, e.g.; sodium silicate is added (6-12 %) to most detergent formulations for just that purpose although it also has anti-corrosion properties, i.e.; it protects the aluminium components of the washing machine (202-204). Although not stated in Table 7, binders are almost certainly used with materials such as aluminium oxide, aluminium hydroxide and aluminium silicate (cf. page 264).

In the past, hydrocarbon waxes have been extensively used as binders and lubricants but these have been gradually replaced by more effective materials such as polyvinyl alcohol (PVA) and polyethylene glycol (PEG) which tend to produce greater particle strength and thus improve handling and machining properties. Alternatively, if a ' softer ' particle is required, binders such as hydroxyethylcellulose, methyl cellulose and mono or polycarboxylic acid derivatives, e.g.; carboxymethylcellulose are used. Binders are discussed further on page 264.

Commercial spray drying details for some of the samples listed in Table 7 are discussed in length by Masters (192), extracts of which are given in Table 8.

Table 8. Drying Specifications of Commercially Spray-Dried Materials (192)

Sample	Feed Solids (%)	Feed Temp. (°C)	Powder Moisture (%)	Drying Temp. Inlet (°C)	Drying Temp. Outlet (°C)	Drier Details
Dyestuffs	20-45	10-40	1.0-6.0	120-450	60-140	PN/R,A/B
Tungsten carbide	70-75	20-25	0.1-0.3	160-180	90-95	PN/R,A/B
Aluminium oxide	45-65	10-20	0.25-2.0	300-500	95-140	PNB,RA
Titanium dioxide	30-55	20-50	0.3-1.0	350-750	110-135	PN/R,A/B
Ferrite	55-70	10-40	0.1-1.0	300-350	110-125	PN/R,A/B
Kaolin	50-65	15-40	1.0-3.0	400-600	95-120	PN/R,A/B
Barium titanate	40-60	10-20	0.3-0.5	250-350	110-125	PNB
Copper oxychloride	35-50	10-20	1.0-1.5	275-400	95-110	PN/R,A/B
Lead chromate	45-50	15-25	0.5-1.0	200-500	100-150	PN/R,A/B
Herbicides †	45-50	10-15	2.0-4.0	140-250	75-110	PN/R,A/B
Coffee (instant)	35-55	20-30	3.0-4.5	220-300	85-100	PNA
Magnesium hydroxide	30-35	5-10	1.0-1.5	300-400	90-110	RA
Tile clay	55-70	15-20	5.0-7.0	450-550	90-100	PN/R,A/B
Detergent	60-70	60-65	6.0-10	300-350	85-110	PNB/C
Skimmed milk	47-52	60-70	3.5-4.0	175-240	75-95	PN/R,A/B
Egg (whole)	20-24	5-10	3.0-4.0	180-200	80-85	PN/R,A
Optical whitener	15-50	20-50	2.5-5.0	150-350	60-85	PN/R,A/B

† 2,3 - dichloropropanoic acid

C Counter-current
PN Pressure nozzle atomization
R Rotary atomization
A Co-current
B Mixed flow

6.2) Powder Characterization

i.) Measurement of Bulk Density

The bulk densities of all thirtynine samples were measured using a method based on British Standard 2955 - Section 508. The results are presented in Table 9 and the raw data in Appendix A 1.0

A cylindrical glass cell of accurately known internal volume, i.e.; 3.1219 cm^3 - approximately 1 cm I.D. x 4 cm, and mass, 2.5853 g, was filled with a representative sample of powder by freely pouring the sample into the cell until it overflowed. The sides were then gently tapped fifteen times to settle the powder down. It was then topped-up with fresh material and tapped a further five times to acheive a consistent packing density. Excess powder was leveled-off from the top of the cell and removed from the external surfaces using a small brush. The cell plus sample were then weighed on a four place decimal balance and the bulk density in g/cm^3, calculated. The procedure was repeated three times per sample for reproducibility and the average bulk density calculated.

Table 9. Bulk Density of Commercially Spray-Dried Samples

Sample	g/cm³	Sample	g/cm³
Aluminium hydroxide	0.276	Detergent	0.524
Aluminium silicate	0.389	Semi-instant skimmed milk	0.548
Dyestuffs	0.461	Yogurt powder	0.584
Tungsten carbide	3.674	Co-dried egg and skimmed milk	0.548
Aluminium oxide	1.153	Titanium dioxide (Drytec - A)	0.452
Titanium dioxide (Niro)	0.634	Polymer (Drytec - A)	0.333
Ferrite	1.422	Instant drink powder	0.281
Kaolin	0.811	Encapsulated flavour	0.397
Barium titanate	1.530	Polymer (sodium salt)	0.458
tri - sodium orthophosphate	0.349	Organic uv brightner	0.274
Copper oxychloride	0.838	Soluble titanium salt (two-fluid nozzle)	0.657
Lead chromate	0.787	Soluble titanium salt (pressure nozzle)	0.558
2,3 - dichloro - propanoic acid	0.341	Soluble titanium salt (rotary)	0.510
Copper ore	1.381	Polymer (Drytec - B)	0.433
Coffee	0.147	Calcium stearate	0.455
Magnesium hydroxide	0.613	Titanium dioxide (Drytec - B)	0.614
Dextran	0.258	Gum acacia	0.391
Clay (Nozzle)	1.021	Skimmed milk (high density powder)	0.633
Clay (Rotary)	1.005		
Glucose	0.451		
Skimmed milk analogue	0.488		

ii.) Estimation of Particle-Size

Because of the high degree of agglomeration in many of the sample powders, particle-sizing methods, such as sieving and laser diffraction, could not be used to determine the particle-size and particle-size distribution of the sample powders. Therefore, direct observation of particle diameters were made using optical microscopy in accordance with British Standard 3406, Pt. 4.

A representative sample of powder, approx. 0.1 g, was placed on a microscope slide and dispersed evenly over the surface by gently tapping the slide to form a monolayer of particles. The density of the field was noted and approximately reproduced for every sample. The slide was then placed under a Zetopan optical microscope (Reichert No. 354033) and illuminated using both transmitted and incident light. By the introduction of different colours, using filters, for the transmitted and incident-light beams the surface and the outline of the particles were both rendered clearly visible at the same time.

The smallest, largest and mean whole particle diameters were recorded at magnifications of x 10, 15, 56 or 84, depending on the particle-size, by comparing values obtained from an internal micrometer graticule with those of a calibrated external graticule, i.e.; 1 mm divided into 10 μm divisions.

The results are presented in Table 10.

Table 10. Particle-Size Range of Commercially Spray-Dried Samples

Sample	Particle Diameter (μm)		
	Smallest	Largest	Mean Value
Aluminium hydroxide	10	270	40
Aluminium silicate	20	430	90
Dyestuffs	50	390	155
Tungsten carbide	7	215	70
Aluminium oxide	8	145	60
Titanium dioxide (Miro)	2	60	30
Ferrite	10	160	85
Kaolin	15	380	175
Barium titanate	35	280	90
tri - sodium orthophosphate	25	500	310
Copper oxychloride	5	90	45
Lead chromate	5	110	40
2,3 - dichloro - propanoic acid	2	140	18
Copper ore	10	120	50
Coffee	20	400	100
Magnesium hydroxide	11	280	50
Dextran	3	75	25
Clay (nozzle)	7	320	120
Clay (rotary)	65	560	300

Sample	Particle Diameter (μm)		
	Smallest	Largest	Mean Value
Glucose	30	360	150
Detergent	30	800	210
S. instant skimmed milk	6	90	40
Yogurt powder	10	135	20
Co-dried egg and skimmed milk	6	280	20
Titanium dioxide (Drytec - A)	5	90	60
Polymer (Drytec - A)	8	250	100
Instant drink powder	5	320	70
Encapsulated flavour	3	120	60
Polymer (sodium salt)	6	280	80
Organic u.v. brightner	45	300	150
Soluble titanium salt (two-fluid nozzle)	4	330	15
Soluble titanium salt (pressure nozzle)	3	90	30
Soluble titanium salt (rotary)	1	140	75
Polymer (Drytec - B)	1	250	45
Calcium stearate	<2	180	17
Titanium dioxide (Drytec - B)	<1	180	40
Gum acacia	5	300	100
Skimmed milk (high density powder)	6	150	40
Skimmed milk analogue	8	110	45

iii.) Measurement of Powder Flowability

The powder flowability, as defined in British Standard 2955 - Section 516, of all thirtynine samples was measured using the method outlined below and the apparatus shown in Figures 29 and 30. The results are presented in Tables 11 to 13, and the raw data in Appendix A 2.0 - A 2.2

The powder inclinometer was filled with a representative sample of powder by rotating the cylindrical glass sample cell to the vertical position and freely pouring the powder into it up to the fillermark (see Figure 30). This gave a sample volume of approximately 1.1 cm^3. The cell was then rotated in a clockwise direction to the horizontal position, i.e.; 0° on scale as indicated by the pointer, and gently tapped until the powder / air interface reached position A on the side of the sample cell. This ensured a consistent packing density.

To measure the angle of repose, the sample cell was rotated clockwise from 0° to 90° on the scale in 1° increments. At each increment the powder was left to settle for a period of 5 seconds or until any displacement of the sample had ceased before increasing the angle of repose. The weight of sample displaced and the angle of displacement were recorded.

The procedure was repeated three times per sample for reproducibility. The results are expressed in terms of cumulative percentage displaced (by weight) versus the angle of repose.

Flowability measurements were carried out at a relative humidity of 62 % and a temperature of 22.3°C, i.e.; ambient temperature and humidity. The powders were left twentyfour hours to equilibrilate at this relative humidity before any measurements were made.

Further measurements were carried out at relative humidities of 15 % and 100 % (to alter the powder moisture content) for a select number of samples by storing them in desiccators filled with silica gel and water respectively. The samples were left for one week to equilibrilate before measurements were made of flowability.

Figure 29. Powder Inclinometer

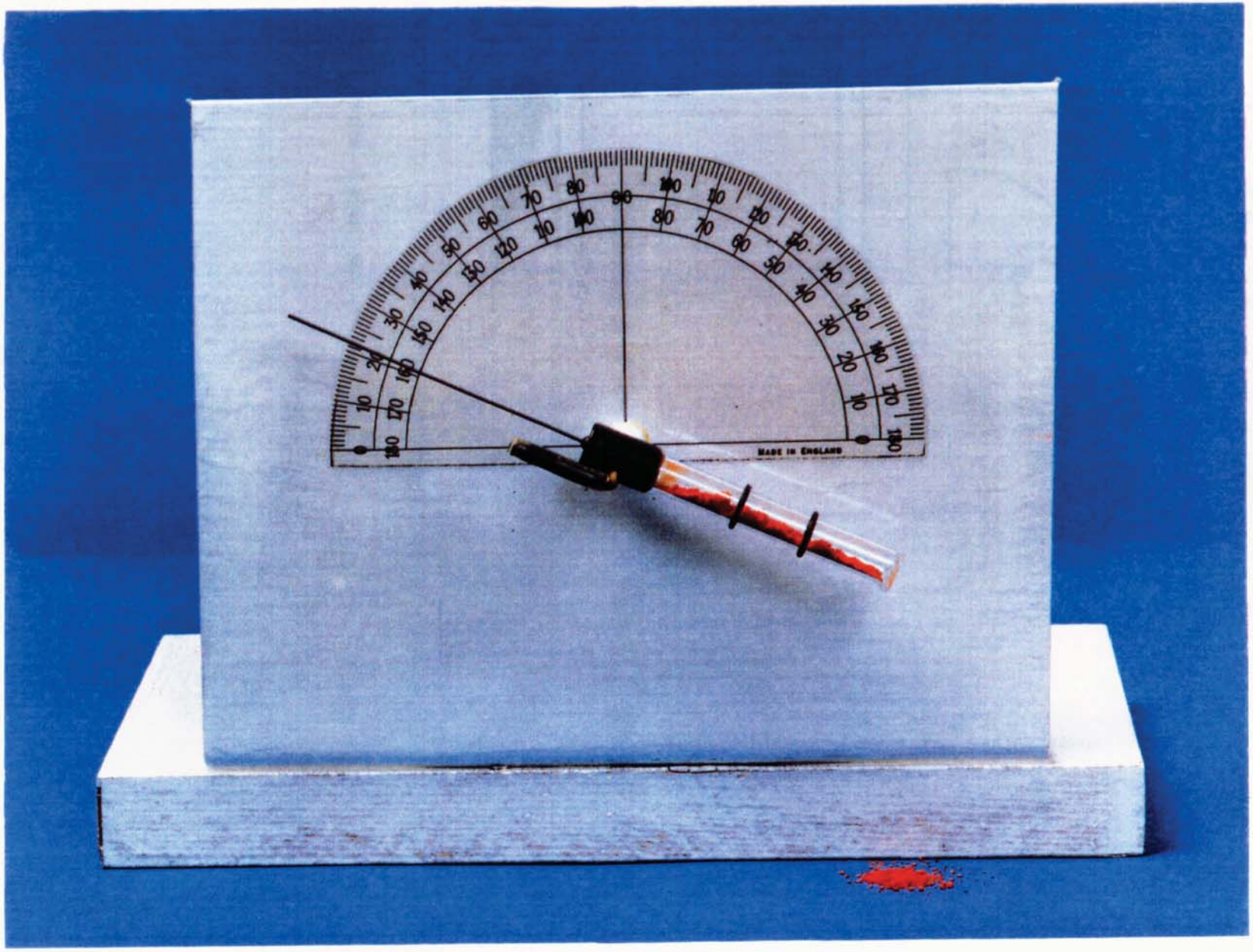

Figure 30. Powder Inclinometer
(Sample Cell Details)

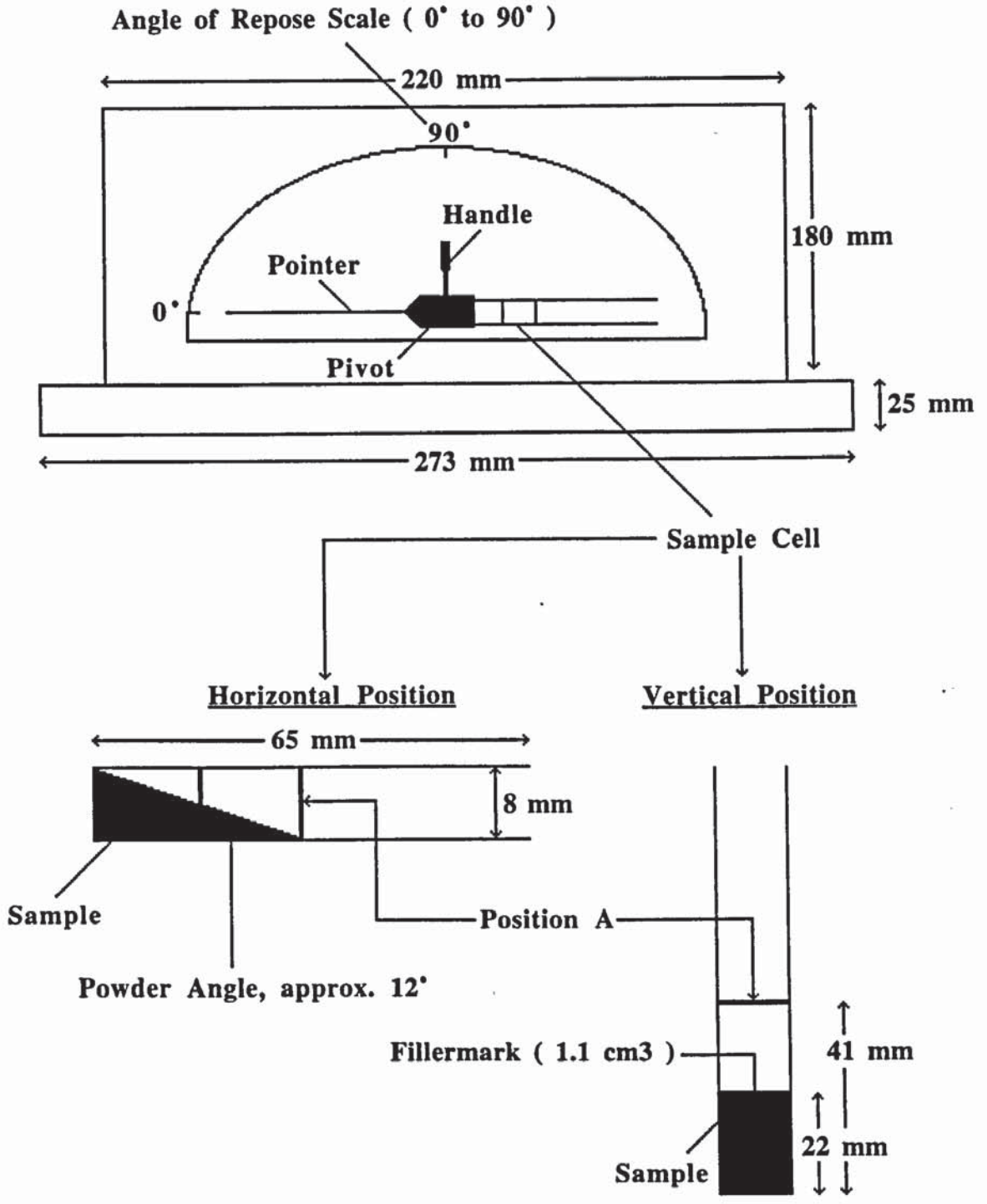

Table 11. Powder Flowability of Commercially Spray-Dried Samples at 62 % Relative Humidity (22.3°C) †

Sample	Angle of Repose	% Weight Displaced	Angle of Repose	% Weight Displaced	Angle of Repose	% Weight Displaced
Aluminium hydroxide	52°	22	49°	15	55°	11
Aluminium silicate	17°	2	18°	2	20°	2
	22°	9	21°	14	24°	92
	25°	100	26°	100	29°	100
Dyestuffs	27°	94	24°	5	25°	3
	35°	100	34°	100	32°	100
Tungsten carbide	22°	2	23°	3	21°	2
	30°	100	30°	9	23°	5
	-	-	35°	100	25°	10
	-	-	-	-	28°	100
Aluminium oxide	30°	98	30°	100	24°	1
	42°	100	-	-	28°	91
	-	-	-	-	29°	95
	-	-	-	-	36°	100
Titanium dioxide	36°	1	44°	8	44°	16
(Miro)	47°	7	51°	9	53°	17
	-	-	58°	35	-	-
Ferrite	41°	15	47°	99	34°	33
	51°	100	75°	100	43°	100
Kaolin	41°	100	35°	5	37°	10
	-	-	45°	100	41°	100
Barium titanate	21°	1	24°	1	24°	12
	26°	75	34°	100	28°	100
	30°	100	-	-	-	-
Tri - sodium orthophosphate	50°	100	48°	100	55°	100
Copper oxychloride	47°	25	46°	23	46°	29
	49°	100	63°	100	47°	43
	-	-	-	-	60°	100
Skimmed milk analogue	58°	67	65°	30	58°	26

† Cumulative Percentage Weight Displaced

Sample	Angle of Repose	% Weight Displaced	Angle of Repose	% Weight Displaced	Angle of Repose	% Weight Displaced
Lead chromate	28°	87	41°	100	26°	90
	40°	100	–	–	29°	96
	–	–	–	–	60°	100
2,3 - dichloro - propanoic acid	79°	33	87°	38	40°	<1
	–	–	–	–	83°	43
Copper ore	40°	16	41°	99	35°	54
	68°	100	62°	100	36°	90
	–	–	–	–	65°	100
Coffee	47°	29	45°	43	58°	37
	57°	53	–	–	–	–
Magnesium hydroxide	32°	36	32°	48	30°	97
	37°	100	36°	97	33°	99
	–	–	47°	100	45°	100
Dextran	49°	9	42°	1	40°	32
	87°	13	54°	7	88°	35
Clay (nozzle)	34°	2	38°	31	49°	100
	42°	90	40°	100	–	–
	50°	100	–	–	–	–
Clay (rotary)	22°	2	26°	100	22°	2
	27°	100	–	–	26°	96
	–	–	–	–	30°	97
	–	–	–	–	32°	100
Glucose	47°	32	40°	5	51°	46
	–	–	66°	21	–	–
Detergent	35°	100	36°	100	40°	100
Semi - instant skimmed milk	40°	8	39°	6	46°	29
	49°	71	50°	67	53°	39
	–	–	–	–	59°	47
	–	–	–	–	61°	100
Yogurt powder	89°	100	85°	100	65°	35
Co - dried egg and skimmed milk	57°	2	64°	100	56°	3
	71°	100	–	–	82°	100
Polymer (Drytec - A)	90°	15	83°	15	73°	84

Sample	Angle of Repose	% Weight Displaced	Angle of Repose	% Weight Displaced	Angle of Repose	% Weight Displaced
Titanium dioxide	39°	6	38°	3	33°	7
(Drytec - A)	65°	60	56°	38	55°	19
	87°	97	65°	49	59°	62
	-	-	77°	60	72°	74
	-	-	88°	74	84°	100
Instant drink powder	37°	<1	60°	<1	64°	26°
	69°	31	70°	18	-	-
Encapsulated flavour	62°	25	55°	30	49°	28
	-	-	-	-	85°	29
Polymer	55°	30	61°	32	35°	1
(sodium salt)	-	-	-	-	40°	3
	-	-	-	-	55°	7
	-	-	-	-	85°	17
Organic u.v. brightner	56°	2	36°	<1	85°	8
	81°	6	43°	3	-	-
	-	-	51°	5	-	-
	-	-	73°	13	-	-
Sol. titanium salt	52°	9	53°	37	56°	31
(two-fluid nozzle)	81°	22	-	-	-	-
Sol. titanium salt (pressure nozzle)	62°	28	61°	33	66°	27
Titanium salt (rotary)	46°	25	70°	34	56°	27
Polymer (Drytec - B)	50°	23	56°	9	58°	24
	70°	97	64°	42	-	-
	-	-	88°	44	-	-
Calcium stearate	70°	37	77°	32	50°	4
	-	-	-	-	69°	18
Titanium dioxide	51°	13	56°	14	45°	24
(Drytec - B)	-	-	78°	16	67°	94
	-	-	-	-	81°	97
Gum acacia	66°	28	67°	33	76°	27
Skimmed milk	61°	43	57°	35	47°	5
(high density	-	-	-	-	66°	24
powder)	-	-	-	-	90°	74

Table 12. Powder Flowability of Commercially Spray-Dried Samples at 15 % Relative Humidity (22.7°C)

Sample	Angle of Repose	% Weight Displaced	Angle of Repose	% Weight Displaced	Angle of Repose	% Weight Displaced
Aluminium silicate	23°	16	22°	3	21°	4
	25°	73	24°	84	25°	84
	32°	100	29°	100	29°	100
Titanium dioxide	41°	14	43°	11	40°	10
(Miro)	49°	76	46°	46	44°	19
	65°	100	55°	100	49°	54
	-	-	-	-	59°	100
Gum acacia	35°	27	60°	38	88°	42
	71°	65	-	-	-	-

Table 13. Powder Flowability of Commercially Spray-Dried Samples at 100 % Relative Humidity (21.4°C)

Sample	Angle of Repose	% Weight Displaced	Angle of Repose	% Weight Displaced	Angle of Repose	% Weight Displaced
Aluminium silicate	23°	100	22°	2	22°	1
	-	-	27°	100	29°	100
Titanium dioxide	34°	50	31°	14	30°	12
(Miro)	49°	100	40°	54	34°	31
	-	-	48°	55	37°	42
	-	-	55°	59	41°	52
	-	-	61°	66	45°	100
	-	-	81°	100	-	-
Gum acacia	45°	11	41°	39	46°	16

iv.) Estimation of Particle Friability

The particle friability of all samples was estimated.

Powder samples were prepared for microscopic examination as described in Section 6.2 ii.

A glass coverslip 22 mm x 22 mm x 0.12 mm was placed on top of a dispersed monolayer of powder particles and a light downward pressure applied evenly over the surface. The slip was carefully removed and the crushed particles examined under an optical microscope at various magnifications.

Particle strength was estimated by applying light pressure to individual particles using a spring steel wire 0.5 mm in diameter and 120 mm long. The particle's relative resistance to compression was estimated.

From the results presented in Table 14 it was possible to place each sample into one of the following four categories,

Friability - F1 to F4

F1 - The particle is soft, i.e.; no resistance to deformation. At yield point, the particle readily crumbles to form a large number of small fragments.

F2 - The particle is soft, i.e.; a slight resistance to deformation, exhibiting plastic behaviour during deformation. The surface or shell is torn with no fragmentation of the particle structure.

F3 - The particle is hard, i.e.; there is a resistance to deformation. At yield point, the particle crumbles into a small number of large fragments.

F4 - The particle is hard and brittle, i.e.; there is a resistance to deformation. At yield point, the particle shatters into a large number of jagged fragments.

Figures 31 to 34 show typical examples of F1 to F4 particles.

Figure 31 shows a crushed particle of barium titanate which had a friability of F1. The particles offered little or no resistance to compression and readily collapsed under pressure to produce a large number of small fragments or dust. Generally, none of the original particle structure remained intact.

Figure 32 shows a crushed or squashed particle of dextran which had a friability of F2. The particles offered some resistance to compression whilst undergoing plastic deformation. During this deformation, the particle surface structure ripped or tore, which, under further compression, could propagate into the centre of the particle. Generally, there was no fragmentation of the particle, consequently, little or no dust was formed and the overall structure remained intact.

Figure 33 shows a crushed particle of clay (rotary) which had a friability of F3. The particles were hard and had a definite resistance to compression. Upon collapse, the

particles fractured into a small number of large fragments with a minimal amount of dust being formed. Although not intact, the general outline of the particles remained recognizable.

Figure 34 shows a crushed particle of coffee which had a friability of F4. The particles were similar to the F3 category in terms of hardness and resistance to compression up to the point of collapse, where, upon fracture, the particles shattered into a large number of jagged sharp fragments. These varied in size from half to quarter spheres down to fragments less than 15 μm long. None of the particles remained intact.

Table 14. Particle Friability of Spray-Dried Samples

Sample	Friability	Sample	Friability
Aluminium hydroxide	F1	Detergent	F3
Aluminium silicate	F3	Semi-instant skimmed milk	F4
Dyestuffs	F4	Yogurt powder	F4
Tungsten carbide	F1	Co-dried egg and skimmed milk	F4
Aluminium oxide	F1	Titanium dioxide (Drytec - A)	F1
Titanium dioxide (Miro)	F1	Polymer (Drytec - A)	F2
Ferrite	F1	Instant drink powder	F2
Kaolin	F1	Encapsulated flavour	F4
Barium titanate	F1	Polymer (sodium salt)	F2
tri - sodium orthophosphate	F3	Organic uv brightner	F1
Copper oxychloride	F1	Soluble titanium salt (two-fluid nozzle)	F4
Lead chromate	F1	Soluble titanium salt (pressure nozzle)	F4
2,3 - dichloro - propanoic acid	F4	Soluble titanium salt (rotary)	F4
Copper ore	F3	Polymer (Drytec - B)	F4
Coffee	F4	Calcium stearate	F2
Magnesium hydroxide	F1	Titanium dioxide (Drytec - B)	F1
Dextran	F2	Gum acacia	F4
Clay (nozzle)	F3	Skimmed milk (high density powder)	F4
Clay (rotary)	F3		
Glucose	F2		
Skimmed milk analogue	F4		

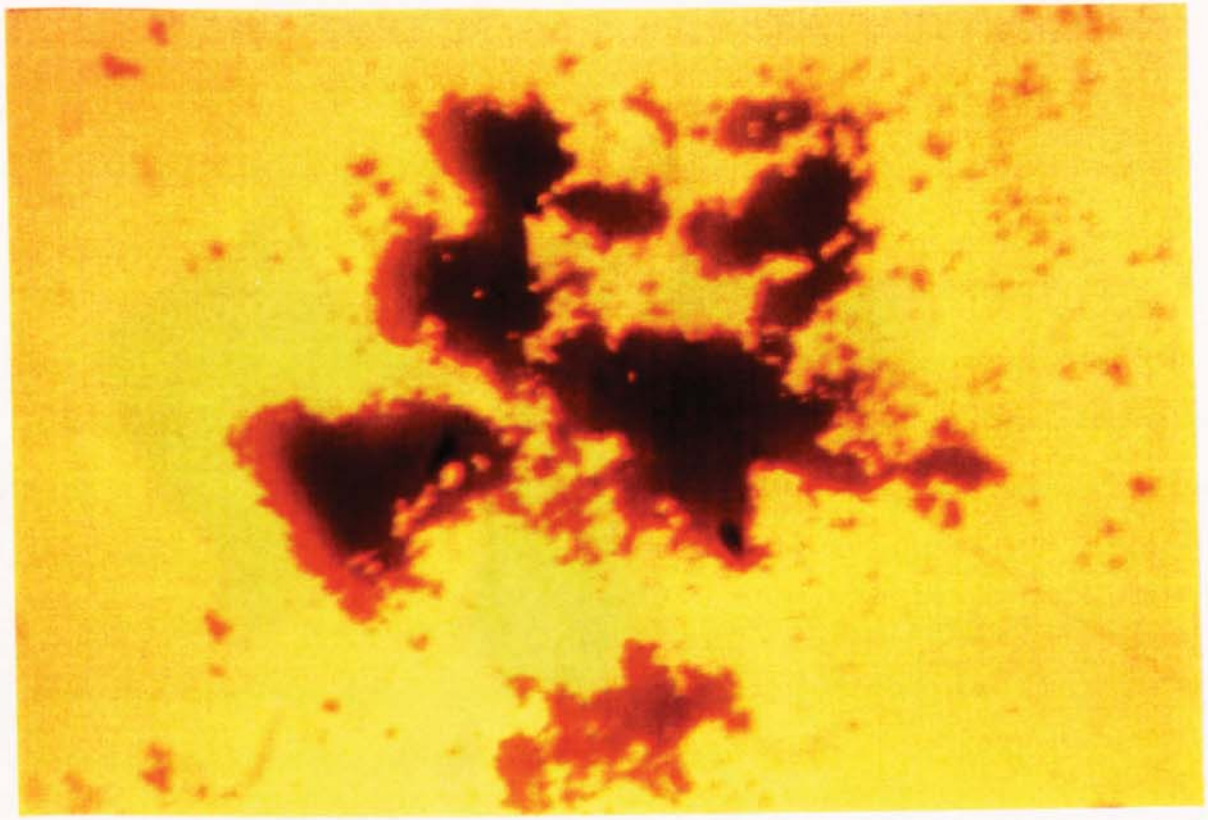

Figure 31. Friability F1 - barium titanate (mag. x 8), In. conc. 50 % w/w
Temp. in 350°C, out 120°C

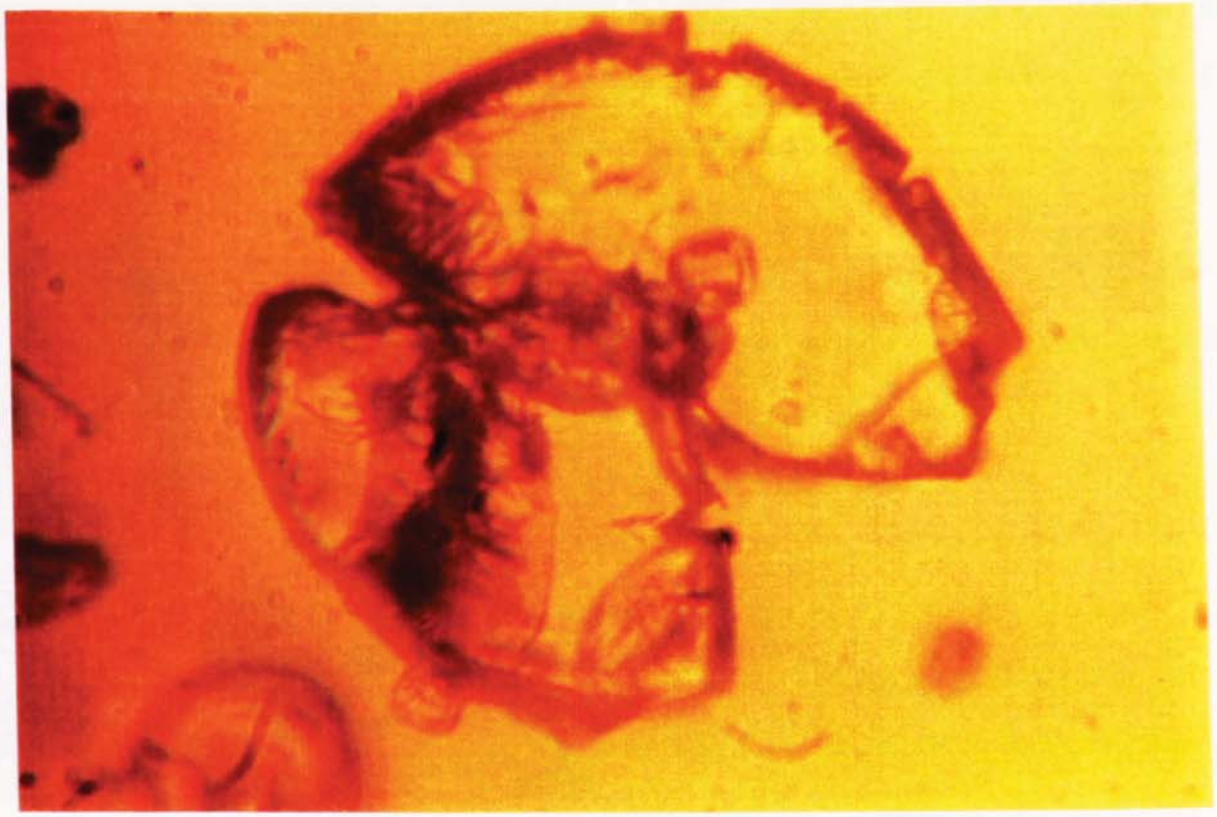

Figure 32. Friability F2 - dextran (mag. x 42), In. conc. 40 % w/w
Temp. in 250°C, out 100°C

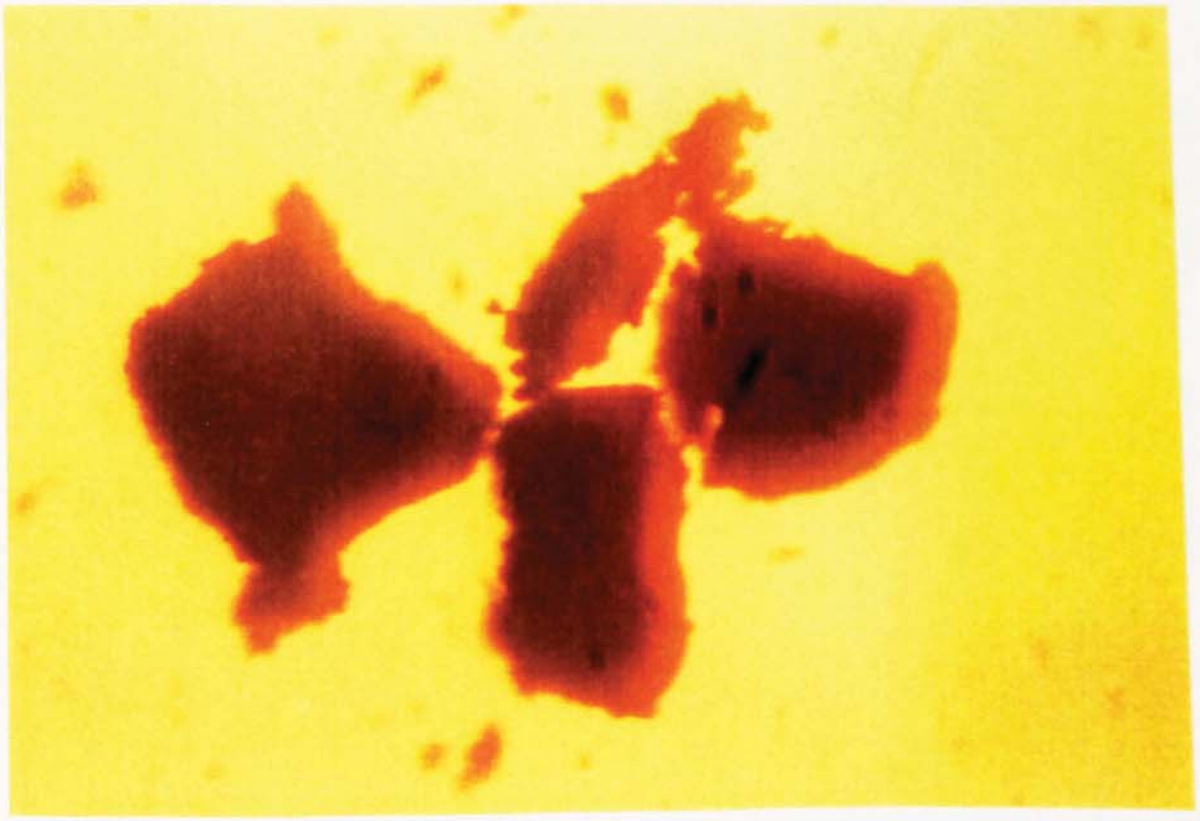

Figure 33. Friability F3 - clay, rotary (mag. x 8), In. conc. --
Temp. in 550°C, out 90°C

Figure 34. Friability F4 - coffee (mag. x 15), In. conc. 30 % to 50 % w/w
Temp. in 230°C, out 115°C

v.) Particle Morphology

The particle morphology of each sample was examined using both optical and scanning electron microscopy. General observations are presented in Appendix A 3.0. Photographs of the particles and a discussion on particle structure are given below (see Figures 35 to 58).

Three distinct morphological types were identified, namely, agglomerate, skin-forming and crystalline. Structurally, these were defined as,

1.) Agglomerate Structure - A particle composed of individual grains of material bound together by sub-micron dust, i.e.; material less than 1 μm in diameter and / or a binder.

2.) Skin Forming - A particle composed of a continuous non-liquid phase which is polymeric or sub-microcrystalline in nature.

3.) Crystalline Structure - A particle composed of large individual crystal nuclei bound together by a continuous micro-crystalline phase.

Typically, the inorganic materials fell into the crystalline and agglomerate categories and could be further sub-divided according to their aqueous solubility, i.e.; materials which are readily soluble in water tend to have crystalline morphologies, whereas, insoluble or partially-soluble materials tend to form agglomerate structures.

Organic materials fall into the skin-forming structural category.

General observations and single droplet studies suggest however that specific inorganic or organic materials can fit into either group. For example, sodium silicate has well known skin-forming properties.

Agglomerate Structures

Particles with an agglomerate structure (see Figures 35 to 46 and Table 15) are composed of individual grains of material bound together by sub-micron dust particles and possibly a binder. The grains or primary particles vary both in size and shape, from relatively large irregular structures up to 10 μm in diameter to regular, almost cubic, grains less than 1 μm in diameter (see Figure 36). Grain-size distributions within particles may also vary or be relatively-uniform.

Most of the agglomerate particles appear externally spherical and regular in shape, but this is not always the case. Figures 37 and 38 for example, show particles of tungsten carbide and aluminium oxide which are pear-shaped and

elongated respectively. This type of deformation is almost certainly due to incomplete atomization, i.e.; the breakdown of ligaments into droplets is incomplete. This phenomenon is by no means restricted to agglomerate structures; both skin-forming and crystalline structures may exhibit similar deformations.

Particle blowholes and cratering are a relatively uncommon feature. This may be due to the highly porous or open nature of the particle structure where movement of water, water vapour and possibly dissolved gases from the interior of the particle to its surface can occur with the minimal amount of resistance, thus minimizing internal pressure build-up and particle distortion. This would account for the high degree of sphericity shown by most of the agglomerate particles.

To explain agglomerate particle structures which do exhibit blowholes and cratering, it is necessary to take into account particle strength, friability, feed specifications and drying conditions. For example, Figure 39 illustrates a fractured particle of tungsten carbide with a blowhole. Although the particles have a relatively open structure they were dried from a volatile non-aqueous feed slurry such as ethanol or hexane to carry a binder. Rapid evaporation of the volatile solvent probably exceeded the rate of liquid and / or vapour diffusion through the porous particle structure resulting in the formation of a blowhole.

The surface morphologies of the clay particles, namely, kaolin, clay (nozzle) and clay (rotary) are in contrast to

this. Clay (rotary) is a particularly good example where particles show a high incidence of cratering (see Figures 42 and 43) and surface structures appear almost polymeric or ' skin-like ' (see Figure 44). This can be explained in terms of the fine nature of the clay primary particles or platelets. Although by definition an agglomerate structure, because of the small size of the platelets, i.e.; in the region of 10^{-6} m to 10^{-9} m, optically, they almost appear to form a continuous phase or skin; for mass transfer purposes this produces a relatively non-porous particle structure. Since most clays have a natural plasticity when wet, particle distortion or some form of vapour pressure release is inevitable during drying, e.g.; particle inflation followed by rupture of the particle wall to form a blowhole which collapses inwards to form a crater.

Agglomeration, in the general sense, is usually limited to two or three particle agglomerates (see Figure 45) or multiple particle agglomerates, never mass agglomeration as shown with the polymeric materials (see Figures 48). The particles appear to be bonded or cemented together by material derived either from each other, or, from a single squashed particle acting as a ' cement '.

The internal structure of agglomerate particles may be either solid (see Figure 46) or hollow (see Figure 39). If hollow, the wall structures are relatively-thick in relation to the overall particle diameter; if solid, particles can sometimes contain vacuoles or trapped air / gas bubbles.

Although not agglomerate structures, a good example of particle vacuolation is shown in Figures 53 and 54.

Both the wall structure and the internal solid structure of agglomerate particles tend to be identical. An exception to this however, are the particles of aluminium silicate. Internally, they have a typical agglomerate structure, i.e.; solid and granular with some degree of vacuolation, but towards the particle surface the composition or texture of the internal structure changes from granular to a very smooth, very compact, dense layer approximately 9 μm to 13 μm thick. The layer extends to the particle surface (see Figure 41) to form a polymeric surface structure with many cracks and fissures (see Figure 40). This change in structural composition is almost certainly due to a binder which has either been applied externally to the particle, or, has migrated to the particle surface, as opposed to being an integral part of the particle structure.

Table 15. Commercially Spray-Dried Samples with an Agglomerate Particle Structure

Aluminium hydroxide	Copper oxychloride
Aluminium silicate	Lead chromate
Tungsten carbide	Copper ore
Aluminium oxide	Magnesium hydroxide
Titanium dioxide (Miro)	Clay (nozzle)
Ferrite	Clay (rotary)
Kaolin	Titanium dioxide (Drytec A)
Barium titanate	Titanium dioxide (Drytec B)

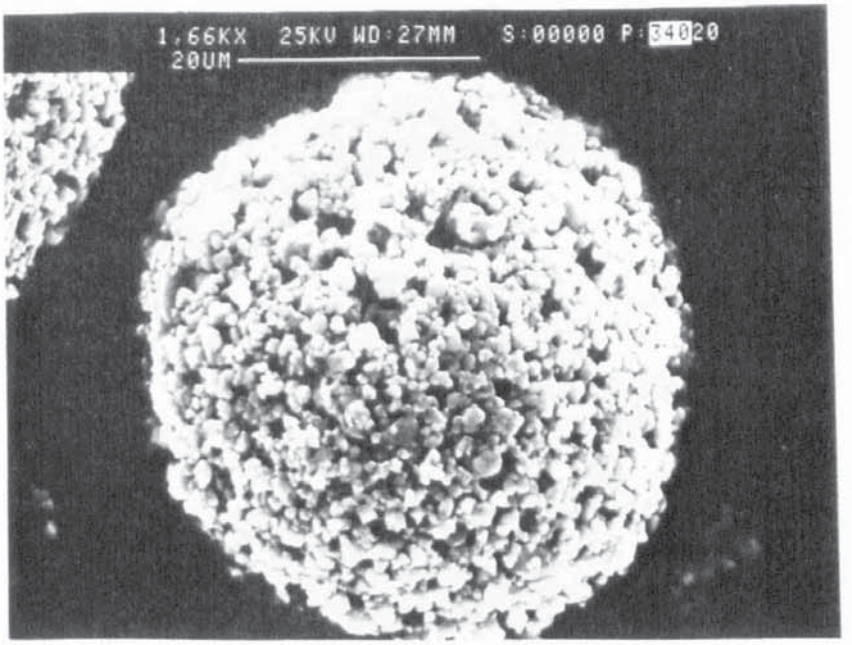

Figure 35.
ferrite
In. conc. 40% w/w
Temp. in 350°C
out 120°C

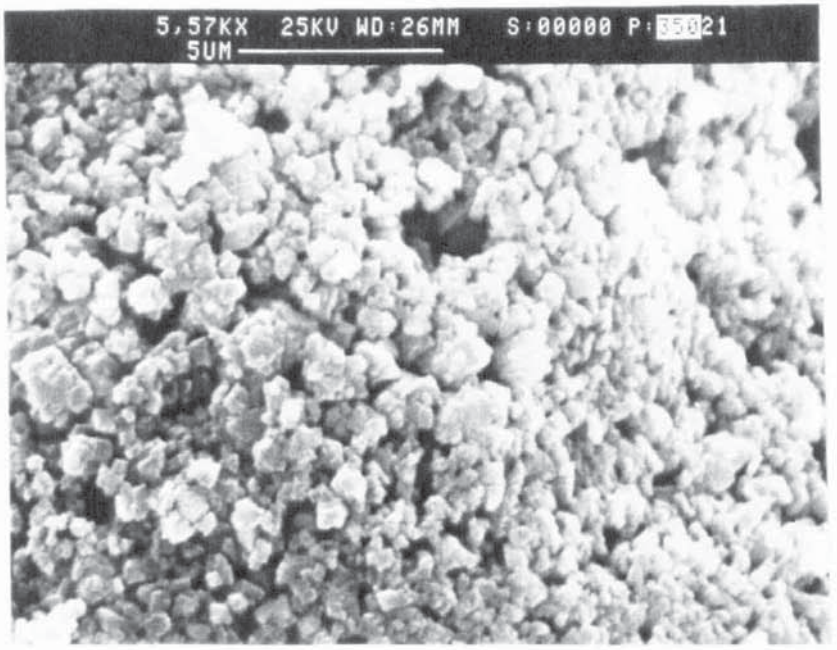

Figure 36.
copper oxychloride
In. conc. --
Temp. in 400°C
out 100°C

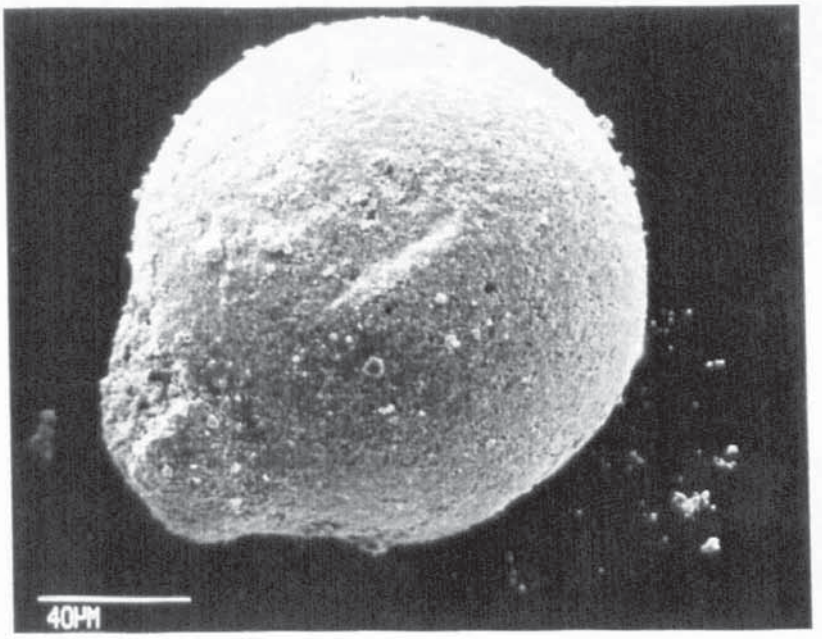

Figure 37.
tungsten carbide
In. conc. 60% w/w
Temp. in 200°C
out 80°C

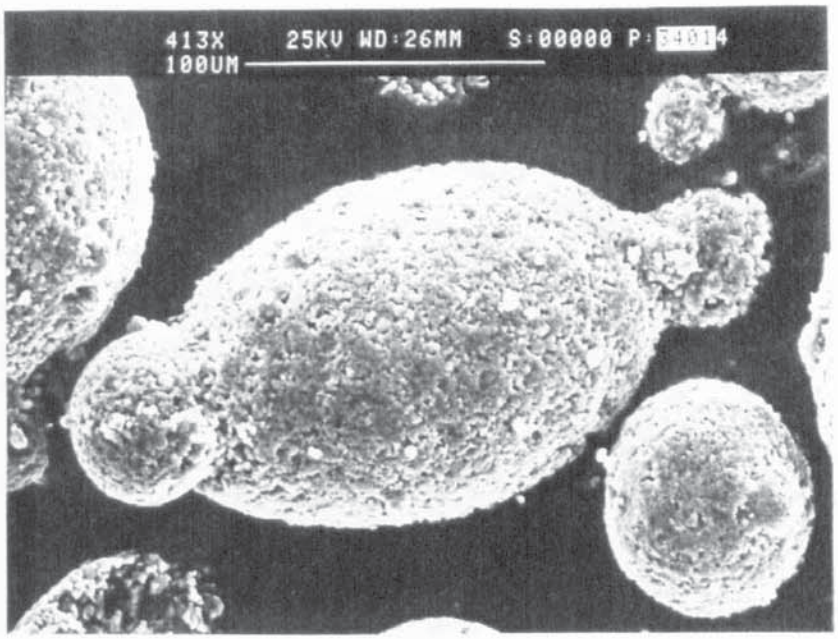

Figure 38.
aluminium oxide
In. conc. 60% w/w
Temp. in 350°C
out 115°C

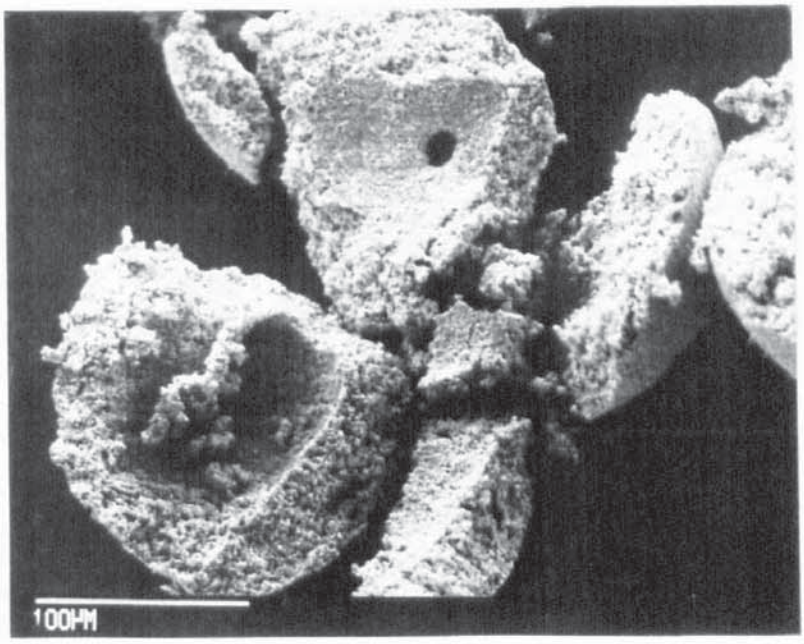

Figure 39.
tungsten carbide
As Figure 37.

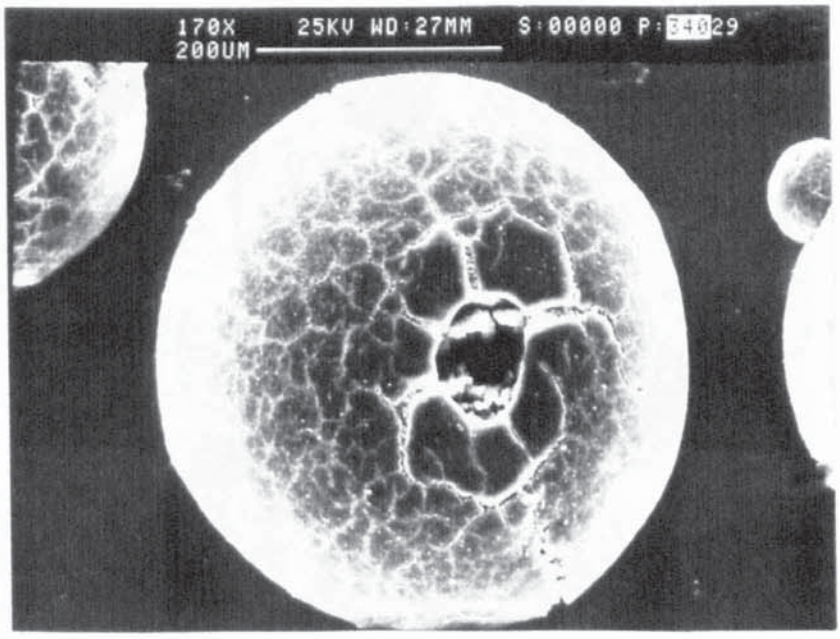

Figure 40.
aluminium silicate
In. conc. 30% to 50% w/w
Temp. in 350°C
out 90°C

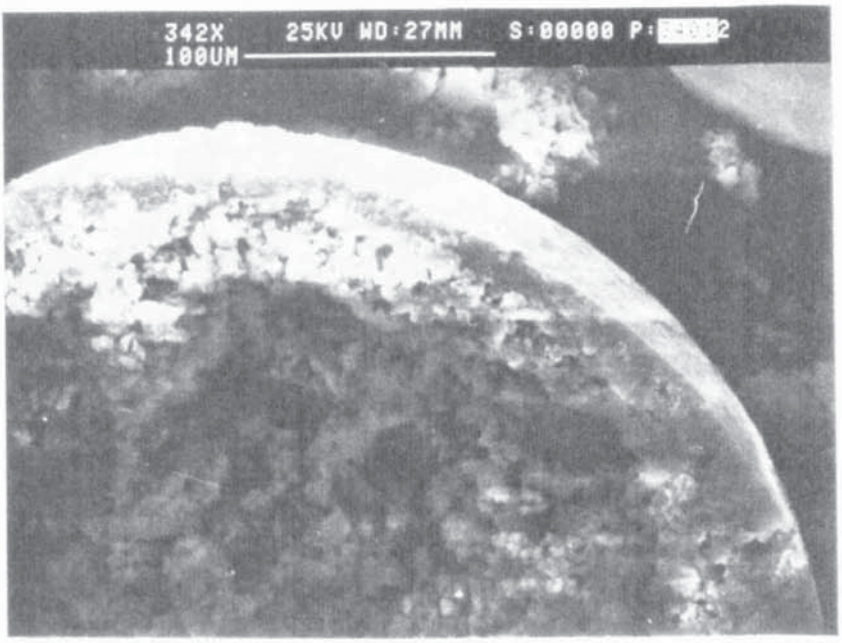

Figure 41.
aluminium silicate
As Figure 40.

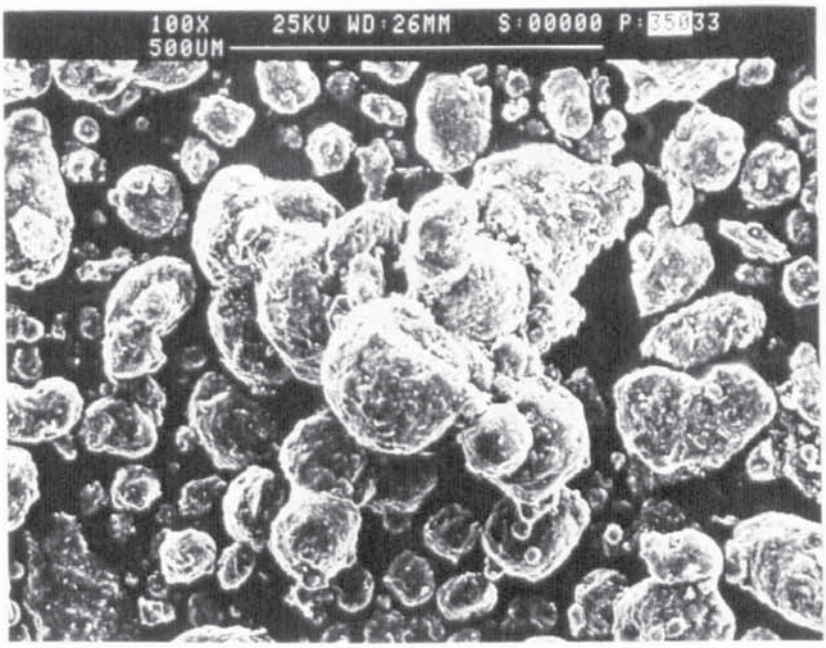

Figure 42.
clay (nozzle)
In. conc. --
Temp. in 550°C
out 100°C

Figure 43.
clay (rotary)
In. conc. --
Temp. in 550°C
out 90°C

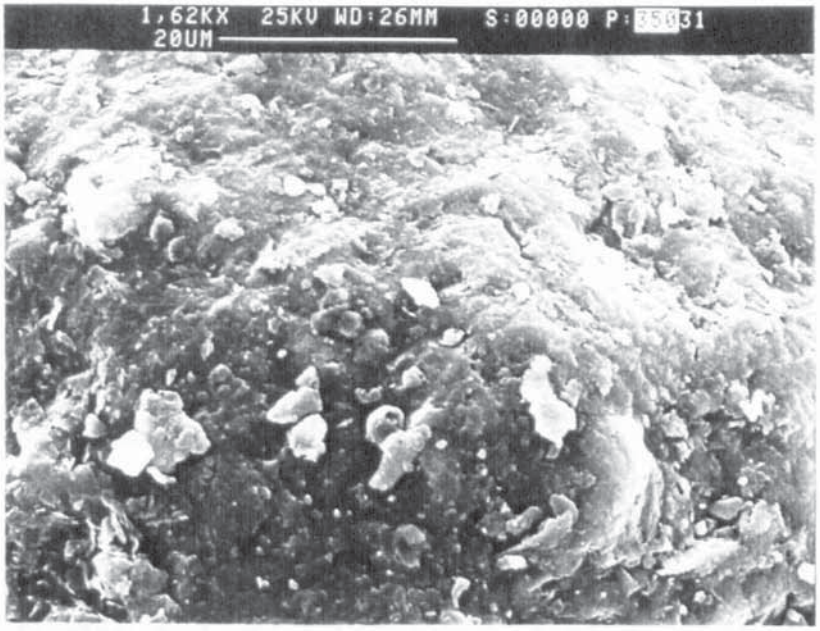

Figure 44.
clay (nozzle)
As Figure 42.

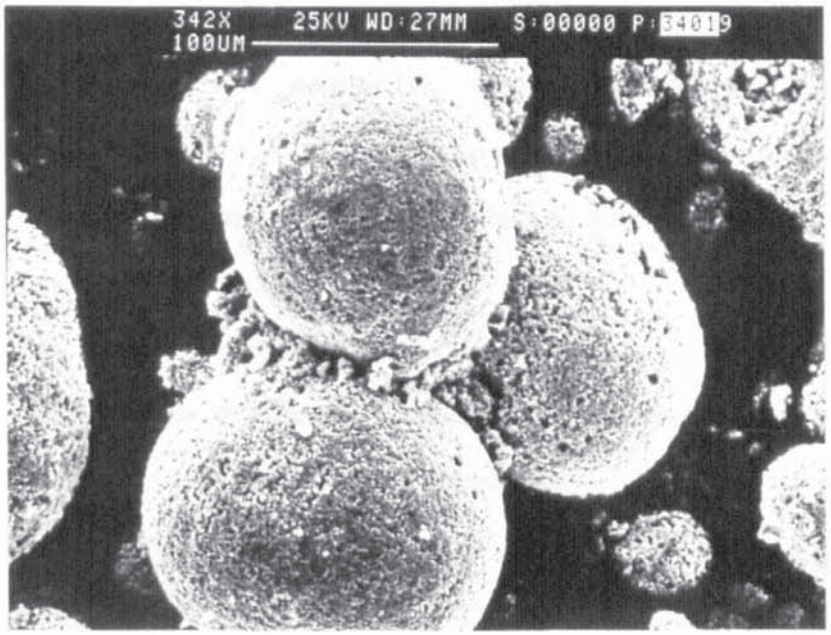

Figure 45.
ferrite
As Figure 35.

Figure 46.
lead chromate
In. conc. --
Temp. in 350°C
out 100°C

Skin Forming Particles

Particles with a skin-like structure or appearance (see Figures 47 to 55) are composed of a continuous non-liquid phase which is very difficult to define from a structural point of view. With dairy products, e.g.; skimmed milk, yogurt powder and co-dried egg and skimmed milk, the non-liquid phase may be composed of denatured proteins such as casein or albumins. For example, when cooking an egg white (which is colourless) the high temperature causes an irreversible denaturation of the albumins which unfold and precipitate to produce a white solid.

Conversely, materials such as glucose, calcium stearate and the soluble titanium salts, have well-ordered, crystalline structures but still display a skin-like particle surface structure and morphology. Such morphologies are somewhat analogous to those displayed by clays, in which the crystalline structure is so fine (sub-micron) that it appears and acts as a continuous phase. Although the clays have a skin-like appearance, they also have a very definite agglomerate texture. These materials have relatively low melting points.

A similar explanation may apply to multicomponent materials whether the particle skins are crystalline in nature or formed by thermal degradation, e.g.; instant drink powder and encapsulated flavour particles are essentially glucose based, whereas coffee contains carbohydrates or carbohydrate

precursors. Furfuryl mercaptan is the essential constituent of natural coffee aroma and is formed from a carbohydrate precursor during the roasting of coffee.

Because many commercially spray-dried materials have skin-like structures, e.g.; food and dairy products, the particle morphology and morphological phenomena associated with the drying of these materials has been widely-studied. It is evident from the literature that the general structural plasticity of the particles during drying has resulted in a greater morphological diversity than both agglomerate and crystalline particle structures. The commercially spray-dried samples reflect this, in that they (see Table 16) show most of the known or recorded morphological features, e.g.; particle inflation (Figure 47), particle collapse / shrivelling (Figure 50), blowholes and cratering (Figures 49 and 51 respectively), agglomeration (Figure 48), particles with cracks and fissures (Figure 52), particle vacuolation (Figures 53 and 54), particles which are hollow (Figures 52 and 55) and particles which are ' solid ' in the sense that they always exhibit vacuolation to some extent (143). Agglomerate and crystalline morphologies are on the other hand restricted to spherical, regular structures with a relatively limited range of morphological features, i.e.; cracks and fissures with occasional cratering and a small number of blowholes.

Table 16. Commercially Spray-Dried Samples with a Skin Forming Particle Structure

Dyestuffs	Co-dried egg and skimmed milk
Polymer (Drytec - A)	2,3 - dichloropropanoic acid
Coffee	Semi-instant skimmed milk
Dextran	Encapsulated flavour
Glucose	Polymer (sodium salt)
Instant drink powder	Soluble titanium salt (two-fluid nozzle)
Yogurt powder	Soluble titanium salt (pressure nozzle)
Polymer (Drytec - B)	Soluble titanium salt (rotary)
Skimmed milk (high density powder)	Calcium stearate
Detergent	Gum acacia
Skimmed milk analogue	

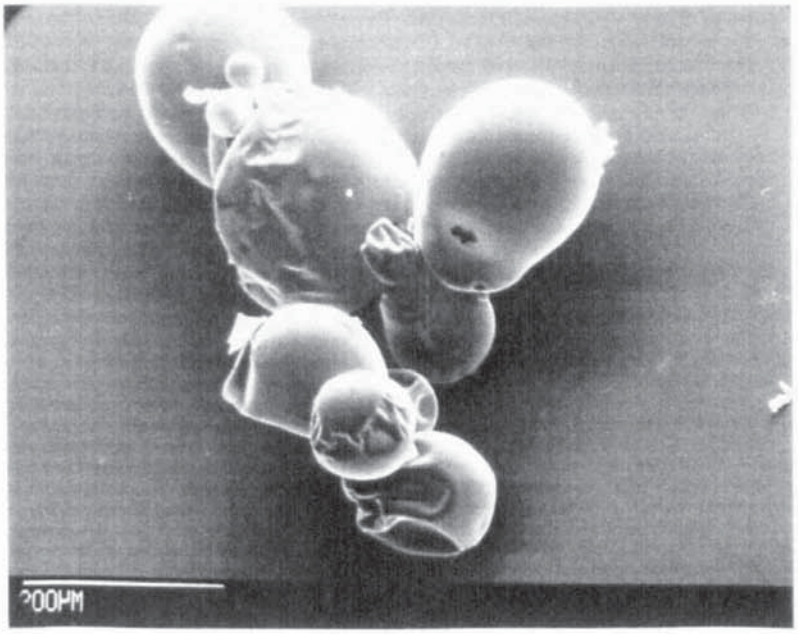

Figure 47.
coffee
In. conc. 30% to 50% w/w
Temp. in 230°C
out 115°C

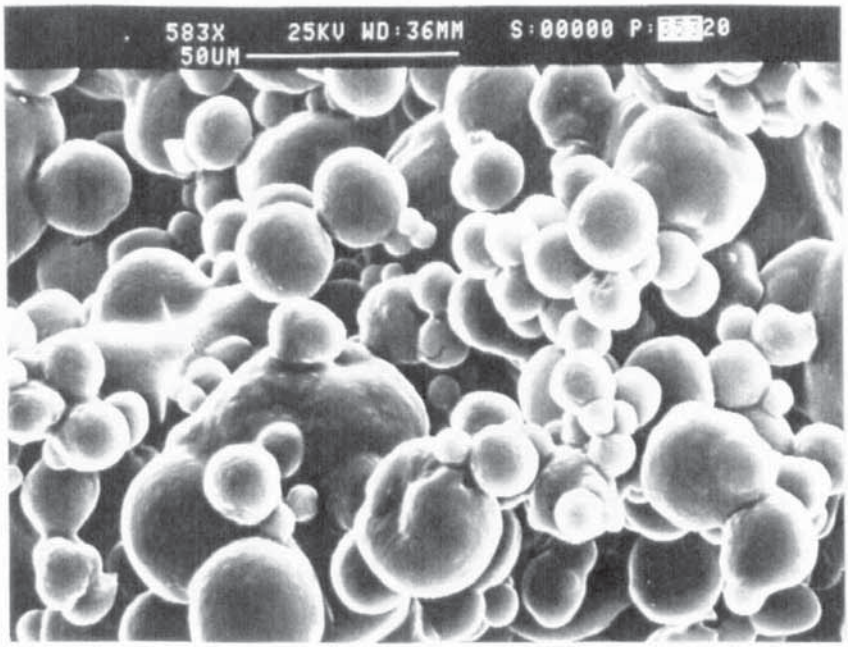

Figure 48.
yogurt powder
In. conc. --
Temp. in --
out --

Figure 49.
yogurt powder
As Figure 48.

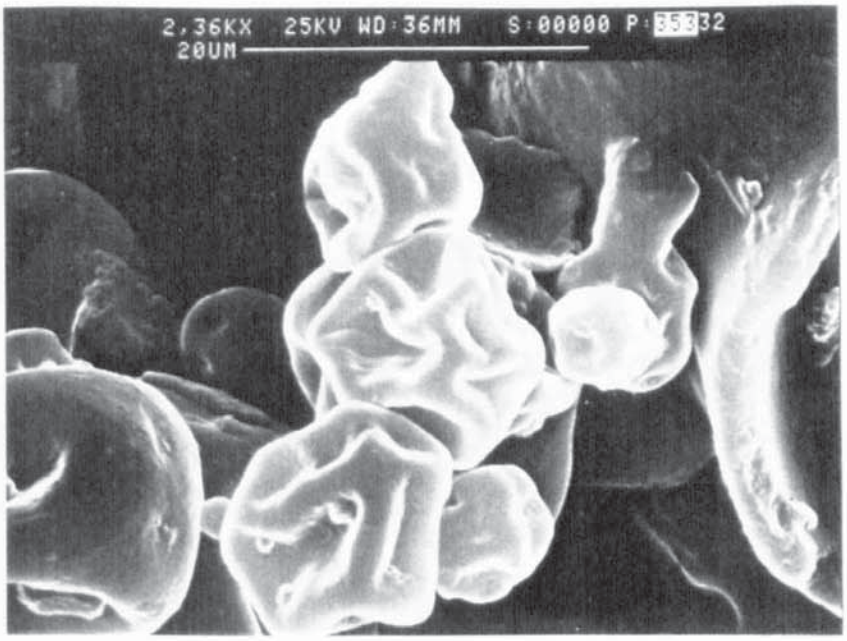

Figure 50.
co-dried egg and skimmed milk
In. conc. --
Temp. in --
out --

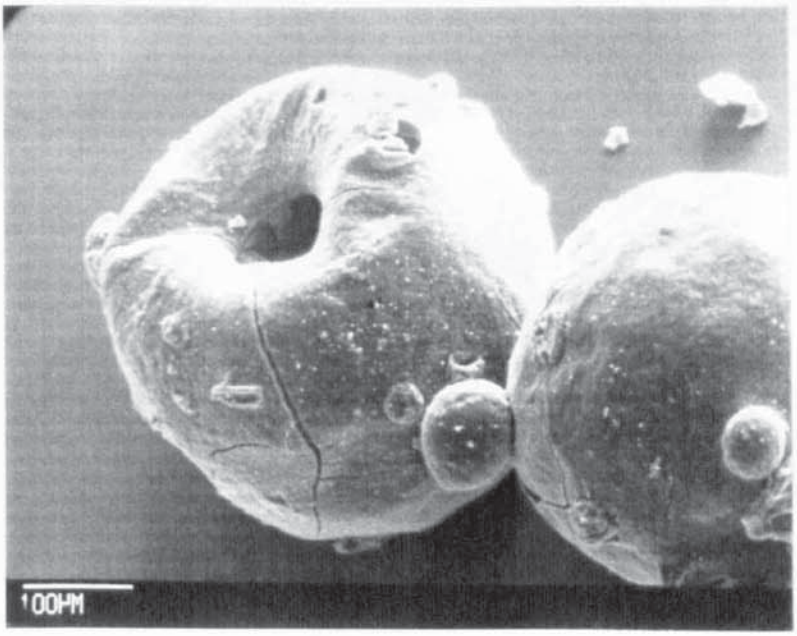

Figure 51.
dyestuffs
In. conc. 30% to 40% w/w
Temp. in 350°C
out 110°C

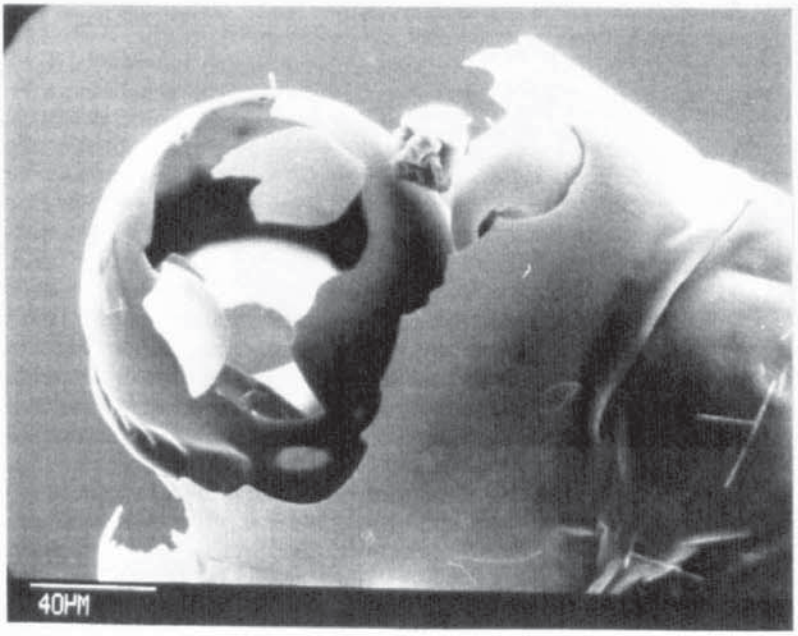

Figure 52.
coffee
As Figure 47.

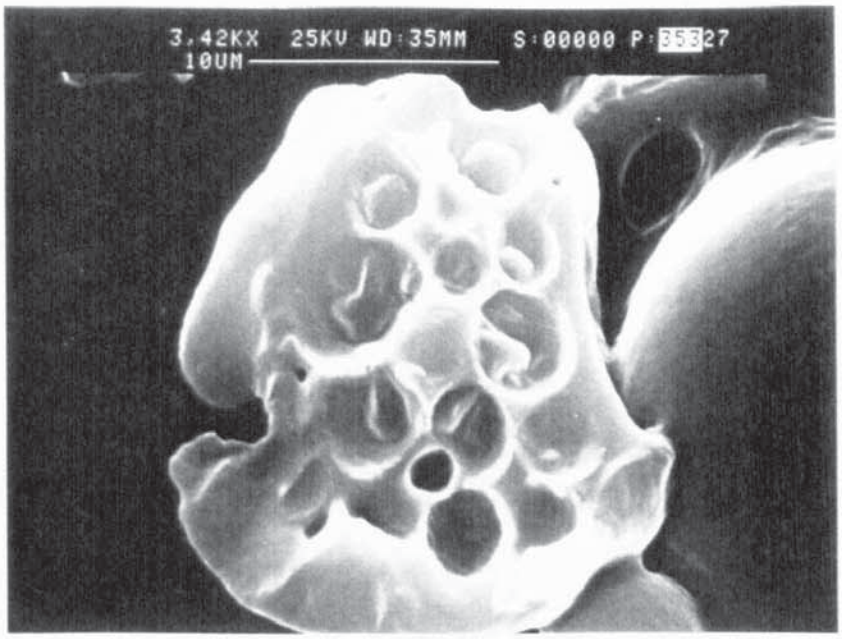

Figure 53.
skimmed milk
(high density powder)
In. conc. --
Temp. in --
out --

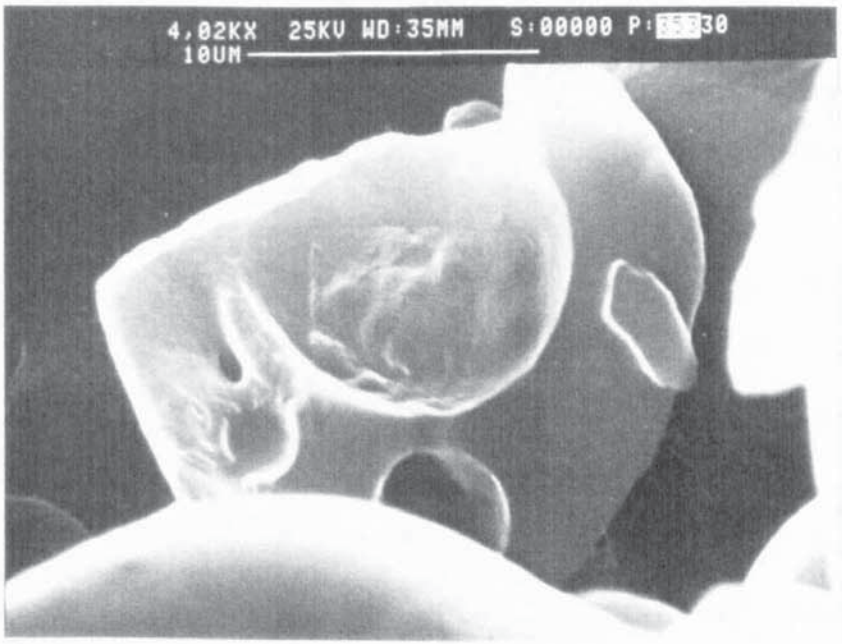

Figure 54.
skimmed milk
(high density powder)
As Figure 53.

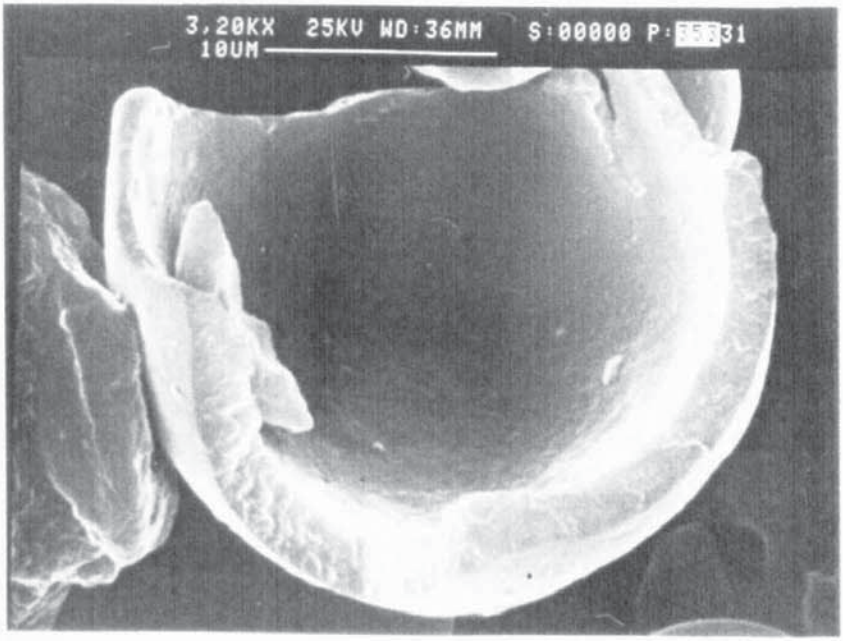

Figure 55.
co-dried egg and
skimmed milk
As Figure 50.

Crystalline Structures

Particles with a crystalline structure are composed of large individual crystal nuclei bound together in a continuous microcrystalline phase (see Figures 56 to 58). They differ structurally from crystalline materials which have a skin-like structure, i.e.; a continuous phase which is sub-microcrystalline in nature, or, crystalline materials with an agglomerate structure, i.e.; individual grains (crystals) bound together by material which does not form a continuous phase.

Of the thirtynine commercially spray-dried samples obtained, only two exhibited a crystalline particle structure, namely, tri-sodium orthophosphate and the organic u.v. brightener.

Morphologically, they were similar to the agglomerate particle structures with no particle inflation or shrivelling and a limited amount of cratering and blowholes. They did however, differ in,

- The extent of surface cracking and fissures. This was excessive in both tri-sodium orthophosphate and the organic u.v. brightner, particularly in tri-sodium orthophosphate where there were many broken shells

- The particles were relatively irregular in shape. The overall shape was not indicative of incomplete atomization

- No solid particles were found

These observations suggest a different drying history from both the agglomerate and skin-like particle structures. The excessive surface cracking and large number of broken shells (assuming they were not produced by mechanical damage) plus the general morphology indicated a relatively non-porous, rigid particle structure where evaporation of the internal liquid had resulted in particle fracture and possibly particle explosion.

The irregular particle shape of both tri-sodium orthophosphate and the organic u.v. brightner did however, suggest some crust or shell movement, not flexibility, during drying. This probably occurred just after crust formation was complete, i.e.; movement of crust segments due to fractures in the overall crust structure caused by escaping water or water vapour from the particle interior.

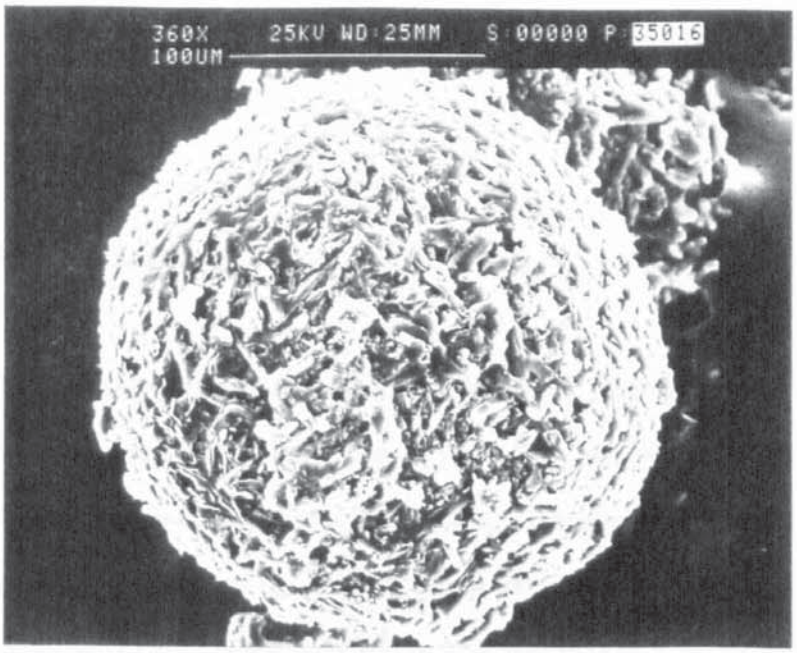

Figure 56.
tri-sodium orthophosphate
In. conc. --
Temp. in 400°C
out 100°C

Figure 57.
tri-sodium orthophosphate
As Figure 56

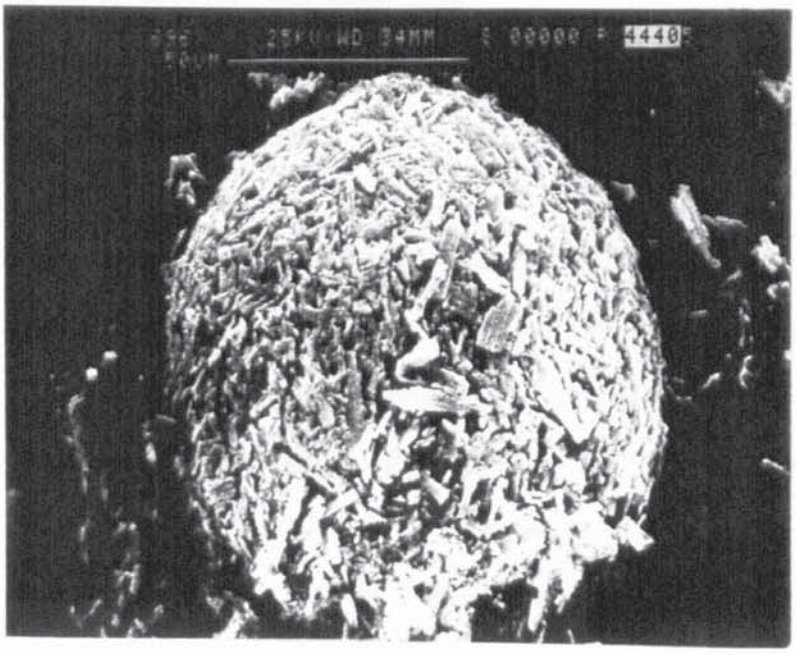

Figure 58.
organic u.v. brightner
In. conc. --
Temp. in --
out --

6.3) Discussion

The samples listed in Table 7 appear to be a reasonably good cross-section of the type of materials spray-dried industrially, but for the absence of biochemicals and pharmaceuticals. The quoted drying specifications, i.e.; feed concentrations, drying temperatures and drier details, show good general agreement with those reported by Masters (192). This would tend to suggest the use of standard drying conditions throughout industry for specific materials or material types. The samples obtained however, can represent only a fraction of the total number of products spray-dried on an industrial basis. Masters (192) for example, lists over a thousand products which have been successfully either spray-dried, or, processed by spray cooling, spray reaction, spray absorption or spray concentration.

Powder Characterization

1.) Bulk Density

Sample bulk densities varied considerably from 0.147 g/cm^3 for coffee to 3.674 g/cm^3 for tungsten carbide, the comparative values being dominated essentially by the material's molecular or formula weight. Most values did not exceed a bulk density of 0.6 g/cm^3 with an average of 0.670 g/cm^3 for all the samples. This bears out Crosby and Marshall's (141) findings,

that the bulk density of most spray-dried material seldom approaches 50 % of the true density of the solid being spray-dried. Experimentally, the highest they recorded was in the region of 0.5 g/cm^3.

Physical factors affecting the bulk densities are difficult to assess due to the differences in formula weight. Particle-size for example, should theoretically be related inversely to bulk density, Tables 9, 10 and Figure 59 however, clearly suggest otherwise, unless the data is grouped into identical or similar material types, i.e.; the titanium dioxide samples show an inverse relationship as do the soluble titanium salts (see Figure 60).

Whilst correlation of bulk densities with formula weights should produce comparative data little or no trend is present. This is probably due to a number of factors,

Structural differences - Particles may be hollow, contain vacuoles or be porous.

Particle-shape - The degree of ' sphericity '. Non-spheroids will generally have a closer packing density. Particle agglomeration must also be taken into account as well as surface roughness.

Broken particles	- Only whole particles were considered when measuring particle diameters. A large number of broken particles would increase bulk density.
Particle-size distribution	- Very few particulate systems are mono-sized.

The bulk density / formula weight to mean particle diameter ratio for samples with skin-like structured particles was significantly lower than for particles with agglomerate or crystalline structures. This cannot be attributed solely to factors such as particle-size distribution, particle shape and the number of broken particles, but would tend to suggest a greater degree of ' hollowness ' within the skin-like structured particles. General observations of particle structures support this (see Appendix A 3.0).

Information in the literature concerning the effects of drying conditions on bulk density are conflicting, indicative of the specific drying behaviour of many materials. Marshall and Seltzer (4) list most of the important considerations, e.g.; feed concentration, drying air temperature and size distribution. Other factors such as feed rate, powder temperature, residual moisture content and the type of atomization and atomization pressure, also influence bulk density.

Figure 59. Bulk Density vs Mean Particle Diameter
(Commercially Spray-Dried Samples)

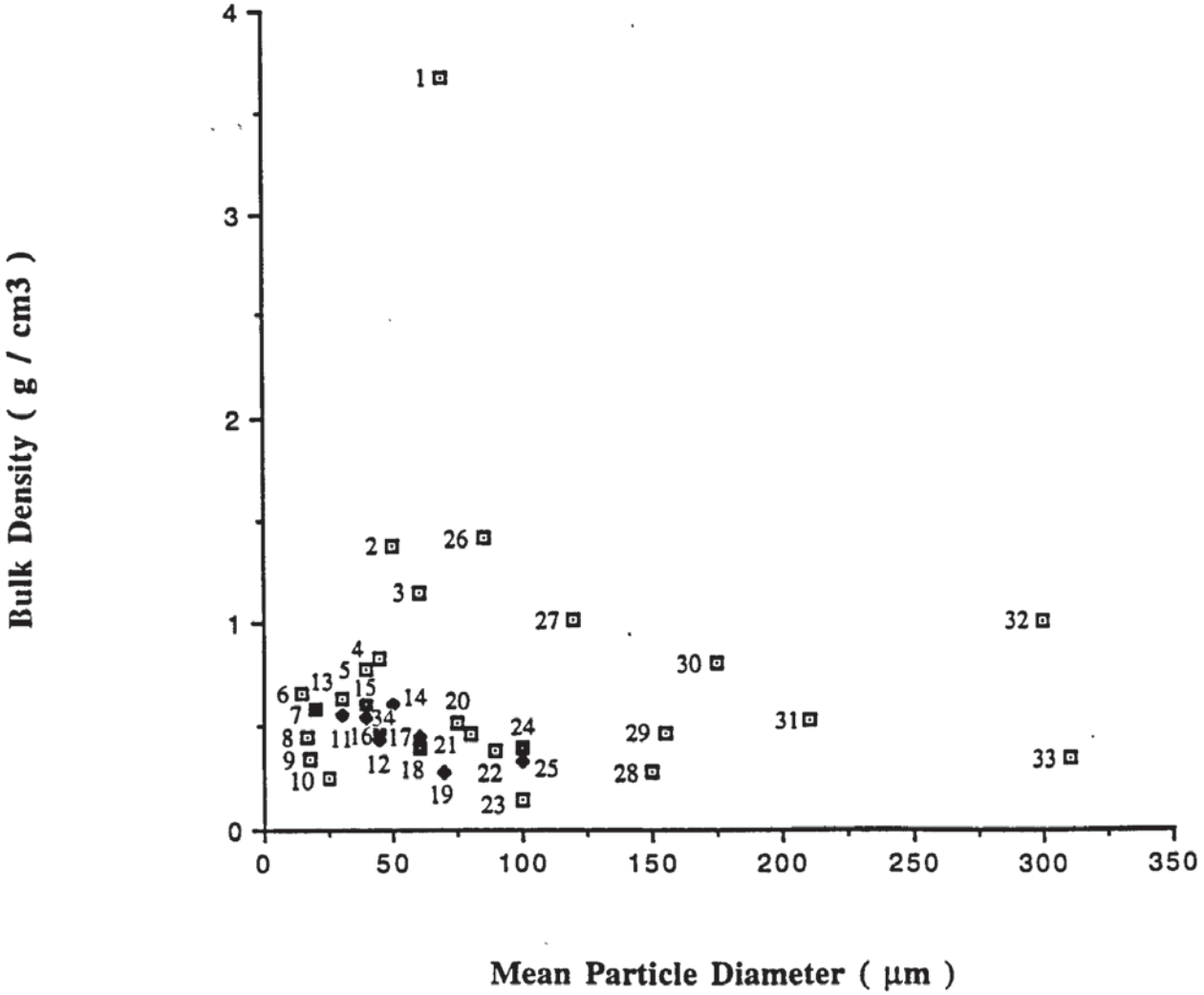

1. tungsten carbide
2. copper ore
3. aluminium oxide
4. copper oxychloride
5. lead chromate
6. soluble titanium salt (two-fluid nozzle)
7. co-dried egg and skimmed milk
8. calcium stearate
9. 2, 3 - dichloro - propanoic acid
10. dextran
11. soluble titanium salt (pressure nozzle)
12. polymer (Drytec B)
13. titanium dioxide (Drytec B)
14. magnesium hydroxide
15. titanium dioxide (Niro)
16. semi - instant skimmed milk
17. titanium dioxide (Drytec A)
18. encapsulated flavour
19. instant drink powder
20. soluble titanium salt (rotary)
21. polymer (sodium salt)
22. aluminium silicate
23. coffee
24. gum acacia
25. polymer (Drytec B)
26. ferrite
27. clay (nozzle)
28. organic u.v. brightner
29. dyestuffs
30. kaolin
31. detergent
32. clay (rotary)
33. tri - sodium orthophosphate
34. skimmed milk analogue

Figure 60. Bulk Density vs Mean Particle Diameter (Identical or Similar Materials)

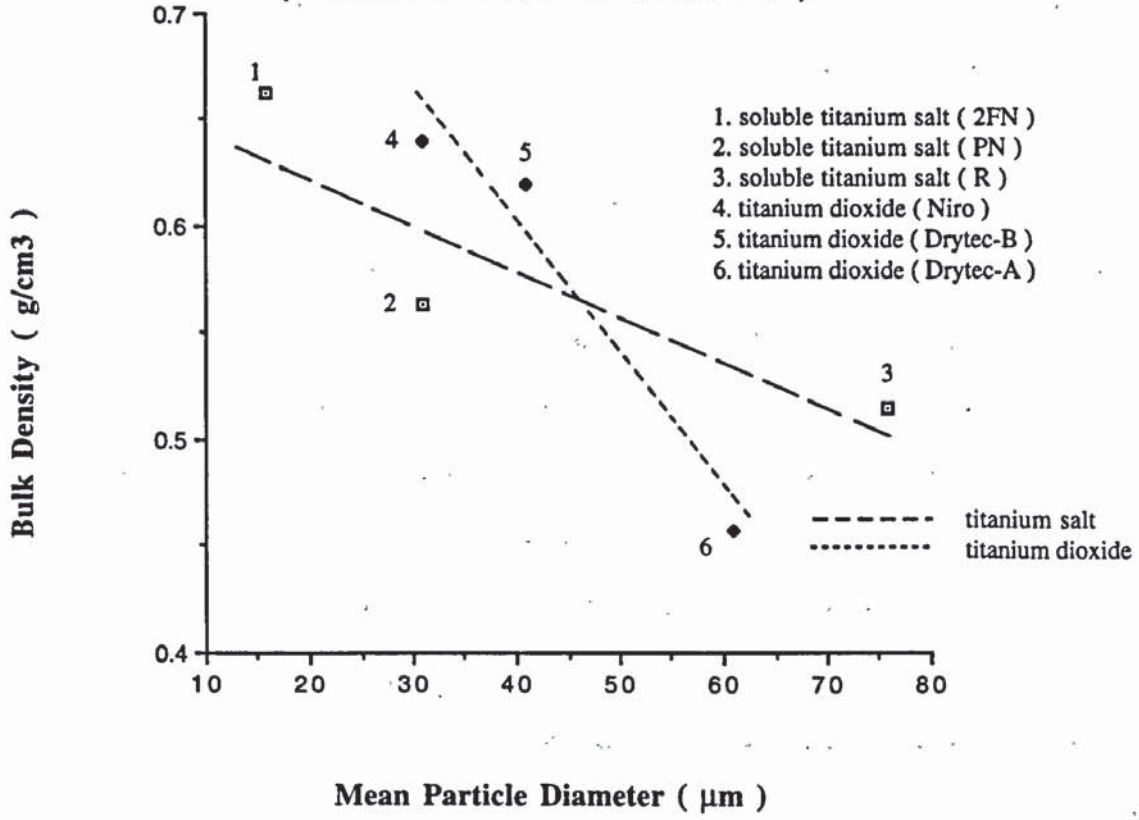

ii.) Particle-Size

Particle diameters ranged from less than 1 μm up to 800 μm with mean values in the region of 17 μm to 310 μm. Measurements were made particularly difficult by the large amount of agglomeration found in most samples. Investigations with relatively rapid methods of sizing such as sieving and laser diffraction, i.e.; the Malvern Droplet and Particle Sizer (Series 2600c) (230), which sample a large number of particles per measurement, were found to be largely unacceptable. Optical microscopy, although labour-intensive and only sampling a relatively small number of particles, was found to be the best alternative.

Particle morphology is likely to be size-dependent, e.g.; small particles have the largest residence time within a spray drier, the largest heat and mass transfer coefficients, and the smallest internal diffusion path. Consequently, they have a lower moisture content initially, dry quicker and are more prone to thermal degradation. Experimental data relating to the sample powders was therefore based upon the mode or most frequent particle-size within the size distribution.

iii.) Powder Flowability

Powders, i.e.; bulk particles, deform and flow in a complex manner. They can exhibit phenomena such as elastic recovery and brittle fracture of the kind found in some solids and may

undergo continuous plastic deformation and flow. In most engineering design situations a bulk powder is often regarded as a plastic continuum, i.e.; the powder exhibits rheological behaviour relating to both ' Hookean ' (the ratio of the stress to the strain produced is constant, within the elastic limit of the body) and plastic deformation. When a powder is subjected to a continuous stress it first deforms elastically in a more or less ' Hookean ' manner but as the stress increases the powder starts to yield and eventually fails completely; after which, deformation becomes completely plastic, the powder dilates and flow sets in. This approach, although relatively successful, fails to give any consideration to particle surface morphology, e.g.; surface asperities of adjacent particles can interlock, clearly an important factor in determining interparticle adhesion and, therefore, powder flowability.

The ' particulate approach ' to powder rheology considers, particle-size, particle shape and particle packing (co-ordination number), interparticle forces, i.e.; surface asperities, surface films and layers (moisture), solid bridges between particles (binders, crystallization, chemical reaction etc.), molecular surface forces (Van der Waals) and electrostatic surface forces. Such considerations are useful in making qualitative predictions. For example, if two powders of the same material, particle-size distribution and particle shape have different strengths, then the difference is likely to lie in the interparticle forces. Questions then

arise as to whether they have the same moisture content, stress histories and have been subjected to similar environments. Flow-property problems of this nature can often be explained and solved from surface considerations, although quantitative modelling of powder behaviour remains a problem.

Flow property testers, e.g.; the Jenike Shear Cell, the Warren Spring Tensile Tester and the Funnel Flow Tester, all tend to be unsatisfactory in some way mainly because powders fail and flow in a complex fashion and no one instrument can take into account all the aspects which govern powder flow. The powder inclinometer described in Section 6.2 iii, was designed to measure the angle of repose of a small quantity of powder, approximately 1.1 cm^3, as accurately as possible. The results, although empirical have been interpreted in relative terms.

Tables 11 and 17 show data on the flowability of all thirtynine samples at 62 % relative humidity (22.3°C). Examination of the data suggests the samples possessed one of three distinct types of flow behaviour, i.e.;

1.) Free-flowing powder,

2.) Semi free-flowing powder, or,

3.) Cohesive powder,

The samples have been categorized in these terms (see Table 18) with typical profiles of all three types of flow behaviour shown in Figure 61.

Sample powders which were free-flowing flowed readily in an even, unbroken manner and had flow patterns characterized by high displacement gradients at low angles of repose. The angle over which displacement occurred was very narrow and, in terms of the test, 100 % of the sample was displaced from the inclinometer.

Semi free-flowing samples tended to flow in an uneven and broken manner, with the powder showing signs of brittle fracture as it separated. Flow patterns were characterized by much lower displacement gradients at higher angles of repose; the angle over which displacement occurred was much wider compared to the free-flowing powders. In some instances, not all the sample was displaced from the inclinometer at 90°.

The cohesive powders exhibited a considerable resistance to flow; flow was very broken and very uneven in fashion, i.e.; via brittle fracture. Flow patterns were characterized by high displacement gradients at very high angles of repose. The angle over which displacement occurred was narrow and, in almost every case, only a relatively small amount of sample was displaced from the inclinometer, even at 90°.

Table 17. Comparison of Flowability Data for Free-flowing, Semi free-flowing and Cohesive Samples

Type of Powder	Angle of Initial Displacement		Displacement Profile		
	Range of Data	Average Angle	Profile Width	Average Width	Average Displacement
Free-flowing	17° - 55°	30°	0° - 34°	7°	100 %
Semi free-flowing	33° - 64°	44°	0° - 51°	21°	95 %
Cohesive	35° - 90°	57°	0° - 50°	10°	34 %

N.B. - A value of 0° for the profile width indicates that all the sample was displaced at one angle.

Figure 61 illustrates how the three types of flow pattern relate to each other. A gradual flattening of the displacement profiles is apparent when moving from a free-flowing powder to a cohesive powder.

The relative ease with which the various powders flowed is also evident from the reproducibility of the data given in Table 11. If the average population standard deviation ($\overline{x}\,\sigma_N$) is calculated for the angle of initial displacement, i.e.; the angle at which displacement first occurs, the results obtained are, 2.6, 2.9 and 7.3, for free-flowing, semi free-flowing and cohesive powders respectively. Although the same number of data points have not been sampled in

Table 18. Categorization of Commercially Spray-Dried Samples in Terms of Flowability

Sample	Category	Sample	Category
Aluminium hydroxide	C	Detergent	FF
Aluminium silicate	FF	Semi - instant skimmed milk	SF
Dyestuffs	FF	Yogurt powder	C
Tungsten carbide	FF	Co - dried egg and skimmed milk	SF
Aluminium oxide	FF		
Titanium dioxide (Miro)	C	Titanium dioxide (Drytec-A)	SF
Ferrite	SF	Polymer (Drytec - A)	C
Kaolin	FF	Instant drink powder	C
Barium titanate	FF	Encapsulated flavour	C
tri - sodium orthophosphate	FF	Polymer (sodium salt)	C
Copper oxychloride	SF	Organic u.v. brightner	C
Lead chromate	FF	Sol. titanium salt (2FN)	C
2,3 - dichloro - propanoic acid	C	Sol. titanium salt (PN)	C
		Sol. titanium salt (R)	C
Copper ore	SF	Polymer (Drytec - B)	C
Coffee	C	Calcium stearate	C
Magnesium hydroxide	FF	Titanium dioxide (Drytec-B)	C
Dextran	C	Gum acacia	C
Clay (nozzle)	FF	Skimmed milk (high density powder)	C
Clay (rotary)	FF	Skimmed milk analogue	C
Glucose	C		

Key : FF = Free-flowing
SF = Semi free-flowing
C = Cohesive
2FN = Two-fluid nozzle
PN = Pressure nozzle
R = Rotary

Figure 61. Flowability of Commercially Spray-Dried Samples at 62% R.H. and 22 C

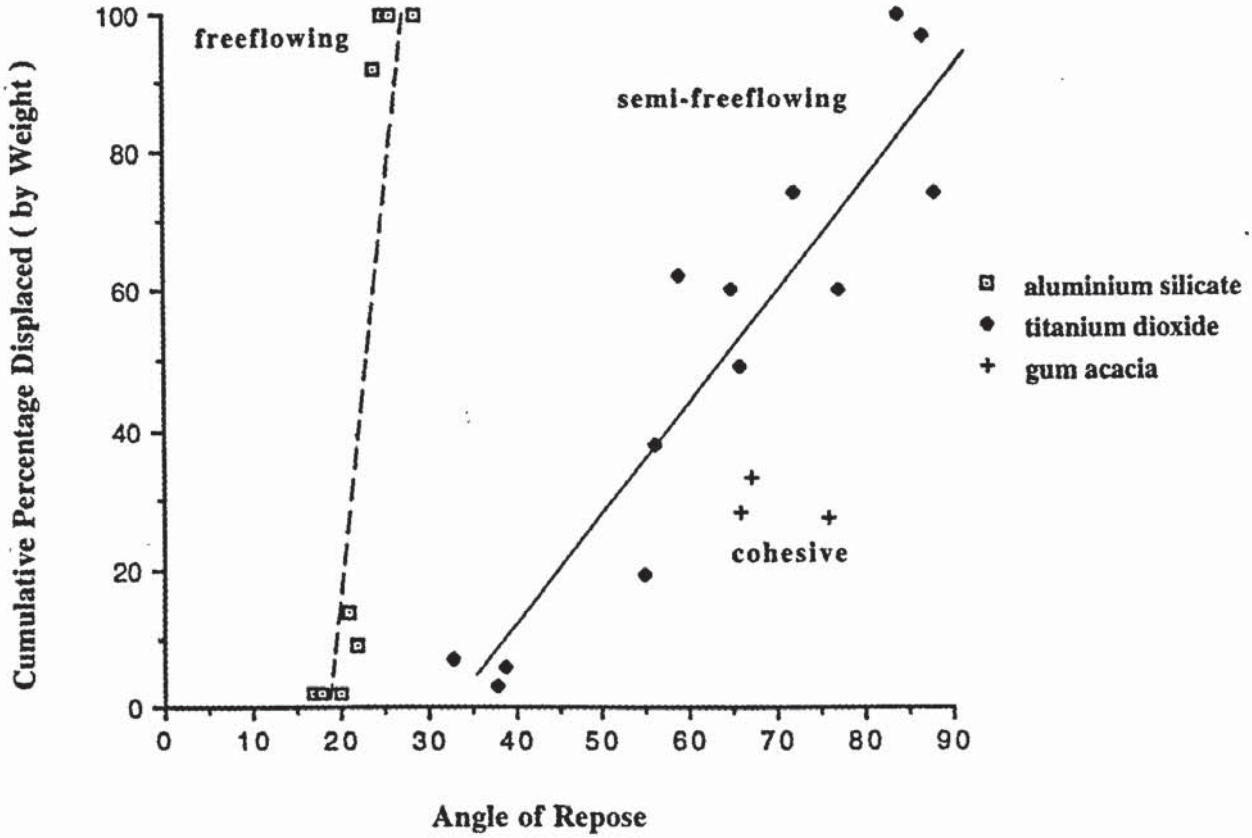

(Data points representative of 3 tests)

calculating $\bar{x}\ \sigma_N$ for each type of powder, the results suggest the data become less reproducible when moving from free-flowing to cohesive powders, i.e.; there is an increasing uncertainty as to whether the powder will flow.

Factors which influence the flowability of a powder have already been considered above, e.g.; particle-size, particle-size distribution, particle shape, moisture content, and the hygroscopic nature of the material. However, one of the most important considerations is the degree of particle agglomeration within the powder sample. Microscopic examination of all three types of powder revealed little or no particle agglomeration for the free-flowing powders, i.e.; agglomerates composed of two, or three particles (see Figures 62 and 63), whereas the semi free-flowing powders contained much larger agglomerates in greater numbers (see Figures 64 and 65). The majority of the cohesive powders exhibited mass agglomeration (see Figures 66 and 67).

Particle-size and particle-size distribution also have a considerable influence on powder flowability. Generally, the larger the particle-size and the narrower the particle-size distribution, the more free-flowing the powder. Comparison of particle-size data (Table 10) with flowability data (Tables 11 and 17) tends to support this, in that, the cohesive powders had a smaller mean particle-size compared to those of the free-flowing and semi free-flowing powders. The smallest and largest particle diameters for free-flowing and semi free-flowing powders were also larger than for cohesive powders.

Apart from the effect of agglomeration on powder flowability, Figures 62 to 67, suggest a correlation between particle morphology and powder flowability. Ideally, the particle surface of a free-flowing powder should be spherical with no surface asperities, i.e.; the particle surfaces should be smooth. The greater the sphericity of the particle and the smoother its surface the more likely it is to flow. Figures 62 to 67 show this, i.e.; the free-flowing powders are composed of very spherical, very smooth particles, whereas particles of the semi free-flowing powders and cohesive powders are far less spherical with increasingly irregular surface structures.

Figure 67 shows an exception to the rule. Although the particles are relatively smooth and spherical the degree of particle agglomeration is presumably the predominant factor determining its flowability.

Variations in powder moisture content had little effect on powder flowability (see Tables 12 and 13). This may be due to a number of reasons. For example, the changes in flowability may be too small for the powder inclinometer to measure. The hygroscopic nature of the samples chosen and factors such as particle-size, particle-size distribution, particle shape etc., may be far more dominant in terms of powder flow. Theoretically, the flowability of a powder should increase with decreasing moisture content since the liquid bridges between the powder particles weaken, i.e.; the capillary and / or viscous forces between the particles decrease.

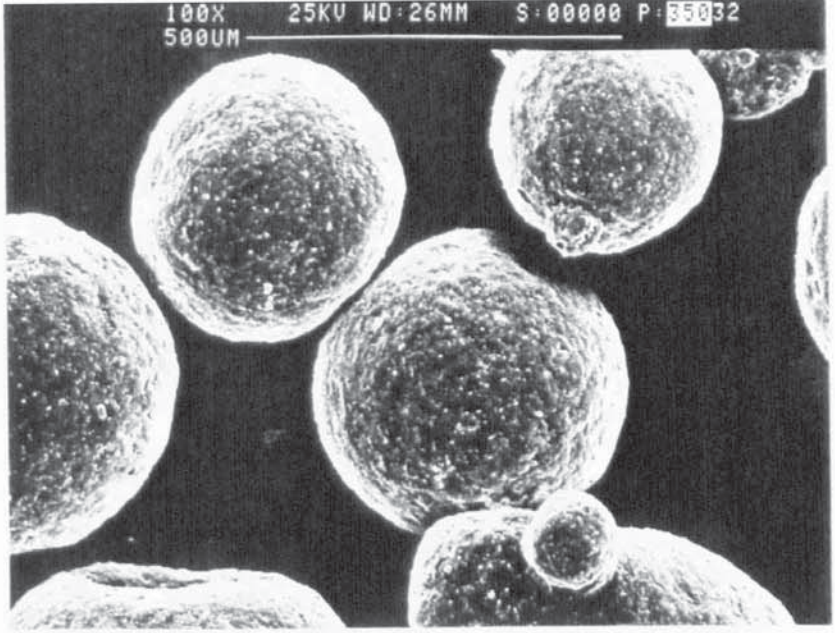

Figure 62.
free-flowing powder clay (rotary)
As Figure 43.

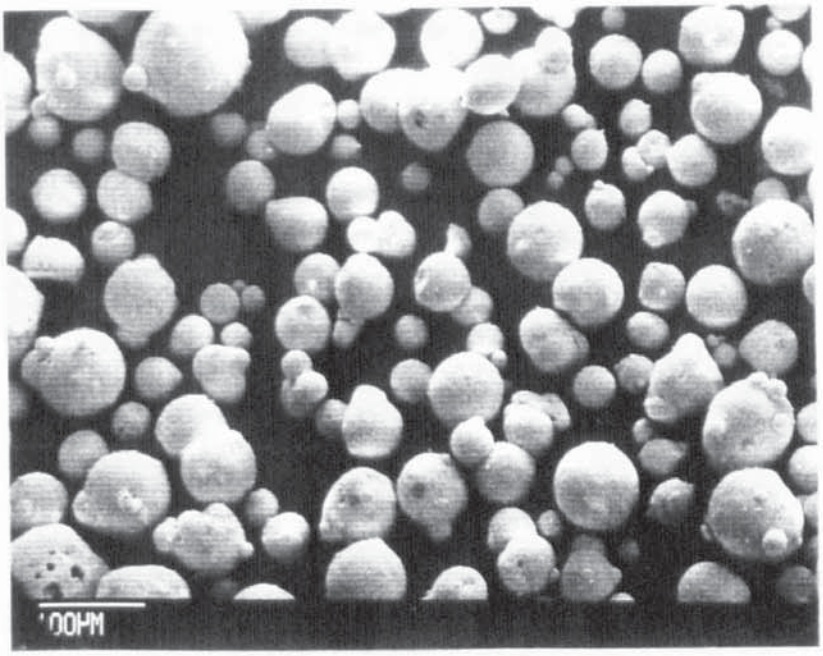

Figure 63.
free-flowing powder lead chromate
As Figure 46.

Figure 64.
semi-free-flowing powder clay (nozzle)
As Figure 42.

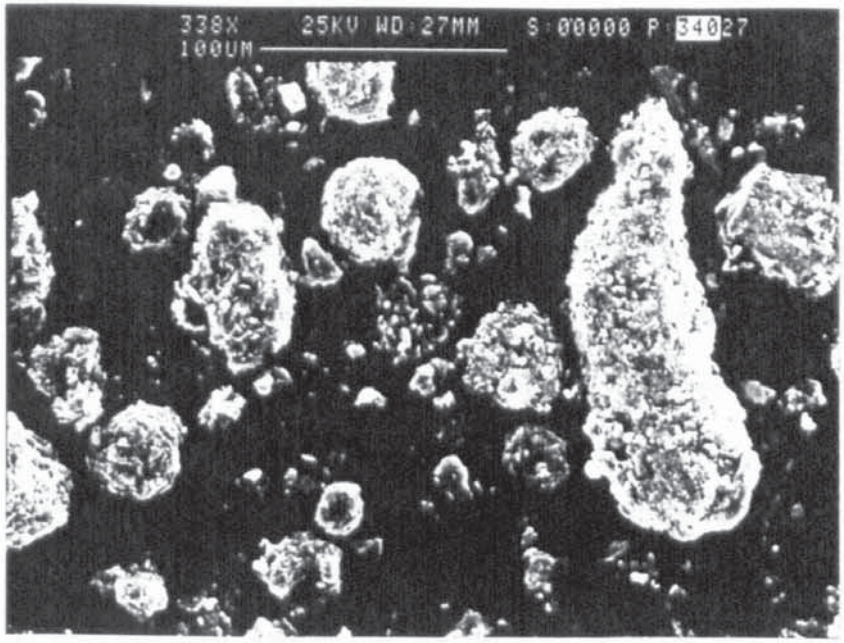

Figure 65.
semi-free-flowing powder
copper ore
In. conc. --
Temp. in 550°C
out 100°C

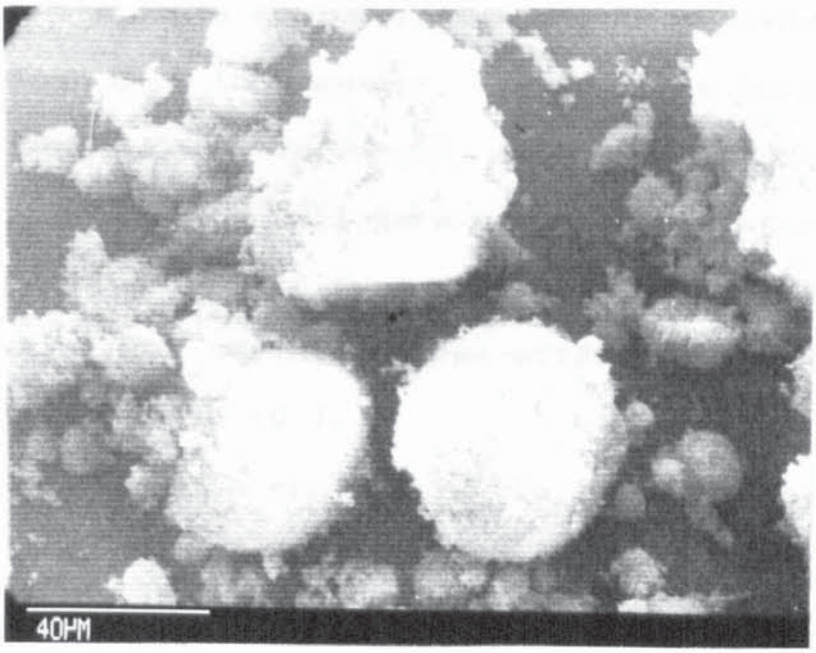

Figure 66.
cohesive powder
titanium dioxide
(Niro)
In. conc. 40% to 50% w/w
Temp. in 550°C
out 200°C

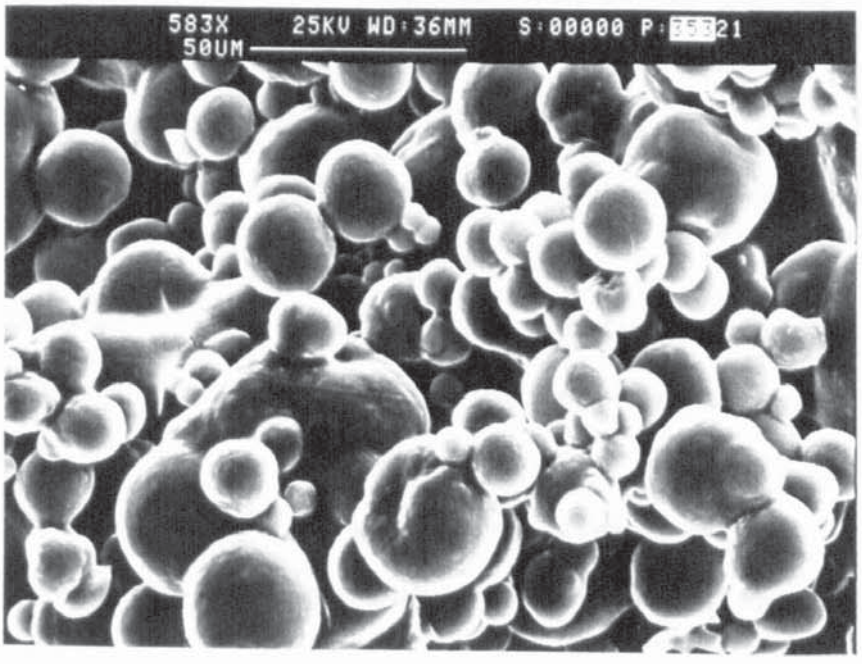

Figure 67.
cohesive powder
yogurt powder
As Figure 48.

Aluminium silicate, titanium dioxide (Drytec - A) and gum acacia were chosen for powder flowability measurements at different relative humidities because they typically represent the three types of flow behaviour, i.e.; free-flowing, semi free-flowing and cohesive respectively.

In an analogous manner to moisture content, interparticle attractions induced by Van der Waals and electrostatic forces can promote agglomeration within a powder. For particles less than 5 μm in diameter, these forces become very large compared to the particle weight. Such small particles are naturally cohesive and will form agglomerates without the need for chemical, solid or liquid bridges. Most of the powder samples show some surface charge effect when electrostatically charged (see Table 19).

The data shown in Table 19 was obtained by electrostatically charging a clean glass rod by rubbing with a silk cloth twenty times and then passing it over the surface of the powder. A similar weight of powder was used for each sample, approximately 0.2g. The relative strength of powder dispersion was noted in terms of,

Very strong - all the powder particles were completely dispersed

Strong - most of the powder particles were dispersed.

Weak - only the surface powder particles were dispersed

None - no particles dispersed

There was no apparent correlation with flowability data.

Table 19. Surface Charge Effects Exhibited by Commercially Spray-Dried Samples

Sample	Surface Charge	Sample	Surface Charge
Aluminium hydroxide	Yes (s)	Detergent	Yes (vs)
Aluminium silicate	Yes (vs)	Semi - instant skimmed milk	Yes (vs)
Dyestuffs	Yes (vs)	Yogurt powder	Yes (s)
Tungsten carbide	Yes (s)	Co - dried egg and skimmed milk	Yes (s)
Aluminium oxide	Yes (s)		
Titanium dioxide (Miro)	Yes (w)	Titanium dioxide (Drytec-A)	Yes (w)
Ferrite	Yes (w)	Polymer (Drytec - A)	None
Kaolin	Yes (s)	Instant drink powder	Yes (w)
Barium titanate	Yes (s)	Encapsulated flavour	Yes (w)
tri - sodium orthophosphate	Yes (vs)	Polymer (sodium salt)	Yes (s)
Copper oxychloride	Yes (s)	Organic u.v. Brightner	Yes (s)
Lead chromate	Yes (s)	Sol. titanium salt (2FM)	Yes (w)
2,3 - dichloro - propanoic acid	Yes (w)	Sol. titanium salt (PM)	Yes (w)
Copper ore	None	Sol. titanium salt (R)	Yes (s)
Coffee	None	Polymer (Drytec - B)	Yes (w)
Magnesium hydroxide	Yes (s)	Calcium stearate	Yes (w)
Dextran	None	Titanium dioxide (Drytec-B)	Yes (w)
Clay (nozzle)	Yes (w)	Gum acacia	Yes (w)
Clay (rotary)	Yes (vs)	Skimmed Milk (high density powder)	Yes (s)
Glucose	Yes (s)	Skimmed milk analogue	Yes (s)

Key : (vs) = Very strongly dispersed (w) = Weakly dispersed
(s) = Strongly dispersed

iv.) Particle Friability

The physical strength or friability of a single spray-dried particle is very difficult to determine because of its small physical size and the minute force needed to crush or test it, i.e.; probably μN or less. The methods used for the strength testing of powders and agglomerates, e.g.; tensile, compressive, attrition / abrasion and impact testing, are not applicable to single particles since the properties of particles in bulk are very different. Experimental apparatus has been built, e.g.; Ghadiri (193) describes a nanotester for measuring the strength of single crystals approximately 2 mm to 5 mm in diameter, but such devices still handle samples many times larger than most spray-dried particles.

Comparison of Table 14 with Tables 15 and 16 suggest there is a direct correlation between particle friability and particle structure. Particles with an agglomerate structure have exclusively F1 and F3 friabilities, whereas, skin-like structured particles have predominantly, but not exclusively, F2 and F4 friabilities. The crystalline morphologies, namely, tri - sodium orthophosphate and the organic u.v. brightner, have F1 and F3 friabilities respectively.

The essential difference between the two types of agglomerate particle in terms of friability lies in the density of the particle structure. Agglomerate particles with a friability of F1 have a very open, porous structure (see

Figures 35 and 36) with a minimum amount of material holding the granular structure together. Upon compression with very little force the grains simply slide apart and the particle structure collapses, producing a large amount of debris (see Figure 31). Conversely, agglomerate particles with a friability of F3 have a much denser structure (see Figure 44) and consequently a greater resistance to compression or deformation. Therefore, upon collapse, a relatively small amount of particle debris is produced (see Figure 33).

Because they are hollow the friability of skin-like particles has a greater dependency upon the rheological properties of the skin rather than the overall particle structure. Factors such as shell thickness must also be taken into account. Dextran ($C_6H_{10}O_5$)n and glucose ($C_6H_{10}O_6$) or glucose-based samples, e.g.; the instant drink powder, form the majority of the F2 category particles in Table 14. These materials are similar chemically, physically and structurally and their spray-dried particles appear to show identical rheological properties, i.e.; deforming under relatively light compression in a plastic manner. The samples with F4 category particles are also of a similar nature, comprising mainly dairy products which contain casein and albumins. On drying, these proteins form a much harder, less plastic skin than the dextran / glucose-based particles and resist deformation up to the yield point. Upon collapse, they shatter into a large number of jagged fragments.

Particles in the F2 and F4 categories which are not dextran, glucose (sub-microcrystalline) or protein based may be presumed to have similar or analogous rheological skin properties.

The particles of aluminium silicate (see Figures 40 and 41) exhibited an interesting anomaly. Their internal structure suggests a friability of F1, i.e.; very open and porous, but externally, the particles are coated with a thick binding material which reinforces the particle structure giving it greater strength and a friability of F3. The identity of the binder is unknown although for ceramic materials of a similar nature, e.g.; aluminium oxide, aluminium nitride, aluminium titanate, aluminosilicates etc., polyvinyl alcohol is commonly used with softening agents such as glycerol or ethylene glycol (192).

The effect of binders on the properties of individual particles, i.e.; particle strength, particle friability etc., is difficult to assess due to the lack of available data. The situation maybe analogous however, to the use of binders in particle agglomeration.

v.) <u>The use of Binders in Particle Agglomeration</u>

Binders and lubricants contribute significantly to agglomerate strength (213). Binders promote particle-particle bonding and lubricants reduce particle-particle friction to allow a lower void fraction and closer particle contact. Lubricants are most

relevant to pressure agglomeration, e.g.; extrusion, rolling, ram pressing etc., where they also act as mould release agents.

Literally hundreds of binders (see Table 20) have been patented, investigated or used for particle agglomeration (214-216). Most however, can be classified according to,

1. physical state - liquid, semi-solid, solid
2. chemical-type - organic, inorganic, compound
3. function - matrix, film, chemical-type

Matrix binders are those in which particles are imbedded in a continuous network of binding material. Film-type binders are commonly used as solutions or dispersions which deposit as a film on drying. Chemical binders develop their strength through a chemical reaction between the components of the binder, or between the binder and the agglomerated material.

The selection of a binder for a given application remains a matter of experience. A preliminary selection however, can be made on the basis of (214),

1. compatibility with the particle system, i.e.; the ability to wet the particle surfaces
2. the strength of binder required
3. waterproof requirements
4. contamination of the product
5. binder availability and cost

Table 20. Examples of Common Binders (214)

Matrix-type	Film-type	Chemical-type
coal-tar pitch	water	$Ca(OH)_2 + CO_2$
petroleum asphalt	sodium silicate	$Ca(OH)_2$ + molasses
Portland cement	plastic resins	$MgO + Fe_3O_4$
carnauba wax	glues/gums	$MgO + MgCl_2$
paraffin	tapioca	$Na_2SiO_3 + CaCl_2$
clay	glucose/sucrose	$Na_2SiO_3 + CO_2$
starch	molasses	
sugars	bentonite	
wood tars	starch	

Bonding mechanisms associated with particle-particle interaction are summarized in Table 21. In practice, more than one mechanism may act simultaneously. For example, in sintering ores, bonding through chemical reaction may also contribute to strength. With very fine powders, it is difficult to determine whether bonding through long-range forces or adsorption predominates. Mechanical interlocking of particles can also influence agglomerate strength, but its contribution is generally considered to be small in comparison with other mechanisms.

Information on the cohesion of particles can be obtained from theoretical considerations (213,217-219) and from direct measurement of particle agglomerate or powder strength (213). Theoretical estimates of bond strength, whether short-range chemical or long-range Van der Waals or electrostatic, are of little use however, due to the presence of other effects which determine the overall bond strength. These effects may be due

to the elastic response and extent of surface asperities on the particles, the existence of residual stresses at the particle-particle interface, and the presence of surface impurities such as oxides. Theoretical treatments of agglomerate strength also assume that interparticle bonds are uniformly distributed throughout the agglomerate interior. This assumption is reasonable in the case of wet agglomerates in the capillary or funicular state. However, in other situations, especially where solid bridging occurs, binder distribution is generally non-uniform, e.g.; in bonding by chemical reaction, bonding by pressure compaction, bonding by sintering or melting, or bonding by deposition of dissolved materials. In the latter case, liquid is drawn to the surface of the agglomerate by capillary action where it evaporates and deposits as a crust at, or near, the particle surface. The crust formation, or ' efflorescence ', is undesirable as it reduces the overall strength of the agglomerate to that of the bonded particle surface layer. One method of preventing this is to incorporate an ' inverse thermal gelling agent ' into the bridging solution. During the early stages of drying, the pore liquid is transformed into a gel which prevents it from moving to the particle surface, consequently, the binder is deposited in-situ.

Suitable gelling agents include (220),

For aqueous bridging liquids.	For organic bridging liquids.
corn starch	aluminium stearate
potato starch	aluminium palmitate
wheat flour	aluminium linoleate
methyl cellulose	

The gelling properties of rice starch and custard (cornflour) have also been noted in some single droplet drying experiments (200,210).

Measured values of agglomerate strength are wide-ranging. For example, the typical compressive strength of a powder agglomerate (221-225) (tests are usually performed on pellets 14 mm to 15 mm in diameter composed of particles 0.13 μm to 209 μm in diameter) ranged from 0.01 kg/cm^2 to 300 kg/cm^2. Values were dependent on, particle-size, void fraction, and the nature of the particle-particle bond. The latter had the greater influence on agglomerate strength, e.g.; a 2 to 3 order-of-magnitude increase in compressive strength was observed when changing from the adhesion of submicron powders by capillary liquid bonding, to bonding by solid bridges, e.g.; chemical binders, sintering etc..

Table 21. Classification of Binding Mechanisms (213,217)

Mechanism	Examples	Application
1. solid bridges	1. sintering, heat hardening	sintering of compacts in powder metallurgy
	2. chemical reaction, hardening binders,' curing '	cement binder for flue dust pellets
	3. melting due to pressure, friction	briquetting of metals, plastics
	4. deposition through drying	crystallization of salts in fertilizer granulation
2. immobile liquids	1. viscous binders, adhesives	sugars, glues, gums in pharmaceutical tablets
	2. adsorption layers	humidity effects in flow of fine powders
3. mobile liquids	1. liquid bridges (pendular state)	moistening / mixing of iron ore sinter mix
	2. void space filled or partly-filled with liquid (capillary and funicular states)	balling (wet pelletization) of ores
4. intermolecular and long-range forces	1. Van der Waals forces 2. electrostatic forces 3. magnetic forces	adhesion of fine powders during storage, flow and handling
5. mechanical interlocking	1. shape-related bonding	fracturing and deformation of particles under pressure

vi.) Particle Morphology

General structural considerations have been discussed in Section 6.2 v.

The three morphological types identified, i.e.; agglomerate, crystalline and skin-forming particles confirms the earlier work of Marshall et al (41,141) who classified laboratory spray-dried particles as crystalline, fine agglomerate and amorphous, or particles with film-forming tendencies. However, few explanations were previously given for the structures.

Two interesting morphological phenomena are the ' mushroom cap-shaped ' particles shown in Figures 69 and 70, and the presence of small particles within large particles (see Figures 52, 71 and 72). Mushroom cap-shaped particles, although not common (i.e.; none were observed in the samples obtained from industry) have been illustrated in the literature on a number of occasions. For example, Duffie and Marshall (41) showed photomicrographs of sodium silicate particles which have ruptured and curled-up to produce the characteristic mushroom cap-shape. Crosby and Marshall (141) reported a similar phenomenon with attapulgus clay slip and suggested the general shape might be caused by the capillary action of the dried particle surfaces drawing liquid and solids outward uniformly around the droplet, thus creating subatmospheric internal pressures which eventually result in collapse of the particle. This seems unlikely however, given

the relative strength of most spray-dried particles, particularly dried clays, in relation to the magnitude of the vacuum produced. Duffie and Marshall's observation of ruptured sodium silicate particles curling up may offer a better explanation, in that, both the sodium silicate and clay particles have skin-forming or analogous skin-forming properties. Consequently, they are pliable during drying. The mushroom cap-shape may therefore be formed due to the particle's resistance to airflow as it moves through the drying chamber (see Figure 68).

The phenomenon of small particles within large particles cannot arise simply from them being able to enter a larger particle via a blowhole or crater, although this probably does occur (see Figure 73). The smaller particles actually appear to be formed inside the larger particle. Figure 71 is a particularly good example, where the larger of the two internal particles is too big to have fallen through the crater or blowhole.

Because of their opaque skin, this phenomenon has been readily observed in the spray-dried coffee sample, where, in some instances, the internal particle(s) are almost half the size of the outer particle.

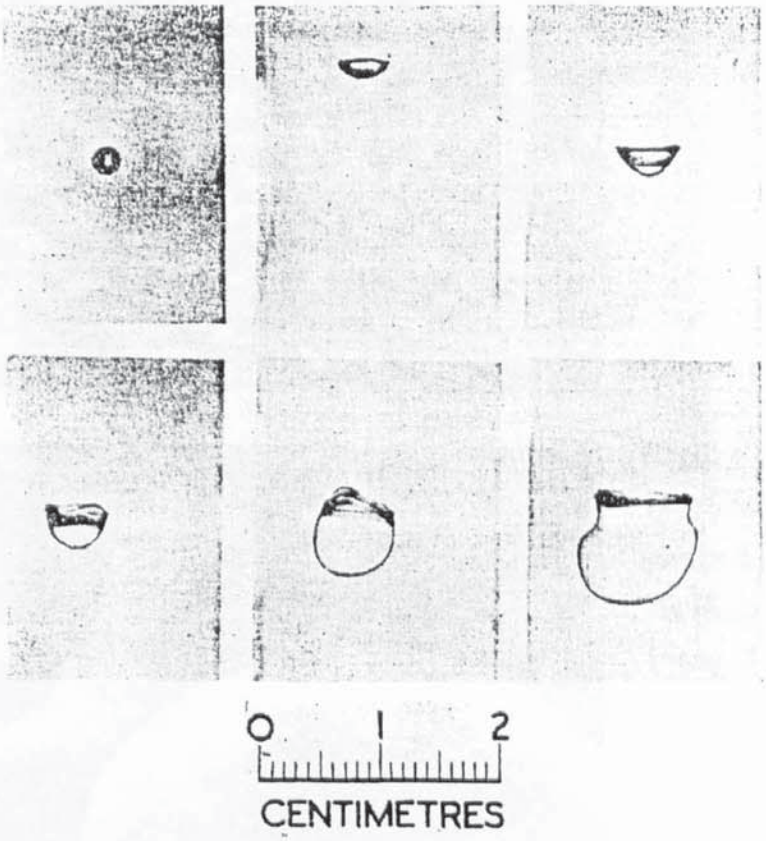

Figure 68. High-speed photographs showing the break-up mechanism of a droplet suddenly impacted by a high-velocity air jet (205)

Figure 69.
mushroom cap shaped particles
procion dye (191)
(mag. x 30)

Figure 70.
mushroom cap shaped particles
As Figure 69.
(mag. x 330)

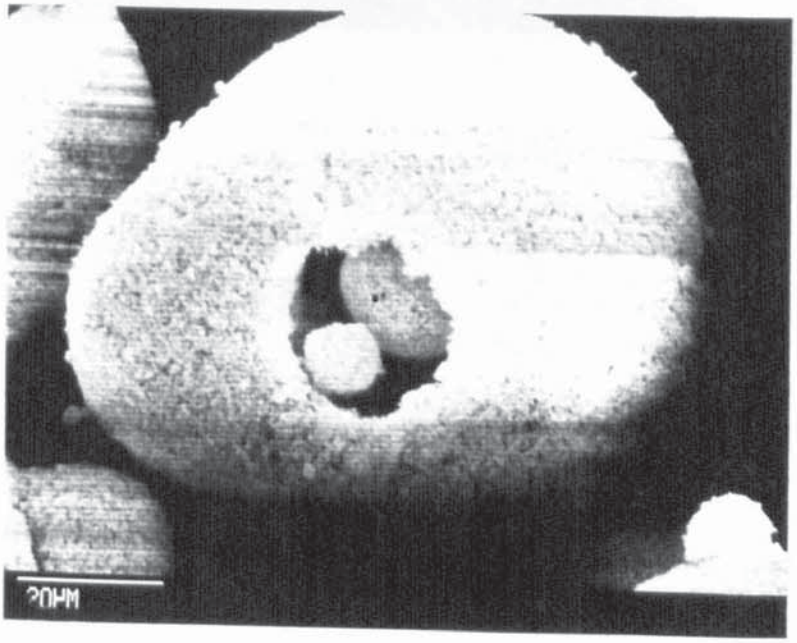

Figure 71.
lead chromate
As Figure 46.

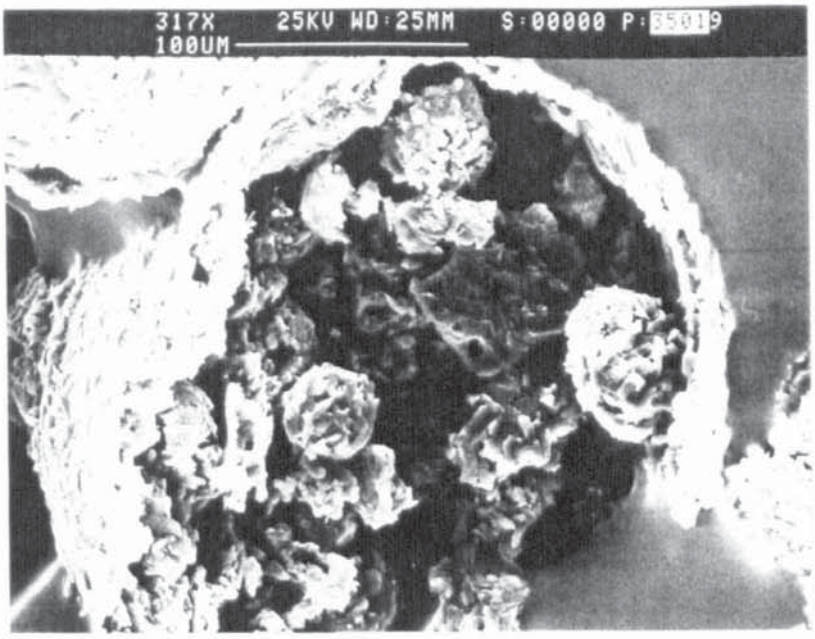

Figure 72.
tri-sodium orthophosphate
As Figure 56.

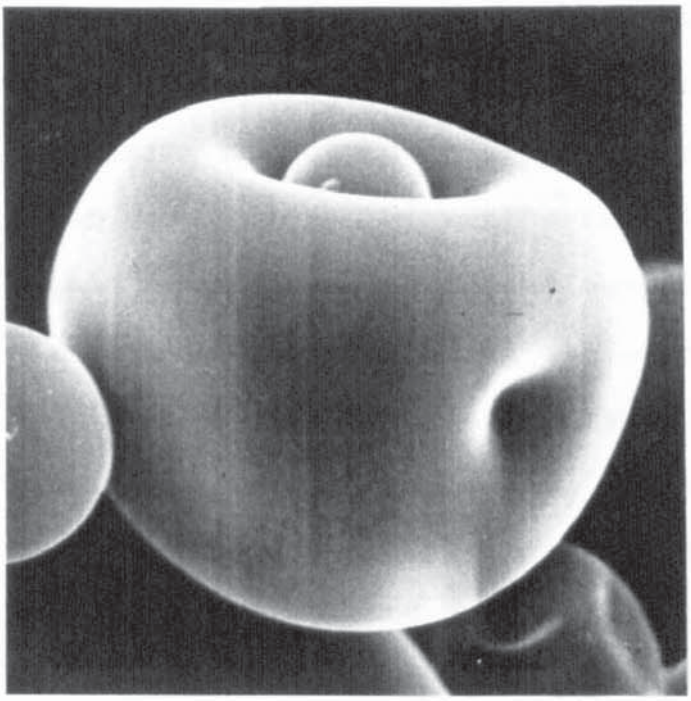

Figure 73.
small particle lodged in larger particle
Procion dye (191)
(mag. x 2000)

THE EVAPORATION OF PURE LIQUID DROPLETS

6.4) Introduction

The single droplet drying apparatus described in Chapter Five was developed to study the drying behaviour of droplets containing dissolved or suspended solids. This apparatus was first commissioned by monitoring the evaporation of pure liquid droplets under forced convection.

Information concerning the evaporation of pure liquid droplets is well-documented. Maxwell (42) considered the problem in terms of molecular diffusion in 1890, and, together with significant contributions by Langmuir (75), Fuchs (102), Frossling (34,35) and Marshall et al (52), provided much of the impetus for research in the area. Over the past one hundred years therefore, the evaporative phenomena both in terms of molecular diffusion and under forced convection have been thoroughly-investigated (65,89,96,97,101). This provides a unique data reference for researchers working in the field and allows the calibration of experimental apparatus in terms of the fluid and flow dynamics which govern the evaporative process by direct comparison of correlated data.

6.5) Determination of Heat and Mass Transfer Coefficients - Calibration of the Single Droplet Drying Apparatus

Using the single droplet drying apparatus (see Sections 5.4 and 5.5) the average heat and mass transfer film coefficients for single droplets of water, butan-1-ol, ethanol and phenol were determined under conditions of forced convection. Experiments were carried out over a temperature range of 50°C to 200°C at a constant air velocity of 1.0 m/s. Data were calculated from the following equations,

for mass transfer (106),

$$k = \frac{dm}{dt} \cdot \frac{1}{Ae} \cdot \frac{RcTa}{Mw(p_s - p_A)} \quad \ldots\ldots\ldots\ldots\ldots (76)$$

and for heat transfer (194),

$$h_T = \frac{\lambda \rho_D}{6 \Delta T} \cdot \frac{1}{De^2} \cdot \frac{d(De^3)}{dt} \quad \ldots\ldots\ldots\ldots\ldots (77)$$

where Ae = equivalent surface area of droplet
Rc = universal gas constant
Mw = molecular weight
ρD = droplet density
De = equivalent droplet diameter

Derivations of equations 76 and 77 are given in Appendix A 4.1. From these, given the physical properties of the system, the film coefficients could be obtained by simply monitoring the decrease in droplet diameter with time.

To compare the results with other published data and thus calibrate the apparatus, equations 76 and 77 were modified to express the mass and heat transfer coefficients in terms of the Sherwood and Nusselt number, i.e.;

$$Sh = \frac{dm}{dt} \cdot \frac{1}{Ae} \cdot \frac{RcTa}{Mw(p_s - p_A)} \cdot \frac{De}{Dv} \quad \ldots\ldots\ldots\ldots (78)$$

and,

$$Nu = - \frac{\lambda \rho_D}{4 \, Kd \, \Delta T} \cdot \frac{d(De^2)}{dt} \quad \ldots\ldots\ldots\ldots\ldots (79)$$

These values were then correlated by the Ranz and Marshall equation (52), a dimensionless equation closely associated with the spray drying process (see equations 13 and 14).

The results are presented in Figures 74 to 78 and the raw data in Appendix A 4.0.

Figure 74. Mass Transfer Correlations for Water Droplets, 50°C to 200°C

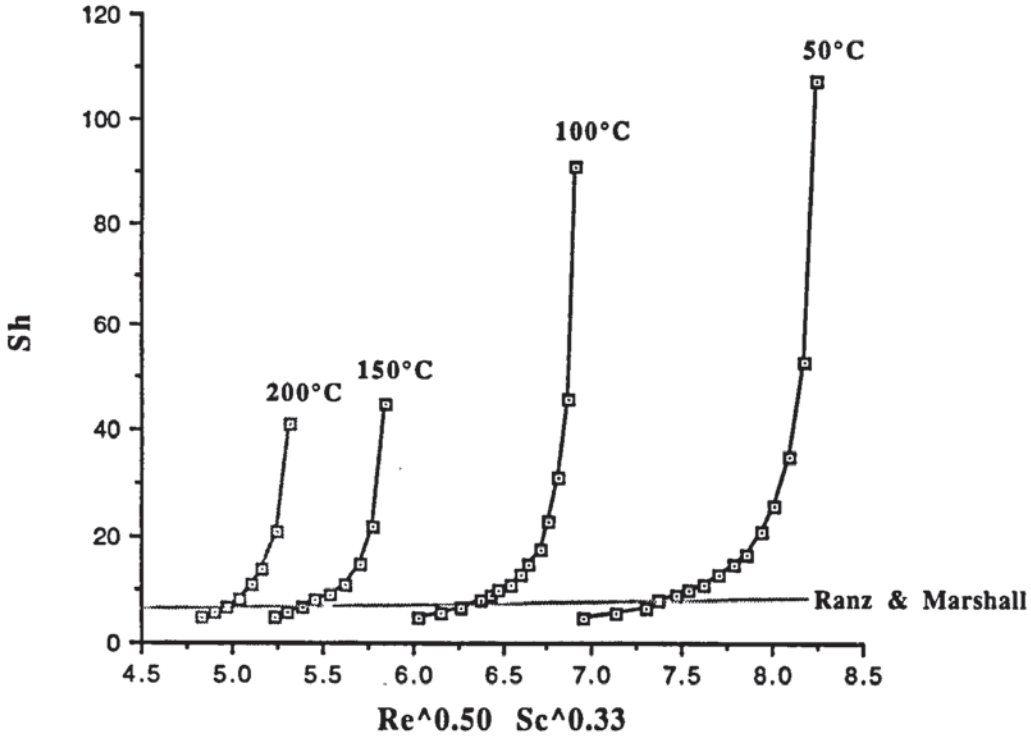

(Data represents an average of 3 plots)

Figure 75. Heat Transfer Correlations for Water Droplets, 50°C to 200°C

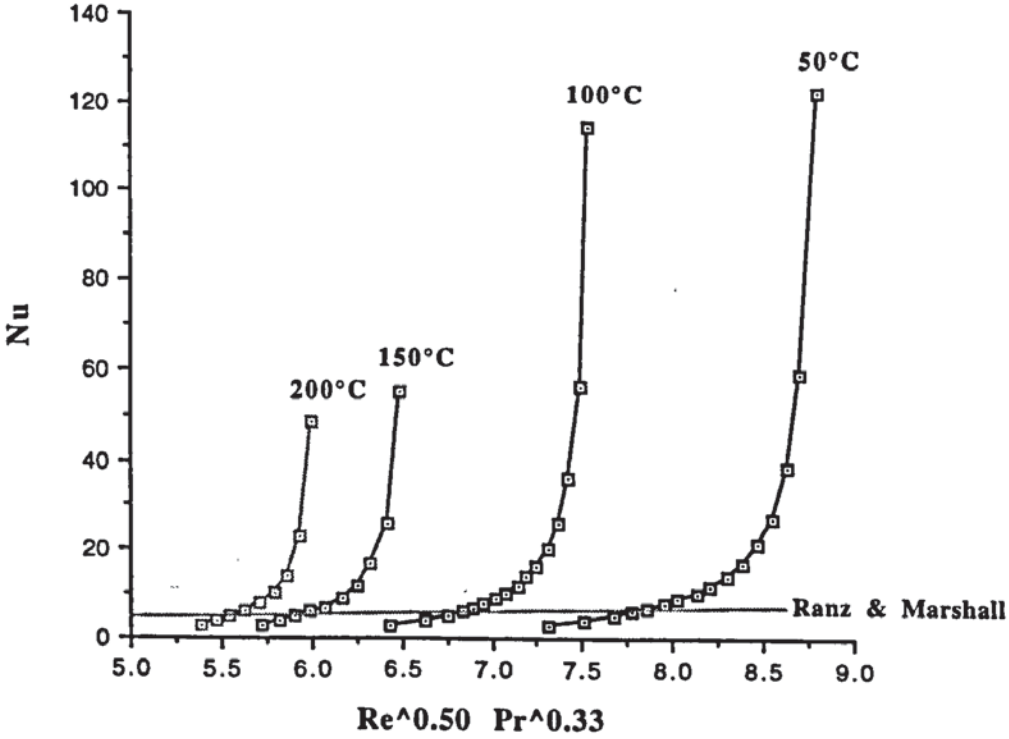

(Data represents an average of 3 plots)

Figure 76. Heat Transfer Correlations for Ethanol Droplets at 50 °C

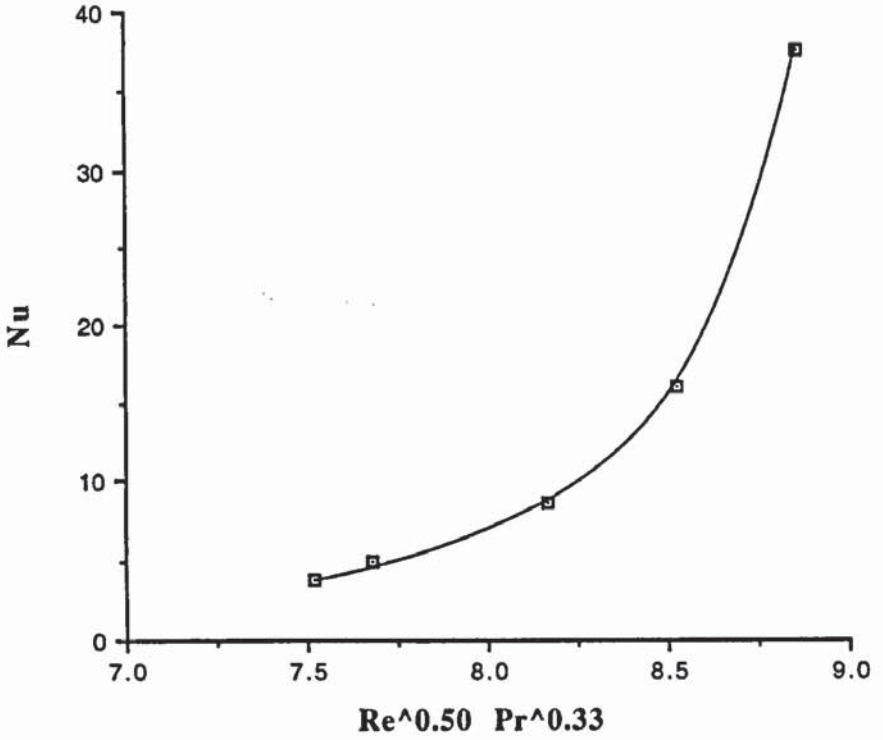

(Data represents an average of 3 plots)

Figure 77. Heat Transfer Correlations for Butan-1-ol Droplets at 50 °C

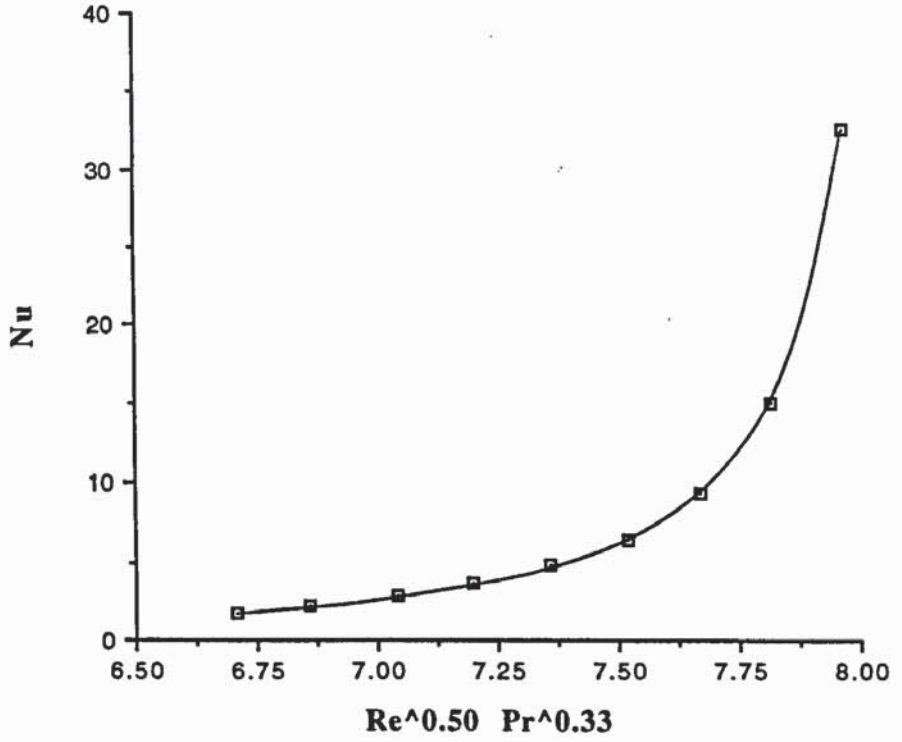

(Data represents an average of 3 plots)

Figure 78. Heat Transfer Correlations for Phenol Droplets at 100°C

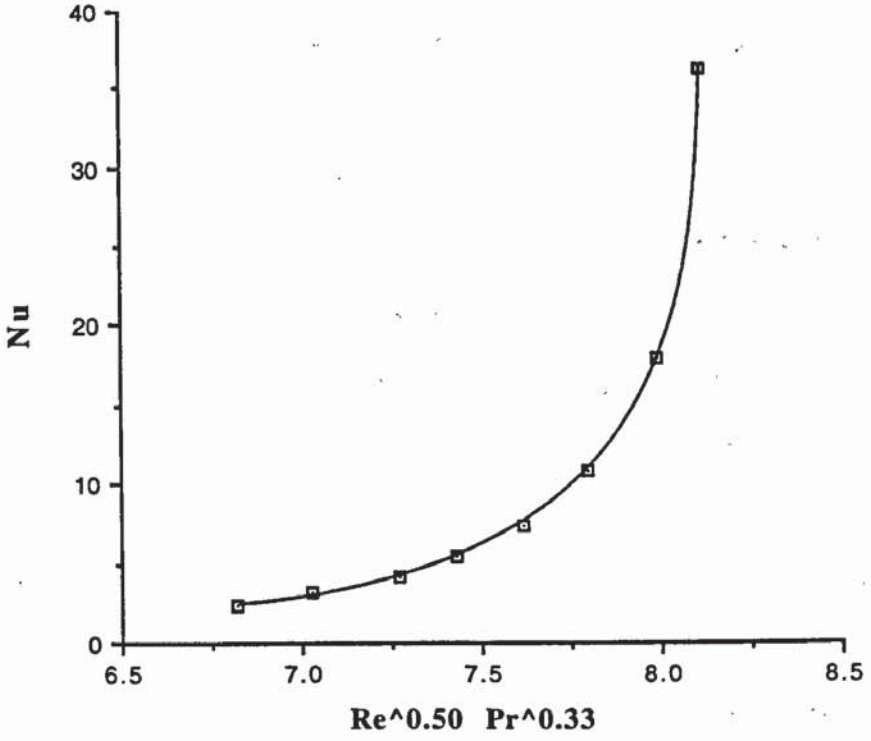

(Data represents an average of 3 plots)

6.6) Measurement of Droplet Diameters

By playing-back a recorded video tape of each experimental run on a 70 cm television screen, the evaporation of a single droplet was monitored by measuring the decrease in the droplet diameter as a function of time. Frame by frame advancement of the video tape gave a resolution of 0.01 s.

Measurements were made by placing a flexible cellulose acetate graticule with a horizontal and vertical millimetre scale directly onto the surface of the television screen, thus counteracting any curvature of the screen surface, so that the intersection of the two scales coincided with the centre of the droplet (see Figure 79). The equatorial (X) and axial (Y) diameters were measured and an equivalent droplet diameter defined. Any optical distortion of the droplet image by the video camera, objective lens and / or the television screen was identified by checking the linearity of a millimetre scale behind the droplet when on screen. The exact magnification of the droplet, and hence the actual size of the droplet, was obtained by comparing the diameters of the on-screen and off-screen support filament. The off-screen or actual filament diameter was measured with a micrometer.

Droplet masses, i.e.; $m = (\pi D^3 \rho_D) / 6$, were calculated from droplet diameter data using regression analysis.

Figure 79. Measurement and Definition of Equivalent Droplet Diameter

The third dimension Dz is assumed to be equivalent to Dx. An equivalent droplet diameter De has therefore been defined as,

$$De = \frac{Dx + Dy + Dz}{3}$$

$$= \frac{2Dx + Dy}{3}$$

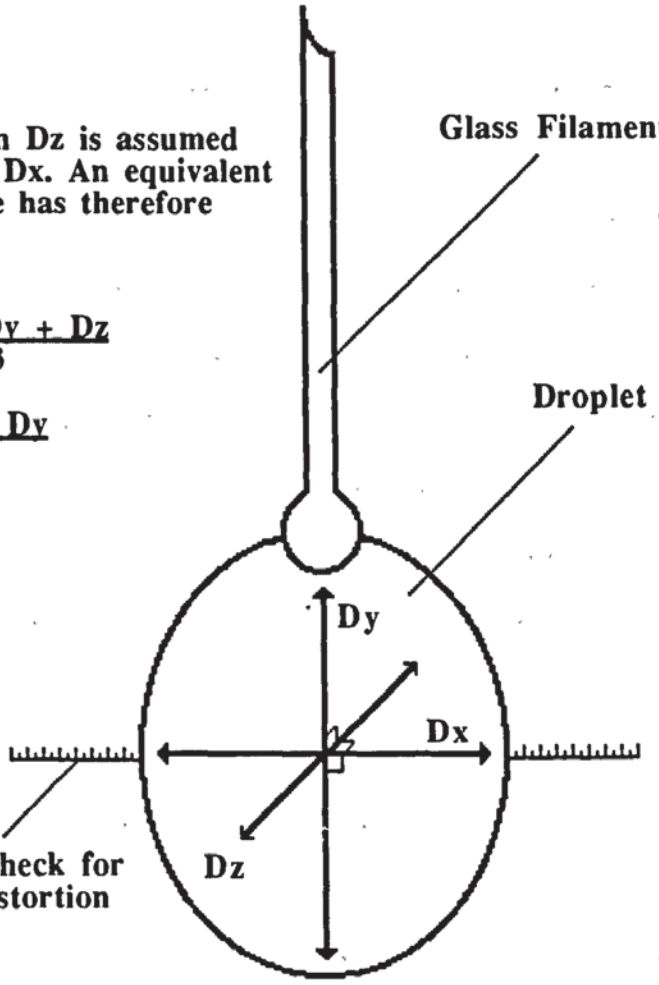

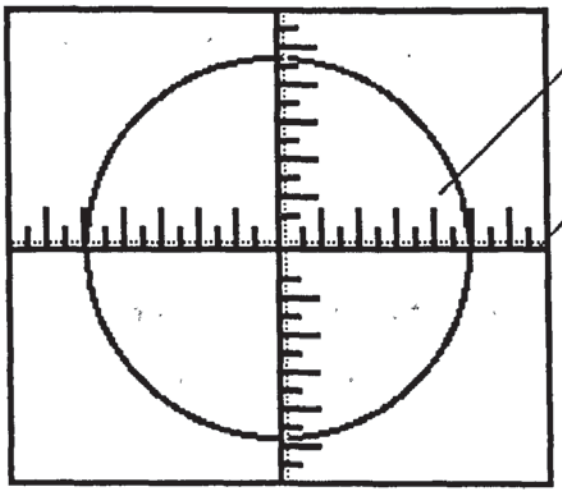

6.7) Discussion

Figures 80 to 86 show the decrease in droplet diameter with time for single droplets of water, butan-1-ol, ethanol and phenol. Measurements were carried out over a Reynolds number range of 581 to 1128, with droplet diameters ranging from 1.40 mm to 1.93 mm. In each case, a straight-line graph, or linear equation of the form $y = mx + c$, was obtained with average correlation coefficients of 0.974 to 0.998 (see Table 22). An increase in scatter of data presented in Table 22 is also apparent for water droplets with an increase in temperature.

All experiments were carried out at an air velocity of 1.0 m/s. Ideally, velocities in the region of 1.8 m/s were considered desirable to produce droplet Reynolds numbers comparable to those found in a commercial spray drier (52), but velocities greater than 1.0 m/s produced excessive movement of the suspended droplet which would have rendered diameter measurement difficult and introduced another variable into the heat and mass transfer processes.

Heat transfer to the droplet via radiation from the surrounding environment, i.e.; the working section of the apparatus, and by conduction through the support filament were calculated. In both cases the amount of heat transferred to the droplet was found to be negligible (see Appendix A 4.1).

Figure 80. Droplet Diameter Squared vs Time for Water Droplets at 50°C

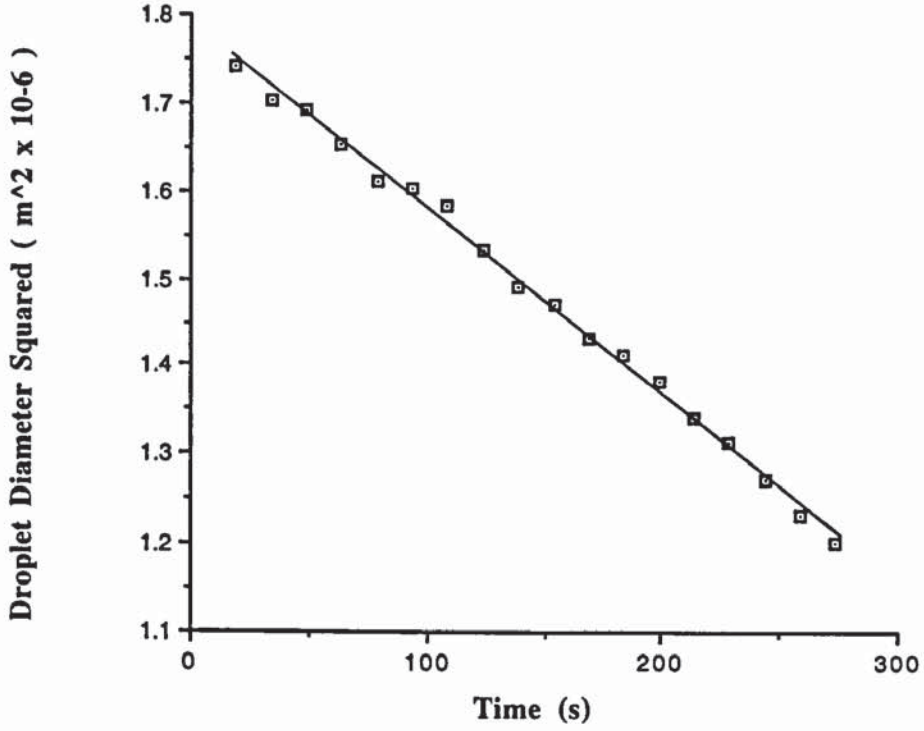

(Data represents an average of 3 plots)

Figure 81. Droplet Diameter Squared vs Time for Water Droplets at 100°C

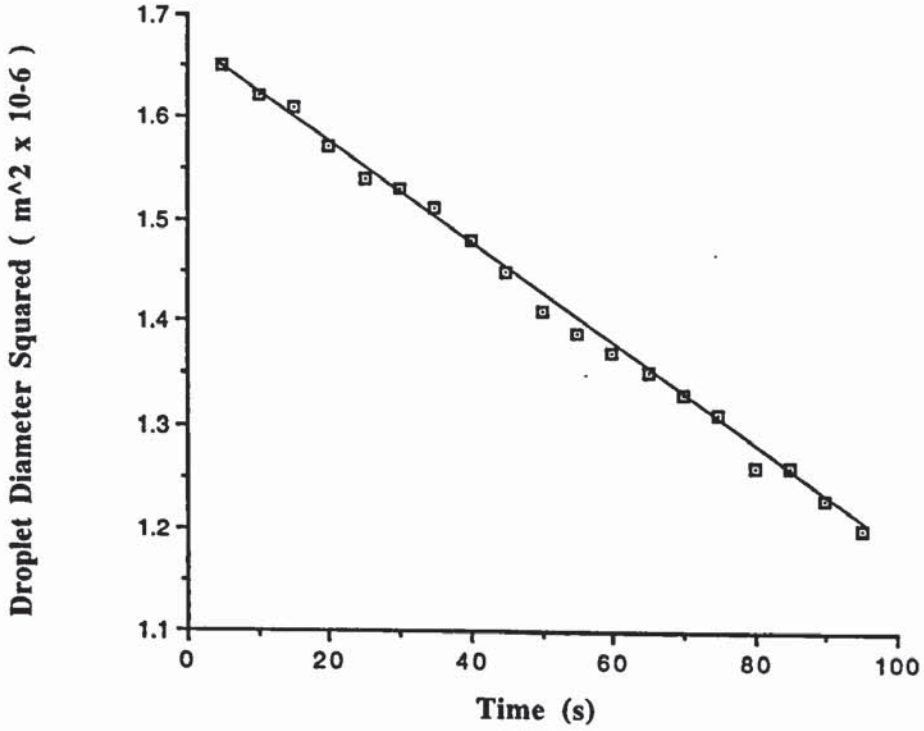

(Data represents an average of 3 plots)

Figure 82. Droplet Diameter Squared vs Time for Water Droplets at 150°C

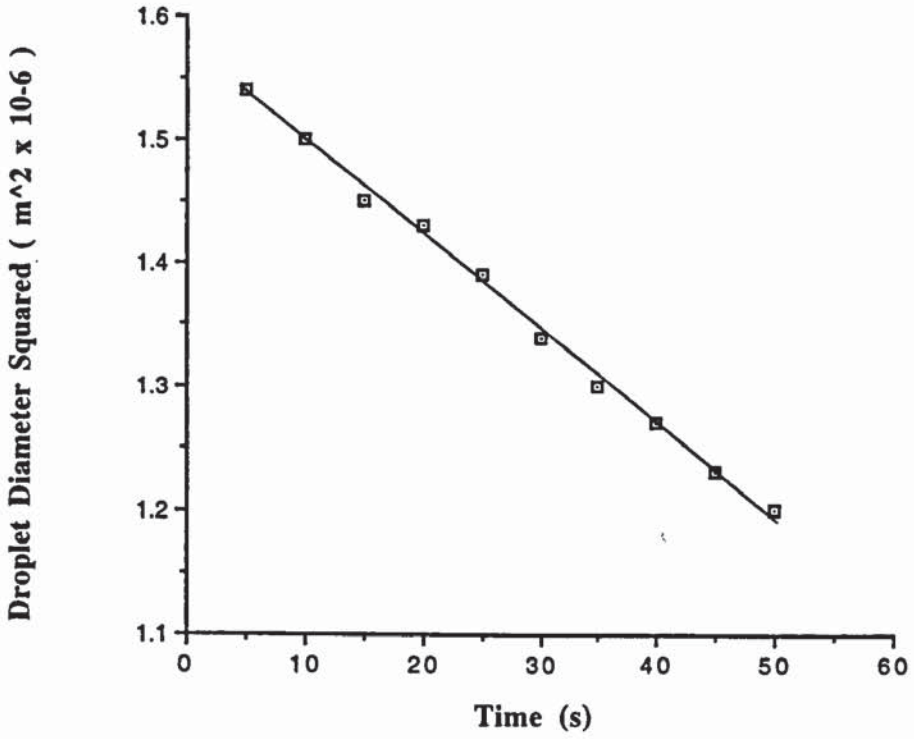

(Data represents an average of 3 plots)

Figure 83. Droplet Diameter Squared vs Time for Water Droplets at 200°C

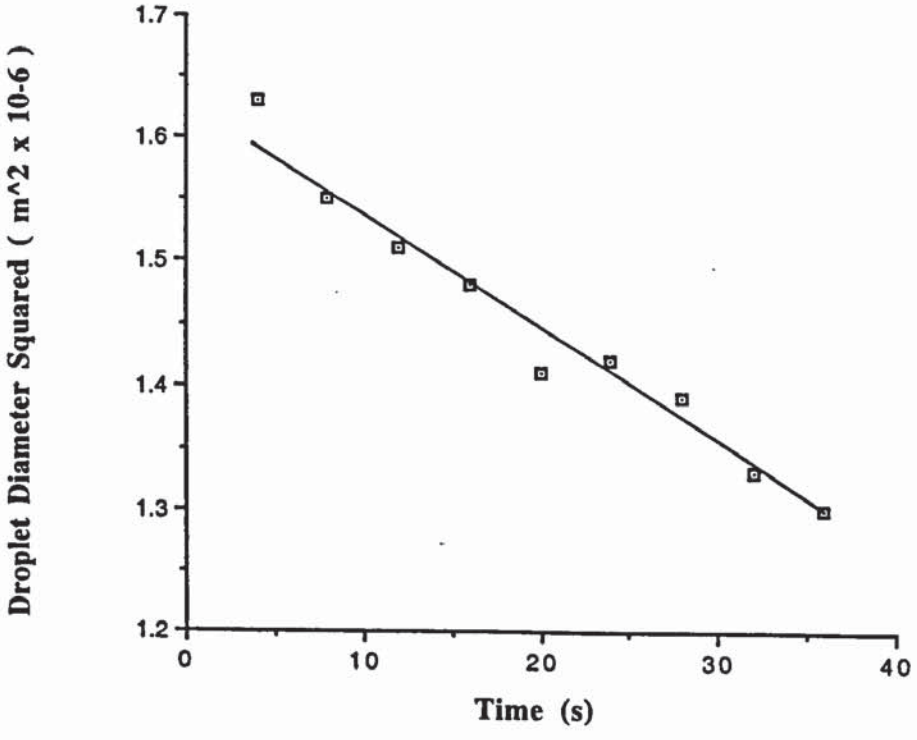

(Data represents an average of 3 plots)

Figure 84. Droplet Diameter Squared vs Time for Ethanol Droplets at 50 °C

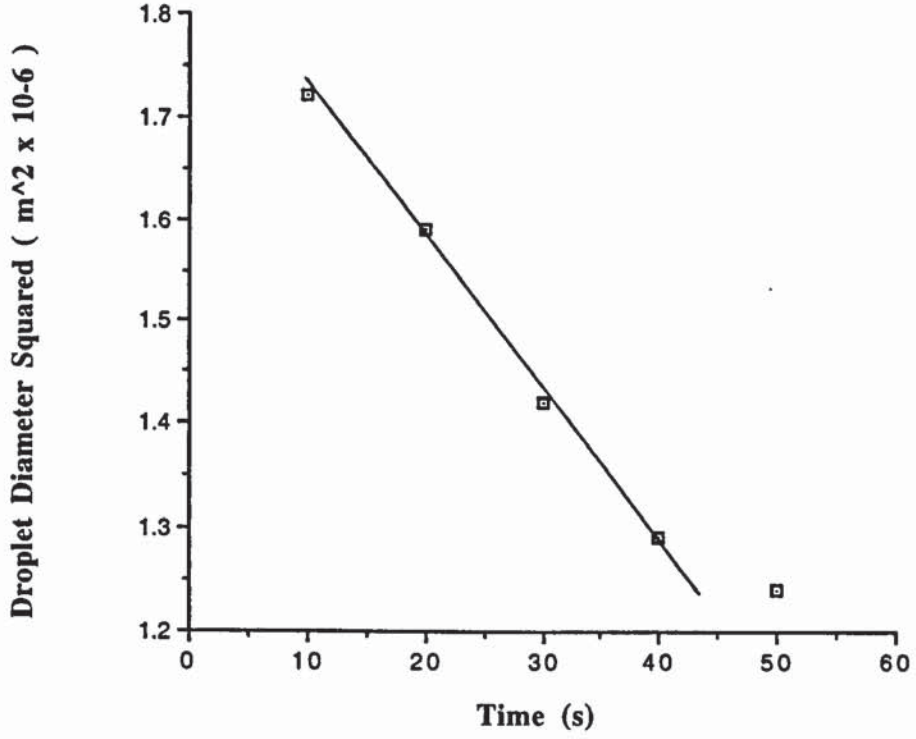

(Data represents an average of 3 plots)

Figure 85. Droplet Diameter Squared vs Time for Butan-1-ol Droplets at 50 °C

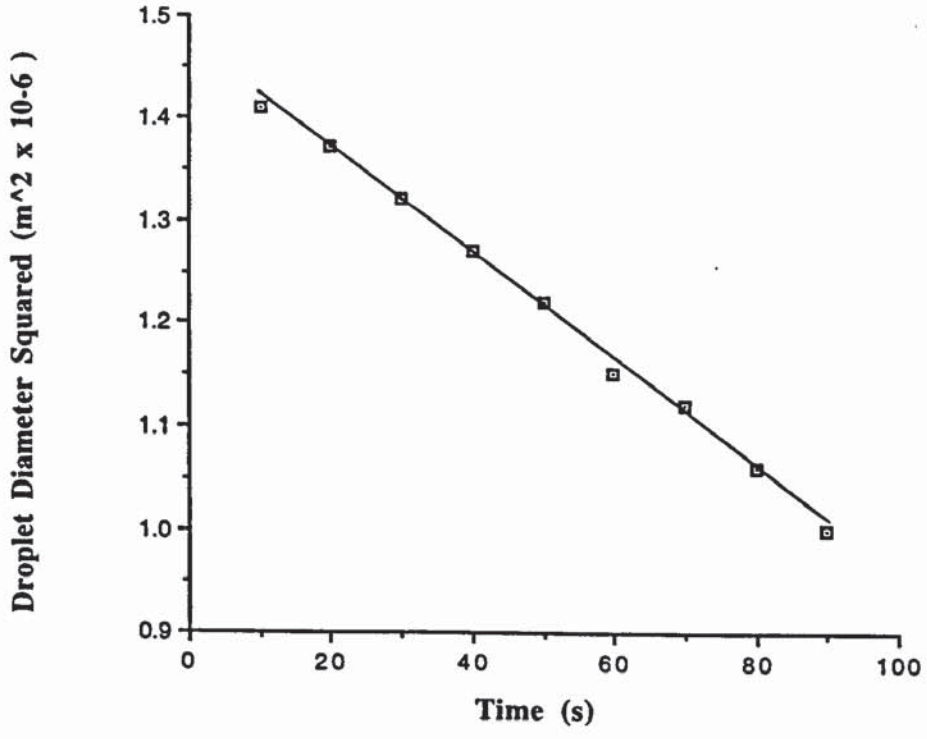

(Data represents an average of 3 plots)

Figure 86. Droplet Diameter Squared vs Time for Phenol Droplets at 100°C

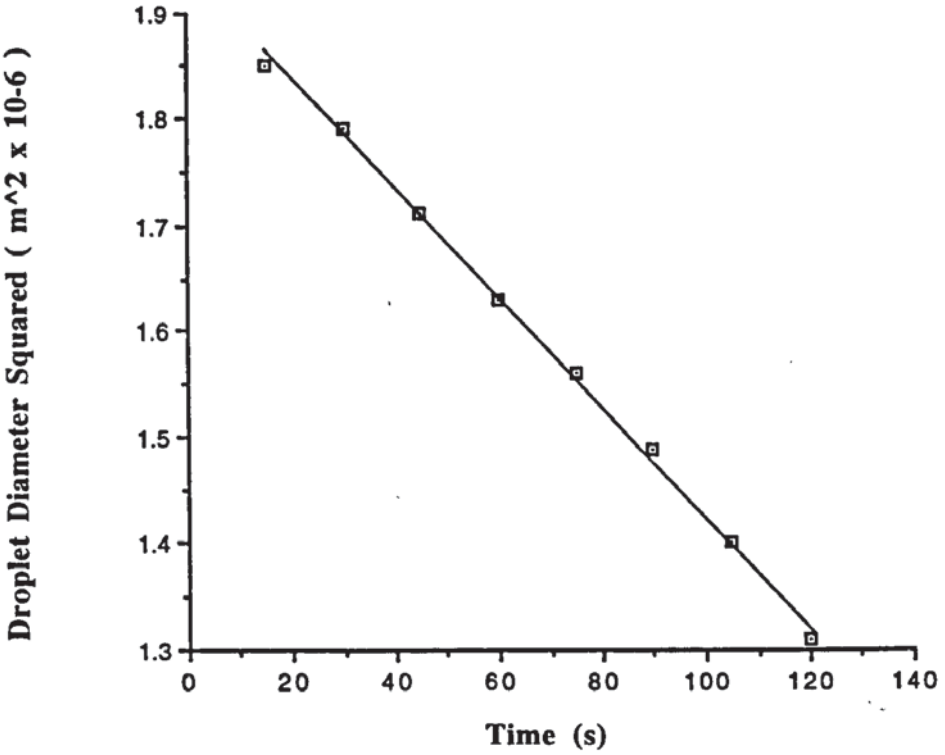

(Data represents an average of 3 plots)

Table 22. Average Correlation Coefficients for Droplet Diameter versus Time Data

Sample Liquid	Air Temperature	Average Correlation Coefficient †	Standard Deviation ††
Water	50°C	0.997	0.001
	100°C	0.994	0.002
	150°C	0.990	0.007
	200°C	0.974	0.006
BuOH	50°C	0.996	0.003
EtOH	50°C	0.995	0.004
PhOH	100°C	0.998	< 0.001

† Average of three runs per temperature
†† Standard deviation of the correlation coefficients

The droplet diameter versus time data is generally consistent with classical evaporation theory. For example, if the rate of evaporation is considered in terms of mass transfer, i.e.; equations 9 and 10, then,

$$\frac{dm}{dt} = Dv2\pi D\ (Ci-Cb) \quad \ldots\ldots\ldots\ldots\ldots\ldots (80)$$

alternately, if $m = (\pi\ D^3\ \rho_D\ ) / 6$,

$$\frac{(\pi\ D^3\ \rho_D\ ) / 6}{t} = Dv2\pi D\ (Ci-Cb) \quad \ldots\ldots\ldots\ldots (81)$$

if $x = (\pi\ \rho_D\ )$ and $y = Dv2\pi\ (Ci-Cb)$, then,

$$\frac{x\ (D^3 / 6\ )}{t} = yD \equiv \frac{(x / 6\ )\ D^3}{t} = yD \quad \ldots\ldots\ldots (82)$$

and,

$$\frac{(x / 6\ )\ D^3}{yD} = t \equiv \frac{(x / 6\ )}{y} D^2 = t \quad \ldots\ldots\ldots (83)$$

therefore, the droplet diameter squared should decrease proportionately with time,

$$D^2 \alpha\ t$$

The heat and mass transfer correlations shown in Figures 74 to 78 show a marked discrepancy from those obtained by Ranz and Marshall - plotted for comparison in Figures 74 and 75 - and many other workers (see Table 23). Instead of the expected linear relationship between Sh versus $Re^{0.5}\ Sc^{0.33}$ and Nu versus $Re^{0.5}\ Pr^{0.33}$, an exponential one was obtained of the form,

$$Sh = A\ e^{-a}\ .\ 10^{(M\ Re^{0.5}\ Sc^{0.33})} \qquad \ldots\ldots\ldots (84)$$

and,

$$Nu = B\ e^{-b}\ .\ 10^{(N\ Re^{0.5}\ Pr^{0.33})} \qquad \ldots\ldots\ldots (85)$$

where A, B, a, b, M and N are correlation factors, values of which are given in Table 24.

Table 23. Correlation of Mass Transfer Data from Suspended Droplets (119)

Investigator	Experimental Range		$Sh = A + KRe^a Sc^b$ Correlation			
	Re	Droplet Diameter (mm)	A	K	b	q
Frossling (34,35)	2-1300	0.1-2	2	0.55	0.33	0.5
Ranz and Marshall (52)	0-200	0.6-1.1	2	0.6	0.33	0.5
Hsu et al (89)	50-350	1.7	2	0.54	0.33	0.5
Garner and Suckling (97)	100-700	9.5-19	2	0.95	0.33	0.5
Manning and Gauvin (65)	1-20	0.01-0.25	2	0.60	0.33	0.5
Garner and Grafton (96)	20-850	12.7	44	0.59	0.33	0.5
Maisel and Sherwood (51)	2000-40000	26-35	0	0.43	0.33	0.56
Linton and Sherwood (195)	800-10000	12.7	0	0.43	0.33	0.56
Yen and Thodos (196)	1750-9000	51	0	0.36	0.33	0.58
Evnochides and Thodos (197)	2000-12000	51	0	0.32	0.33	0.6
Pasternak and Gauvin (101)	500-5000	10	0	0.69	0.33	0.51

Table 24. Correlations for Equations 84 and 85

Sample Liquid		Temperature	Correlation						Correlation Coefficient	
			A	a	M	B	b	N	Sh	Nu
Water	1	50°C	8.98	6	0.82	1.35	5	0.74	0.956	0.940
	2		1.75	6	0.94	6.32	6	0.81	0.962	0.923
	3		1.73	7	0.97	2.66	7	0.89	0.949	0.930
	4	100°C	6.20	7	1.11	4.23	7	1.05	0.940	0.926
	5		1.68	7	1.20	2.54	7	1.08	0.950	0.932
	6		5.06	7	1.15	5.87	7	1.05	0.947	0.928
	7	150°C	1.12	7	1.43	2.18	7	1.24	0.964	0.942
	8		1.96	7	1.40	5.84	7	1.19	0.977	0.966
	9		1.19	6	1.24	4.87	7	1.18	0.948	0.967
	10	200°C	1.73	7	1.54	6.27	7	1.26	0.962	0.942
	11		4.11	7	1.46	1.64	7	1.36	0.939	0.978
	12		1.26	9	1.93	1.40	8	1.52	0.987	0.973
BuOH	1	50°C	4.79	6	0.71	1.86	6	0.87	0.981	0.979
	2		8.96	6	0.69	5.85	5	0.68	0.991	0.962
	3		1.37	5	0.66	1.23	5	0.77	0.961	0.974
EtOH	1	50°C	-	-	-	8.79	5	0.60	-	0.922
	2		-	-	-	3.18	4	0.57	-	0.995
	3		-	-	-	5.54	4	0.52	-	0.985
PhOH	1	100°C	-	-	-	6.96	4	0.56	-	0.953
	2		-	-	-	2.24	6	0.83	-	0.955
	3		-	-	-	6.07	6	0.79	-	0.964

Figures 74 and 75 for water droplets clearly show an increase in the rate of heat and mass transfer with an increase in drying air temperature. This is to be expected as the driving force ΔT, Ta - Td, is increased.

The general exponential nature of all the data, which indicates enhanced heat and mass transfer, is more difficult to explain. Although this phenomenon has been reported previously (117,119-121) and more recently by Akbar (198) and Oteng-Attakora et al (199), most data correlated in the form of the Ranz and Marshall equation has produced linear equations typified by the correlations quoted in Table 23. When applying these equations however, certain limitations must be taken into account, namely,

1.) Steady-state drag coefficients must apply.
2.) The temperature gradient in the gas-film surrounding the droplet is assumed to be constant.
3.) Heat transfer to evaporated moisture is neglected.
4.) The droplet is assumed to be stable within the airflow.

Throughout all the experimental runs a constant air velocity of 1.0 m/s has been used; consequently, steady-state drag coefficients are assumed to apply. With regard to the temperature gradient surrounding the droplet being altered by high rates of evaporation, and heat being taken-up by vapour moving away from the droplet, a number of workers (44,55-57,126) have analysed the problem mathematically and produced

correction factors. Most engineering calculations ignore these effects which are reported to become significant only at temperatures exceeding 300°C (37). For example, using techniques similar to the present investigation, and under similar experimental conditions (cf. pages 86 and 156), Audu (106) and Cheong (194) proposed the following correlations to account for temperature variations in the gas-film surrounding a single droplet and for heat taken up by the evaporating moisture as it leaves the droplet,

Audu (106), $$\frac{(Tb - Td)}{Tamb} - 0.008$$

Cheong (194), $$(1/B)^{0.24}$$

In both cases, the exponents were found to be too small to have any significant effect on the data.

A more likely explanation for the enhanced heat and mass transfer is dimensional instability of a droplet within the airflow, i.e.; oscillations or any form of surface distortion would increase droplet surface area and reduce the boundary layer; both would increase the rate of heat and mass transfer. Throughout all the experimental runs a certain amount of droplet oscillation was noted at the beginning of each run (see Figure 87), but as a droplet evaporated and became smaller these oscillations tended to die down. This is probably due to an increase in droplet surface tension forces

Figure 87. Observed Droplet Oscillations and Distortions

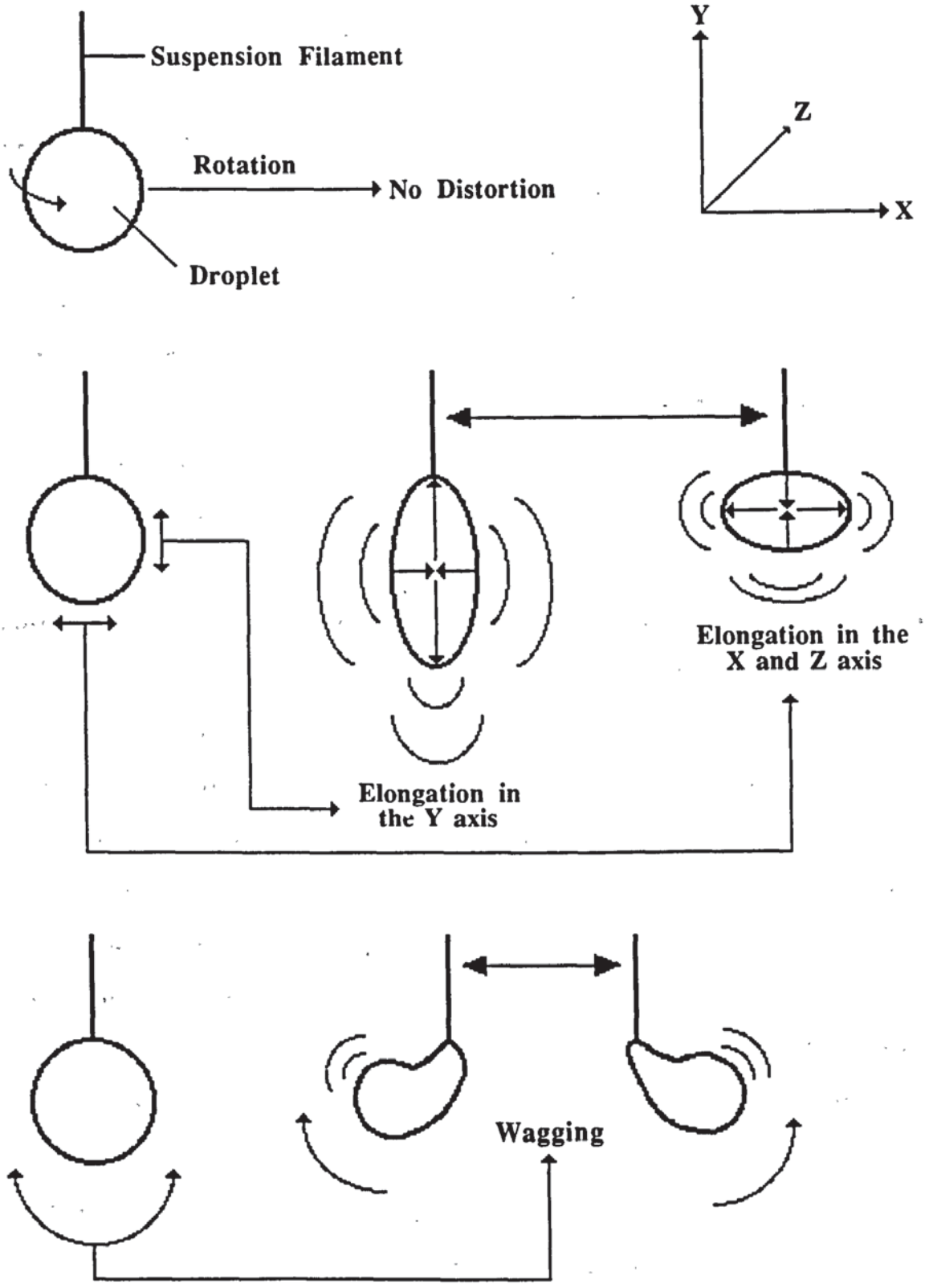

relative to droplet viscosity, i.e.; interaction with the drying medium causes the droplet to deform and produce the type of oscillations shown in Figure 87. The extent of the deformation, and hence the degree of oscillation, depends upon droplet viscosity; the lower the viscosity the greater the deformation or oscillation. As the droplet evaporates and decreases in size surface tension forces become increasingly predominant and retain the droplet at the minimum spherical surface area. Any oscillations are hence gradually damped-down. The process may be analogous to the die-away curve of any damped oscillation or wave motion, the oscillation amplitude decreasing exponentially with time. This is clearly demonstrated in Figures 88 and 89 where at maximum oscillation the rates of heat and mass transfer are considerably enhanced but rapidly decrease as the oscillations die down. The maximum oscillation corresponds to droplet ' wagging ' which occurs during the first few seconds of suspension as the droplet equilibrilates with the airflow. When oscillations are at a minimum, the plots of heat and mass transfer coefficients versus droplet diameter start to approximate to straight lines which suggests they are proportional to the droplet diameter.

Recent work in collaboration with Oteng-Attakora (199) using water droplets of inhibited surface behaviour, high viscosity liquids, e.g.; glycerol and ethanolamine, and solid spheres of naphthalene in free-flight, shows a gradual smoothing out of exponential mass transfer data with the solid

spheres of naphthalene exhibiting linear mass transfer rates as a function of $Re^{0.5}\ Sc^{0.33}$ predicted by Ranz and Marshall.

Figure 88. Mass Transfer Coefficients for Water Droplets at 50°C

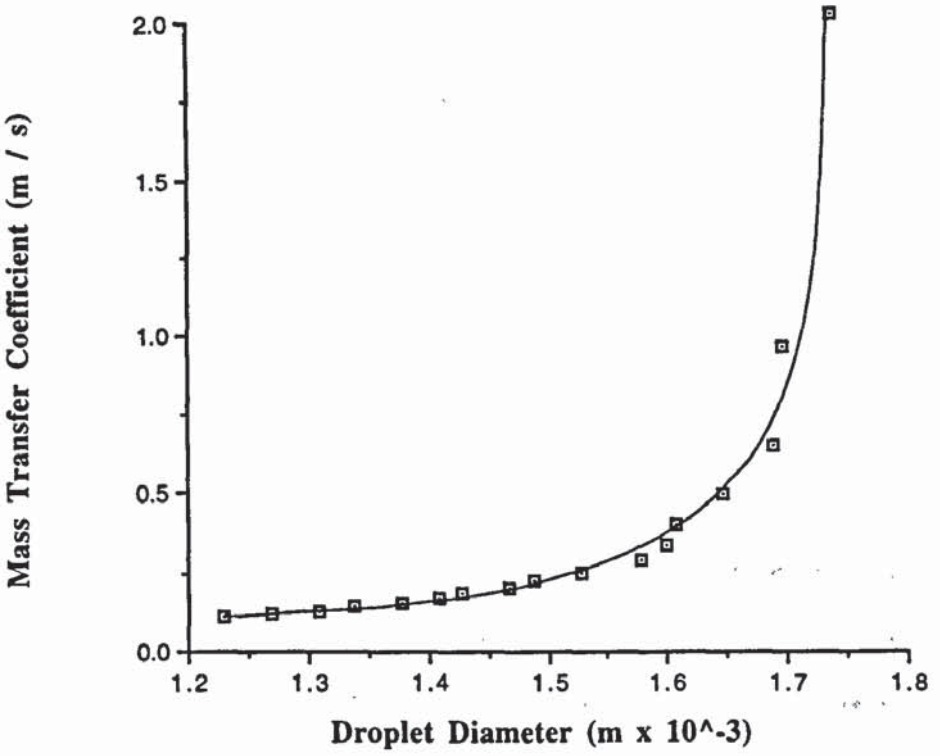

(Data represents an average of 3 plots)

Figure 89. Heat Transfer Coefficients for Water Droplets at 50°C

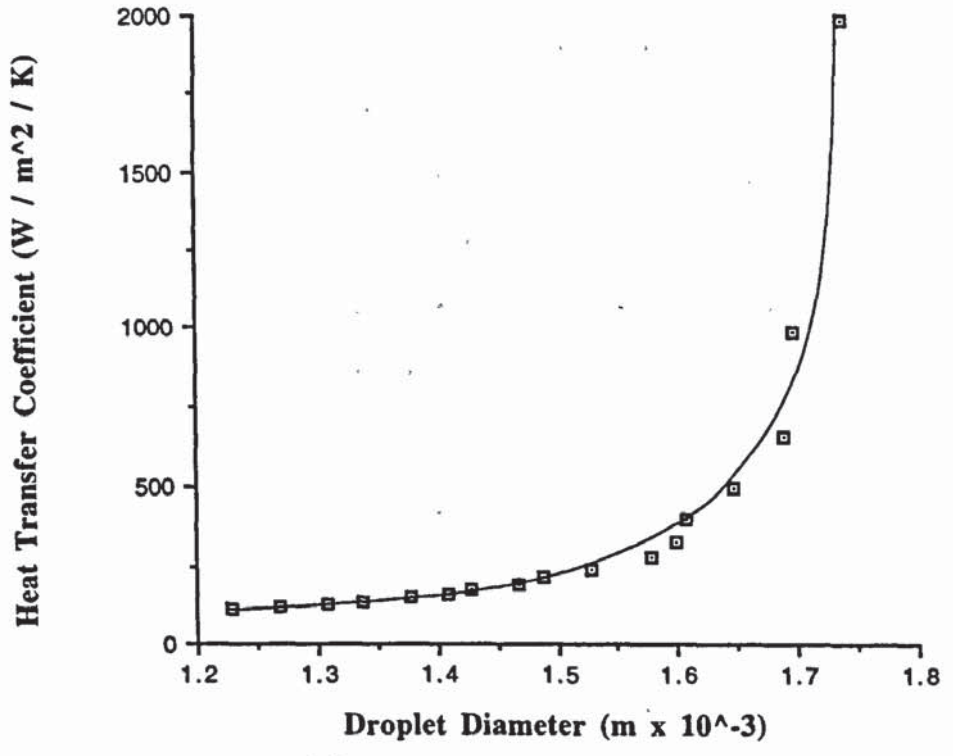

(Data represents an average of 3 plots)

SINGLE DROPLET DRYING STUDIES

6.8) Introduction

Single droplet drying studies were carried out on a range of individual inorganic and organic materials and with a number of proprietary and commercial products (see Table 25). The materials were chosen to represent the types of industrial spray-dried material listed in Table 7, the criteria being that they were available in a pure form or to a specification.

The main aim of the work was,

- to identify and classify the various types of particle morphology produced;
- to identify factors which influence droplet / particle behaviour, under controlled drying conditions;
- to provide a greater understanding of the drying fundamentals involved; and,
- to determine whether the single droplet drying method is analogous to the spray drying process.

Materials were dried from aqueous solutions, suspensions, slurries and pastes as single droplets at various concentrations and temperatures. Other parameters, e.g.; feed

Table 25. Materials Chosen for the Single Droplet Drying Study

Inorganic	Organic	Proprietary
sodium silicate	sodium benzoate	semi-instant skimmed milk powder
ammonium dihydrogen orthophosphate	sodium dodecyl sulphate	co-dried egg and skimmed milk powder
sodium chloride	gelatine	detergent (anionic)
potassium nitrate	sodium formate	
sodium carbonate	ethylenediaminetetra-acetic disodium salt (E.D.T.A.- $2Na^{+}$)	
zinc sulphate		
sodium pyrophosphate		
silica		
colloidal carbon		

aeration / deaeration and the retention of volatiles, were also investigated. The results have been interpreted in terms of the particle morphologies produced and their associated drying behaviour.

6.9) Evaluation of Drying Behaviour - The Effect of Temperature and Concentration on Particle Morphology

Aqueous solutions or suspensions of the materials listed in Table 25 were dried as single droplets at various temperatures and concentrations. Initially, concentrations were fixed at a value of 15 % w/w and the droplets were dried at temperatures below and above the respective boiling point of the solution

or suspension liquid, i.e.; 70.0°C (32.5°C WB) and 200.0°C (58.4°C WB) respectively. Droplets of a limited number of materials were subsequently dried at a temperature of 200°C from feed concentrations of 1 % w/w, 15 % w/w and concentrations ranging from 23 % to 36 % w/w.

Generalized drying behaviour are reported based upon observations during drying of three droplets per material for each condition of temperature and feed concentration.

The reconstituted proprietary materials may have different properties to the initial feedstock. However, this was of no consequence to the present study since the types of drying behaviour were investigated rather than one specific product.

The Effect of Drying Temperature on Particle Morphology

Drying Sequence 1 - Materials which form particles with a skin-like structure.

Applicable to : sodium silicate †
sodium dodecyl sulphate †
semi - instant skimmed milk ††
potassium nitrate †
gelatine †
co - dried egg and skimmed milk ††

(† solution, †† suspension / emulsion)

Drying Behaviour at 70.0°C

Solid precipitation occurred by the formation of a skin. This covered the whole droplet surface within seconds, trapping the

bulk of the droplet liquid internally. As evaporation took place the particle gradually decreased in size, and became darker and finally opaque in appearance as the skin thickened, to form either a solid or hollow particle depending on the material being dried. All the particles had a relatively smooth, surface structure. If the particle was hollow, on complete drying it tended to shrivel and deform, although particles of semi - instant skimmed milk and gelatine showed signs of internal bubble nucleation and partial inflation. Crust thicknesses ranged from approximately 50 μm to 130 μm. Figures 90 and 91 show typical examples of this type of drying behaviour. Sodium silicate for example, formed a solid particle which retained its general spherical shape, whereas, co - dried egg and skimmed milk formed a hollow particle which collapsed and shrivelled. In both cases skin formation is clearly evident. Figure 92 shows a hollow particle of semi - instant skimmed milk in which a limited amount of internal bubble nucleation has occurred. This has caused the particle to partially inflate producing a spherical surface structure which is smooth with no folding. A relatively thick wall structure is apparent.

Drying Behaviour at 200.0°C

A skin covered the whole droplet surface virtually instantaneously. This was rapidly followed by internal bubble nucleation. The bubbles expanded to violently distort, and

eventually rupture, the skin surface causing the particle to collapse, shrivel and then re-inflate. This cycle repeated three or four times until most of the internal moisture had evaporated. As the skin dried-out and hardened the vaporization of residual moisture inflated the particle permanently (see Figure 93) to form a hollow particle with, in the majority of cases, a relatively smooth surface structure (see Figure 94). No solid particles were produced. However, some shrivelled particles with uneven surface structures were formed (see Figure 95). Crust thicknesses were slightly less than those produced at 70°C and ranged from approximately 30 µm to 50 µm. In some materials, i.e.; sodium silicate and sodium dodecyl sulphate, a type of internal blistering occurred which produced small particles or blisters within the larger parent particle. This was particularly evident in sodium silicate (see Figures 96 to 98) with which the evaporation of a residual liquid ' heel ' inside partially dried particles resulted in the liquid heel boiling causing it to foam and bubble. On fully drying, the foam / bubbles hardened to give a blistered appearance. This phenomenon resembles the small particles within large particles observed in some of the industrial spray-dried materials (see Figures 71 and 72).

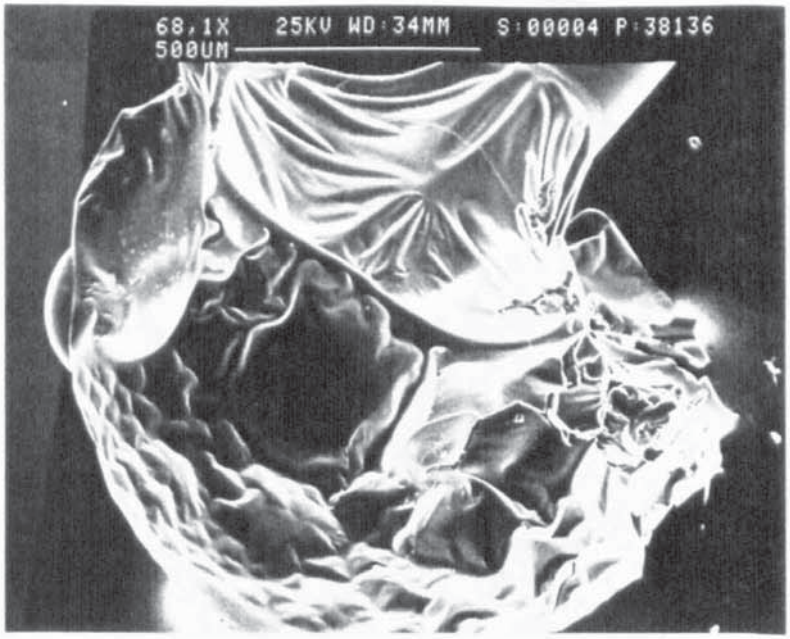

Figure 90.
sodium silicate
In. conc. 15% w/w
Temp. 70°C

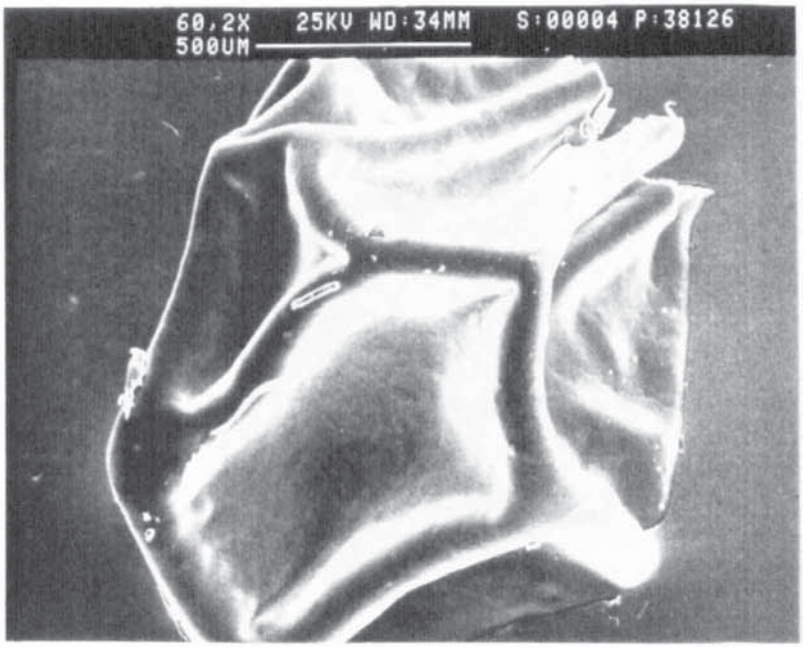

Figure 91.
co-dried egg and skimmed milk
In. conc. 15% w/w
Temp. 70°C

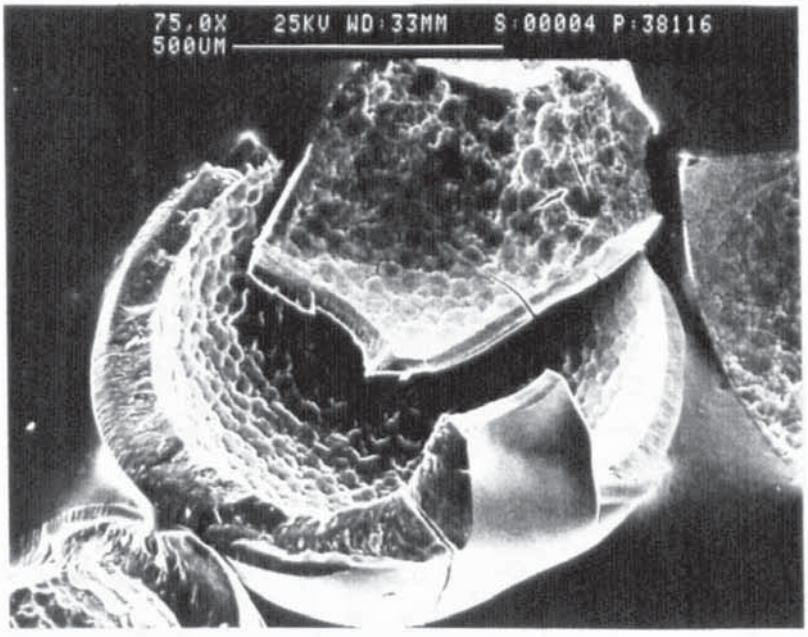

Figure 92.
semi-instant skimmed milk
In. conc. 15% w/w
Temp. 70°C

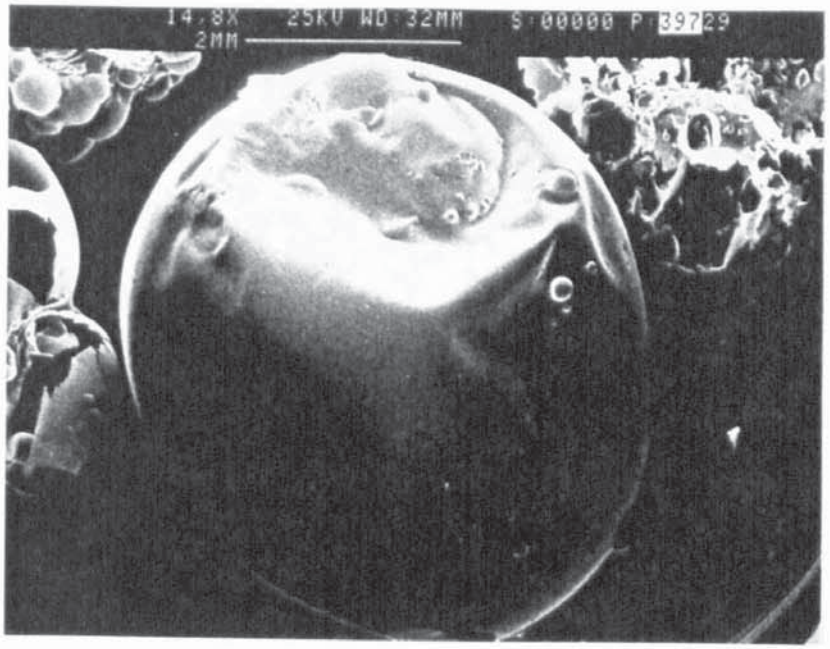

Figure 93.
sodium silicate
In. conc. 15% w/w
Temp. 200°C

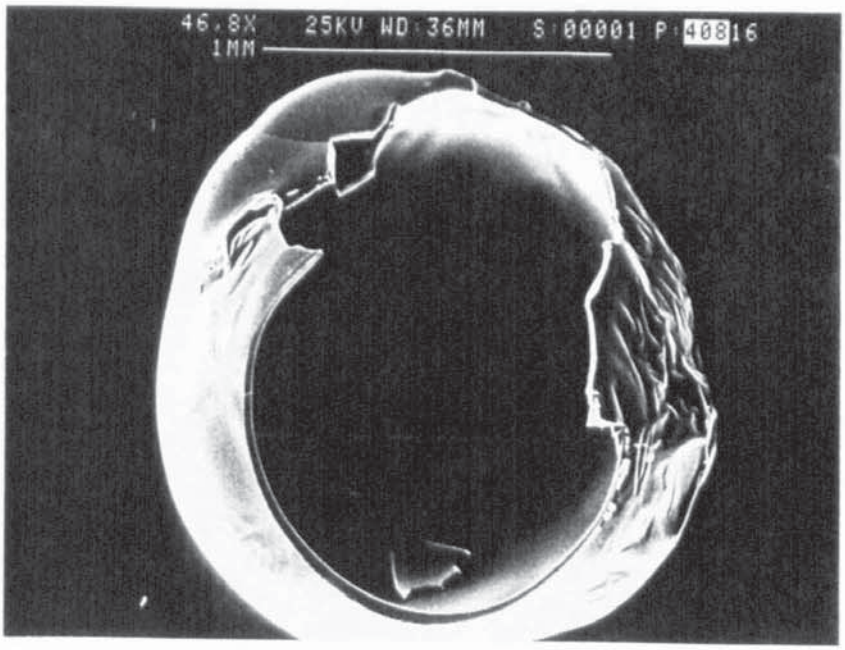

Figure 94.
gelatine
In. conc. 15% w/w
Temp. 200°C

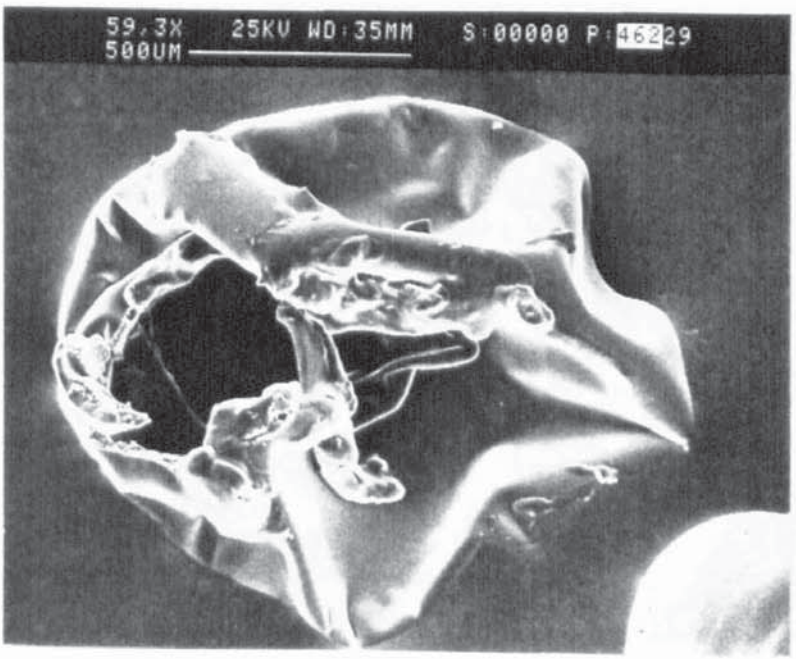

Figure 95.
semi-instant skimmed milk
In. conc .15% w/w
Temp. 200°C

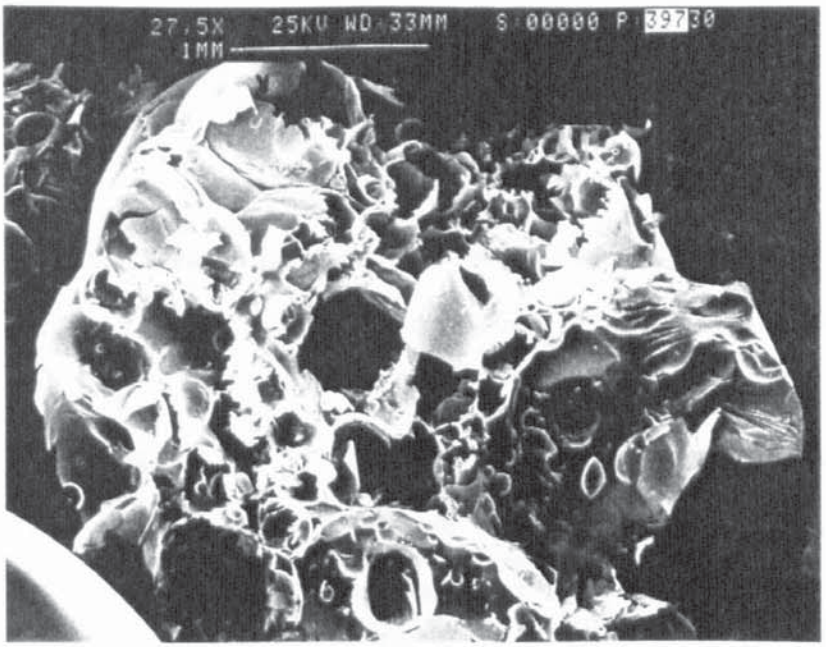

Figure 96.
sodium silicate
As Figure 93.

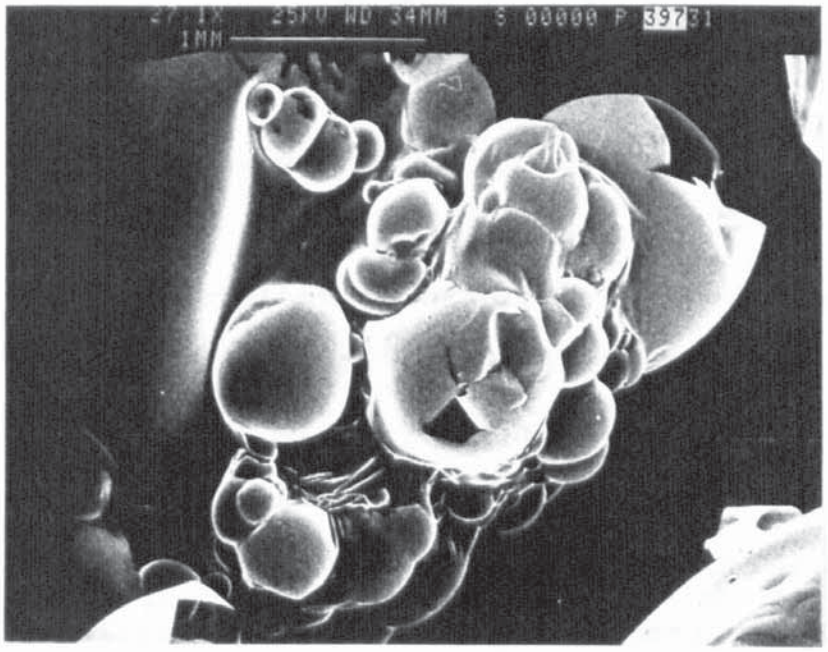

Figure 97.
sodium silicate
As Figure 93.

Figure 98.
sodium dodecyl sulphate
In. conc. 15% w/w
Temp. 200°C

Drying Sequence 2 - Materials which form particles with a crystalline structure.

Applicable to : ammonium dihydrogen orthophosphate †
sodium chloride †
sodium carbonate †
zinc sulphate †
sodium pyrophosphate †
sodium benzoate †
sodium formate †
ethylenediaminetetra-acetic disodium salt †

(† solution)

Drying Behaviour at 70.0°C

Solid precipitation occurred by the formation of crystals from single or multiple nucleation sites located at the surface of the droplet, usually around the equator. The crystal size and shape depended upon the type of material being dried (see Figures 99 to 101), e.g.; sodium chloride formed large cubic crystals, whereas, sodium benzoate and E.D.T.A.- $2Na^{+}$ formed fine needle-shaped crystals. The instant a crystal formed it started to rapidly rotate about the droplet equator gradually sinking to the bottom of the droplet as it became larger. Once anchored, the nuclei linked-up to form a large crystal mass which eventually covered the whole droplet surface trapping liquid inside. Internal bubble nucleation then took place, albeit to a lesser extent than in the skin-forming materials. Some of the samples did however, exhibit surface cracks and fissures with a limited amount of crust deformation, i.e.; sodium chloride and sodium formate. At this point, all the

materials clearly showed saturated surface drying with particle surfaces appearing wet. Once the bulk of the liquid had evaporated the surface of the particle started to dry-out leaving a hollow, semi-hollow or solid crystalline structure with either a smooth or irregular surface structure (see Figure 99 and Figures 102 to 105). The type of morphology formed was very dependent upon the crystalline nature of the material being dried. Crust thicknesses of hollow and semi-hollow particles were comparatively thick and ranged from approximately 200 μm to 300 μm. Sodium chloride, sodium formate, sodium carbonate and sodium benzoate particles formed surface structures covered with dendritic crystalline growth. This gave the particles a rough, ' furry ' appearance (see Figures 106 and 107).

Drying Behaviour at 200.0°C

The initial stages of solid precipitation at 200°C were virtually identical to those at 70°C, but the rate of drying was considerably faster and there was an apparent increase in the number of initial crystal nuclei. Differences started to arise however, when crust formation was complete. With the exception of zinc sulphate, which tended to form a solid particle with a smooth surface structure (see Figure 110), the particle structure formed was violently distorted by internal bubble nucleation; however, once the majority of the bulk liquid had evaporated this subsided and the particle

surface adopted a more permanant structure. As with the skin-forming materials, it was the removal of the residual moisture that determined the final particle morphology. This usually resulted in the formation of a hollow, partially-inflated structure with a rough crystalline surface (see Figures 108 and 109). The component crystal nuclei were smaller and had a more uniform size distribution with particle crust thicknesses much less than those formed at 70°C, i.e.; they ranged from approximately 50 μm to 100 μm. Particle inflation did not occur with sodium pyrophosphate, sodium benzoate and E.D.T.A.-$2Na^{+}$. These particles had a tendency to explode with an audible ' pop ' completely destroying the entire particle structure.

At both 70°C and 200°C droplets of zinc sulphate and sodium formate exhibited a transition period just before solid precipitation occurred which resulted in the formation of a ' sticky ' droplet. This was probably due to the loss of water of crystallization, e.g.; for $ZnSO_4$, - $5H_2O$ occurs at 70°C.

NB - Droplets of ammonium dihydrogen orthophosphate solution were dried at 170°C (53°C WB) rather than 200°C due to the relatively low melting point of the solid, i.e.; 190°C.

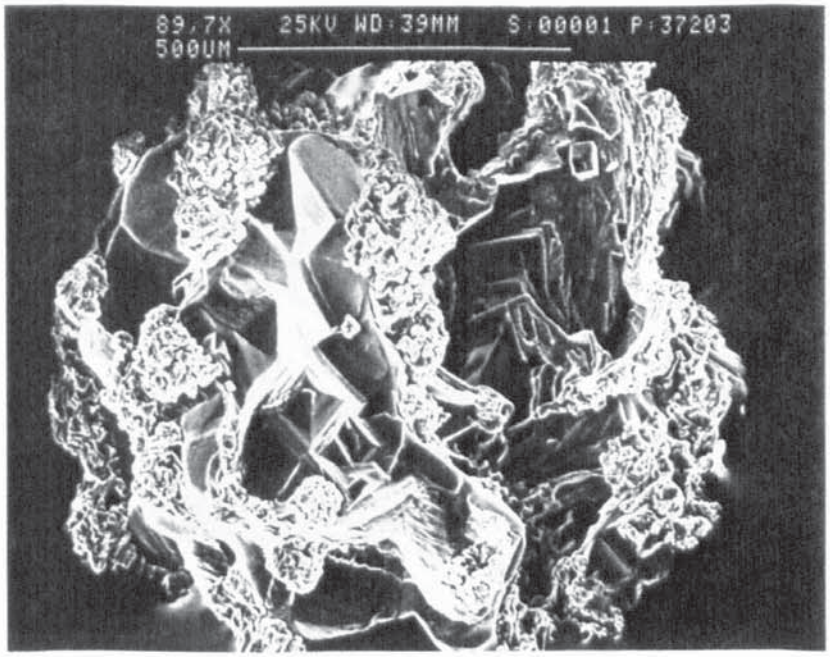

Figure 99.
sodium chloride
In. conc. 15% w/w
Temp. 70°C

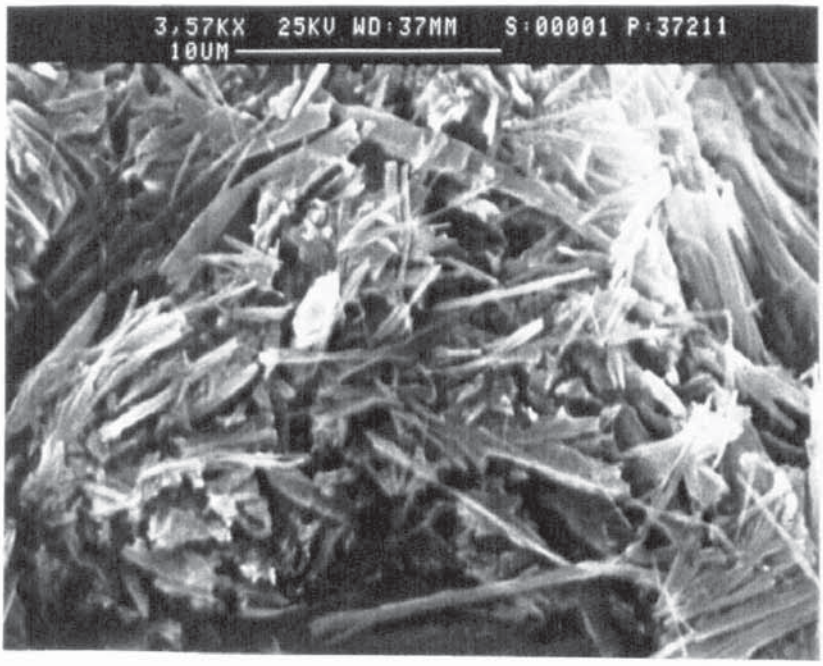

Figure 100.
sodium benzoate
In. conc. 15% w/w
Temp. 70°C

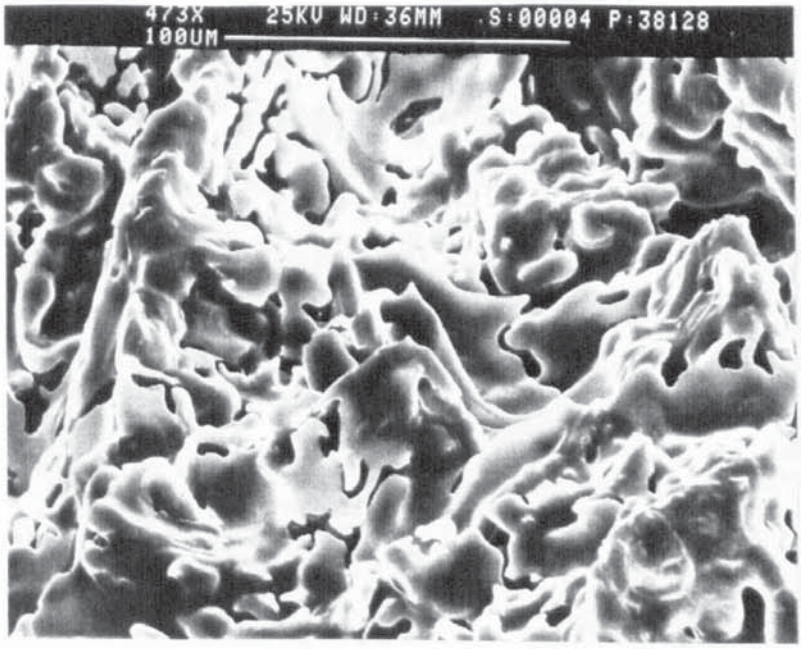

Figure 101.
sodium formate
In. conc. 15% w/w
Temp. 70°C

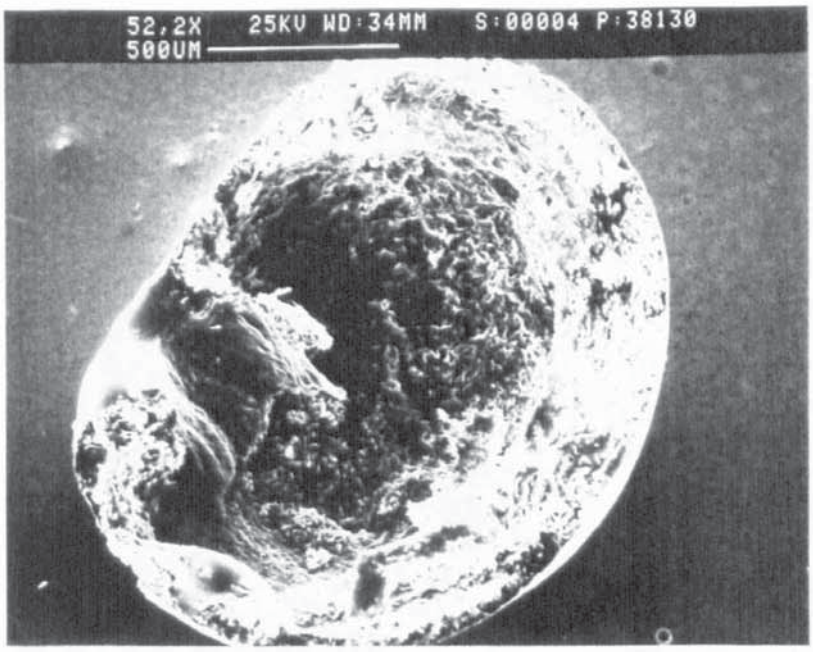

Figure 102.
ethylenediaminetetra-acetic acid disodium sal
In. conc. 15% w/w
Temp. 70°C

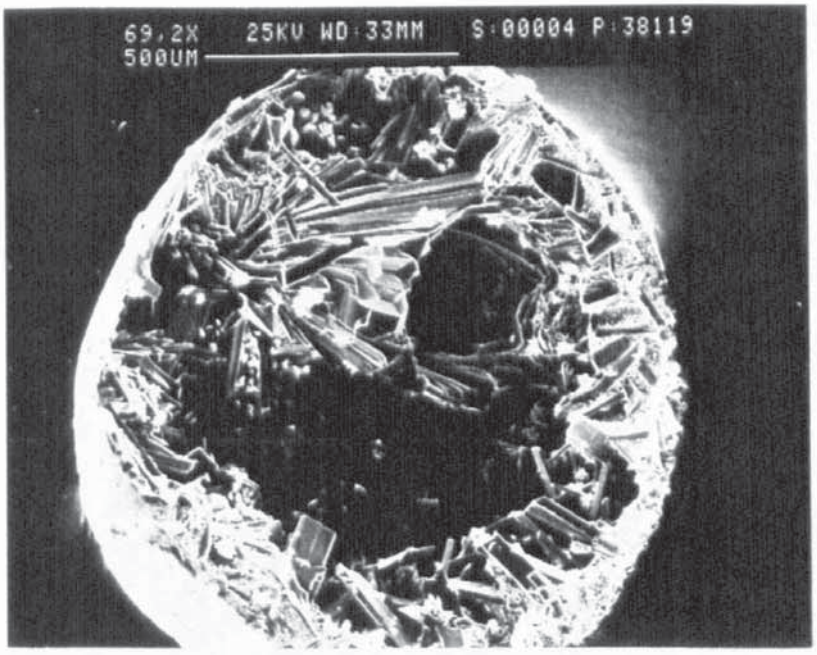

Figure 103.
sodium pyrophosphate
In. conc. 15% w/w
Temp. 70°C

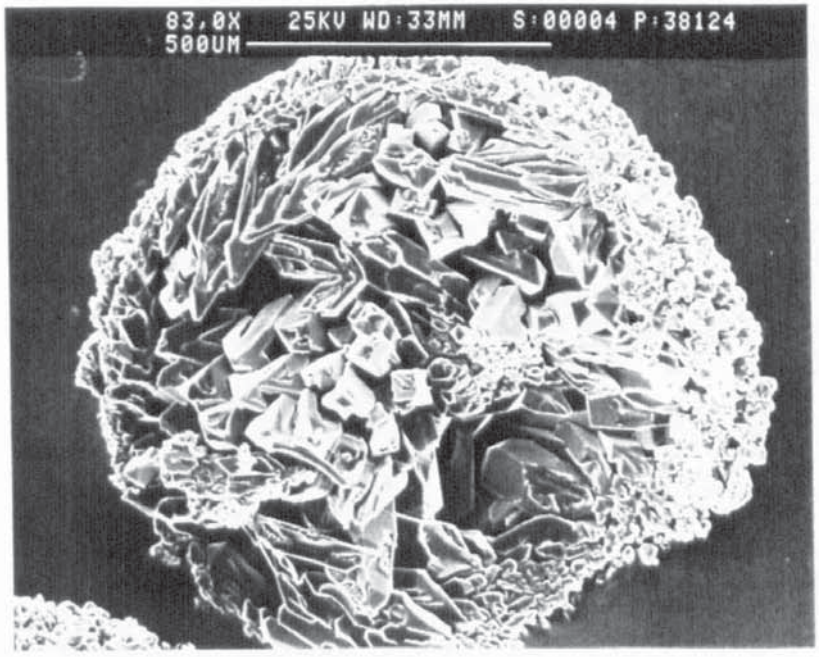

Figure 104.
ammonium dihydrogen orthophosphate
In. conc. 15% w/w
Temp. 70°C

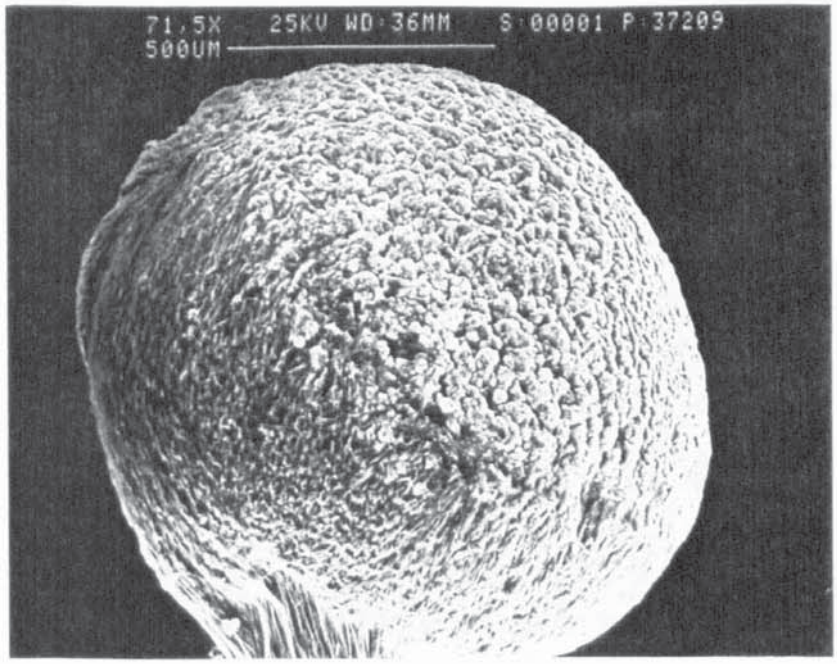

Figure 105.
sodium benzoate
As Figure 100.

Figure 106.
sodium carbonate
In. conc. 15% w/w
Temp. 70°C

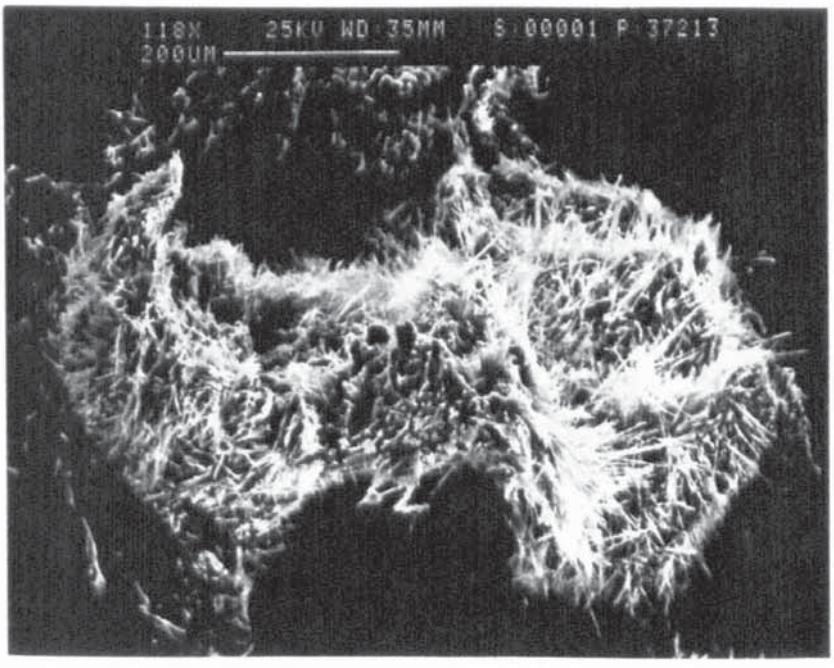

Figure 107.
sodium benzoate
As Figure 100.

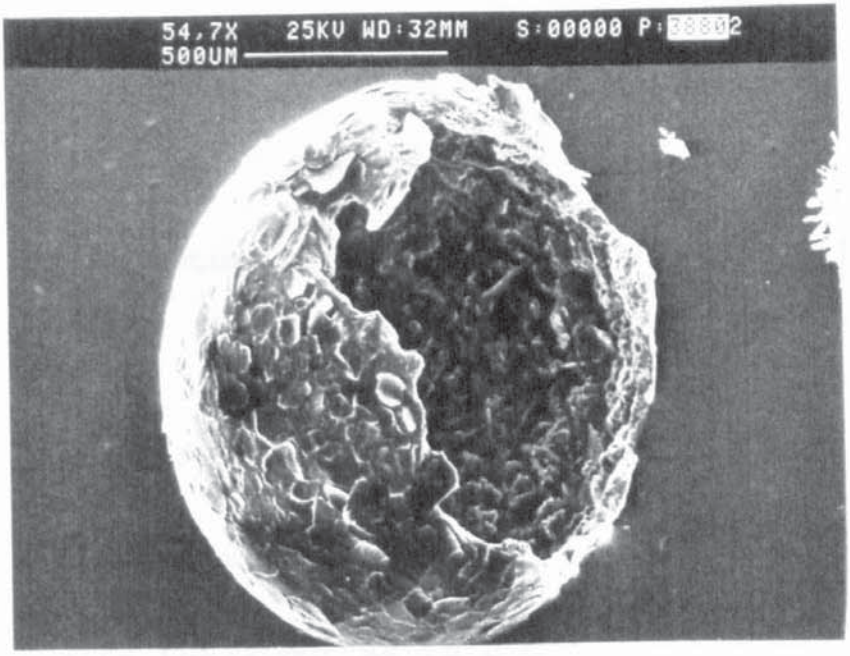

Figure 108.
ethylenediaminetetra-acetic acid disodium salt
In. conc. 15% w/w
Temp. 200°C

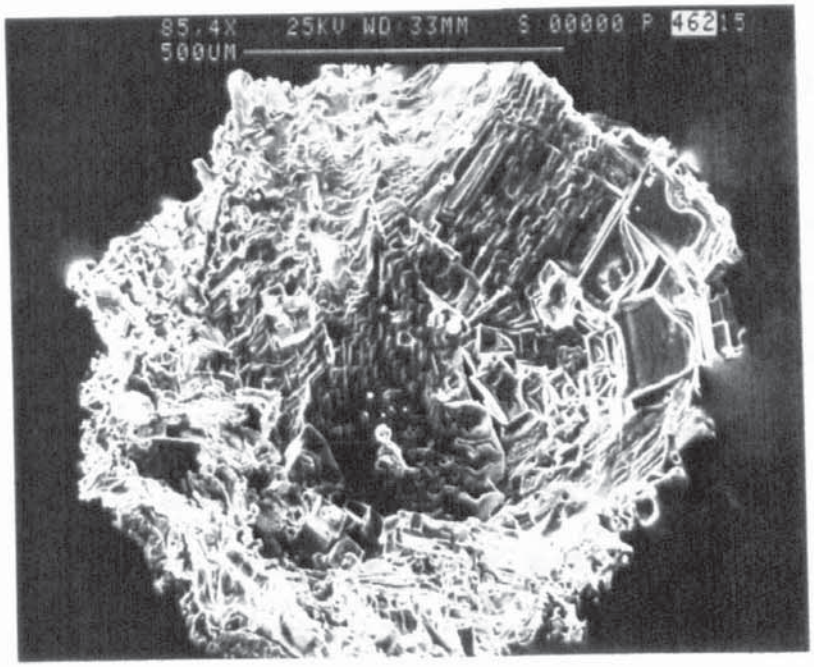

Figure 109.
sodium chloride
In. conc. 15% w/w
Temp. 200°C

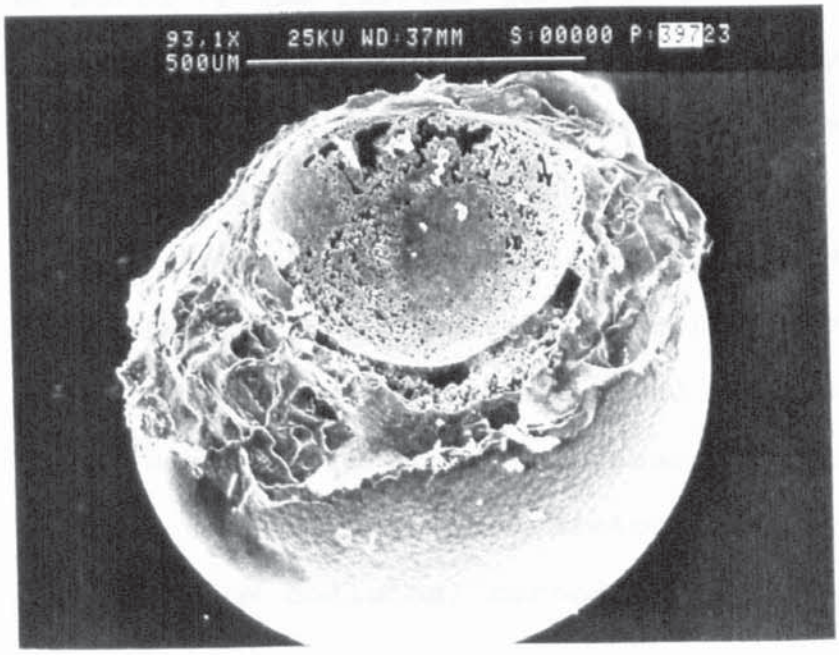

Figure 110.
zinc sulphate
In. conc. 15% w/w
Temp. 200°C

Drying Sequence 3 - Materials which form particles with an agglomerate structure.

Applicable to : silica †
colloidal carbon †

(† suspension)

Drying Behaviour at 70.0°C

Because the above materials are aqueously insoluble, and therefore, form a suspension not a solution, no solid precipitation occurred. The droplets simply decreased in size until most of the bulk liquid had evaporated leaving particles with a high degree of sphericity. Residual moisture was removed via saturated and non-saturated surface drying to form either solid or hollow particles with a very smooth surface structure; the period of saturated surface drying was of short-duration, i.e.; approx. 5-10 s. The particle tended to be solid if the initial particle-size of the suspended material was >> 1 μm, but hollow if the particle-size was approximately < 1 μm. For example, silica (see Figures 111 to 113) formed solid particles composed of material 6 μm to 50 μm in diameter (77 % of the suspended material was within this size range), whereas, colloidal carbon (see Figures 114 and 115) formed hollow particles composed of material far less than 1 μm in diameter. Internal bubble nucleation and a limited amount of surface distortion only occurred in particles of colloidal carbon.

Drying Behaviour at 200.0°C

Drying behaviour and particle morphologies were identical to those produced at 70°C, although particle drying rates were increased. The colloidal carbon particles showed a greater tendency to inflate at 200°C, i.e.; by approximately 5 %.

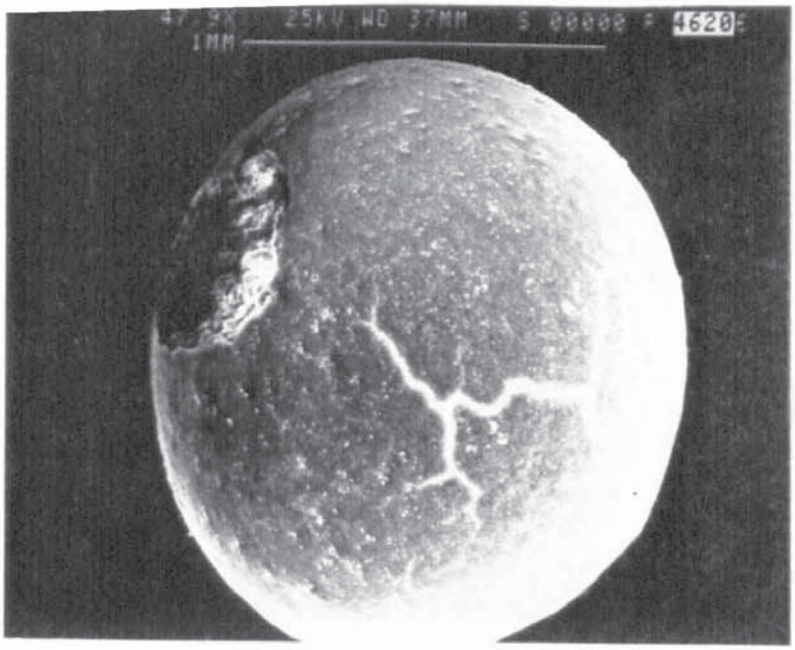

Figure 111.
silica
In. conc. 15% w/w
Temp. 200°C

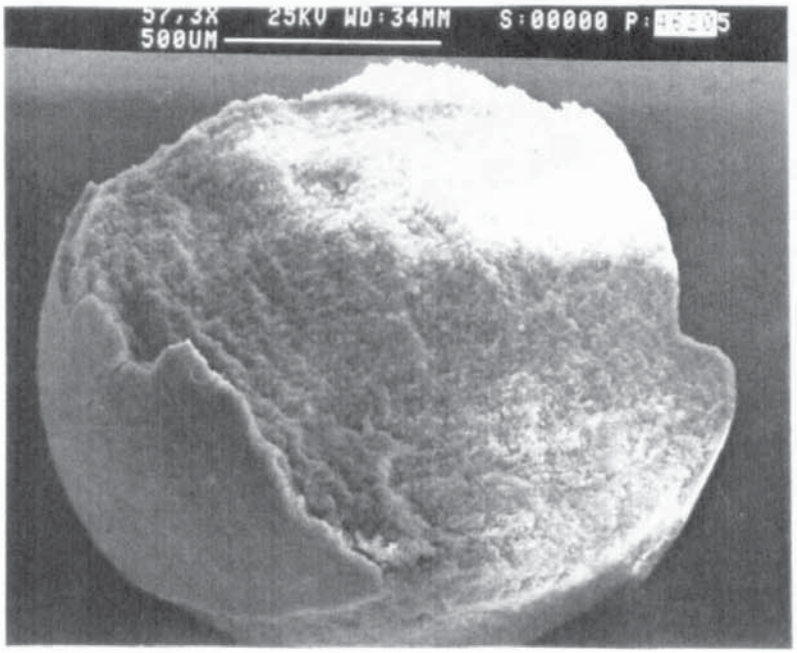

Figure 112.
silica
As Figure 111.

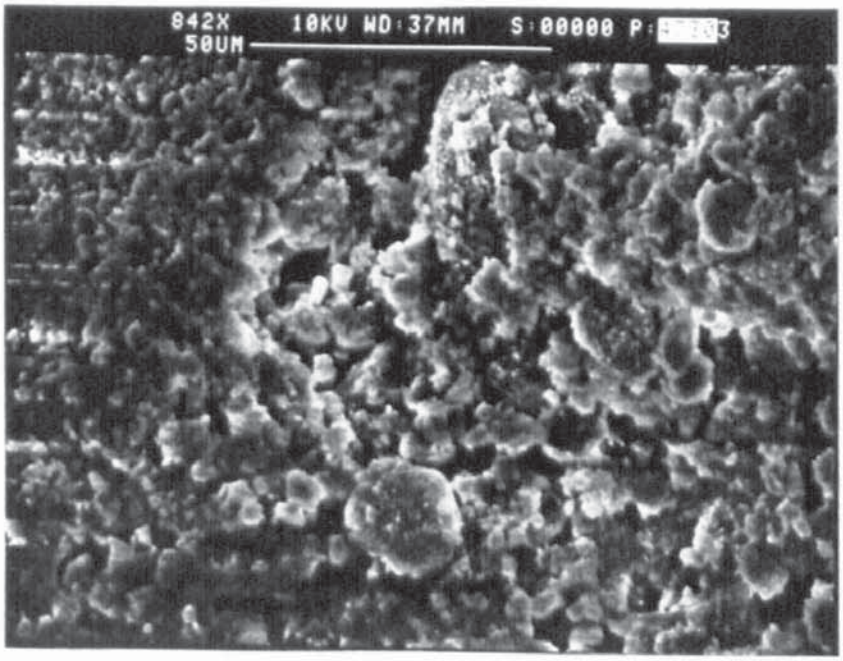

Figure 113.
silica
In. conc. 15% w/w
Temp. 70°C

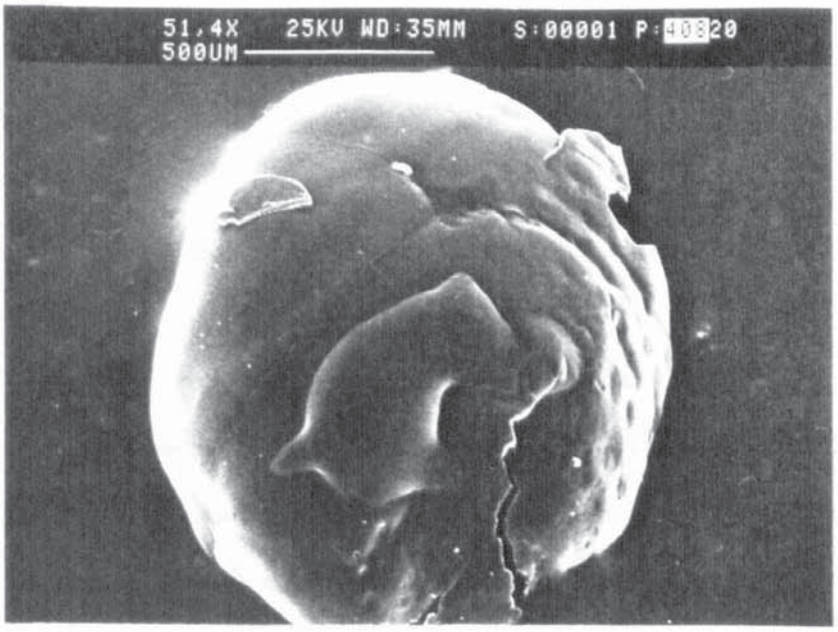

Figure 114.
colloidal carbon
In. conc. --
Temp. 200°C

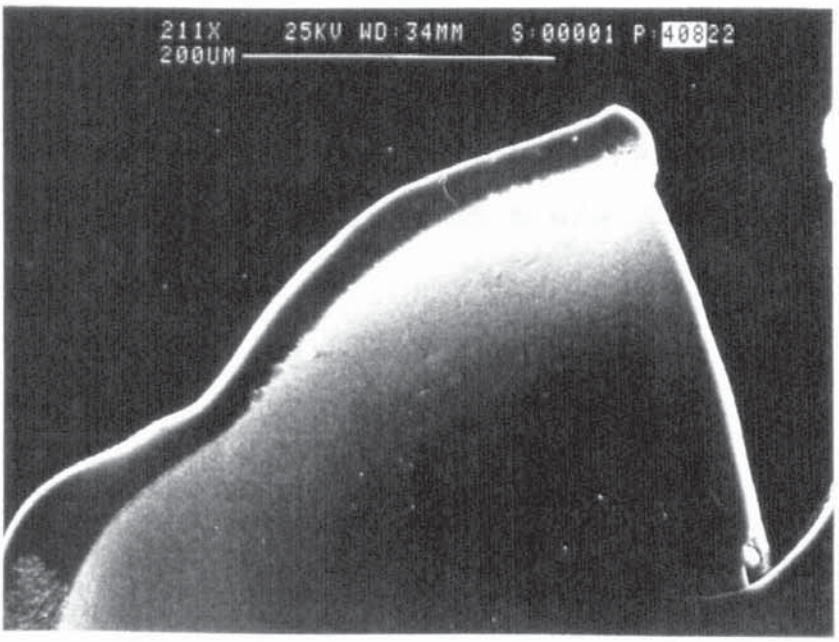

Figure 115.
colloidal carbon
As Figure 114.

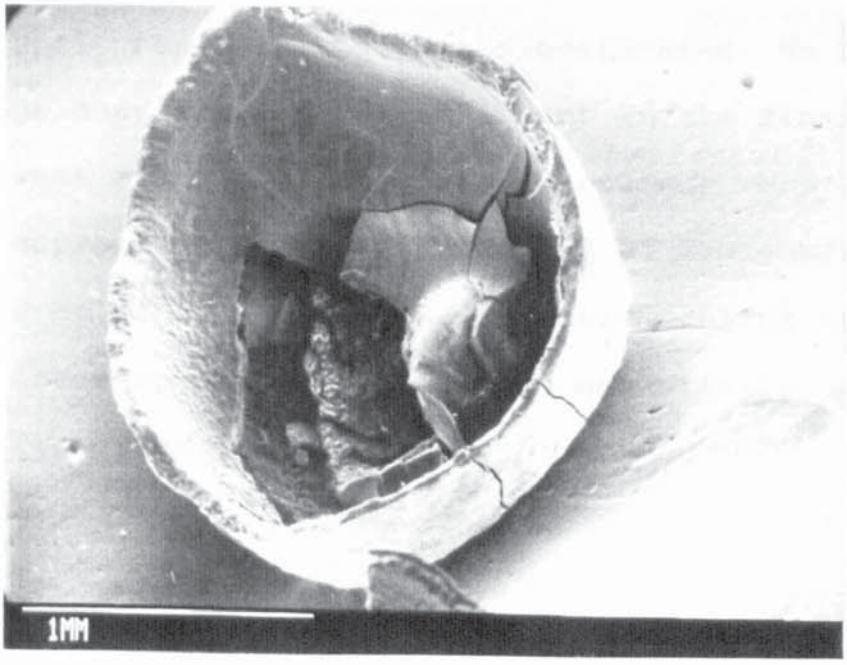

Figure 116.
aqueous soluble proprietary dye
In. conc. 15% w/w
Temp. 200°C
Temp. in 400°C
out 100°C

The Effect of Concentration on Particle Morophology

Three of the materials listed in Table 25 were selected to study the effects of concentration on drying behaviour and particle morphology. Single droplets of semi - instant skimmed milk, sodium chloride and silica, i.e.; materials which represent the three morphological types - polymeric, crystalline and agglomerate - were dried at a temperature of 200°C from feed concentrations of 1 % w/w, 15 % w/w and the highest possible working concentration of 30 % w/w for semi - instant skimmed milk, 36 % w/w for sodium chloride and 23 % w/w for silica.

The following observations were made,

Feed Concentration of 1 % w/w

Droplets of all three materials dried in a similar manner to the evaporation of pure liquids, gradually decreased in size until the bulk liquid had evaporated. No solid precipitation or deposition occurred except in the final stages of drying when small amounts of solid residue were deposited on the support filament. Figures 117 to 119 confirm this since droplet surface areas decreased continuously with time, but the evaporation process was essentially unhindered by solid formation.

Feed Concentration of 15 % w/w

All three materials formed particles. Drying behaviours and particle morphologies were as described above. Figures 120 to 122 show graphically, and would tend to confirm, the three distinct types of drying behaviour previously characterized. For comparison, apparent surface areas calculated after the particle inflated and deformed are also shown in Figures 121 and 122. Since viewing was only in one plane, the accuracy of these values is not quantifiable *; they are simply reported to demonstrate the degree of inflation and deformation. The mean values are quoted as a1 and a2. Droplets of semi - instant skimmed milk initially decreased in size as the bulk of the liquid evaporated. This period appeared to be relatively-unhindered by initial skin formation, although the gradient of the curve in Figure 122 is somewhat less than those in Figures 120 and 121 for particles of silica and sodium chloride. Surface areas tended to stabilize as particle skins / crusts adopted a more permanent structure. This was followed by a slight increase in surface area as the particles inflated. Because the particles were rotated as they dried (one complete revolution every 20 s) any permanent surface deformation was recorded as a series of repetitive peaks and troughs. The greater the amplitude of the peak, the greater the surface deformation. Localized dynamic events, such as inflation, rupturing and collapse were not however recorded since they occur too rapidly, i.e.; in the region of 1 to 5 s.

* It was subsequently demonstrated that this limitation can be overcome by the use of angled mirrors allowing double images of droplets to be recorded on high-speed video (199).

Figure 122 suggests the surface structure or skin of the semi - instant skimmed milk particles were relatively smooth due to inflation. Conversely, Figure 121 suggests the sodium chloride particles had a considerable degree of surface or crust deformation. Behaviour during the initial evaporation period appeared to be similar to those of semi - instant skimmed milk particles, although a greater degree of inflation had occurred. In contrast to both semi - instant skimmed milk and sodium chloride particles, Figure 120 suggests the silica particles had little or no surface deformation, i.e.; the particles were smooth, relatively spherical and exhibited no inflation.

The Highest Possible Working Concentration

Silica at 23 % w/w had the consistency of a paste and was difficult to apply to the suspension filament in the form of a spherical droplet. Consequently, the paste tended to adopt the same irregular shape throughout drying. Figure 123 clearly shows such surface irregularities. Figure 123 is characteristic of a non-inflating deformed particle. The mean areas are quoted as a1 and a2 but are somewhat arbitrary due to the high initial paste viscosity. Drying behaviour and particle morphologies were in general identical to particles dried from a feed concentration of 15 % w/w (see Figure 128) with no surface deformation or particle inflation.

Droplets of sodium chloride (36 % w/w) formed a crust instantly, the crystal nuclei being much finer than those produced from a feed concentration of 15 % w/w. All the particles displayed internal bubble nucleation, particle inflation and particle surface deformation during drying, but not to the same extent as particles dried from a feed concentration of 15 % w/w. Figure 124 illustrates the behaviour of a supersaturated solution with inflation and deformation following crust formation. The morphology of the fully-dried particles was generally hollow and irregular in shape with wall structures in the region of 500 μm thick. However, a small number were solid and relatively spherical (see Figure 127). The latter corresponded to particles which had dried with a limited amount of internal bubble nucleation, no particle inflation, and very little surface deformation.

Particles of semi - instant skimmed milk (30 % w/w) displayed a similar drying behaviour to particles dried from a feed concentration of 15 % w/w. The initial evaporation periods were however considerably shorter (see Figure 125) and cycles of particle inflation, rupture and collapse appeared to be less exaggerated. Wall or skin thickness of the fully-dried particles appeared to be thicker than those dried from a feed concentration of 15 % w/w and ranged from approximately 50 μm to 70 μm thick, although overall particle diameters increased. The data in Figure 125 show both the normally-observed behaviour (Run 2), and the occasional grossly inflated particle (Run 1); see Figure 126.

Figure 117. Apparent Surface Area vs Time for Droplets of 1% w/w Silica

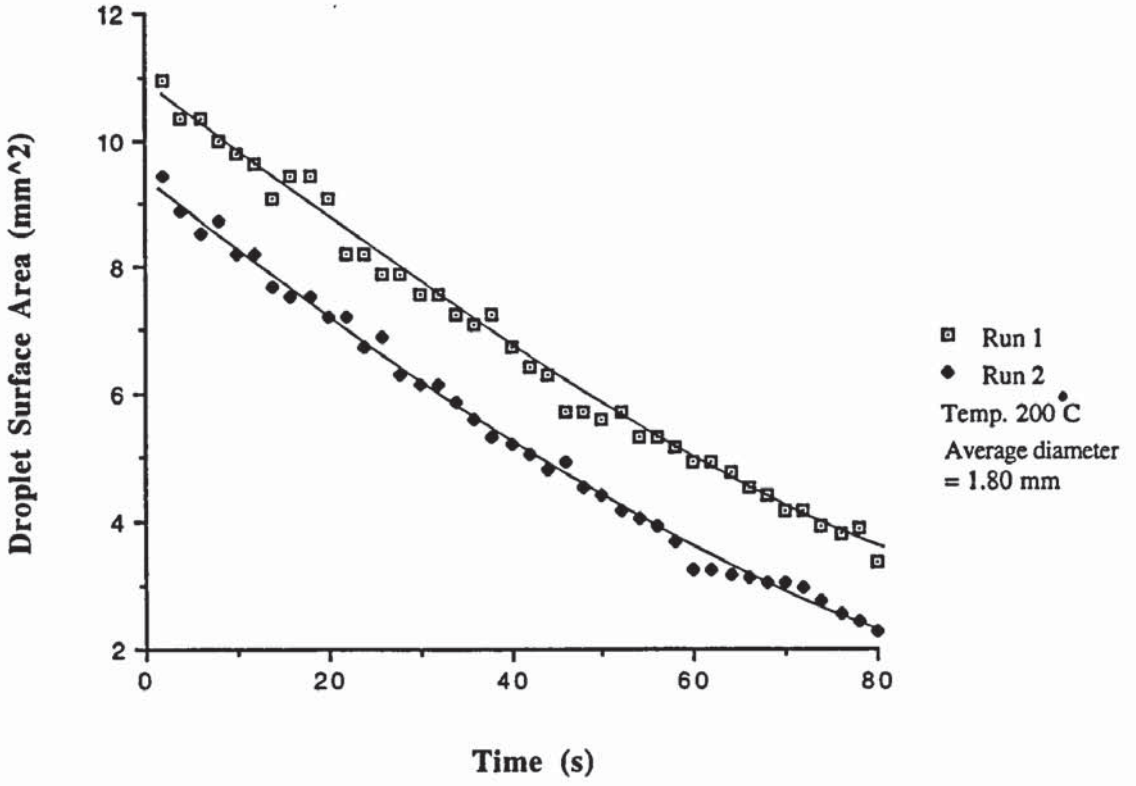

Figure 118. Apparent Surface Area vs Time for Droplets of 1% w/w Sodium Chloride

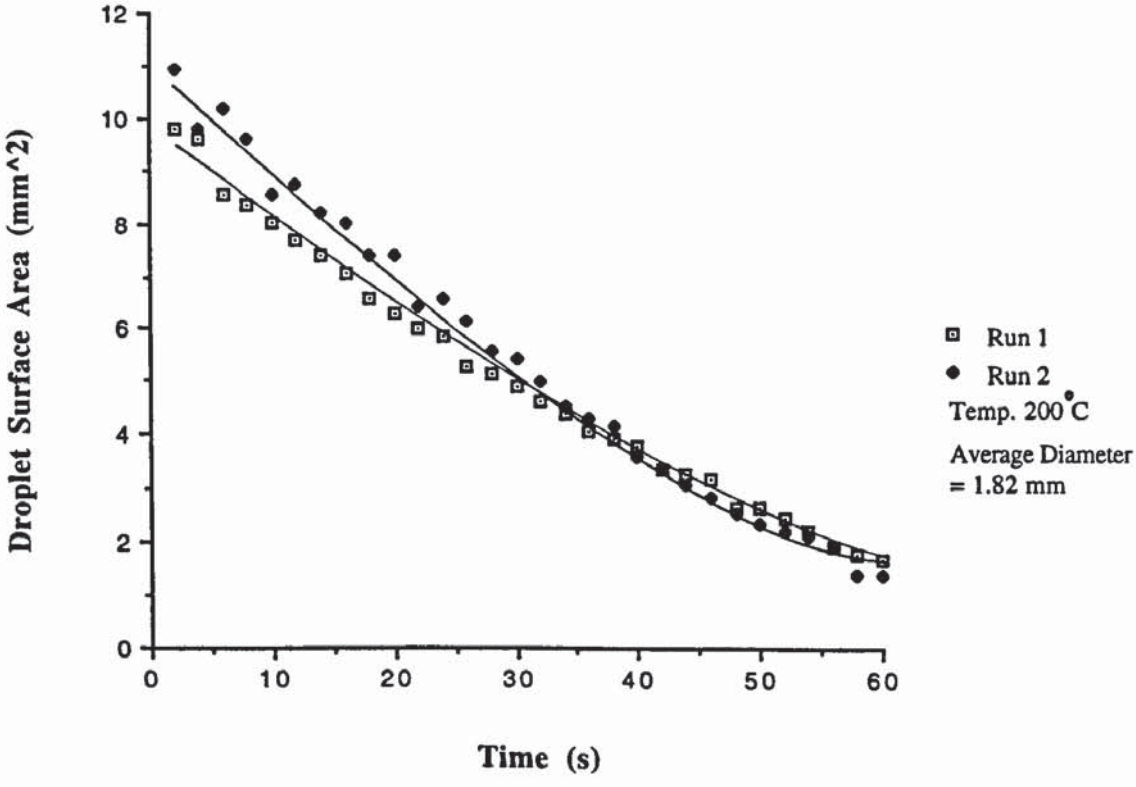

Figure 119. Apparent Surface Area vs Time for Droplets of 1% w/w Semi-Instant Skimmed Milk

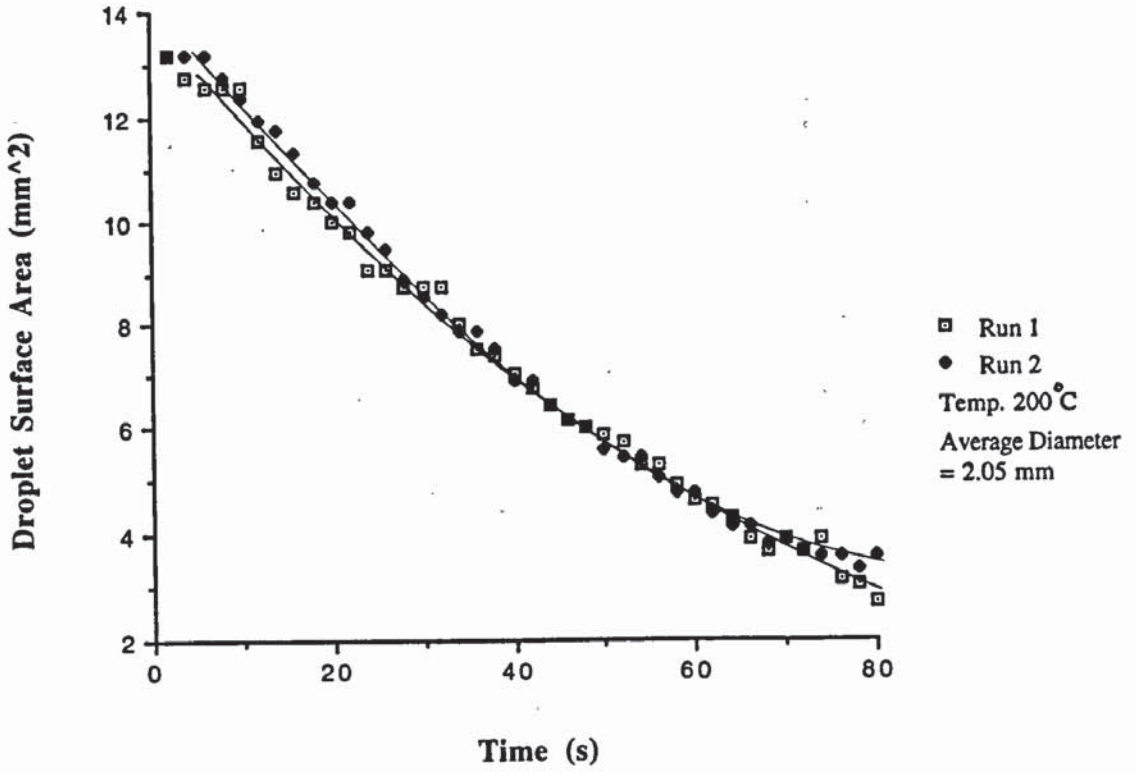

Figure 120. Apparent Surface Area vs Time for Droplets of 15% w/w Silica

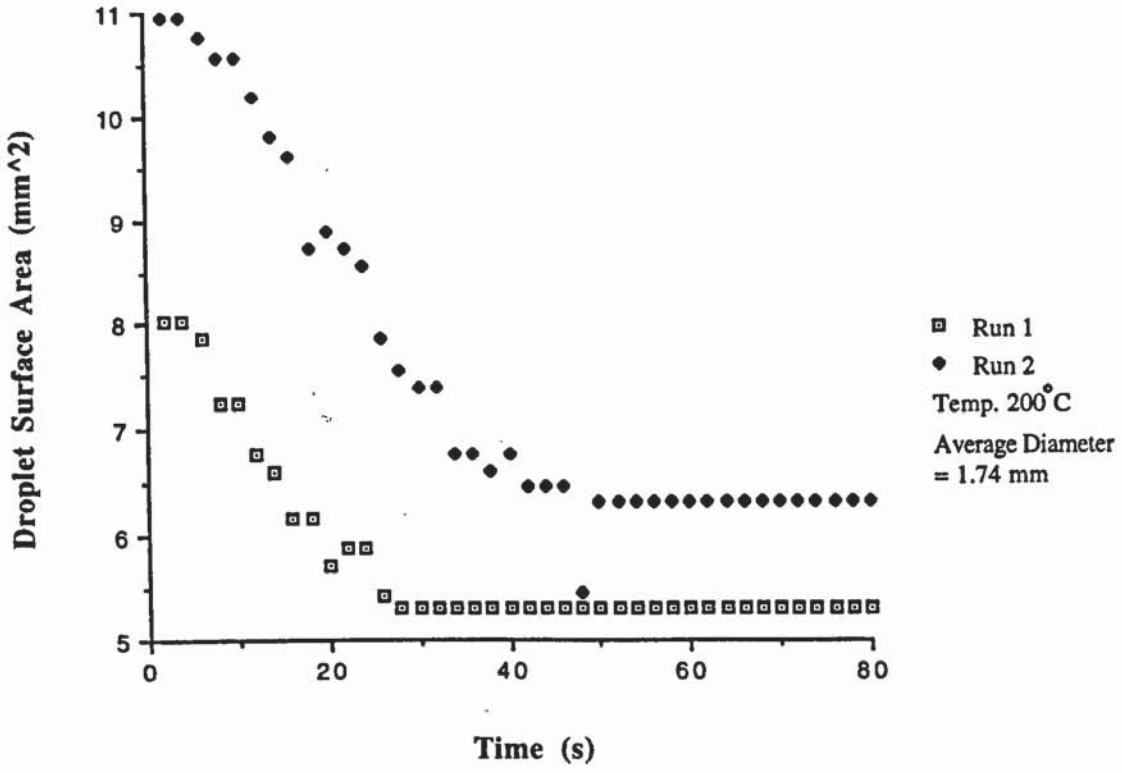

Figure 121. Apparent Surface Area vs Time for Droplets of 15% w/w Sodium Chloride

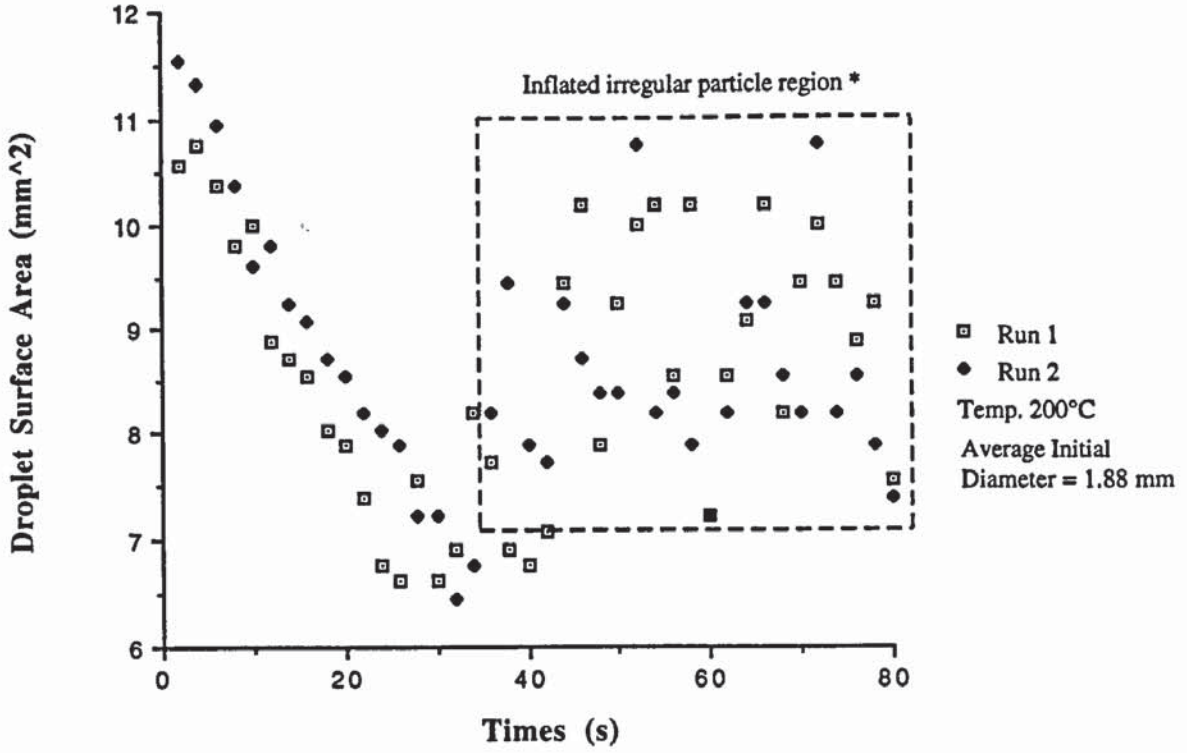

* a1 (Run 1) -- 6.58 mm^2, a2 (Run 2) -- 4.27 mm^2

Figure 122. Apparent Surface Area vs Time for Droplets of 15% w/w Semi-Instant Skimmed Milk

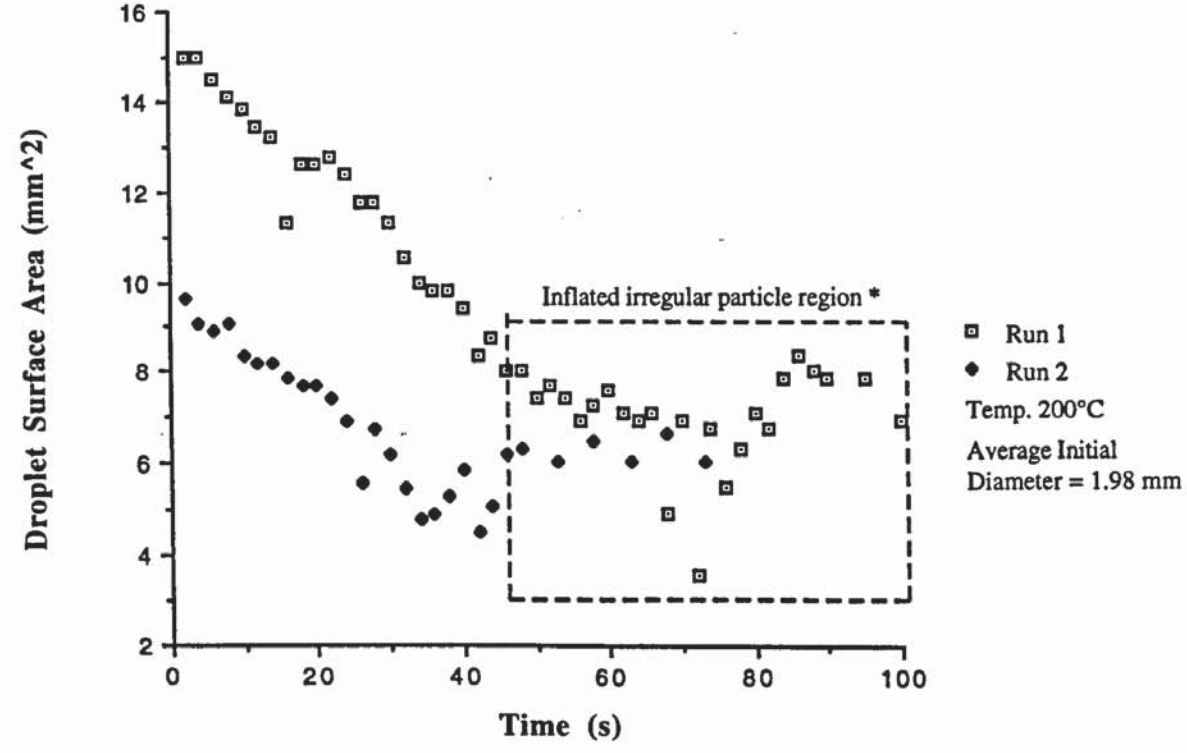

* a1 (Run 1) -- 7.89 mm^2, a2 (Run 2) -- 5.80 mm^2

Figure 123. Apparent Surface Area vs Time for Droplets of 23% w/w Silica

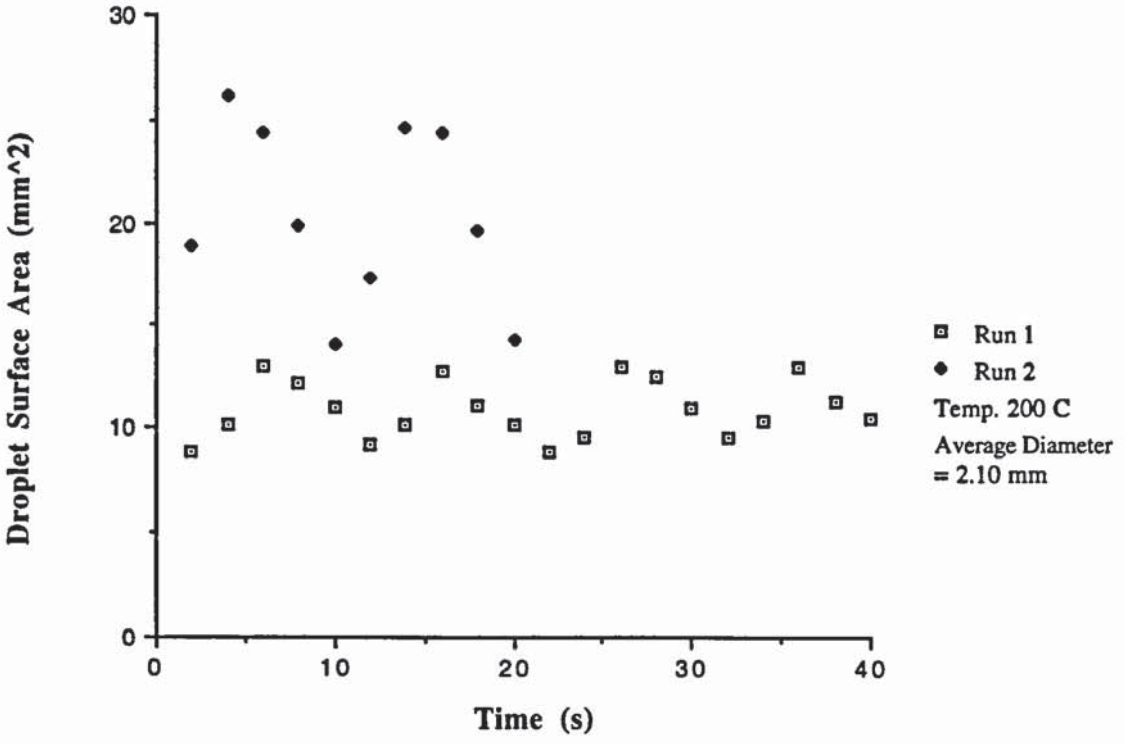

* a1 (Run 1) = 10.87 mm^2, a2 (Run 2) = 20.36 mm^2

Figure 124. Apparent Surface Area vs Time for Droplets of 36% w/w Sodium Chloride

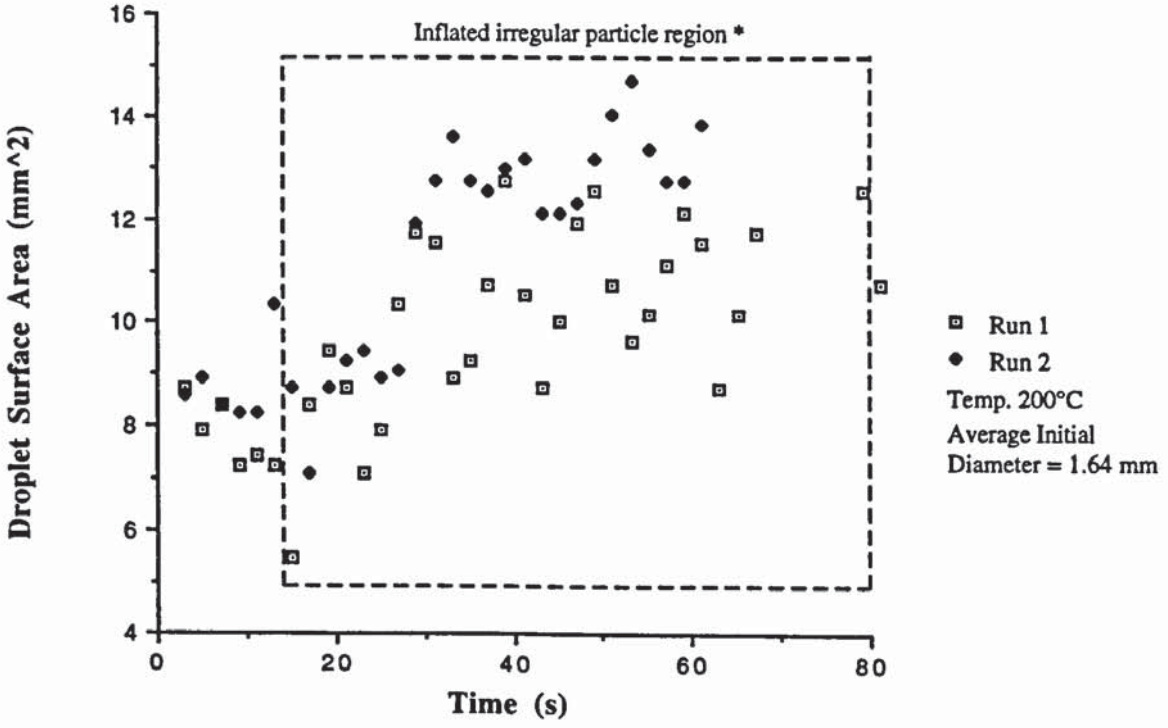

* a1 (Run 1) = 10.64 mm^2, a2 (Run 2) = 12.94 mm^2

Figure 125. Apparent Surface Area vs Time for Droplets of 30% w/w Semi-Instant Skimmed Milk

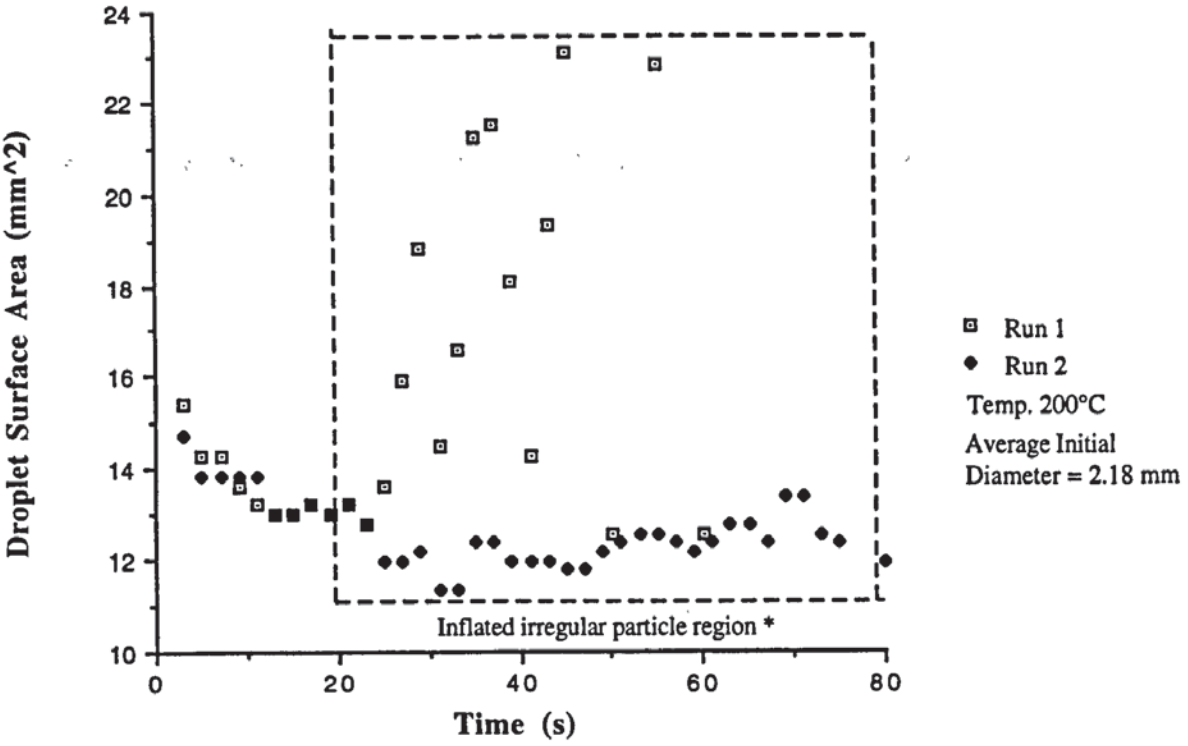

* a1 (Run 1) = 23.19 mm^2, a2 (Run 2) = 11.97 mm^2

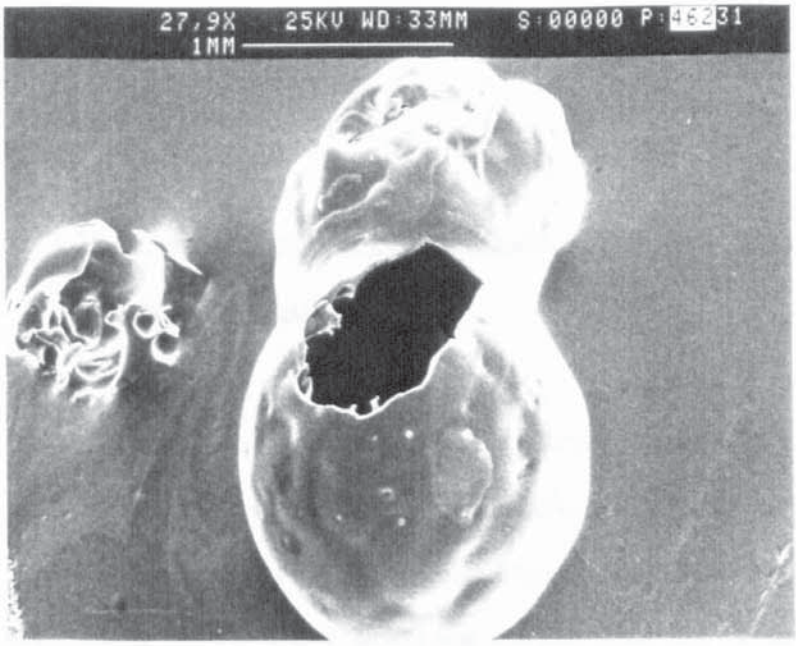

Figure 126.
semi-instant skimmed milk
In. conc. 30% w/w
Temp. 200°C

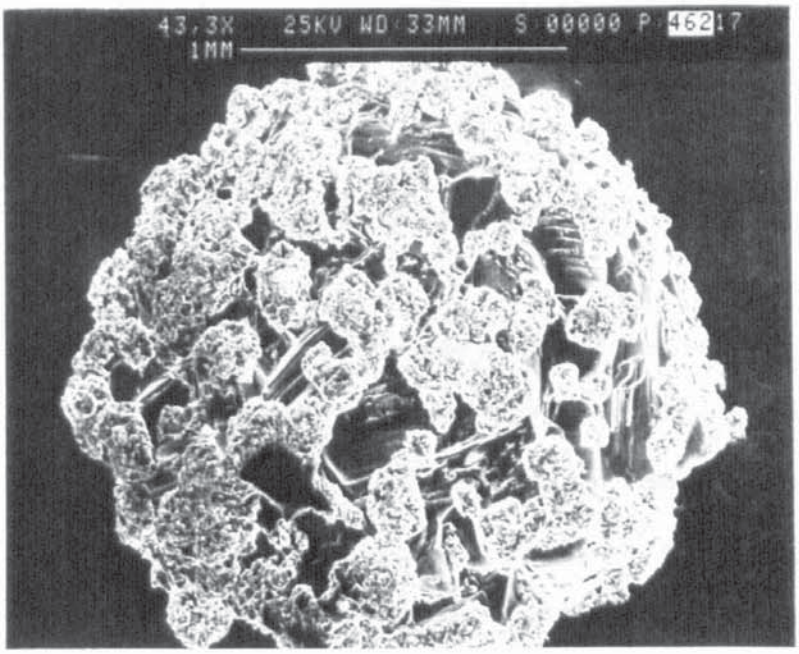

Figure 127.
sodium chloride
In. conc. 36% w/w
Temp. 200°C

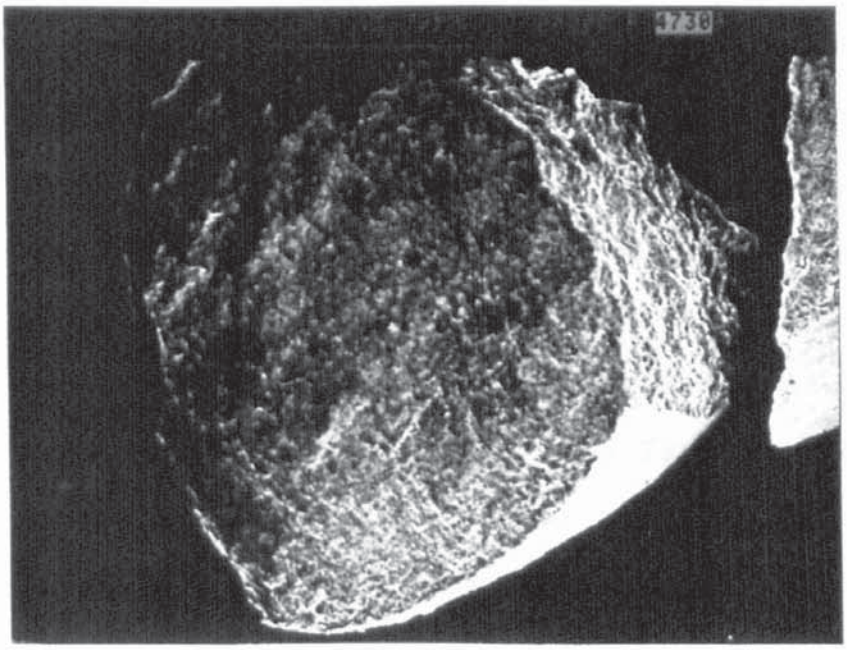

Figure 128.
silica
In. conc. 23% w/w
Temp. 200°C

6.10) Particle Morphologies Derived from Multicomponent Solutions

Two mixed solutions, the first containing sodium silicate and sodium chloride, both at a concentration of 5 % w/w (10 % w/w total solids), and the second containing semi - instant skimmed milk and sodium chloride at the same concentration, were dried as single droplets at temperatures of 70°C and 200°C. The following general observations were made,

sodium silicate / sodium chloride

Initial evaporation periods were longer at both 70°C and 200°C than for either of the two individual solutes dried at the same temperature. Sodium chloride appeared to show the first visible signs of precipitation, although the crystal nuclei did not travel throughout the droplet surface as previously observed with the individual solute. This suggests they may have been held in situ by a thin film of sodium silicate, which has the lower aqueous solubility. The drying behaviour of the particles was dominated at both temperatures by characteristics due to sodium chloride. Cycles of particle inflation, collapse and re-inflation were however, far more subdued than with either of the two individual solutes. This appeared to be the result of a lack of mobility or flexibility within the particle crust or skin surface. Although there was no violent surface deformation during drying, a certain amount

of internal bubble nucleation did take place. This resulted in the formation of hollow particles with wall thicknesses in the region of 80 μm at 70°C and 60 μm at 200°C. The surface morphologies of particles dried at 70°C were relatively spherical with little or no deformation (see Figure 129), and with sodium chloride comprising the major constituent of the surface structure. Similar morphologies were produced at 200°C, although the sodium chloride nuclei were smaller, approximately 30 μm in diameter as opposed to 50 μm in diameter at 70°C. The majority of particles dried at 200°C exhibited inflation of the sodium silicate matrix. This forced the sodium silicate through the surface of the sodium chloride crust (see Figures 130 and 131) which suggests the formation of a double skinned particle, i.e.; an outer layer of sodium chloride encapsulating an inner layer of sodium silicate.

<u>semi - instant skimmed milk / sodium chloride</u>

The overall drying behaviour of these particles was very similar to that of semi - instant milk particles. Consequently, and in complete contrast to the sodium silicate / sodium chloride particles, it was the skin-forming material rather than the crystalline material which dominated both particle drying behaviour and particle morphology. Cycles of particle inflation, collapse and re-inflation occurred at both 70°C and 200°C, albeit to a lesser extent than with the individual solutes and, as with particles of sodium

silicate / sodium chloride, there was a noticeable increase in skin or crust rigidity. The morphologies of the fully-dried particles varied from being partially-inflated to shrivelled and collapsed. All the particles produced were hollow with skin / crust thicknesses ranging from approximately 50 μm to 60 μm at 70°C and 20 μm to 50 μm at 200°C. At both drying temperatures the majority of the sodium chloride was located on the inside of the particle structure and the semi - instant skimmed milk on the outside. However, a large number of individual sodium chloride nuclei were evenly distributed over the surface of all the particles (see Figures 132 and 133). The concentration of these nuclei increased with drying temperature so that the particles dried at 200°C appeared white (see Figure 134). Such nuclei deposition could have resulted from, sodium chloride solution being ejected from beneath the particle skin / crust surface during drying, i.e.; through a rupture. Alternatively, the uniformity of the crystal nuclei in terms of size and distribution (see Figure 133) may be indicative of diffusion of the solution through submicron pores in the skin / crust surface.

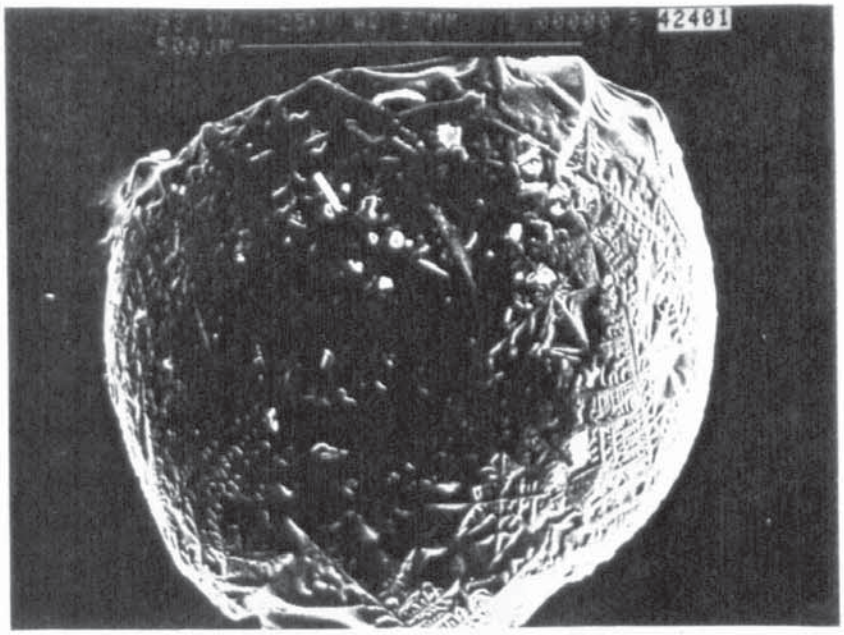

Figure 129.
sodium silicate plus sodium chloride
In. conc. 5% w/w
(10% w/w total)
Temp. 70°C

Figure 130.
sodium silicate plus sodium chloride
In. conc. 5% w/w
(10% w/w total)
Temp. 200°C

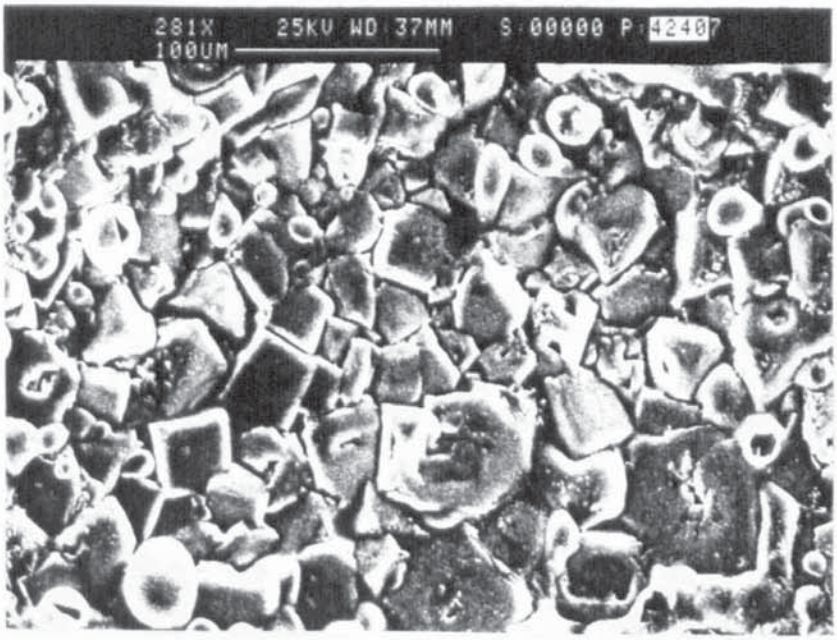

Figure 131.
sodium silicate plus sodium chloride
As Figure 130.

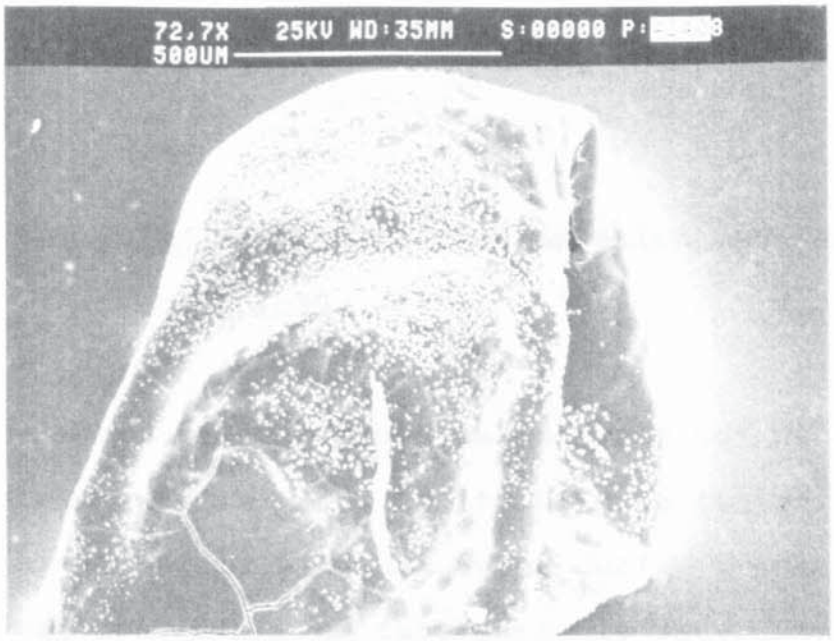

Figure 132.
semi-instant
skimmed milk plus
sodium chloride
In. conc. 5% w/w
(10% w/w total)
Temp. 70°C

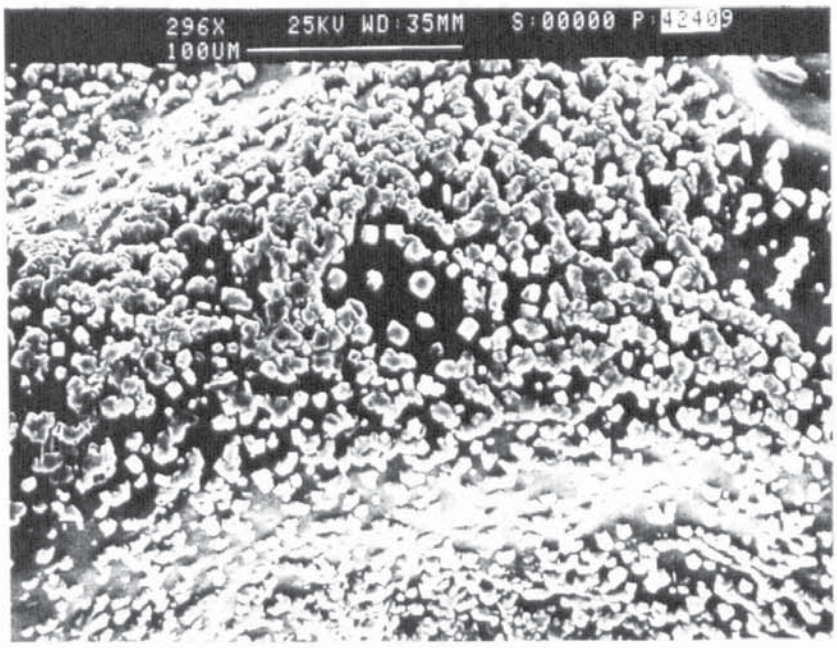

Figure 133.
semi-instant
skimmed milk plus
sodium chloride
As Figure 132.

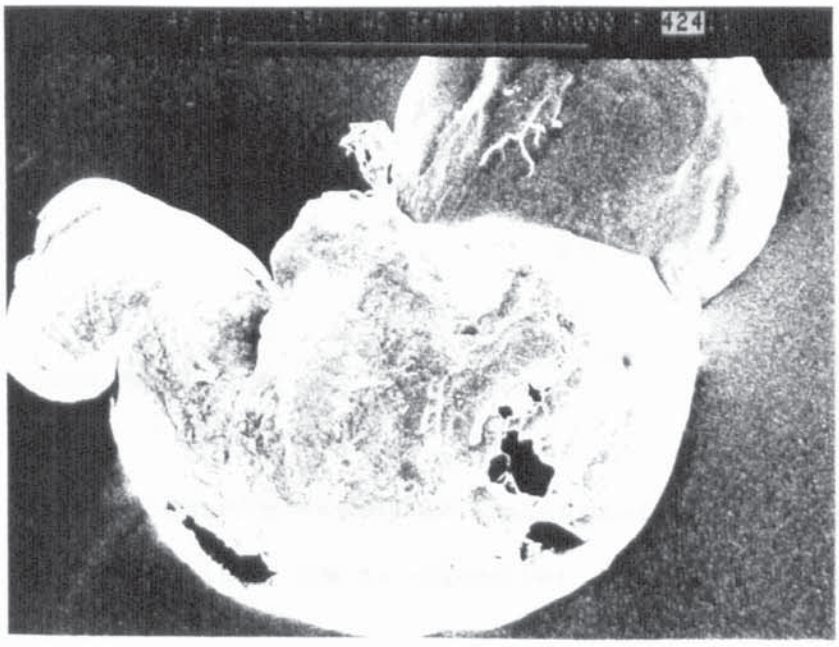

Figure 134.
semi-instant
skimmed milk plus
sodium chloride
In. conc. 5% w/w
(10% w/w total)
Temp. 200°C

6.11) The Effects of Feed Aeration and Deaeration on Particle Morphology

A morphological study was carried out on a commercial anionic detergent in order to investigate the effects of feed aeration, such as can arise during processing and transfer, and deaeration on intraparticle vacuolation. The extent of particle vacuolation, i.e.; the formation of holes, pores or bubbles within the solid matrix, has a considerable bearing on the particle / bulk density produced, e.g.; through particle inflation in drying. It is of considerable commercial importance.

Single droplets of detergent were dried under the following conditions using both aerated and deaerated feed stocks,

Drying Air Temperature	65°C (29°C WB)
	82°C (32°C WB)
	107°C (41°C WB)
Solids Concentration	50 % w/w
	70 % w/w

Feed Aeration

Approximately 2000g of detergent were weighted out into a 5l beaker (16.5 cm in diameter) and the appropriate amount of

distilled water added to give a solids concentration of either 50 % or 70 % w/w. The contents of the beaker were gently stirred with a glass rod for approximately 1 minute to ensure partial suspension of the solids. A pitched blade turbine 7.5 cm in diameter, giving an impeller to beaker diameter ratio of 0.45, and rotating at 800 rpm was then used for complete mixing. The impeller was positioned centrally to promote vortexing and hence ensure air entrainment during continuous agitation. The beaker was covered with a damp cloth to minimize evaporation. Thirty minutes was found to be the optimum mixing time for the 70 % solids concentration, i.e.; the shortest time to produce an air saturated paste of even consistency. The paste had a viscosity of 2194 mP/s. Up to two hours continuous mixing did not alter the level of air entrainment.

An identical mixing time was used for the 50 % solids concentration to standardize mixing procedures. This produced a paste with a viscosity of 147 mP/s.

Figures 135 and 139 show the size distribution of entrained air bubbles found in a typical sample of aerated detergent paste. Both the photographic and graphical data, obtained by optical microscopy, represents a sample area of approximately 0.2 mm^2, i.e.; the microscope's field of view. Bubble diameters ranged from 3 μm to almost 100 μm, with the majority below 25 μm in diameter.

Feed Deaeration (Chemical)

A commercial antifoaming agent, Dow Corning ® 544 silicone fluid (an emulsion of polydimethylsiloxane with a non-ionic emulsifier) and hexane, were added to separate batches of an aerated 70 % w/w detergent paste, i.e.; the silicone fluid in one batch and hexane in the other, at concentrations of 500 ppm and 1 % w/w respectively. The pastes were then continuously stirred for 60 minutes under identical conditions with the same apparatus and procedure used to aerate the feed. The effectiveness and stability of deaeration was monitored as a function of time by taking samples every 15 minutes and examining them under an optical microscope for bubbles of entrained air. The aerated paste, i.e.; the paste prior to the addition of the deaerants (t = 0 min) was used for comparison.

Figures 135 to 147 suggest that both the silicone fluid and the hexane successfully deaerated the detergent paste. The silicone fluid significantly reduced the level of air entrainment after 15 minutes continuous stirring. Both the size and the number of air bubbles within the paste decreased as illustrated by a comparison of Figure 139 with Figures 140 to 143. The level of deaeration remained stable for over 60 minutes, although the number of small bubbles, i.e.; 3 μm in diameter, were found to increase in samples taken at 60 minutes. Hexane did not achieve the same level and stability

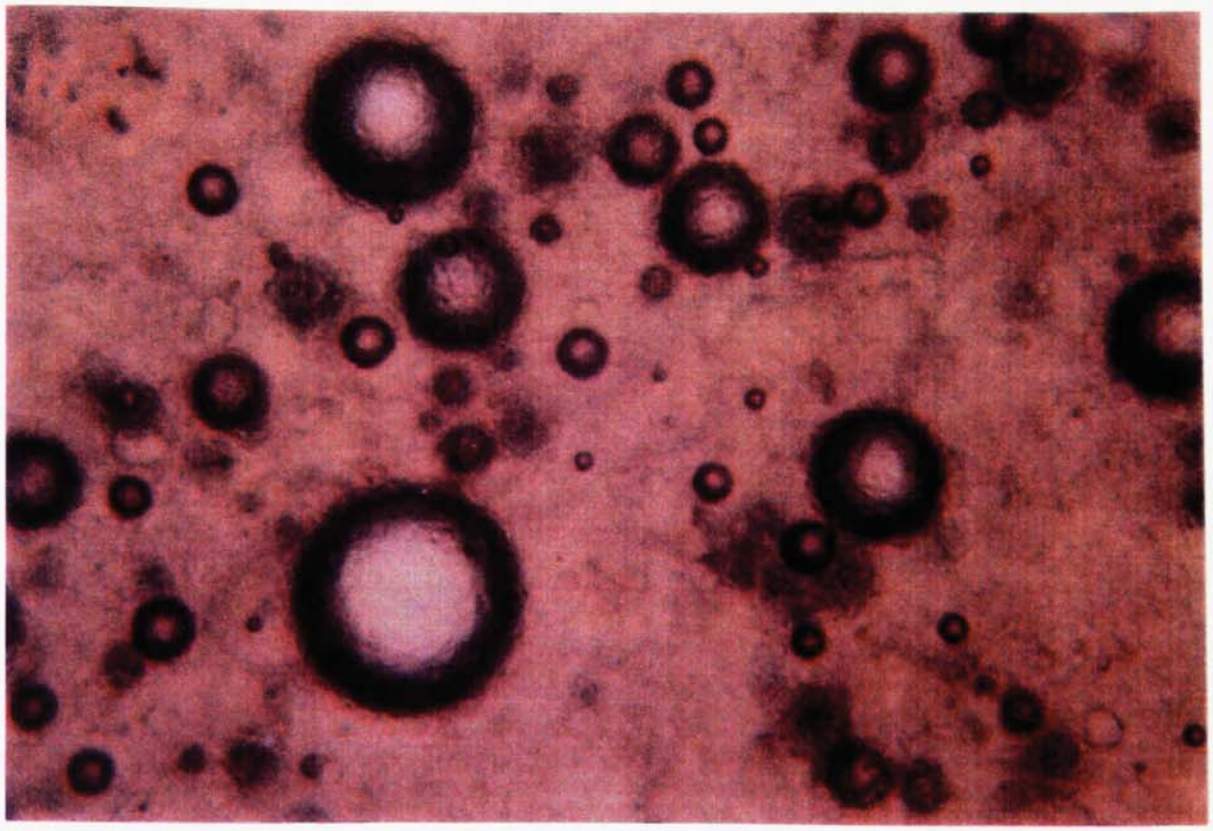

Figure 135. Aerated Detergent Paste (mag. x 300)

(mixing time 30 mins., In. conc. 70% w/w)

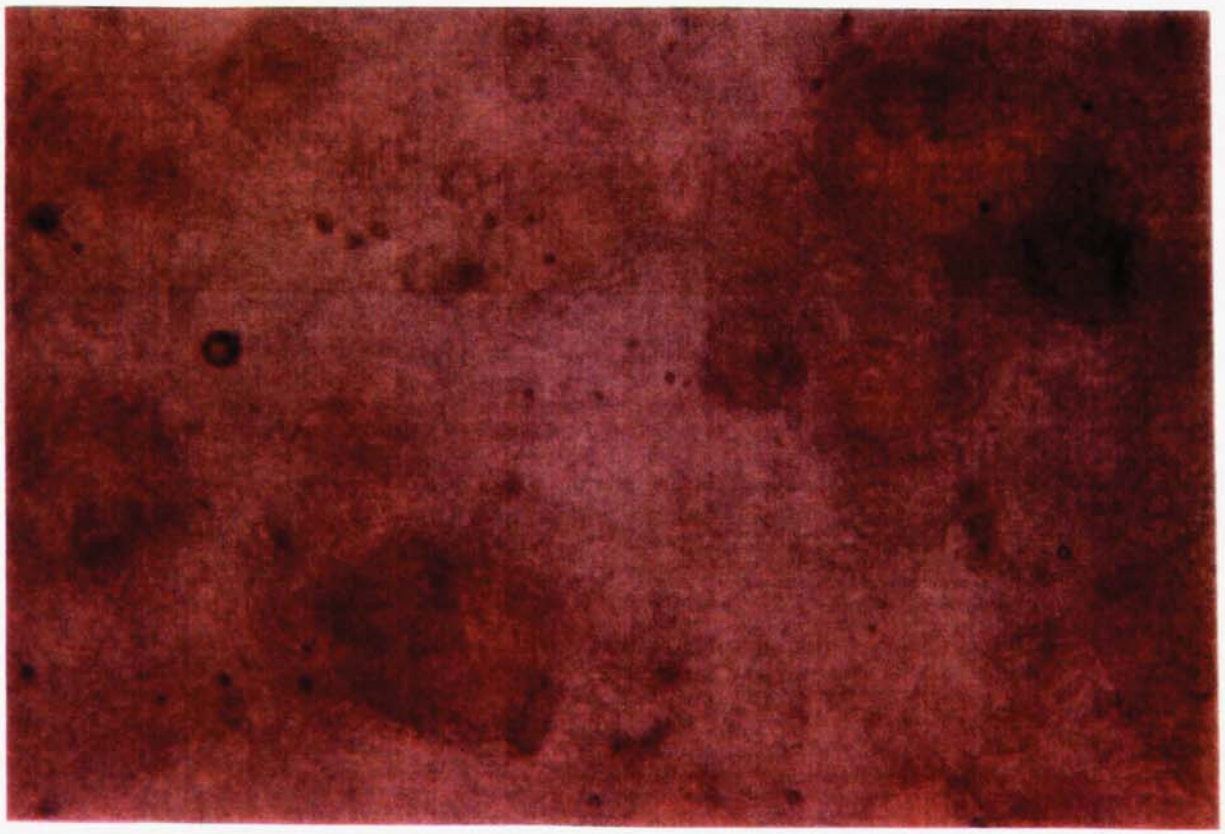

Figure 136. Detergent Paste Deaerated with 500 ppm Silicone DC544 (mag. x 300)

(mixing time 60 mins., In. conc. 70% w/w)

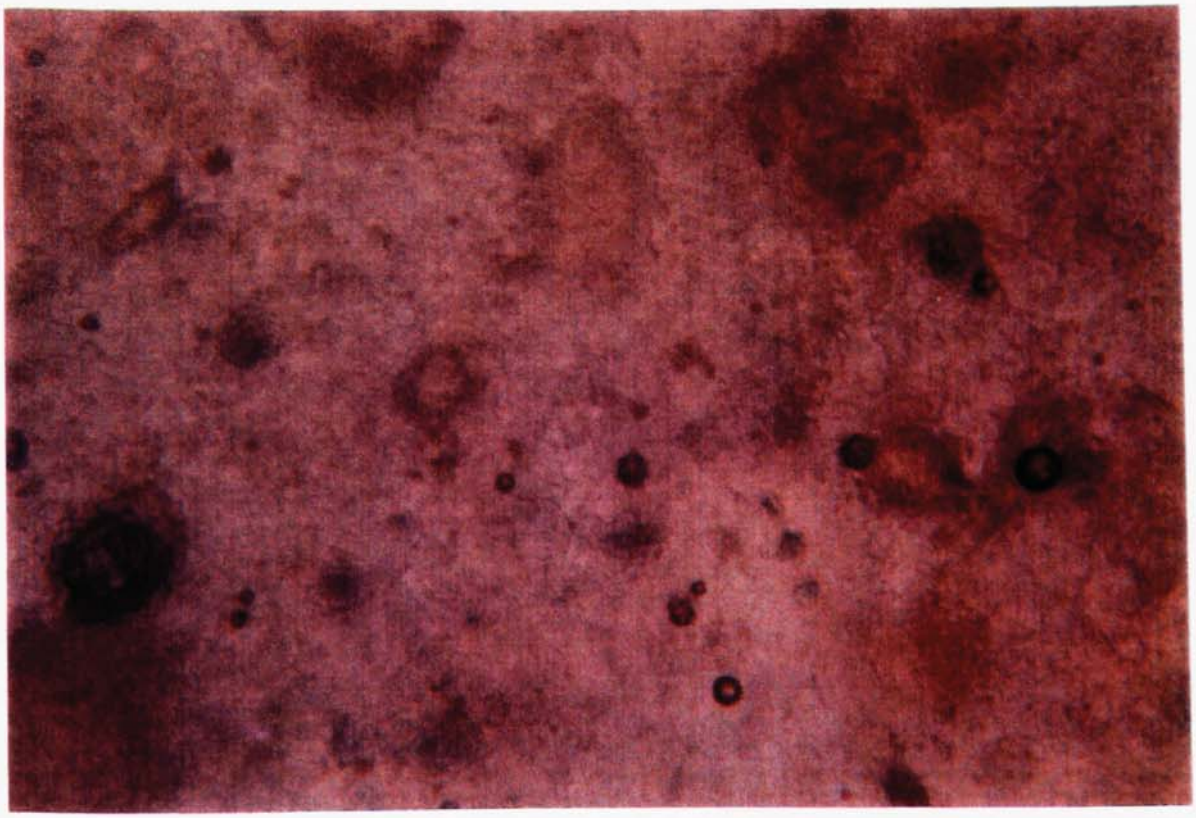

Figure 137. Detergent Paste Deaerated with 1% w/w hexane (mag. x 300)
(mixing time 45 mins., In conc. 70% w/w)

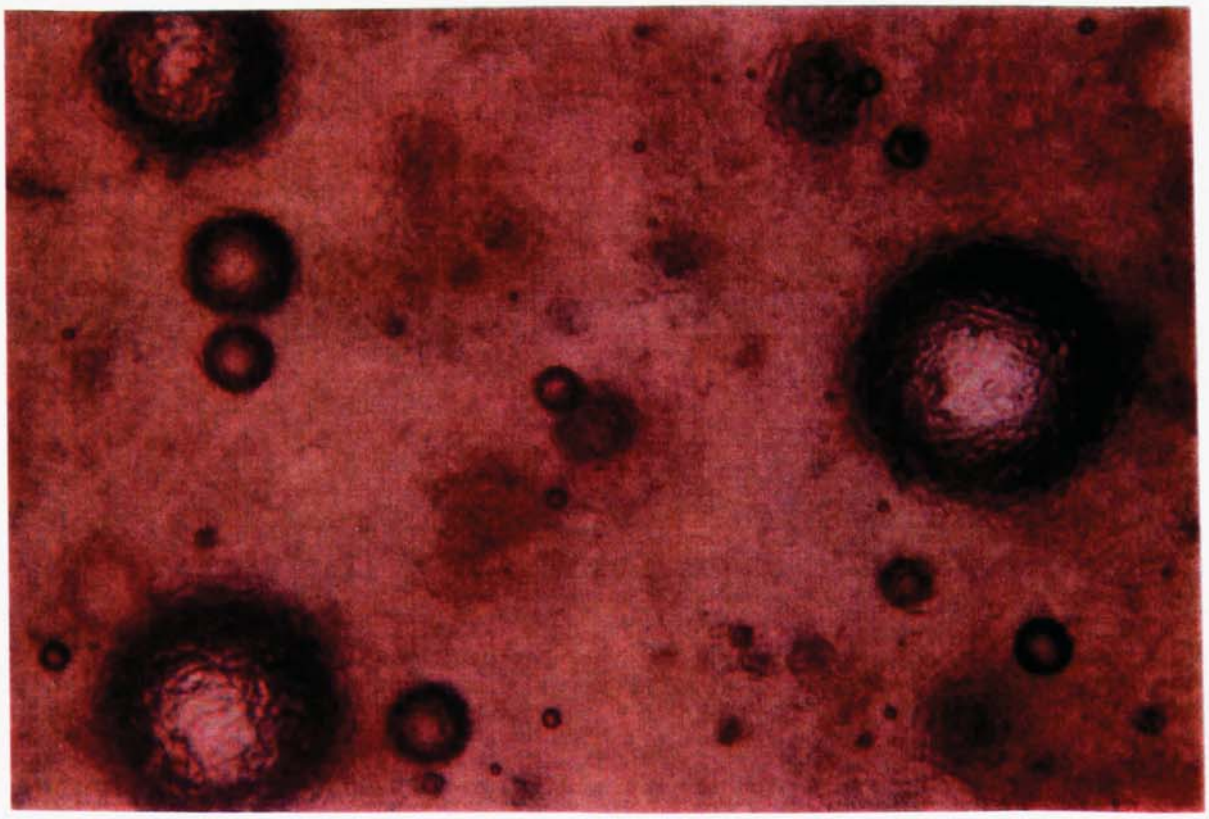

Figure 138. Detergent Paste Deaerated with 1% w/w hexane (mag. x 300)
(mixing time 60 mins., In. conc. 70% w/w)

Figure 139. Aerated Detergent (t = 0 min)

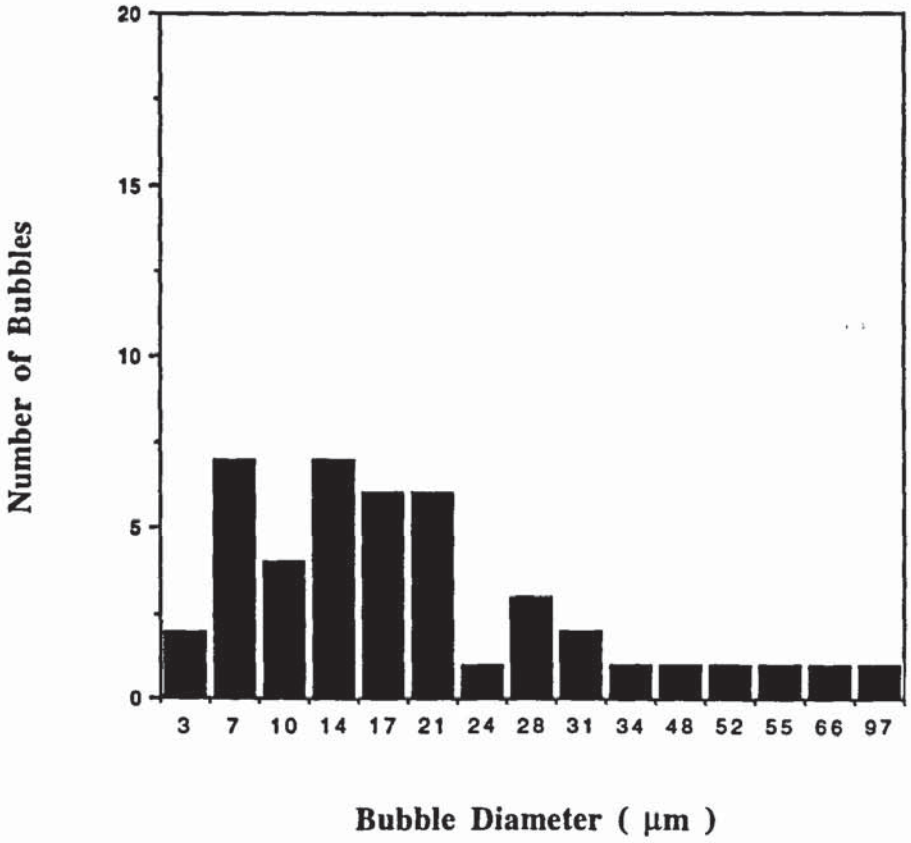

Figure 140. Silicone Deaerated (t = 15 min)

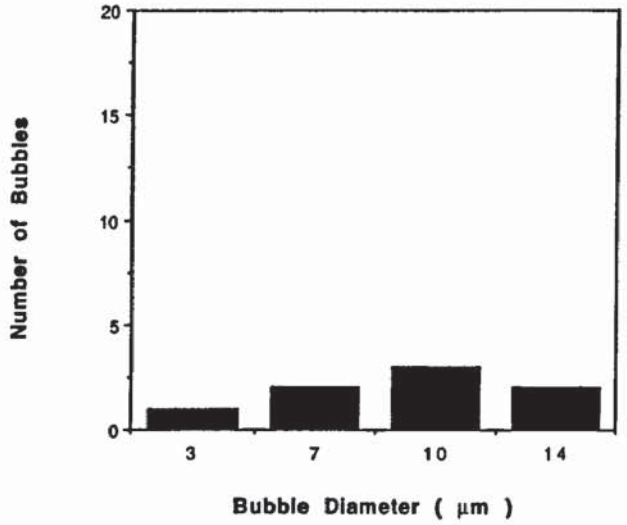

Figure 141. Silicone Deaerated (t = 30 min)

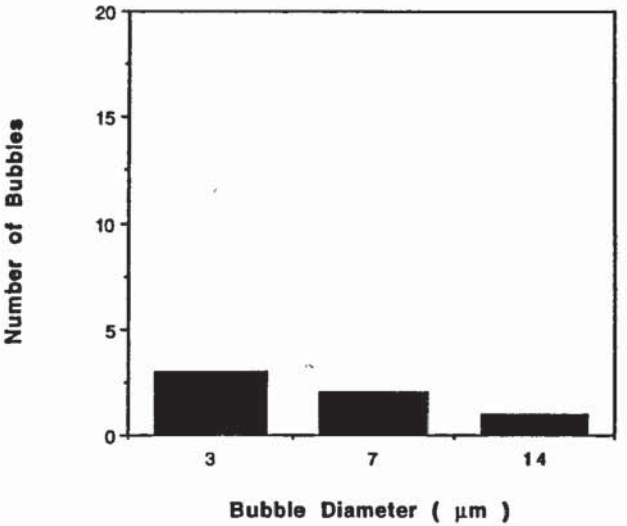

Figure 142. Silicone Deaerated (t = 45 min)

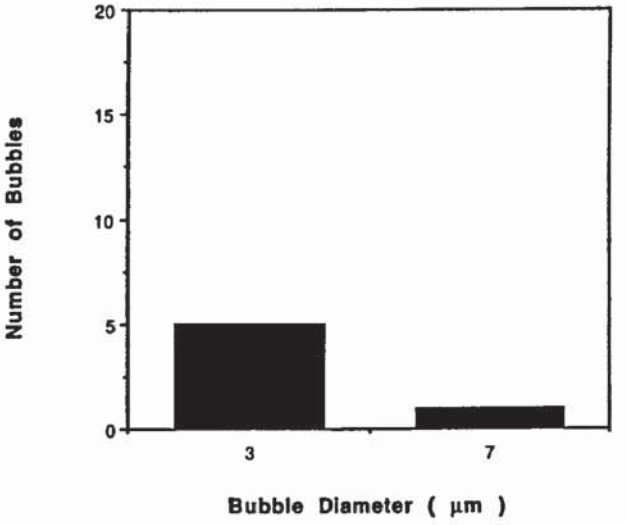

Figure 143. Silicone Deaerated (t = 60 min)

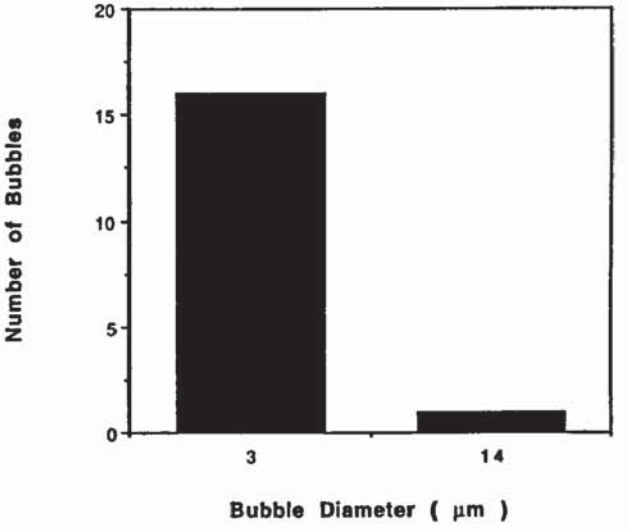

Figure 144. Hexane Deaerated (t = 15 min)

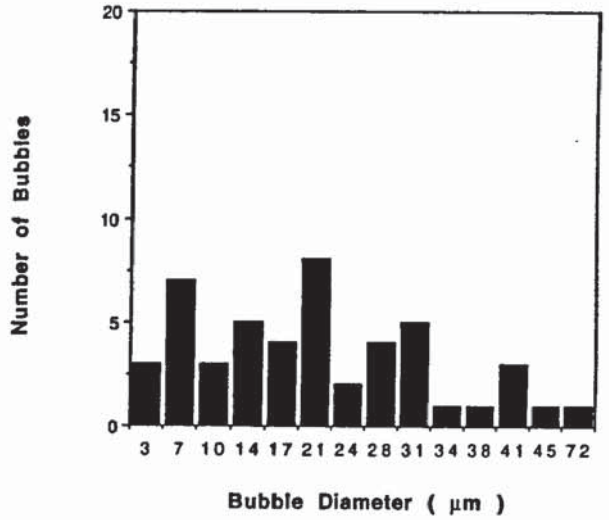

Figure 145. Hexane Deaerated (t = 30 min)

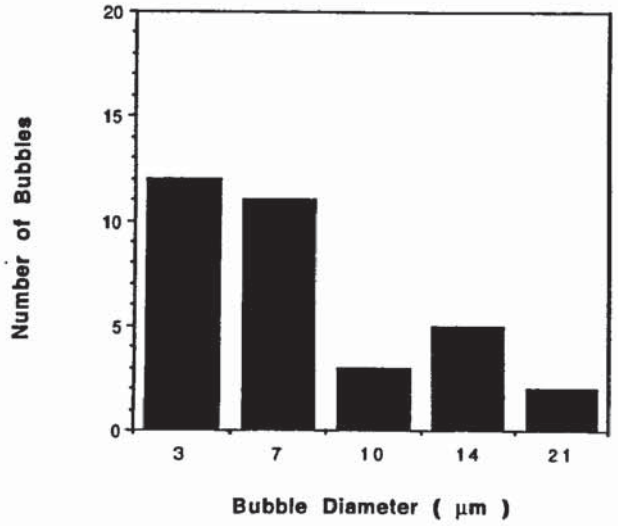

Figure 146. Hexane Deaerated (t = 45 min)

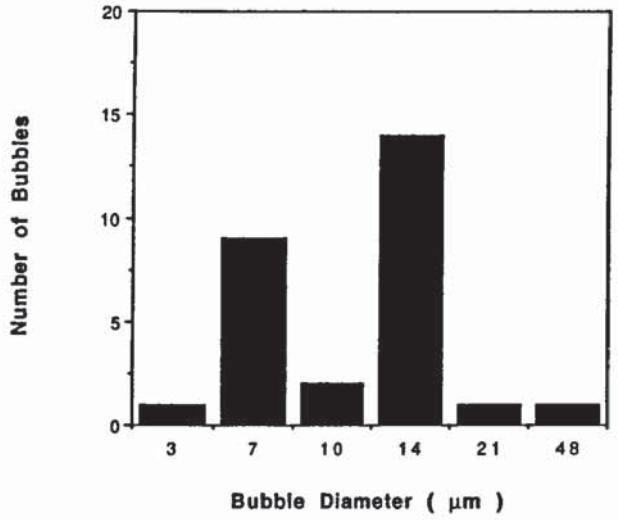

Figure 147. Hexane Deaerated (t = 60 min)

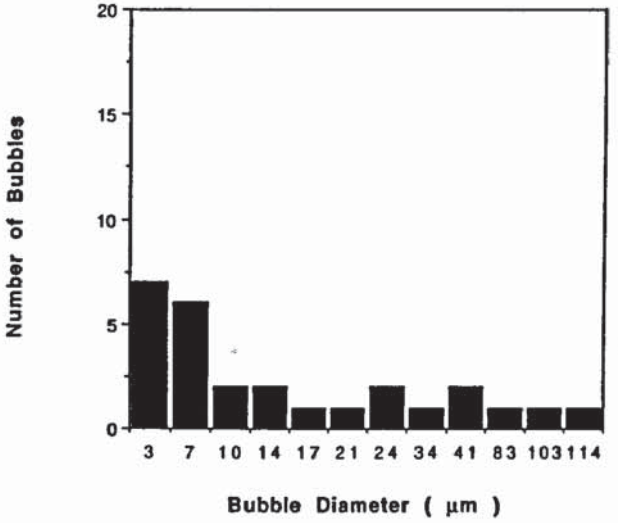

of deaeration as the silicone fluid (see Figures 144 to 147). After 15 minutes continuous stirring, no significant changes in the level of air entrainment had occurred. This may have been due to the hexane taking longer to disperse. Samples taken after 30 minutes did however show significant changes in bubble-size distribution, albeit to a lesser extent than with the silicone deaerant, i.e. there was an overall decrease in the number and size of air bubbles within the paste, but after 60 minutes, bubble sizes started to increase again. A number of bubbles larger than those found in the aerated paste were also found in samples taken after 60 minutes. This suggests the hexane vaporized to form bubbles of hexane vapour or / and air bubbles contaminated with hexane vapour - the air bubbles being formed by re-entrainment.

Single Droplet Drying Studies

All three detergent pastes, i.e.; the aerated, silicone deaerated and hexane deaerated, produced relatively similar particle morphologies, namely, particles with smooth exteriors and highly porous interiors. Both the exterior and interior structures were dependent on the concentration of the detergent paste, the level of paste aeration / deaeration and the drying temperature.

The exterior or surface structures of particles dried from pastes containing 50 % w/w solids were very smooth, almost spherical, with little or no surface distortion, i.e.; no

folds or wrinkles. However, most of the particles exhibited blowholes which varied in size and shape depending on the drying temperature. At 65°C and 82°C, blowhole diameters ranged from approximately 90 μm up to 150 μm, whereas, at 107°C they were in the region of 200 μm in diameter. With the exception of particles dried at 65°C, the blowholes were almost invariably located in cavities (see Figures 148 and 149). These appear to have been caused by the collapse of the particle surface structure, a feature grossly exaggerated in particles dried from the hexane-deaerated paste.

Particles dried from both the aerated and silicone deaerated pastes showed random increases in surface area during drying, i.e.; between 9 % to 15 % inflation, regardless of the drying temperature. Particles dried from the hexane-deaerated paste however, showed considerable increases in surface area which were very dependent on the drying temperature, i.e.; increases of between 20 % to 30 % at 65°C, 40 % to 50 % at 82°C and 250 % to 350 % at 107°C.

The surface structures of particles dried from detergent pastes containing 70 % w/w solids (see Figure 150) were very irregular with many folds and wrinkles. These probably arose during application of the paste to the suspension filament before drying. In general, surface morphologies were not significantly altered by increases in drying temperature or variations in the level of paste aeration / deaeration, although particles dried from the hexane-deaerated paste had a

greater tendency to inflate with surface areas increasing by approximately 20 % at 65°C and up to 80 % at 107°C.

The internal structures of all the particles were highly porous, irrespective of the drying condition, paste concentration and level of paste aeration / deaeration. The degree of porosity did however depend on these parameters.

The internal porosity of particles dried from detergent pastes containing 70 % w/w solids (see Figures 151 and 152) varied depending upon whether the paste was aerated or deaerated, and, with the type of detergent. The aerated paste produced particles with evenly-dispersed vacuoles which increased in size as the drying temperature increased; i.e. at 65°C vacuole diameters were approximately 40 μm in diameter, at 107°C they were in the region of 100 μm in diameter. In some cases the vacuoles were so large that particles might be regarded as being hollow rather than porous. Surprisingly, there was very little particle inflation during drying with less than a 10 % increase in particle surface areas at all three drying temperatures. Particles dried from the silicone deaerated paste had much denser internal structures. Both the size and number of vacuoles had decreased relative to the internal structures of particles dried from the aerated paste at the same temperatures. Changes in particle surface areas during drying were similar to those dried from the aerated paste. By far the greatest variation in internal porosity occurred with particles dried from the hexane deaerated paste. Vacuole diameters were considerably larger than any of those

found in particles dried from both the aerated and silicone deaerated pastes, i.e.; particles dried from the hexane-deaerated paste produced vacuoles ranging from approximately 70 μm to 500 μm in diameter at 65°C and 500 μm to 700 μm in diameter at 82°C. Vacuole diameters at 107°C were so large they coincided, essentially to form hollow particles. The extent of the internal porosity and the excessive amount of particle inflation observed at all three drying temperatures was almost certainly attributable to the vaporization of hexane within the detergent paste.

The internal structures of particles dried from pastes containing 50 % w/w solids showed identical trends to those dried from pastes containing 70 % w/w solids. Vacuole diameters were however, much larger ranging from approximately 70 μm to 600 μm at 65°C, 90 μm to 700 μm at 82°C and 200 μm to 800 μm at 107°C. Particles dried from the hexane-deaerated paste at 107°C were completely hollow with crust thicknesses of approximately 30 μm (see Figure 153).

The Addition of High Surface Area Powders

To asses the effect which addition of a high surface area powder might have upon dried particle properties, activated carbon and sodium aluminosilicate hydrate powders were first left to equilibrilate under ambient conditions of temperature, humidity and pressure for 24 hours. The powders were then added (5 % w/w) to separate batches of a 70 % w/w aerated

detergent paste. Single droplets of the pastes were then dried at 65°C. The addition of high surface area powders such as activated carbon (≈ 0.8 - 1.8 km^2/kg) and sodium aluminosilicate (≈ 0.7 km^2/kg), i.e.; powders with good gas adsorption properties, would be expected to increase the internal porosity of the particles by desorption of adsorbed gases during drying. Figures 154 and 155 tend to confirm this. The internal structure of particles dried from both batches showed a considerable increase in the size of vacuoles relative to particles dried from the standard aerated paste at the same temperature (compare Figures 154 and 155 with Figure 151). The overall number of vacuoles within the particles was not however increased.

Stirring under Vacuum

To simulate possible process improvements, a batch of aerated detergent paste (70 % w/w) was stirred under a vacuum of 635 mm Hg for approximately 30 minutes at 600 rpm. Single droplets of the paste were then dried at 65°C. Stirring the detergent paste under vacuum would be expected to decrease the internal porosity of the particles by decreasing the level of air entrainment within the paste. Figure 156 shows exactly that. The internal structure of particles dried from the ' outgassed ' detergent paste were much denser than those dried from the aerated paste, i.e.; only a limited amount of vacuolation had occurred.

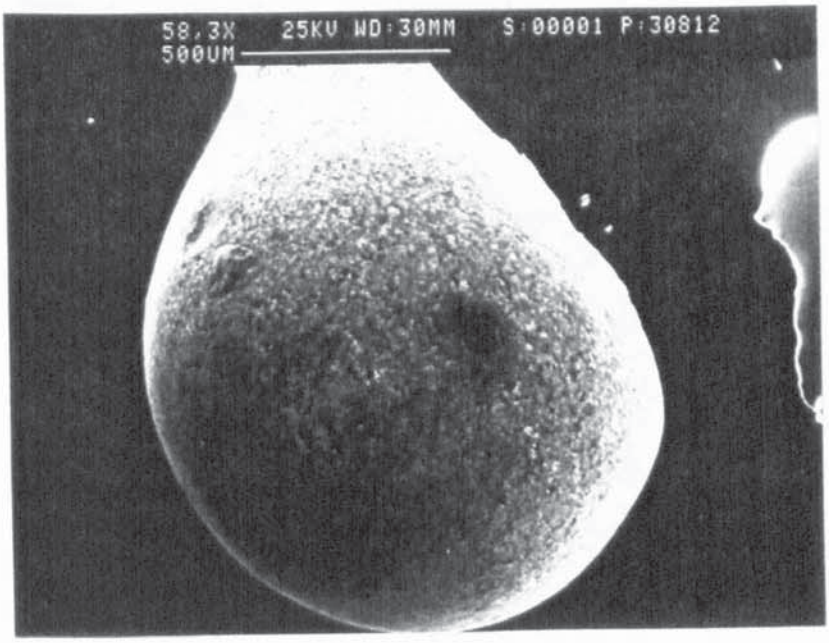

Figure 148.
aerated detergent paste
In. conc. 50% w/w
Temp. 65°C

Figure 149.
detergent paste deaerated with 500 ppm silicone DC544
In. conc. 50% w/w
Temp. 107°C

Figure 150.
aerated detergent paste
In. conc. 70% w/w
Temp. 107°C

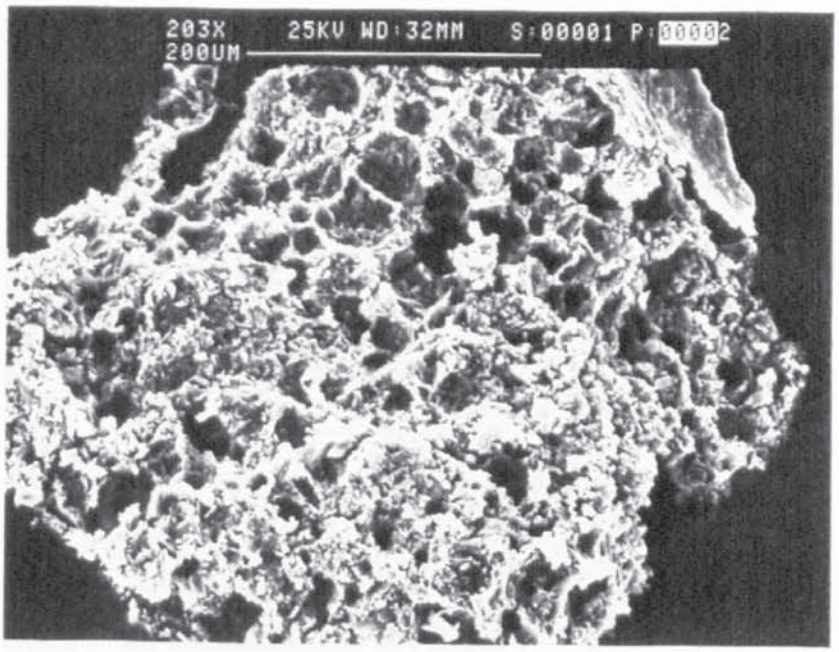

Figure 151.
aerated detergent paste
In. conc. 70% w/w
Temp. 65°C

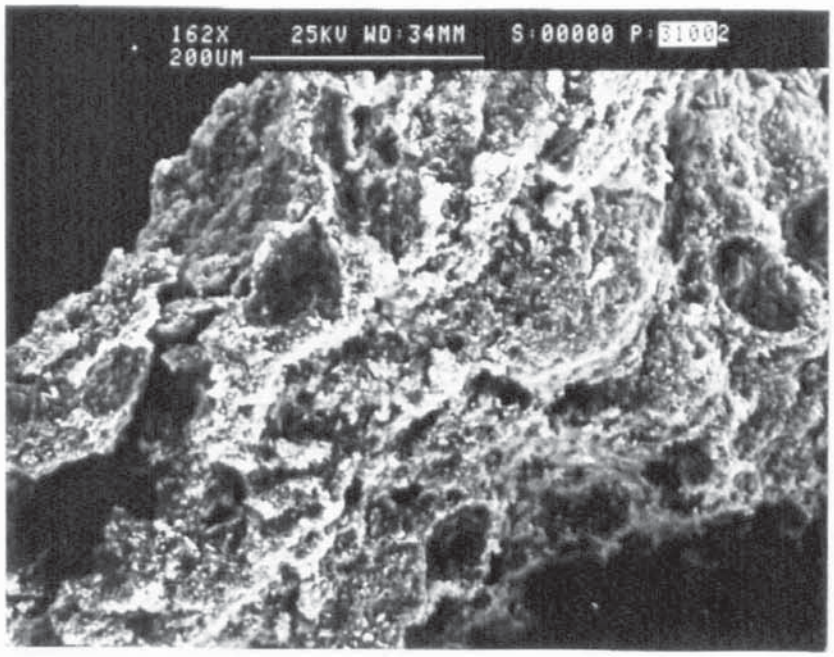

Figure 152.
detergent paste deaerated with 500 ppm silicone DC544
In. conc. 70% w/w
Temp. 65°C

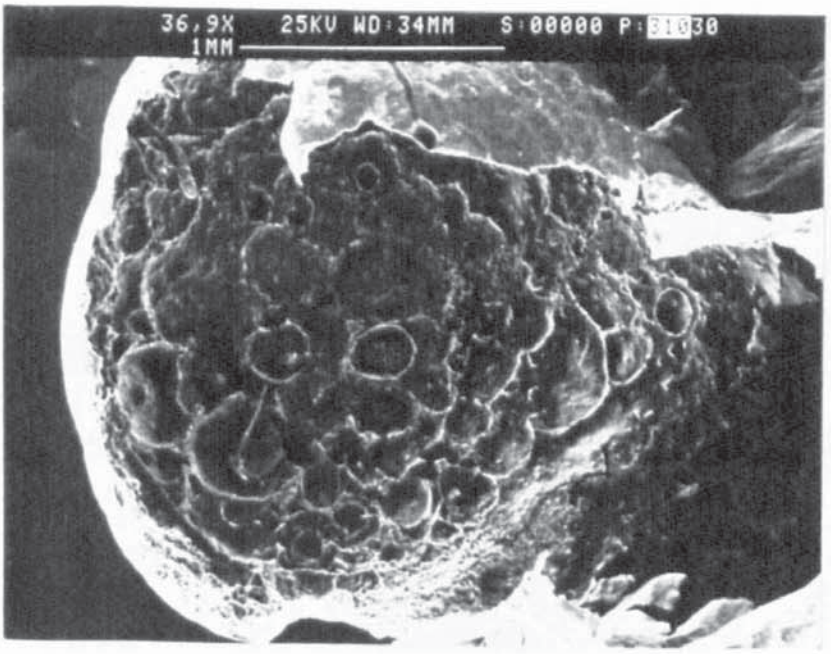

Figure 153.
detergent paste deaerated with 1% w/w hexane
In. conc. 50% w/w
Temp. 107°C

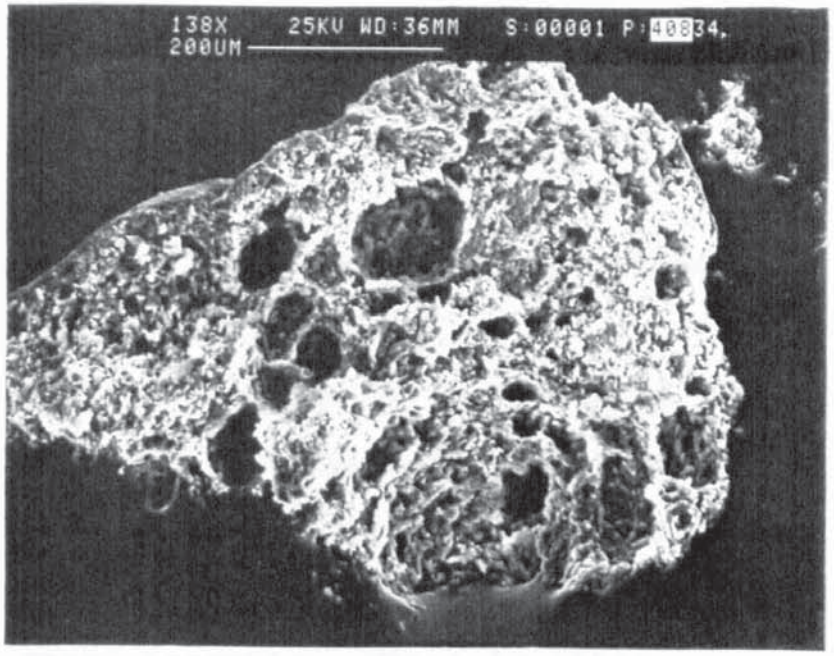

Figure 154.
aerated detergent paste plus activated carbon
In. conc.
detergent 70% w/w
carbon 5% w/w
Temp. 65°C

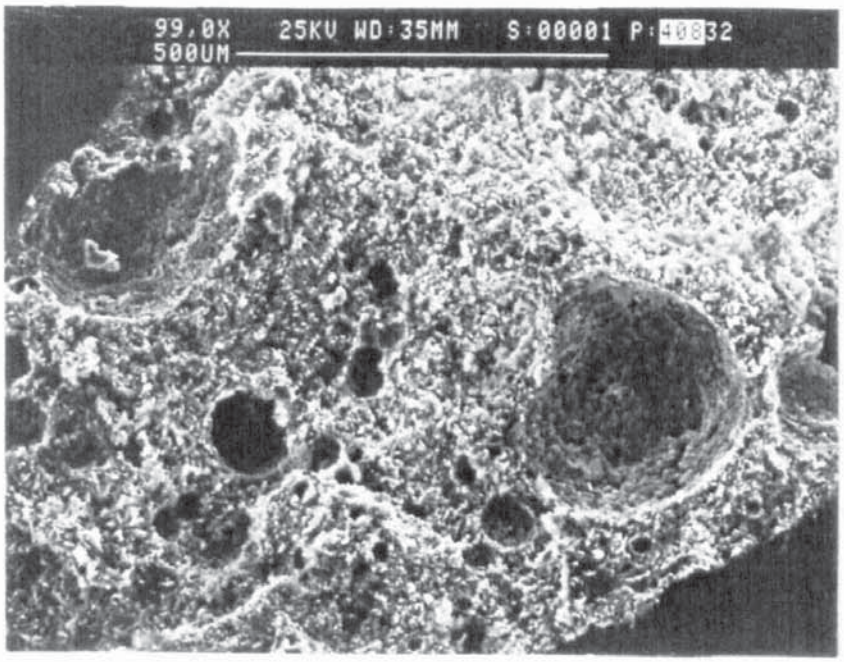

Figure 155.
aerated detergent paste plus sodium aluminosilicate hydrate
In. conc.
detergent 70% w/w
aluminosilicate 5% w/w
Temp. 65°C

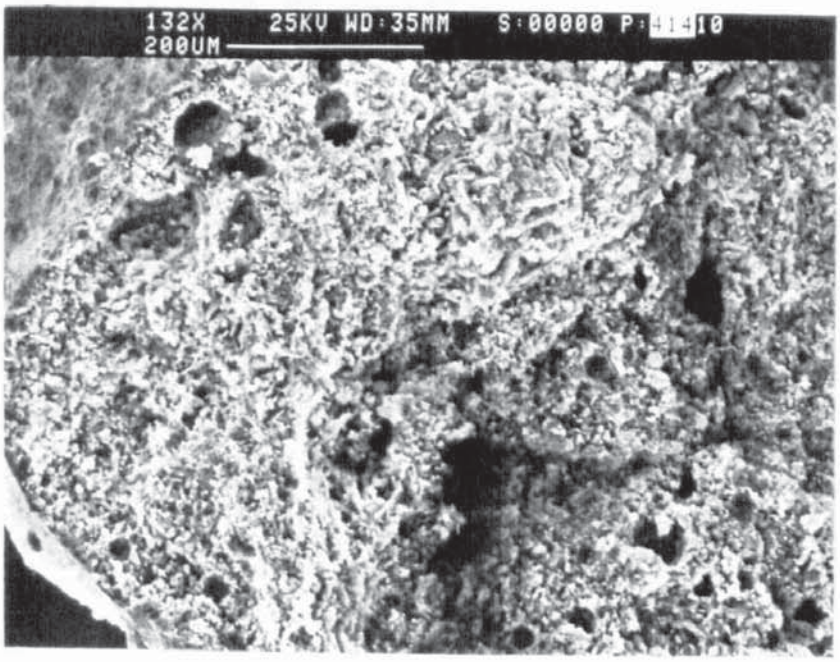

Figure 156.
aerated detergent paste stirred under vacuum for 30 mins.
In. conc. 70% w/w
Temp. 65°C

6.12.0) The Retention of Volatiles

Work carried out by Thijssen (72,154) King et al (189) suggests that the majority of volatiles, flavour and aroma loss in spray drying occurs during atomization and in the initial stages of droplet evaporation, i.e.; before skin or crust formation. There is little or no experimental information however, concerning the effects of particle morphology upon the retention, or loss, of volatiles during spray drying.

A study was therefore made of the effects of particle morphology, feed concentration, and drying temperature upon the retention of a ' model volatile ', namely ethanol. Ethanol was chosen because its rate of evaporation from the droplets was readily quantifiable throughout drying using an established G.L.C. analytical technique.

6.12.1) Feed Preparation

15.0000g of sodium chloride, semi - instant skimmed milk (SIM) and silica, i.e.; typical representatives of the three types of morphological structure, were separately dissolved or suspended in 75.0000g of distilled water and 10.0000g of absolute ethanol (0.2 % water) to give a solid and volatile feed concentration of 15 % w/w and 10 % w/w respectively. All three solutions / suspensions were thoroughly mixed by

vigorously shaking in a stoppered 150 ml screw topped glass bottle for approximately 5 minutes.

Additional feed concentrations of semi - instant skimmed milk, 1 % w/w and 25 % w/w, were also prepared.

6.12.2) Experimental Procedure

Single droplets from each of the three different types of morphological feed were dried at 120.0°C (44.3°C WB) for ' 0 s ', 20 s, 40 s, 60 s, 80 s and 100 s. Four consecutive droplets were dried for each time interval and the total amount of ethanol contained within each was subsequently determined by gas liquid chromatography as described later (see Appendix A 5.0). This ensured a detectable level of ethanol after drying. The relative percentage of ethanol remaining in all four droplets was then calculated by comparing the analytical results, i.e.; peak area, with the theoretical amount of ethanol present in the droplets before drying. This allowed for any variations in the initial droplet size. Theoretical values were obtained by calculating the total volume of feed dried per time interval - obtained by measuring initial droplet diameters - and comparing it with the analytical results of the total volume of feed ' dried ' at t = 0 s.

Thus if the time interval t = 0 s was assumed to have 100 % ethanol retention then,

$$\text{Relative percentage of ethanol remaining} = \frac{A}{(B / C) D} \times 100$$

where, A = ethanol peak area per time interval
B = ethanol peak area at t = 0s
C = total volume of feed taken at t = 0s
D = total volume of feed taken per time interval

Further experiments were performed with semi - instant skimmed milk dried at different feed concentrations and drying temperatures. Droplets were dried at 120°C from feed concentrations of 1 % w/w, 15 % w/w and 25 % w/w, and, from a feed concentration of 15 % w/w at temperatures of 120°C, 150°C and 200°C.

The results are presented in Table 26 and Figures 157 to 159, and the raw data in Appendix A 5.0. Water droplets containing 10 % w/w ethanol and no solids were used as a reference in Figure 157.

6.12.3 Analysis - Gas Liquid Chromatography

Immediately after drying, the four droplets or particles dried per time interval were placed in a 1.5 ml Eppendorf tube containing 0.5000g of distilled water. The tube was sealed and covered with Parafilm ● to prevent any loss of ethanol. The contents were then thoroughly mixed using a vortex mixer which effectively broke-up the particles. Once all six tubes had

been prepared, i.e.; 0 s to 100 s, they were left in a refrigerator at 5°C for 24 hours to allow any ethanol trapped within the solids to leach out. After 24 hours, the tubes were taken out of the refrigerator and left for approximately 1 hour to attain room temperature and then re-mixed using the vortex mixer.

The samples were analysed under the following conditions using a Pye Unicam 204 Gas Liquid Chromatograph,

Mobile phase	- Helium, 30 ml / min.
Stationary phase	- Porapak ® Q (s.s. column, 4 mm i.d. x 1.8 m)
Detector	- TCD (atten. 2 x 10)
Temperatures	- Detector (250°C), Injector (250°C), Oven (180°C)
Injection size	- 4 µl

Each sample was analysed three times and the average ethanol peak area calculated.

Table 26. The Effects of Particle Morphology, Feed Concentration and Drying Temperature on the Retention of Ethanol

Sample	Solids Concentration	Drying Temperature	Drying Time	Relative % of Ethanol Remaining
	% w/w	°C	s	
sodium chloride	15	120	0	100.0
			20	1.4
			40	1.2
			60	0.7
			80	0.7
			100	0.6
silica	15	120	0	100.0
			20	36.6
			40	26.3
			60	7.5
			80	2.1
			100	0.8
SIN	15	120	0	100.0
			20	49.0
			40	40.2
			60	42.5
			80	42.0
			100	39.9
SIN	1	120	0	100.0
			20	35.4
			40	13.3
			60	6.4
			80	5.6
			100	Trace
SIN	25	120	0	100.0
			20	95.5
			40	88.2
			60	85.1
			80	77.6
			100	68.4

Sample	Solids Concentration	Drying Temperature	Drying Time	Relative % of Ethanol Remaining
	% w/w	°C	s	
SIM	15	150	0	100.0
			20	83.6
			40	61.1
			60	51.2
			80	52.9
			100	47.5
SIM	15	200	0	100.0
			20	64.4
			40	54.4
			60	27.8
			80	13.5
			100	18.2
Water	--	120	0	100.0
			20	23.2
			40	3.3
			60	1.4
			80	0.7
			100	---

Figure 157. The Effect of Particle Morphology on the Retention of Ethanol

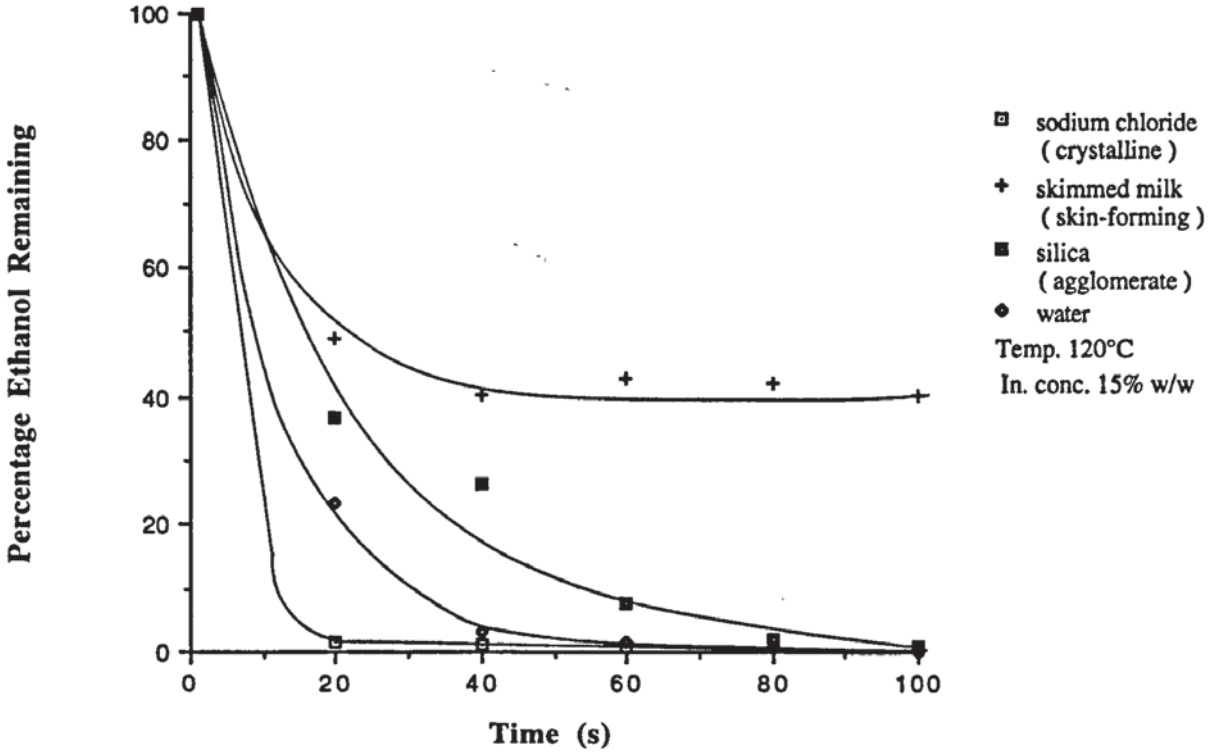

(Data representative of 3 tests)

Figure 158. The Effect of Concentration on the Retention of Ethanol in Droplets of Semi-Instant Skimmed Milk

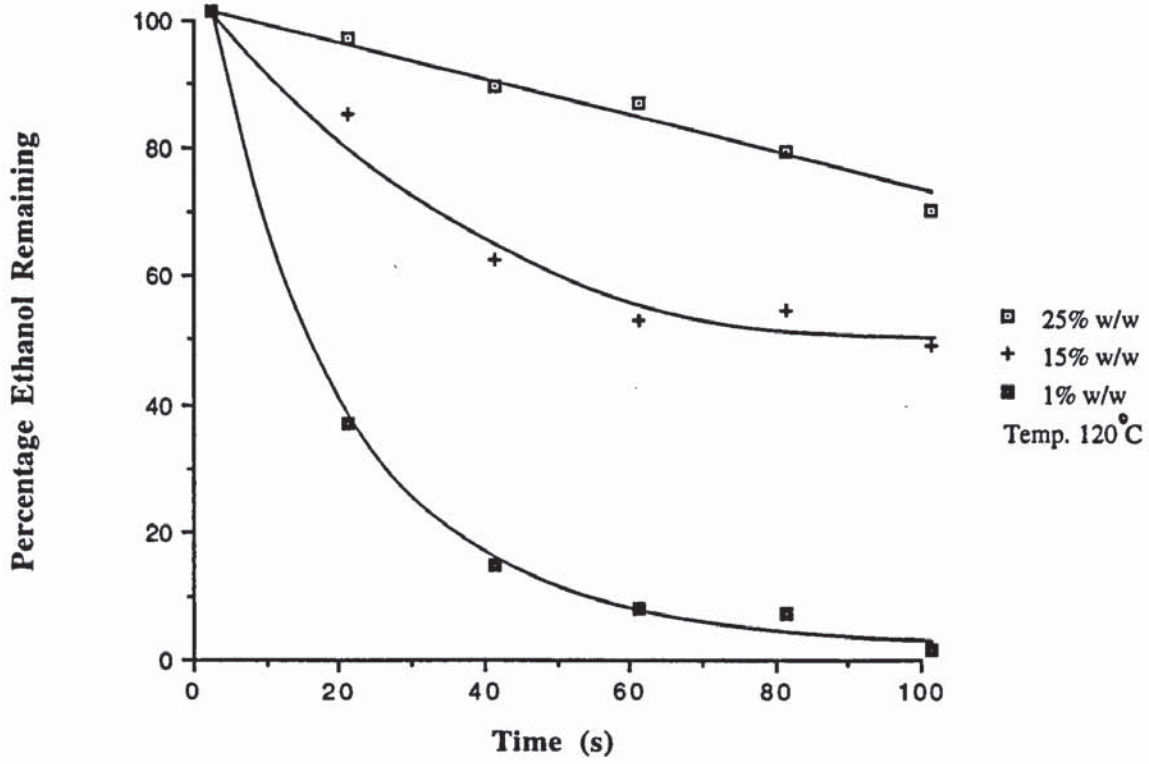

(Data representative of 3 tests)

Figure 159. The Effect of Temperature on the Retention of Ethanol in Droplets of Semi-Instant Skimmed Milk

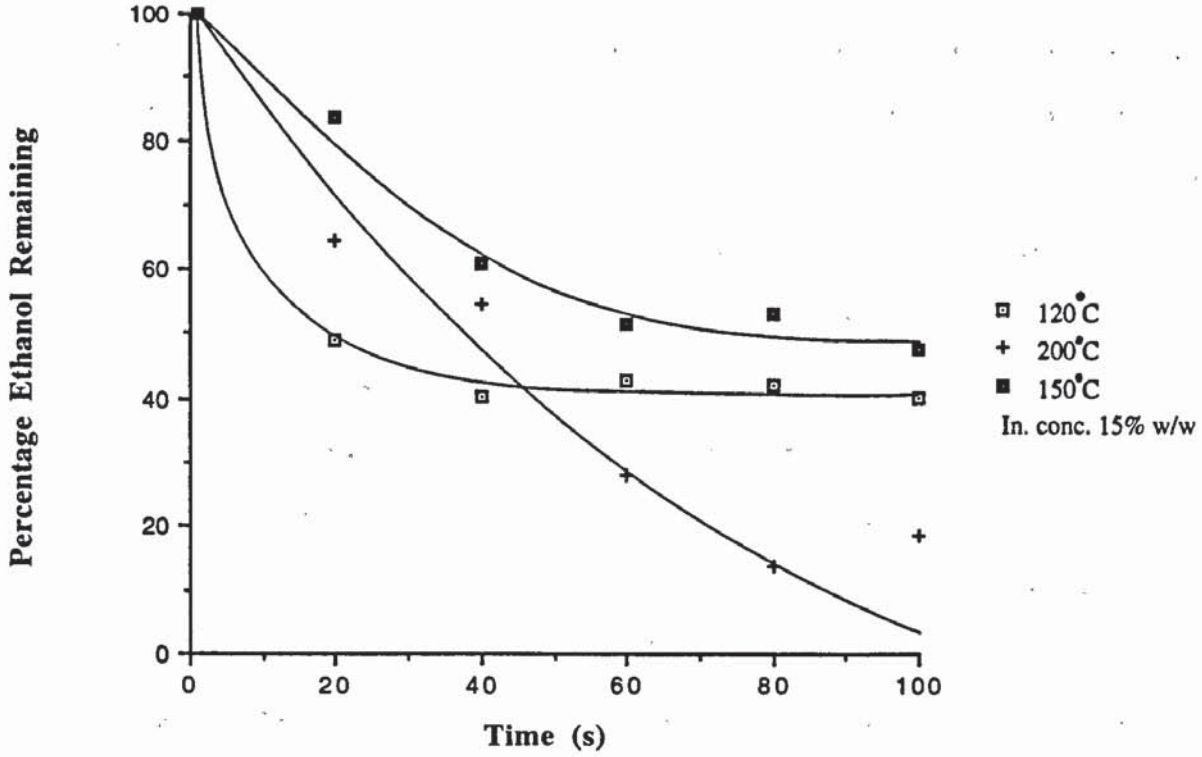

(Data representative of 3 tests)

(Demonstrating the beneficial effects of accelerated skin formation at 150°C which are overridden by inflation and rupture at 200°C)

6.13) Discussion

Evaluation of Drying Behaviour

The single droplet drying studies demonstrated that all of the particle morphologies exhibited by the materials listed in Table 25 can be categorized according to structure under the headings skin-forming, crystalline or agglomerate, i.e.; the same structural categories previously identified with the industrial spray-dried materials. Particles from each of these categories displayed the characteristic drying behaviour represented schematically in Figures 160 to 162.

The general morphology of the particles was markedly similar to those produced industrially. Features such as particle inflation, particle shrivelling, hollow particles, solid particles with varying degrees of vacuolation, smooth spherical particles, rough irregular particles and fractured particles were all produced on the single droplet drying apparatus. Such morphological features are clearly identifiable in the industrial spray-dried materials. Experiments were also carried out on a number of organic dyes and detergents with feed specifications and drying air temperatures identical to the industrial spray-dried material. The particle morphologies produced showed a good general agreement with those produced by industrial spray drying (230).

These studies demonstrated that both the chemical and physical nature of a material are important in determining its drying behaviour and particle morphology. For example, the rheological properties of skin-forming materials allow particles to inflate, collapse and then re-inflate many times. Ruptures in the skin surface are quickly sealed and surface folds and wrinkles readily accomodated. The pliable or plastic nature of the skin is related to its chemical and / or physical structure. The term ' skin ' must however be regarded as a generalization, since it has been used to describe particle surface structures which are polymeric (amorphous) and sub-microcrystalline in nature. The chemical nature of polymeric skins are largely uncharacterized but probably range from denatured proteins, such as casein or albumins found in many food and dairy products, to tetrameric and polymerized species of $[SiO_2(OH)_2]^{2-}$ found in aqueous solutions of sodium silicate. Particle skins composed of sub-microcrystalline material, such as those formed by potassium nitrate, were less pliable than those of a polymeric nature and tended to form partially-inflated particles which were smooth and unwrinkled with relatively thick surface structures, as opposed to the grossly-inflated or shrivelled thin-walled particles formed by polymeric skins. Once a skin has formed moisture movement within the particle may also be different. Particles with a polymeric skin showed an initial drying period during which they decreased in size without any rupture of the skin surface; this tends to suggest the skin is porous (200).

Conversely, particles with a skin composed of a sub-microcrystalline structure underwent saturated surface drying with moisture transported from the particle interior to the surface via cracks and fissures.

Particles with crystalline (macro) surface structures were far less pliable during drying than particles with a skin-type surface structure. This was evident from the type of particle morphologies they formed, i.e.; spherical with irregular surfaces and thick crusts. Although relatively violent surface distortion can occur during drying, and partially inflated particles were formed by some of the materials, there was a tendency towards the formation of hollow, semi-hollow or solid particles which did not inflate. Particle diameters did however show a gradual increase. Moisture movement during drying occurred by saturated surface drying through cracks and fissures in the crust surface with quite substantial additional losses occurring by rupture of the crust surface. If the packing of the crystal nuclei within the crust was particularly dense and the particle rigid, e.g.; as with sodium benzoate and E.D.T.D.- $2Na^{+}$, then mass transfer can be retarded which may result in the particle exploding.

Particles with an agglomerate structure exhibited relatively simple drying behaviour in comparison to both skin forming and crystalline morphologies. If the interstices or pores within the particle structure were sufficiently large to allow free liquid movement, i.e.; via capillary flow, from the

centre of the particle to the surface, then solid, very spherical and very smooth particles were formed. If liquid movement was restricted by pore size, then the surface structure acted as a pseudo-skin and hollow, partially-inflated particles were formed.

An increase in drying temperature from 70°C to 200°C increased the rate of heat and mass transfer experienced by both droplet and particle. With skin forming and crystalline morphologies this resulted in shorter drying times and a more violent drying behaviour to produce particles with a greater tendency to inflate, shrivel and in some cases explode.

None of the materials dried from a feed concentration of 1 % w/w formed recognizable particle structures. At what point a particle becomes recognizable was however, difficult to assess, although it presumably occurs somewhere between a solid concentration of 1 % and 15 % w/w. For particles of semi-instant skimmed milk, an increase in feed concentration from 15 % to 30 % w/w resulted in a decrease in particle distortion, surface rupture and internal bubble nucleation. Sphericity and skin thickness also increased. Sodium chloride showed similar trends but to a lesser extent, i.e.; an increase in feed concentration from 15 % to 36 % w/w had less effect on drying behaviour and particle morphology.

Changes in drying temperature and feed concentration had little or no effect upon the morphology of silica particles. However, as would be expected, drying times decreased with an increase in drying temperature or feed concentration.

Particle morphologies produced from solutions of sodium silicate / sodium chloride and semi-instant skimmed milk / sodium chloride, i.e.; a combination of skin forming and crystalline materials, demonstrated the complexity of multicomponent morphology. Commercial products may for example, contain many different components all of which could migrate at formulation-dependent rates. Detergents are one example in which it is not uncommon to have between 10 to 12 different components, i.e.; a typical detergent may contain,

	Percentage by Weight
anionic paste (alkylbenzenesulphonates)	21.1
sodium silicate	7.1
brightener	0.4
polyacrylate	1.0
water	4.6
polyethylene glycol (Mw.8000)	0.7
sodium carbonate	15.8
sodium tripolyphosphate	7.5
tetrasodium pyrophosphate	30.0
sodium silicate	11.8

By increasing the drying temperature from 70°C to 200°C it was possible to alter the respective migration rates of the two solutes studied in this work. The migration of sodium chloride through the semi-instant skimmed milk skin tends to suggest it is porous, whereas, the migration of sodium silicate through the sodium chloride crust appeared to be via cracks and fissures in the particle surface and between individual crystal nuclei.

Figure 160. The Effect of Temperature and Concentration on the Particle Morphology of Skin-Forming Materials

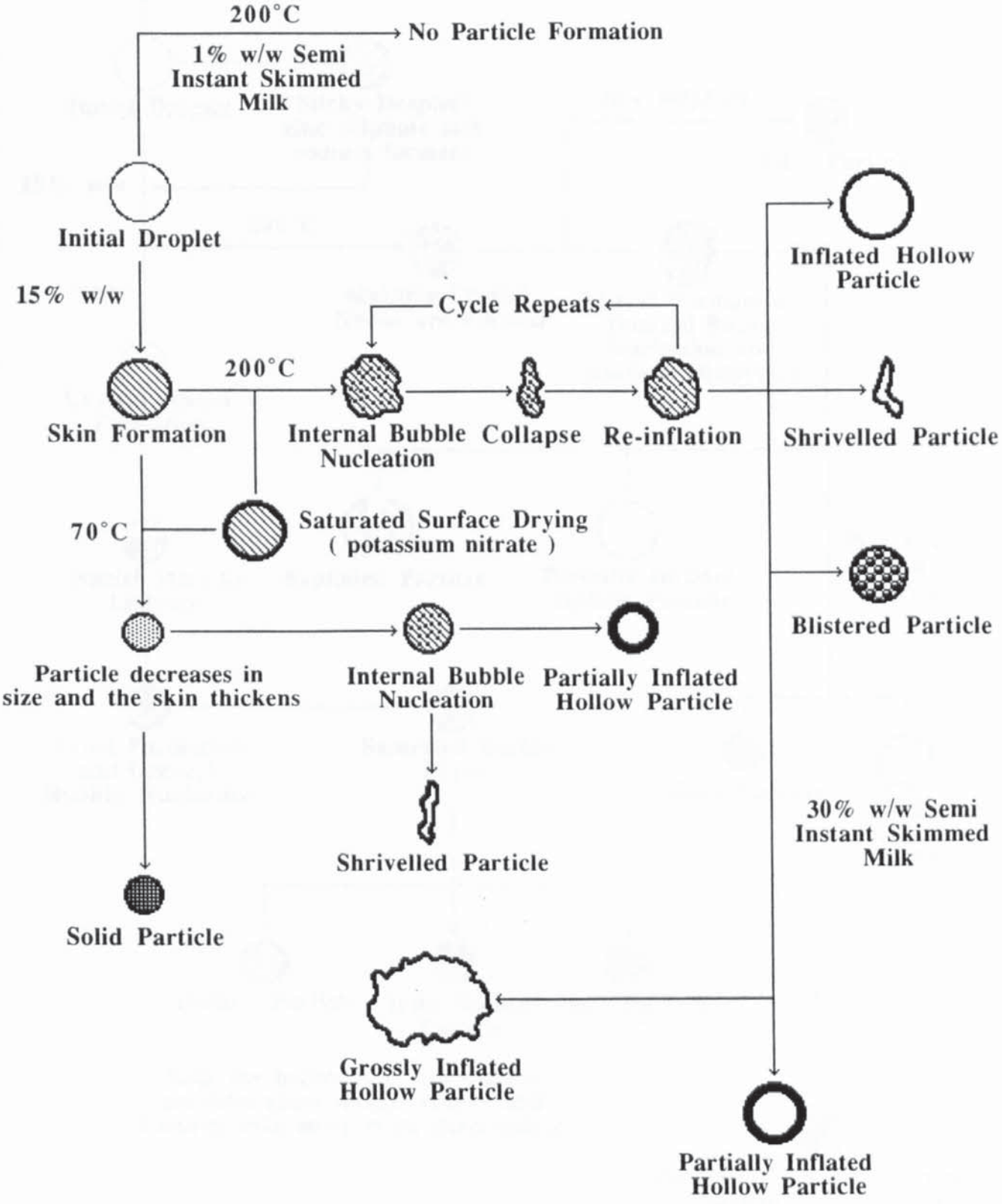

Figure 161. The Effect of Temperature and Concentration on the Particle Morphology of Crystalline Materials

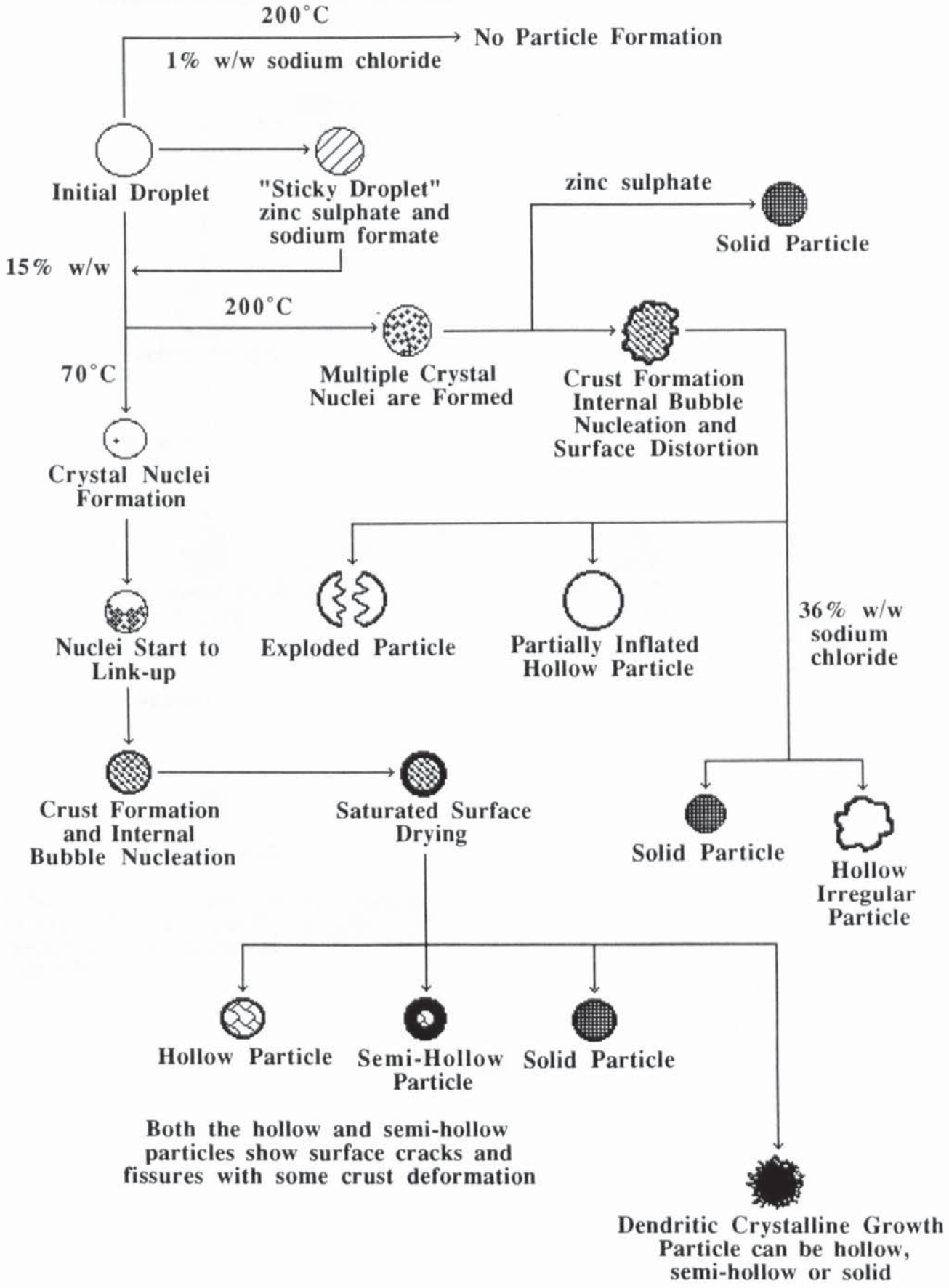

Figure 162. The Effect of Temperature and Concentration on the Particle Morphology of Agglomerate Materials

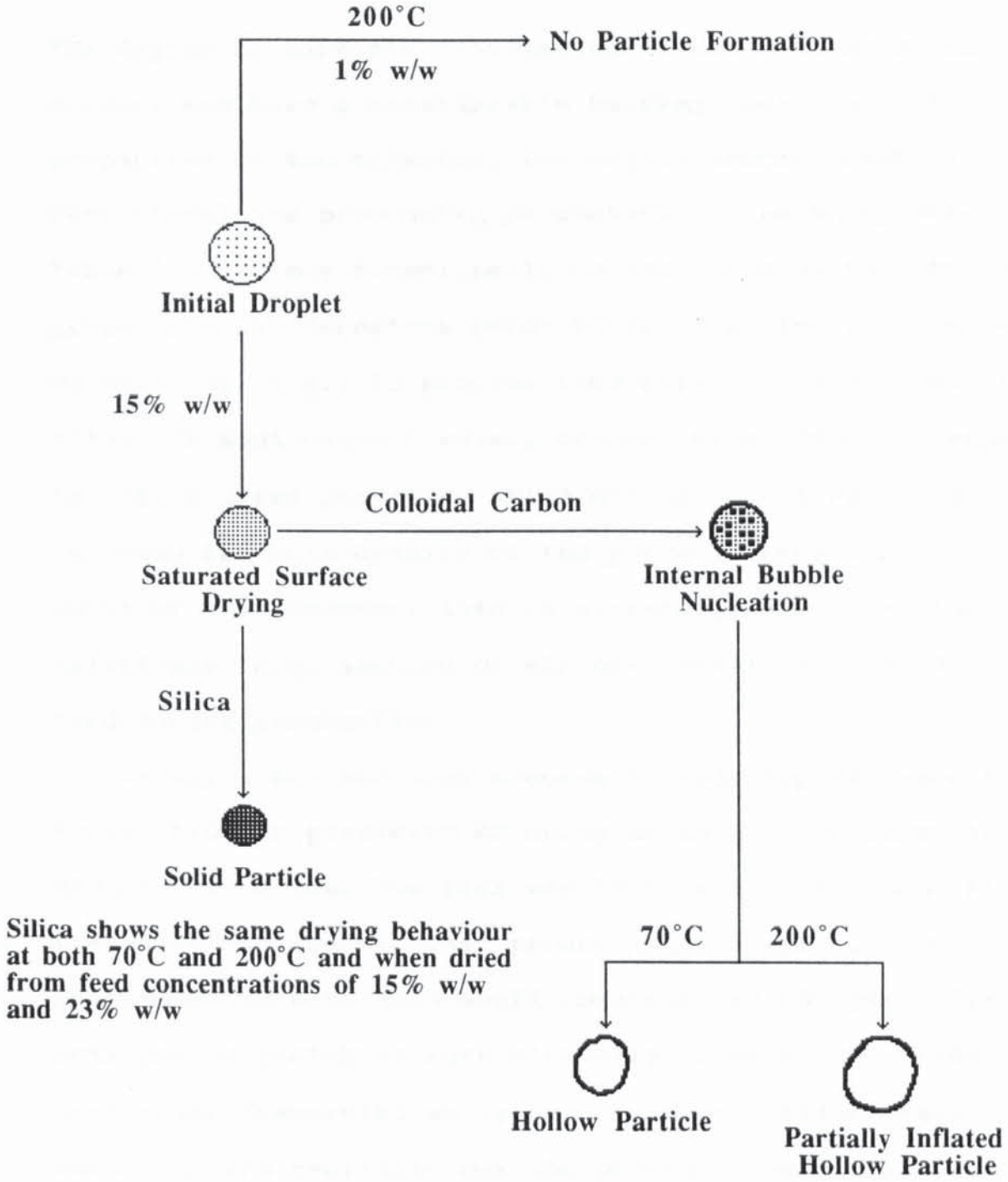

Feed Aeration and Deaeration

The degree of particle vacuolation within a spray-dried product may have a considerable bearing upon the bulk properties of the material, its drying characteristics and the operational and processing parameters of the spray drier (see Table 4). It may occasionally be advantageous to introduce gases into the feedstock prior to spray drying to promote vacuolation, e.g.; to produce foam dried cottage cheese whey (146). In most cases however, considerable effort is expended to obtain dried particles which are vacuole-free, primarily to increase the bulk density of the product. From a practical point of view however, this is extremely difficult since relatively large amounts of air are usually entrained into the feed during atomization.

Verhey (143) had some success in reducing the amount of vacuolation in particles of spray-dried milk by shrouding the atomizer in steam. The idea was to incorporate steam rather than air into the atomized product so that on cooling the entrapped steam bubbles would condense and the particles collapse or shrink to form virtually vacuole-free powder particles. Commercial spray driers incorporating steam shrouding are available but the process remains technically difficult.

A possible alternative route for reducing particle vacuolation, although not as effective as steam shrouding, involves deaeration of the feed prior to atomization. Both

physical (e.g.; thermal, mechanical) and chemical methods can be specifically chosen to suit the type or nature of the feed being spray-dried. Chemical deaerators function by producing localized depressions in the surface tension of the bubble walls which causes them to burst and consequently collapse. Efficient dispersion of the deaerant is therefore essential. The polydimethylsiloxane and hexane * used to deaerate the detergent paste in this investigation function in exactly this way, although since both were essentially insoluble in the aqueous based paste, dispersion was poor. To overcome this problem most commercial deaerators or antifoaming agents contain a finely-divided filler (e.g.; silica, titanium dioxide or magnesium oxide) which improves dispersion but increases viscosity. Silicone deaerators function only in aqueous, well-agitated systems and for maximum dispersion it is necessary to emulsify the compound. The stability and droplet-size distribution of the emulsion can then further influence the deaeration effect. Once fully dispersed, the droplets of deaerant cannot spread and are therefore deposited on the bubble walls as sites of low surface tension. However, all deaerators tend to lose their efficiency after a period of time. This is either due to the mutual saturation of the deaerant with the feed, i.e.; such that there is no longer any significant difference between the surface tension of the two materials, or, to the ' solubilization ' of the deaerant into aggregates or micelles. This effectively removes the droplets of deaerant

* Hexane was chosen because of its physical properties, i.e.; hexane is immiscible with water, its surface tension is approximately 4 times less than the surface tension of water at 20°C, and hexane is extensively used

from the bubble walls so that it can no longer operate effectively.

The detergent aeration and deaeration experiments demonstrated that an increase in feed moisture content and drying temperature will result in increased levels of particle vacuolation. This is entirely consistent with previous observations involving other skin forming materials. By increasing the drying temperature the amount of dissolved or entrained air desorbed within the particles during drying will increase. The driving force for desorption occurs as water evaporates from the droplet and the droplet temperature rises, i.e.; the solubility of air decreases. According to Greenwald and King (173), following formation the air bubbles grow by vaporization of water until the equilibrium partial pressure of water is reached. This will increase as the droplet temperature rises. As the mole fraction of air within the bubbles decreases the interior bubbles, and hence the droplet, will start to grow in size. The morphology of a particle can hence be strongly influenced by the initial nucleation step for air bubbles, the occurrence of which requires the presence of a hetrogeneous nucleation site within the droplet which is a statistical phenomenon. With some materials, particularly those which are skin forming, e.g.; semi-instant skimmed milk, this can result in particle inflation and the formation of completely hollow particles.

A similar explanation presumably applies when the moisture content of the feed is increased. In general, the greater the

volume of dissolved or entrained air trapped within the particle liquid the greater the incidence of particle vacuolation (cf. page 167). An increase in feed moisture content therefore, would increase the ratio of the volume of dissolved or entrained air within the particle liquid to that of its solid content, and, by the mechanism(s) described above, should increase particle vacuolation. However, any differences in the rheological properties of the feed must also be taken into account. The silicone fluid proved to be a very effective and stable feed deaerator which successfully reduced the level of particle vacuolation within the detergent paste. Deaeration with hexane was less effective, probably due to the incomplete dispersion of the hexane throughout the paste and its greater relative volatility (BP = 69°C, VP = ~ 1800 mmHg at 100°C). With both deaerators, continued agitation of the paste after deaeration increased air entrainment. In the case of hexane, this occurred after approximately 45 minutes with bubbles larger than those found in the aerated feed being formed, i.e.; ranging from approximately 103 μm to 114 μm in diameter compared with 97 μm in diameter in the aerated feed. The enlarged bubbles were probably caused by the vaporization of hexane within the entrained air bubbles and would tend to confirm the mechanism described by Greenwald and King for vacuolation growth. Particles produced from the hexane deaerated feed were grossly inflated and exhibited multiple nucleation sites or voids.

Both the aerated and deaerated detergent particles exhibited vacuolation to some extent so that it may be impossible to produce completely vacuole-free particles. This is in contrast to the work carried out by Verhey (143) who produced ' virtually ' vacuole-free milk powders using steam shrouded rotary atomization. It is possible however, that the powdered raw materials retain a small amount of air, possibly only a monolayer, which is sufficient to result in residual vacuoles. To test this hypothesis high surface area powders, i.e.; activated carbon and sodium aluminosilicate hydrate, materials with good gas / air adsorption properties, were added to the detergent feed (details given on page 344) prior to drying. The particles produced showed an increase in vacuolation relative to particles dried from purely the aerated feed. Alternatively, when the feed was mixed under vacuum, particle vacuolation was reduced. This suggests that air adsorbed onto the surface of the raw materials promotes particle vacuolation.

The Retention of Volatiles

The loss of volatile flavours and aromas during the spray drying of many food and dairy products has been a major industrial problem for many years. The corresponding reduction in product quality is undesirable both to the consumer and the manufacturer. Coffee for example, contains less than 10 % of its original aromas after spray drying (152). The essential

oils (see Table 27), which are very expensive, are usually steam distilled from the feed prior to spray drying and then re-added to the dried product after spray drying. This obviously increases manufacturing costs. The problem arises because of the high volatilities, at low concentrations, i.e.; ppm, of the complex mixture of components which comprise most flavours and aromas relative to water (see Table 28). Therefore, they tend to evaporate much faster from aqueous solutions than water. However, if the solution or suspension concentration is sufficiently high, the reverse is generally true. At some level of solids concentration, optimally between 40 % to 45 % w/w when spray drying coffee (152), the diffusion coefficients of many relatively volatile materials become far less than the diffusion coefficient of water (see Figure 17) and they are therefore retained to a much greater extent during drying. This ' selective diffusion ', a concept introduced by Thijssen (72) some thirty years ago, has led to a better understanding of the fundamental mechanisms and operational parameters which influence volatile loss during many drying or preconcentration processes. In the case of spray drying, selective diffusion explains how atomization conditions, inlet air temperature, flow dynamics, feed concentration, feed foaming and feed additives for example, can be optimized to give far greater volatile retention.

Nevertheless, the effect of particle morphology or changes in particle morphology, upon the retention of volatiles during spray drying still remains largely uncharacterized and

Table 27. The Major Compounds Responsible for Flavour Quality Retention in Coffee (201)

acetaldehyde	propionaldehyde
acetone	methanol
isobutyraldehyde	butyraldehyde
methyl ethyl ketone	ethanol
ethyl acetate	diacetyl
isovaleraldehyde	diethyl ketone
valeraldehyde	propanol
methyl propyl ketone	furfuryl mercaptan

Table 28. Relative Volatilities of Some Model Aroma Compounds at Infinite Dilution in Water (72)

	R. Volatility
water	1
pyridine	3
methanol	8
ethanol	12
n-propanol	16
n-butanol	27
n-pentanol	32
acetone	46

speculative. Even work relating to the above spray drying parameters has been carried out exclusively with food or food-related substances which are predominantly skin forming, i.e.; carbohydrate materials such as maltodextrin, sucrose, coffee, etc..

Figure 157 shows the effects of various types of particle morphology upon the retention of ethanol. The particles were dried from feed concentrations of 15 % w/w at a temperature of 120°C.

All three materials, including the water droplets used as a reference, exhibited similar retention profiles and varied only in the level of ethanol retained and the rate of ethanol loss. By far the greatest retention was shown by particles of semi-instant skimmed milk, a skin-forming material. After 20 s, approximately 50 % of the ethanol had been lost rising to almost 60 % at 40 s. No further losses of ethanol occurred between a drying time of 40 s and 100 s. Direct observation of the drying histories of these particles and the material, and of such materials in general, suggests the period of greatest ethanol loss, i.e.; 0 to 40 s, occurred during skin formation, and that the period of constant ethanol retention occurred after the skin formation was complete, approximately 40 s. At the relatively low drying temperature of 120°C no particle surface eruptions or distortions occurred apart from a small amount of particle expansion (each data point represents the ' average ' drying history of four droplets). Consequently, there was no direct route for ethanol or moisture loss during

this period and the skin can be regarded as being relatively impermeable. If the particles were dried for long enough however, the level of ethanol decreased, reinforcing the earlier proposal that the skin may be porous or act as a membrane. This assumes that no thermal decomposition of the solid has taken place.

The silica particles, which have an agglomerate structure, showed an almost exponential loss of ethanol during drying with levels decreasing to less than 1 % after 100 s. This is entirely consistent with the porous nature of the particle structure. Once the initial particle structure had been formed, ethanol / moisture loss occurred by saturated and non-saturated surface drying. In both cases, liquid movement occurred by capillary flow through the interstices or pores within the particle structure. With no impermeable surface barrier or skin to restrict liquid movement and, as already demonstrated, the silica particles being relatively stable during drying, i.e.; no surface eruptions, distortion or particle inflation (see Figure 120), the loss of ethanol / moisture can take place relatively unhindered. The solid however, did show some retentive properties.

Unlike silica, sodium chloride cannot be regarded as an inert solid. When in aqueous solution the salt depresses the vapour pressure of water and therefore increases its boiling point (226). This should increase ethanol loss. This is confirmed by the data shown in Figure 157; i.e. the sodium chloride droplets exhibited far less ethanol-retention than

the water droplets. After drying for 20 s the droplets had lost > 98 % ethanol compared with approximately 77 % for the water droplets. Alternatively, the total vapour pressure of water-ethanol systems is greater than the vapour pressure of pure water (226). This should increase ethanol loss, albeit possibly to a lesser extent than that demonstrated. The only other possible explanation is a morphological one. The violent crust deformation observed during drying resulted in the formation of hollow or semi-hollow particles with surface cracks and fissures which would provide ample routes for considerable volatile / ethanol loss.

The drastic effect sodium chloride has on the retention of ethanol may be particularly relevant from an industrial point of view as sodium chloride is added to many feed stocks (which may or may not contain volatiles) prior to spray drying to increase the bulk density of the spray-dried product and / or to ' salt out ', i.e.; to crystallize or precipitate, the feed solid during spray drying.

Figure 158 shows the effects of feed concentration upon the retention of ethanol in particles of semi-instant skimmed milk dried at 120°C. At a solid concentration of 1 % w/w the amount of ethanol retained by the particles appeared to be very similar to the water droplets shown in Figure 157. This suggests, and general observations confirm, that no substantial solid formation occurred on the surface of the droplets during drying. Increasing the solid concentration to 15 % w/w however, has resulted in the retention of

approximately 40 % ethanol. Therefore, a sufficiently high concentration of solids has built-up on the surface of the droplets early enough during the initial stages of drying to render their surfaces effectively impermeable to volatile loss. Droplets dried from a solid concentration of 25 % w/w showed a marked increase in the amount of ethanol retained with almost 70 % retention after a drying time of 100 s. The linear loss of ethanol with time, compared with the characteristically exponential one, suggests a critical surface concentration was reached almost immediately.

These results clearly demonstrate that an increase in feed concentration drastically improved ethanol retention. This can be explained in terms of selective diffusion. As the solid concentration of the feed increases the concentration gradient within the particles decreases which means the critical surface concentration required for selective diffusion is attained more rapidly and volatile retention is increased.

At 120°C particles of semi-instant skimmed milk underwent minimal changes in particle morphology during drying, i.e.; little or no surface distortion occurred. However, previous work at higher drying temperatures has shown that an increase in feed solid concentration will decrease or minimize such distortions.

The effects of drying air temperature upon the retention of ethanol in particles of semi-instant skimmed milk (15 % w/w) are shown in Figure 159. At 120°C approximately

40 % ethanol was retained; this rose to just over 50 % at 150°C and decreased to less than 20 % at 200°C.

Theoretically, any drying parameter which promotes a more rapid build-up of solid on the surface of the droplets during the initial stages of drying should increase the amount of volatiles retained. This would explain the 10 % increase in the amount of ethanol retained by particles dried at 150°C relative to those dried at 120°C, since the process is essentially analogous to increasing the feed concentration. At 200°C however, the amount of ethanol retained by the particles decreased to less than 20 %. This suggests the optimum drying temperature lies between 150°C and 200°C. The decrease in ethanol, which apparently conflicts with previous data, is almost certainly due to changes in particle morphology during drying. Particles of semi-instant skimmed milk dried at 200°C, particularly from a feed concentration of 15 % w/w, exhibited a considerable amount of surface distortion (see Figure 122), i.e.; the particles can inflate, rupture, collapse and re-inflate three or four times during the initial stages of drying. This would give ample opportunity for substantial volatile loss. Alternatively some ethanol loss could be due to thermal decomposition of the semi-instant skimmed milk, but this would seem unlikely since no browning of the particles was observed and the material is dried industrially, albeit with shorter residence times, at air temperatures ranging from 175°C to 240°C (192).

CONCLUSIONS

All conclusions are made with reference to sections 6.3, 6.7 and 6.13.

1.) Following-on from previous studies, e.g.; that of Cheong (194) and Bains (207) in developing a receding-interface model, Audu (106) and Ali (190) into mechanisms in the drying of single droplets of particulate slurries and solutions, Akbar (198) into the drying of droplets in free-flight, and Hassan (200) into mechanisms of skin formation, the present investigation confirmed the value of single droplet drying studies under carefully-controlled conditions in simulating spray drying.

2.) The commercially spray-dried samples obtained from various manufacturers represent a reasonably good cross-section of the type of materials spray-dried industrially. Drying specifications also show a good general agreement with those reported (192).

Three distinct categories of particle morphology have been identified, i.e.; crystalline, skin-forming and agglomerate. Although, of course, material-specific, each category is evidence of a characteristic drying behaviour which is dependent on feed concentration, the degree of feed aeration, and drying temperature. Selected

properties, e.g.; powder flowability, particle and bulk density, particle-size, particle friability, and the retention of volatiles bear a direct relationship to morphological structure.

Morphologies of multicomponent mixtures, typified by mixtures of sodium chloride and sodium silicate or sodium chloride and semi-instant milk were complex. The respective migration rates of the solutes were however, dependent on drying temperature.

The generalized droplet drying behaviours, depicted in Figures 160 to 162, provide a valuable insight into particle formation and the various drying mechanisms which govern particle morphology. This should assist prediction of optimum drying formulations and conditions in specific industrial drying operations.

3.) The similarity between the industrial spray-dried morphologies and those dried experimentally suggest that, within limitations, it is possible using single droplet drying studies to reproduce, and therefore predict the morphology of production-dried formulations without recourse to expensive plant trials. Moreover, it has been demonstrated that such studies permit rapid comparison of drying rates between different formulations. Hence they can save on expensive pilot-plant trials to test changes in formulations and drying conditions. Morphological phenomena of spray-dried particles are also identifiable.

For example, the relatively common feature of small particles within large particles (see Figures 71 and 72) may result from a similar type of drying behaviour to that observed for sodium silicate and sodium dodecyl sulphate droplets dried at 200°C, i.e.; internal blistering (see Figures 96 to 98).

4.) The exponential nature or enhancement of heat and mass transfer data of single droplets of water, ethanol, butan-1-ol and phenol suspended under forced convection, and representative of the constant-rate drying period for solution drying, has been attributed to droplet oscillation. This effect has been considered in detail elsewhere (199).

In summary, this work has made a significant contribution to identifying the types of particle morphology produced by spray drying. Physical methods were devised to test powder properties, e.g.; the powder inclinometer, and a single droplet drying technique was developed which allowed droplet and particle drying behaviour to be observed and drying mechanisms to be deduced. The apparatus successfully reproduced the types of particle morphology produced by spray drying.

A unique study has been carried out into the morphology of multicomponent particles and the effect of particle morphology on the retention of volatiles.

RECOMMENDATIONS FOR FURTHER WORK

1.) Further work is required covering a greater range of materials.

This applies,

- to the types of material already studied, e.g.;
  - to identify the structural nature of polymeric skins,
  - to confirm and extend morphological observations and their associated drying mechanisms (e.g. mushroom cap-shaped particles were not produced or identified in any of the industrial spray-dried samples),
  - to compare the morphological properties of materials with the same general formula, e.g.; quality control or batch identification,

- to include biochemical and pharmaceutical materials to parallel work in progress separately on their thermal degradative mechanisms (227),

- to more viscous feeds to investigate the effects of droplet oscillation on the enhancement of rates of heat and mass transfer. As in on-going free-flight studies (231), the results can be compared with rigid particles which cannot undergo such behaviour.

2.) The development of a more accurate method for measuring particle strength. A recent study concerning the effect of binders on particle strength found this to be a limitation (228). It is desirable to differentiate between ' bulk-strength ' tests which are particle-size distribution-dependent and fundamental single particle strength, although the former is the one of interest to the user - since it indicates the degree of free-flow ability likely in processing etc.

3.) The control of particle vacuolation. It may be necessary to minimize particle vacuolation, e.g.; to increase particle and bulk density. Alternatively, specific advantages may result from promoting vacuolation, e.g.; to produce foamed droplets (see Table 5). For example, the incorporation of ' explosion puffing ' into a dehydration process for banana slices (232), analogous to that tested for other fruits and vegetables (233), has been found to result in faster drying rates due to the formation of a more porous structure. As would be expected such products also have faster rehydration rates when used.

4.) The drying of multicomponent particles to examine the factors affecting solute / solute interaction. This encompasses many possible considerations, e.g.;

chemical interaction - possible reactions during drying,

e.g.; ' curing ',

- the rate of any such reaction,
- chemical decomposition during use or storage, this may or may not be desirable,

physical phenomena

- the rate of individual solute migration,
- location of individual solutes after drying (particle morphology) and their effect on physical properties, e.g.; strength (binders),
- the use of binders, thermal gelling agents (see section 6.3 v),
- microencapsulation, i.e.; permanent encapsulation of the product for storage, or, slow / quick release,

5.) The effect of particle morphology on the retention of volatiles compared with the time to formation of a skin or crust (i.e.; by the presence or addition of skin-forming agents). Experiments should be performed with volatiles other than ethanol as many of the compounds responsible for flavour and aroma quality in foodstuffs are large, complex molecules (see Table 27) with widely differing volatilities, e.g.; methyl mercaptan or methanethiol, a constituent in coffee aroma, has a relative volatility

≈ 42 times greater than ethanol when dissolved in water at ppm concentration (72).

This is an extremely complex area since the selective-diffusion phenomena noted on pages 158 to 166 are also present (160).

6.) The correlation of data derived from other single droplet drying techniques. This would help to assess the validity of the technique. For example, in a recent study concerning the rate of heat and mass transfer of oscillating droplets (199), there was a good general agreement of transfer data derived from single suspended droplets and single droplets in free-flight. In a further study however, the use of a domestic microwave to dry single droplets proved unsuccessful due to the non-uniform nature of the microwave field (229).

REFERENCES

1.) Butcher, C.,
The Chemical Engineer, No. 489, 17-22 (1991).

2.) Masters, K.,
Spray Drying Handbook, 5th Ed., p. 9-20.
Longman Scientific & Technical (UK) (1991).

3.) MacTaggart, E.F.,
Trans. Inst. Chem. Engrs., 27, 23-46 (1949).

4.) Marshall, W.R., Jr. and Seltzer, E.,
Chem. Eng. Progr., 46, 10, 501-508 &
46, 11, 575-584 (1950).

5.) Friedman, S.J.,
Ind. Eng. Chem., 40, 1, 18-22 Jan. (1948) &
41, 1, 27-31 Jan. (1949).
Ind. Eng. Chem., 42, 1, 38-44 Jan. (1950).

6.) Calus, W.F.,
Chem. Proc. Eng., 41, 10, 448-452 Oct. (1960) &
43, 1, 28-32 Jan. (1962) & 44, 5, 273-278 May (1963).

7.) Gluckert, F.A.,
Ind. Eng. Chem., 46, 1, 82-86 Jan. (1954) &
47, 3, 527-531 Mar. (1955).

8.) Bagnoli, E.,
Ind. Eng. Chem., 48, 3, 500-504 Mar. (1956) & 49, 3, Pt. 2,
476-480 Mar. (1957) & 50, 3, Pt. 2, 435-437 Mar. (1958).

9.) McCormick, P.Y.,
Ind. Eng. Chem., 51, 3, Pt. 2, 352-353 Mar. (1959) &
52, 5, 439-440 May (1960) & 58, 11, 58-62 Nov. (1966).

10.) Belcher, D.W., et al.
Chem. Eng., 70, 83-88 & 201-208
30th Sept. & 14th Oct. (1963).

11.) Marshall, W.R., Jr.,
Ind. Eng. Chem., 45, 1, 47-54 Jan. (1951).

12.) Genskow, L.R.,
Considerations In Drying Consumer Products,
6th International Drying Symposium.
IDS'88, Versailles Sept., KL. 39-46 (1988).

13.) Filkova,T. and Cedik,P.,
Nozzle Atomization In Spray Drying,
Advances In Drying,Vol.3,p.181-217 (1984).

14.) APV Anhydro A/S.Information bulletins (A-2 ENG),
7 Ostmarken,DK-2860 Soborg-Copenhagen,Denmark.
(Denton Holme,Carlisle,Cumbria CA2 5DU.)

15.) Dombrowski,N. and Fraser,R.P.,
Phil.Trans.R.Soc.,247A,101 (1953).

16.) Dombrowski,N. and Munday,G.,
Biochemical And Biological Engineering Science,
Vol.2,p.209-305.
Academic Press,Edited by N.Blakebrough (1968).

17.) Perry,J.H.,
Chemical Engineers Handbook,
Sixth Edition,Sec.18,p.49,
McGraw-Hill Book Co.,Inc.,London (1984).

18.) Garner,F.H.,Nissan,A.H. and Wood,G.F.,
Phil.Trans.R.Soc.,243A,37 (1950).

19.) Fraser,R.P.,Eisenklam,P. and Dombrowski,N.,
J.Inst.Fuel.,30,399 (1957).

20.) Addison,C.C.,
J.Chem.Soc.,5,35 (1943).

21.) Dombrowski,N. and Hooper,P.C.,
Chem.Eng.Sci.,17,291 (1962).

22.) Rayleigh,Lord.,
Proc.Lond.Math.Soc.,10,4 (1878/9).

23.) Weber,C.,
Z.angew.Math.Mech.,11,136 (1931).

24.) Nukiyama.S. and Tanasawa,Y.,
Jap.Trans.Soc.Mech.Engrs.,4,86 (1938).

25.) Ryley,D.J.,
J.Appl.Phys.,10,180 (1959).

26.) Weinberg,S.,
Proc.Instn.Mech.Engrs.,18,240 (1952/3).

27.) Whitman,W.G.,
Chem.Met.Eng.,29,147 (1923).

28.) Higbie,R.,
Trans.Amer.Inst.Chem.Eng.,31,365 (1935).

29.) Danckwerts, P.V.,
Ind. Eng. Chem., 43, 1460 (1951).

30.) Toor, H.L. and Marchello, J.M.,
A.I.Ch.E.J., 4, 97 (1958).

31.) Prandtl, L.,
Proc. III Intern. Math. Congr., Heidelberg (1904).

32.) *ibid.*, Ref. 21, Sec. 5, p. 63.

33.) Garner, F.H., Jenson, V.G. and Keey. R.B.,
Trans. Instn. Chem. Engrs., 37, 14 (1959).

34.) Frossling, N.,
Beitr. Geophys., 52, 170 (1938).

35.) Frossling, N.,
Lunds. Univ. Arskr., 36, 4 (1940).

36.) Linton, M. and Sutherland, K.L.,
Chem. Engng. Sci., 12, 214 (1960).

37.) Marshall, W.R., Jr.,
Chem. Eng. Prog., Monograph Series, 2, 50, 81-94 (1954).

38.) *ibid.*, Ref. 37, p. 89.

39.) *ibid.*, Ref. 53, p. 173.

40.) Sjenitzer, F.,
Chem. Eng. Sci., 1, 101-117 (1952).

41.) Duffie, J.A. and Marshall, W.R., Jr.,
Chem. Eng. Prog., 49, 417, 480 (1953).

42.) Maxwell, J.C.,
Collected Scientific Papers, Cambridge, 11, 625 (1890).

43.) Coulson, J.M. and Richardson, J.F.,
Chemical Engineering, Vol. 1, 2nd Ed. Chap. 8, 324.
Pergamon Press, London (1968).

44.) Marshall, W.R., Jr.,
Trans. Amer. Soc. Mech. Eng., 77, 11, 1377 (1955).

45.) Dlouhy, J. and Gauvin, W.H.,
A.I.Ch.E.J., 6, 1, 29 (1960).

46.) Soo, S.L.,
Chem. Engng. Sci., 5, 57 (1956).

47.) Hoffman, T.W. and Gauvin, W.H.,
Can. J. Chem. Eng., 40, 170 (1962).

48.) Gwyn, J.E., Crosby, E.J. and Marshall, W.R., Ind. Eng. Chem. Fund., 2, 204 (1965).

49.) Frazer, R.P., Eisenklam, P. and Dombrowski, N., Brit. Chem. Eng., 2, 414, 536, 610 (1957).

50.) Kramers, H., Physica, 12, 61 (1946).

51.) Maisel, D.S. and Sherwood, T.K., Chem. Engng. Prog., 46, 131, 172 (1950).

52.) Ranz, W.E. and Marshall, W.R., Jr., Chem. Engng. Prog., 48, 141 (1952).

53.) Rowe, P.N., Claxton, K.T. and Lewis, J.B., Trans. Ins. Chem. Eng., 43, T, 14 (1965).

54.) *ibid.*, Ref. 2, p. 315-317.

55.) Marshall, W.R., Jr., Chem. in Can., 7, 37 (1955).

56.) Ranz, W.E., Trans. Am. Soc. Mech. Engrs., 78, 909 (1956).

57.) Sleicker, C.A., Jr. and Churchill, S.W., Ind. Eng. Chem., 48, 1819 (1956).

58.) *ibid.*, Ref. 16, p. 303.

59.) Miesse, C.C., Paper presented at Am. Rocket Soc. meeting, New York (1954).

60.) Probert, R.P., Phil. Mag., 37, 94 (1946).

61.) *ibid.*, Ref. 37, p. 93.

62.) Sapiro, A.H. and Erickson, A.J., Trans. Am. Soc. Mech. Engs., 79, 775 (1957).

63.) Fledderman, R.G. and Hanson, A.R., Univ. Michigan Eng. Research Rept. CM667 (1951).

64.) Dickinson, D.R. and Marshall, W.R., Jr., A.I.Ch.E.J., 14, 4, 541 (1960).

65.) Manning, W.P. and Gauvin, W.H., A.I.Ch.E.J., 6, 2, 184 (1960).

66.) Bose, A.K. and Pei, D.C.T., Canad. J. Ch. Eng., 42, 6, 259 (1964).

67.) *ibid.*, Ref. 16, p. 304.

68.) *ibid.*, Ref. 2, p. 326-329.

69.) *ibid.*, Ref. 21, Sec. 20, p. 10.

70.) Williams, G.C. and Schmidt, R.O.,
Ind. Engng. Chem., 38, 967 (1946).

71.) Charlesworth, D.H. and Marshall, W.R., Jr.,
A.I.Ch.E.J., 6, No. 1, 9-23 (1960).

72.) Thijssen, H.A.C.,
Colloq. Inst. Chim. Cafes Verts, Torrefies Leurs
Deriv., 4, 108-117 (1970).

73.) Sreznevskii, V.,
Zh. R. Ph. Kh. O., 14, 420, 483 (1882).

74.) Morse, H.W.,
Proc. Amer. Acad. Sci., 45, 363 (1910).

75.) Langmuir, I.,
Phys. Rev., 12, 2, 368 (1918).

76.) Whytlaw-Gray, R. and Patterson, H.,
Smoke (Dyme), Goskhimizdat, M., 149 (1934).

77.) Topley, B. and Whytlaw-Gray, R.,
Phyl. Mag., 4, 873 (1927).

78.) Houghton, H.G.,
Physics., 4, 419 (1933).

79.) Kiriukhin, B.V.,
Trudy NIU Gidrometsl., 1, 7, 35 (1945).

80.) Langstroth, G.O., Diehl, C.H.H. and Winhold, E.J.,
Can. J. Research, 28A, 580 (1950).

81.) Mathers, W.G., Madden, A.J. and Piret, E.L.,
Ind. Eng. Chem., 49, 16, 961 (1957).

82.) Steinberger, R.L. and Treybal, R.E.,
A.I.Ch.E.J., 6, 227 (1960).

83.) Yuge, T.,
Trans. A.S.M.E., 82, Series C, 214 (1960).

84.) Gudris, N. and Kulikova, L.,
Z. Physik, 25, 121 (1924).

85.) Nestle, R.Z.,
Physics., 77, 174 (1932).

86.) Woodland, D.J. and Mack, E.,
J. Amer. Chem. Soc., 55, 3149 (1933).

87.) Toei, R. and Furuta, T.,
A. I. Ch. E. J., Symp. Ser., 78, 218, 111 (1982).

88.) Majama, T.,
Bull, Inst. Phys. Chem. Res. (Tokyo), 9, 339 (1930).

89.) Hsu, N. T., Sato, J. and Sage, B. H.,
Ind. Engng. Chem., 46, 870 (1954).

90.) Tverskaia, N. P.,
Uchen. Zap. Leningrad Univ., Phys., 7, 241 (1949).

91.) Tverskaia, N. P.,
IZV. Akad. Nauk USSR., Geogr. Geoph., 14, 164 (1950).

92.) Tverskaia, N. P.,
IZV. Akad. Nauk USSR., Geoph., 259 (1953).

93.) Sokolskii, A. P. and Timofeyeva, F. A.,
Studies on the combustion process of natural fuels
Energoizdat, M.-L., 182 (1948).

94.) Van Krevelen, D. W. and Hoftijzer, P. J.,
J. Soc. Chem. Ind., 68, 59 (1949)

95.) Ingebo, R. D.,
Chem. Eng. Prog., 48, 403 (1952).

96.) Garner, F. H. and Grafton, R. W.,
Proc. R. Soc., A224, 64 (1954).

97.) Garner, F. H. and Suckling, R. D.,
A. I. Ch. E. J., 4, 114 (1958).

98.) Garner, F. H. and Keey, R. B.,
Chem. Eng. Sci., 9, 119-129 (1958).

99.) Garner, F. H. and Hoffman, J. M.,
A. I. Ch. E. J., 6, 579 (1960).

100.) Pasternak, I. S. and Gauvin, W. H.,
Can. J. Chem. Eng., 38, 35 (1960).

101.) Pasternak, I. S. and Gauvin, W. H.,
A. I. Ch. E. J., 7, 254 (1961).

102.) Fuchs, N. A.,
Evaporation and Droplet Growth in Gaseous Media,
Pergamon Press, London (1959).

103.) Bowman, C.W., Ward, D.M., Johnson, A.I. and Trass, O.,
Can.J.Chem.Eng., 39, 9 (1961).

104.) Ward, D.M., Trass, O. and Johnson, A.I.,
Can.J.Chem.Eng., 40, 164 (1962).

105.) Kinard, G.E., Manning, F.S. and Manning, W.P.,
Brit.Chem.Eng., 8, 326 (1963).

106.) Audu, T.O.K.,
Studies of the Drying of Particulate Slurries,
Ph.D Thesis, University of Aston in Birmingham (1973).

107.) Sandovles-Robles, J.G., Riba, J.P. and Conderc, J.P.,
Trans.Inst.Chem.Eng., 58, 132 (1980).

108.) Sandovles-Robles, J.G., Delmas, H. and Conderc, J.P.,
A.I.Ch.E.J., 27, 819 (1981).

109.) Tsubouchi, T. and Sato, S.,
Chem.Eng.Prog.Symp.Ser., 56, 269, 285 (1960).

110.) Adams, A.E.S. and Pinder, K.L.,
Canad.J.Chem.Eng., 50, 707 (1972).

111.) Schafer, K.,
Z.Physik., 77, 198 (1932).

112.) Monchik, L. and Reiss, H.,
J.Chem.Phys., 22, 831 (1954).

113.) Vyrubov, D.N.,
J.Tech.Phys.Moscow, 9, 1923 (1939), Canadian Defence
Research Board Translation, September (1949).

114.) Kinzer, G.D. and Gunn, R.,
J.Meteor., 81, 71 (1951).

115.) Jones, S.J.R. and Smith, W.,
Proc.Symp.Interaction Between Fluid and Particles.,
Inst.Chem.Eng., London, 190 (1962).

116.) Garner, F.H. and Skelland, A.H.P.,
Ind.Eng.Chem., 46, 1255 (1954).

117.) Finlay, B.A.,
Study of Liquid Droplets in an Airstream,
Ph.D Thesis, University of Birmingham (1957).

118.) Jarvis, J.,
Ph.D Thesis, University of Birmingham (1957).

119.) Ahmadzadeh, J. and Harker, J.H.,
Trans.Inst.Chem.Eng., 52, 108 (1974).

120.) Garner, F.H. and Lane, J.J.,
Trans. Inst. Chem. Eng., 37, 162 (1959).

121.) Yao, S. and Schrock, V.E.,
T.A.S.M.E., Journ. of Heat Tran., 120-126 (1976).

122.) Miura, K., Miura, T. and Ohtani, S.,
A.I.Ch.E. Symp. Series, 73, 95, 163-164 (1977).

123.) Garner, F.H. and Kendrick, P.,
Trans. Inst. Chem. Eng., 37, 155 (1959).

124.) Yuen, M.C. and Chen, L.W.,
Int. J. Heat and Mass Transfer, 21, 537-542 (1978).

125.) Colburn, A.P. and Drew, T.B.,
Trans. Am. Inst. Chem. Engrs., 33, 197 (1937).

126.) Godsave, G.A.E.,
Nat. Gas Turb. Establish. Rept. R66, R88, England (1950, 1952).

127.) Eisenklam, P., Armachalam, S.A. and Weston, J.A.,
Evaporation Rates and Drag Resistance of Burning Drops,
Eleventh International Symposium on Combustion.,
715-725 (1967).

128.) Hoffman, T.W. and Gauvin, W.H.,
Canad. J. Chem. Eng., 38, 129, (1960).

129.) Pei, D.C.T. and Gauvin, W.H.,
A.I.Ch.E.J., 9, 375 (1963).

130.) Pei, D.C.T., Narasimhan, C. and Gauvin, W.H.,
Proc. Symp. Interaction Between Fluid and Particles.,
Inst. Chem. Eng. London, 243 (1962).

131.) Downing, C.G.,
A.I.Ch.E.J., 12, 760 (1966).

132.) Narashimhan, C. and Gauvin, W.H.,
Can. J. Chem. Eng., 45, 181-188 (1967).

133.) Lee, K. and Ryley, D.J.,
J. Heat Transfer, Trans. A.S.M.E., 90, 445 (1968).

134.) Frazier, G.C. and Hellier, W.W.,
Ind. Eng. Chem. Fundam., 8, 807 (1969).

135.) Cosby, E.J. and Stewart, W.E.,
Ind. Eng. Chem. Fundam., 9, 515 (1970).

136.) Trommelen, A.M. and Crosby, E.J.,
A.I.Ch.E.J., 16, 857 (1970).

137.) Sano,U. and Nishikawa,S.,
Chem.Eng.Japan,28,275 (1964).

138.) Kadota,T. and Hiroyasu,H.,
Bull.J.S.M.E.,19,1515 (1976).

139.) Hiroyasu,H.,et al.,
Trans.J.S.M.E.,40,3147 (1974).

140.) Renksizbulut,M. and Yuen,M.C.,
Journal of Heat Transfer,105,384 (1983).

141.) Crosby,E.J. and Marshall,W.R.,Jr.,
Chem.Eng.Prog.,54,7,56 (1958).

142.) Buma,T.J. and Henstra,S.,
Netherlands Milk and Dairy J.,25,278 (1971).

143.) Verhey,J.G.P.,
Netherlands Milk and Dairy J.,25,246 (1971).
ibid.,26,186,203 (1972).*ibid.*,27,3 (1973).

144.) Fuchs,V.M.,
Phys.Z.Sowjet.,6,224 (1934).

145.) Greenwald,C.G. and King,C.J.,
J.Food Process.Eng.,4,171 (1981).

146.) Abdul-Rahman,Y.A.K.,Crosby,E.J. and Bradley,R.L.,Jr.,
J.Dairy Sci.,54,8,1111-1118 (1971).

147.) Crosby,E.J. and Weyl,R.W.,
A.I.Ch.E.Symp.Ser.,73,163,82 (1977).

148.) Chu,J.C.,Stout,L.E. and Busche,R.M.,
Chem.Eng.Prog.,47,1,29-38 (1951).

149.) Wallman,H. and Blyth,H.A.,
Ind.Eng.Chem.,43,1480 (1951).

150.) *ibid.*,Ref.41,p.483.

151.) Buckham,J.A. and Moulton,R.W.,
Chem.Eng.Prog.,51,3,126-133 (1955).

152.) Menting,L.C. and Hoogstad,B.,
J.Food Sci.,32,87-90 (1967).

153.) Hikita,H.,Asai,S. and Azuma,Y.,
Canad.J.Chem.Eng.,56,371-374 (1978).

154.) Rulkens,W.H. and Thijssen,H.A.C.,
J.Food Technol.,7,1,95-105 (1972).

155.) Menting, L.C., Hoogstad, B. and Thijssen, H.A.C., J.Food Technol., 5, 2, 127-139 (1970).

156.) Menting, L.C., Hoogstad, B. and Thijssen, H.A.C., J.Food Technol., 5, 2, 111-126 (1970).

157.) Chandrasekaran, S.K. and King, C.J., A.I.Ch.E.J., 18, 520-526 (1972).

158.) Kerkhof, P.J.A.M. and Thijssen, H.A.C., A.I.Ch.E.J., Symp.Ser., 73, 163, 33-46 (1977).

159.) King, C.J., Freeze Drying of Foods, CRC Press, Appendix (1971).

160.) King, C.J., Chem.Eng.Prog., 86, 33-39 (1990).

161.) Heath, W.P. and Washburn, R.M., Process of Manufacturing Powdered Milk and Other Feeds, U.S. Pat. 1,406,381 (1922).

162.) Reich, I.M. and Johnston, W.R., Spray Drying Foamed Material, U.S. Pat. 2,788,276 (1957).

163.) Chase, F.A. and Laursen, G.E., Carbonation of Coffee Extract, U.S. Pat. 2,771, 364 (1956).

164.) Oakes, E.T. et al, Preparation for Soluble Milk Powder, U.S. Pat. 3,072, 486 (1963).

165.) Hanrahan, F.P., Tamsma, A., Fox, K.K. and Pallansch, M.J., J.Dairy Sci., 45, 1, 27-31 (1962).

166.) Bell, R.W., Hanrahan, F.P. and Webb, B.H., J.Dairy Sci., 46, 1352 (1963).

167.) Bradley, R.L. and Stine, C.M., Foam Spray Drying of Natural Cheese, Manufactured Milk Prod.J., 55, 6, 8 (1964).

168.) Audu, T.O.K. and Jeffreys, G.V., Trans.I.Ch.E., 53, 165-172 (1975).

169.) Leong, K.H., J.Aerosol Sci., 12, 5, 417-435 (1981).

170.) Leong, K.H., J.Aerosol Sci., 18, 5, 511-524 (1987).

171.) *ibid.*, Ref.170, p.525-552.

172.) Sano, Y. and Keey, R.B.,
Chem. Eng. Sci., 37, 6, 881-889 (1982).

173.) Greenwald, C.G. and King, C.J.,
A.I.Ch.E.J., Symp. Ser., 78, 218, 101-110 (1982).

174.) Van der Lijn, L.,
Simulation of Heat and Mass Transfer in Spray Drying,
Ph.D Thesis, University of Wageningen, Netherlands (1976).

175.) Kerkhof, P.J.A.M. and Schoeber, W.J.A.H.,
Advances in Pre-concentration and Dehydration of Food,
Ed. by Arnold, Applied Science Pub., London (1974).

176.) Wijlhuizen, A.E., Kerkhof, P.J.A.M. and Bruin, S.,
Chem. Eng. Sci., 34, 651 (1979).

177.) Downton, G.E., Flores-Luna, J.L. and King, C.J.,
Ind. Eng. Chem. Fundam., 21, 447 (1982).

178.) Alexander, K. and King, C.J.,
Drying Technology, 3, 3, 321-348 (1985).

179.) Bellows, R.J. and King, C.J.,
A.I.Ch.E.J., Symp. Ser., 69, 132, 33-41 (1973).

180.) Cheong, H.W., Jeffreys, G.V. and Mumford, C.J.,
A.I.Ch.E.J., 32, 8, 1334 (1986).

181.) Bains. G.,
Mechanisms of Drying of Particulate Slurries,
Ph.D Thesis, University of Aston in Birmingham (1990).

182.) *ibid.*, Ref. 12, p. OP. 471-477.

183.) *ibid.*, Ref. 12, p. PC. 43-50.

184.) *ibid.*, Ref. 12, p. OP. 449-453.

185.) *ibid.*, Ref. 12, p. PC. 15-19.

186.) El-Sayed, T.M., Wallack, D.A. and King, C.J.,
Ind. Eng. Chem. Res., 29, 12, 2346-2357 (1990).

187.) Supran, M.K., Acton, J.C., Howell, A.J. and Saffle, R.L.,
J. Milk Food Technol., 34, 584-585 (1971).

188.) Wallack, D.A. and King, C.J.,
Biotechnol. Prog., 4, 1, 31-35 (1988).

189.) Frey, D.D. and King, C.J.,
Ind. Eng. Chem. Fundam., 25, 723-730 (1986).

190.) Ali,H.H.,
Mechanisms of Drying of Single Droplets,
Ph.D Thesis,University of Aston in Birmingham (1985).

191.) Wood,W.M.L.,
Solids Drying Subject Group Symposium,
I.Ch.E.,7th January (1986).
Photographs courtesy of I.C.I. plc,Fine Chemicals
Manufacturing Organisation,Process Technology
Department,Blackley,Manchester.

192.) ibid.,Ref.2,p.499-511 & 538-676.

193.) Ghadiri,M.,
Attrition and Comminution, Lecture given at S.E.R.C.
Summer School in Particle Tecchnology,
University of Surrey,19th to 23rd July (1992).

194.) Cheong,H.W.,
The Drying of Small Droplets of Particulate Slurries,
Ph.D Thesis,University of Aston in Birmingham (1983).

195.) Linton,W.H. and Sherwood,T.K.,
Chem.Engng.Prog.,46,258 (1950).

196.) Yen,Y.C. and Thodos,E.,
A.I.Ch.E.J.,8,34 (1962).

197.) Ernochides,S. and Thodos,E.,
A.I.Ch.E.J.,7,78 (1961).

198.) Akbar,S.,
The Drying of Droplets in Free-Flight,
Ph.D Thesis,University of Aston in Birmingham (1988).

199.) Oteng-Attakora,G.,Walton,D.E. and Mumford,C.J.,
I.Chem.E. Research Event,
University College London (1994).

200.) Hassan,H.M.,
Mechanisms of Drying of Skin Forming Materials,
Ph.D Thesis,University of Aston in Birmingham (1991).

201.) Flink,J.,
Freeze Drying and Advanced Food Technology,
International Course on Freeze Drying and Advanced Food
Technology,Ed. by Goldblith,Rey and Rothmayer,
Academic Press,London (1975).

202.) Murphy,A.P.,
Procter and Gamble
U.S. Patent Document 4,379,080 (1983).

203.) Grecsek, J.J., Giordano, S.W. and Grey, S.,
Colgate-Palmolive
U.K. Patent Application GB 2 095 274 A (1992).

204.) Hendrik, E.J., et al,
Unilever
European Patent Specification EP 0 240 356 B1 (1987).

205.) Lane, W.R.,
Ind. Eng. Chem., 43, 12 (1951).

206.) Walton, D.E. and Mumford, C.J.,
I.Chem.E. Research Event,
University of Manchester Institute of Science and Technology (1992).

207.) Ali, H.H., Mumford, C.J., Jeffreys, G.V. and Bains, G.S.,
6th International Drying Symposium, p.OP.463-470.
IDS'88, Versailles, September (1988).

208.) Verderber, A. and King, C.J.,
Drying Technology, 10, 4, 875-891 (1992).

209.) Sunkel, J.M. and King, C.J.,
Ind. Eng. Chem. Res., 32, 10, 2357-2364 (1993).

210.) Hassan, H.M. and Mumford, C.J.,
Drying Technology, 11, 7, 1713-1782 (1993).

211.) Riera, F., Walton, D.E. and Mumford, C.J.,
Paper presented at the 23rd Annual Meeting of the Spanish Chemical Society, Salemanca, Sept. 23-28 (1990).

212.) Lihou, D.,
Droplets in Gaseous Streams,
Ph.D Thesis, University of Birmingham (1963).

213.) Handbook of Powder Technology, Vol. 1,
Particle Size Enlargement by C.E. Capes, p.23-51,
Edited by Williams and Allen, Bradford, England (1980).

214.) Komarek, K.R.,
Chem. Eng., 74, 25, p.154-155 (1967).

215.) Waters, P.L.,
Proc. Inst. Briquet. Agglom. Bien. Conf., 12, p.145-159 (1971).

216.) Waters, P.L.,
Technical Communication No.51, CSIRO, Division of Mineral Chemistry, N.S.W., Australia, p.75 (1969).

217.) Rumpf, H.,
The Strength of Granules and Agglomerates, In Knepper Ed. of Agglomeration, Interscience (NY), p.379-414 (1962).

218.) Pietsch, W. and Rumpf, H.,
Proc. Int. Coll. C. M. R. S., p. 213-235 (1966).

219.) Krupp, H., Colloid Interface Sci., 1, p. 11-239 (1967).

220.) Capes, C. E. and McIlhinney, A. E.,
Methods of Preparing Agglomerates of Reduced Efflorescence, U.S. Patent 3,493,642 (1970).

221.) Capes, C. E., Powder Technol., 4, p. 77-82 (1970-71).

222.) Ball, D. F. et al,
Agglomeration of Iron Ores, Heinemann, London (1973).

223.) Kapur, P. C. and Fuerstenau, D. W.,
J. Am. Ceram. Soc., 50, p. 14-18 (1967).

224.) Cahn, D. S.,
Trans. Soc. Mining Eng. AIME, 250, p. 173-177 (1971).

225.) Meissner, H. P. et al,
Ind. Eng. Chem. Process Des. Dev., 5, p. 10-14 (1966).

226.) Chemistry An Integrated Approach, by Lowrie and Ferguson,
Pergamon Press Ltd., p. 156-168 (1975).

227.) Sayed, A. A.,
The Single-Droplet Drying of Heat Sensitive Materials,
23rd Annual Chemical Engineering and Applied Chemistry Research Symposium,
University of Aston in Birmingham, July (1992).

228.) Morris, N. A. and Parkinson, J.,
The Enhancement of Spray-Dried Particle Properties Using Trace Additives,
Final year undergraduate industrial project, University of Aston in Birmingham, Dept. C. E. A. C., Jan. (1994).

229.) Sud, D. and Woollatt, S.,
Microwave Drying,
Final year undergraduate industrial project, University of Aston in Birmingham, Dept. C. E. A. C., Jan. (1993).

230.) Walton, D. E., et. al., Contract Research (unpublished work), 1985-1994.

231.) Oteng-Attakora, G., Aston University (unpublished work).

232.) Saca, S. A., & Lozano, J. E., International Journal of Food Science and Technology, 2, 419-426 (1992).

233.) Kozempel, M. F., Sullivan, J. F., Craig, J. C., &
Konstance, R. P., Journal of Food Science, 54,
772-773 (1989).

APPENDICES

A 1.0) Bulk Density of Commercially Spray-Dried Samples

Sample	Bulk Density (g/cm^3)			
	1	2	3	Average
Aluminium hydroxide	0.273	0.275	0.280	0.276
Aluminium silicate	0.390	0.389	0.388	0.389
Dyestuffs	0.463	0.461	0.459	0.461
Tungsten carbide	3.673	3.675	3.673	3.674
Aluminium oxide	1.155	1.154	1.151	1.153
Titanium dioxide (Niro)	0.632	0.637	0.633	0.634
Ferrite	1.422	1.422	1.421	1.422
Kaolin	0.813	0.810	0.809	0.811
Barium titanate	1.527	1.530	1.533	1.530
tri - sodium orthophosphate	0.351	0.347	0.349	0.349
Copper oxychloride	0.835	0.834	0.844	0.838
Lead chromate	0.783	0.785	0.794	0.787
2,3 - dichloro - propanoic acid	0.339	0.341	0.343	0.341
Copper ore	1.379	1.385	0.379	0.381
Coffee	0.147	0.143	0.152	0.147
Magnesium hydroxide	0.609	0.619	0.611	0.613

Sample	Bulk Density (g/cm³)			
	1	2	3	Average
Dextran	0.259	0.258	0.258	0.258
Clay (nozzle)	1.025	1.017	1.021	1.021
Clay (rotary)	1.005	1.009	1.002	1.005
Glucose	0.441	0.456	0.455	0.451
Detergent	0.520	0.526	0.525	0.524
Semi - instant skimmed milk	0.557	0.561	0.527	0.548
Yogurt powder	0.586	0.588	0.577	0.584
Co - dried egg and skimmed milk	0.559	0.536	0.549	0.548
Titanium dioxide (Drytec - A)	0.477	0.432	0.446	0.452
Polymer (Drytec - A)	0.329	0.328	0.342	0.333
Instant drink powder	0.288	0.286	0.269	0.281
Encapsulated flavour	0.396	0.397	0.398	0.397
Polymer (sodium salt)	0.456	0.454	0.463	0.458
Organic UV brightner	0.265	0.281	0.277	0.274
Sol. titanium salt (two-fluid nozzle)	0.642	0.673	0.656	0.657
Sol. titanium salt (pressure nozzle)	0.568	0.547	0.560	0.558
Sol. titanium salt (rotary)	0.504	0.486	0.540	0.510
Polymer (Drytec - B)	0.425	0.425	0.448	0.433
Calcium stearate	0.450	0.453	0.462	0.455

Sample	Bulk Density (g/cm^3)			
	1	2	3	Average
Titanium dioxide (Drytec - B)	0.617	0.619	0.605	0.614
Gum acacia	0.391	0.386	0.396	0.391
Skimmed milk (high density powder)	0.627	0.626	0.645	0.633
Skimmed milk analogue	0.491	0.488	0.486	0.488

A 2.0) Flowability of Commercially Spray-Dried Samples at 62 % Relative Humidity (22.3°C) †

Sample	Angle of Repose	Weight Displaced (g)	Angle of Repose	Weight Displaced (g)	Angle of Repose	Weight Displaced (g)
Aluminium hydroxide	52°	0.0701	49°	0.0441	55°	0.0352
	-	0.3240	-	0.2904	-	0.3301
Aluminium silicate	17°	0.0081	18°	0.0082	20°	0.0106
	22°	0.0442	21°	0.0694	24°	0.3932
	25°	0.4842	25°	0.4931	29°	0.4287
Dyestuffs	27°	0.4633	24°	0.0291	25°	0.0142
	35°	0.4923	34°	0.5321	32°	0.5100
Tungsten carbide	22°	0.0906	23°	0.0980	21°	0.0202
	30°	3.8204	30°	0.3322	23°	0.0506
	-	-	35°	3.7592	25°	0.1027
	-	-	-	-	28°	3.1156
Aluminium oxide	30°	1.2018	30°	1.1872	25°	0.1187
	42°	1.2315	-	-	28°	0.9077
	-	-	-	-	29°	0.9491
	-	-	-	-	32°	0.9717
	-	-	-	-	36°	1.0025
Titanium dioxide (Niro)	36°	0.0072	44°	0.0649	44°	0.0929
	47°	0.0703	51°	0.0768	53°	0.1028
	-	0.9429	58°	0.2836	-	0.5900
	-	-	-	0.8142	-	-
Ferrite	41°	0.2360	47°	1.4889	34°	0.5294
	51°	1.5485	75°	1.4979	43°	1.5886
Kaolin	41°	0.9258	35°	0.0412	37°	0.0871
	-	-	45°	0.8584	41°	0.8449
Barium titanate	21°	0.0093	24°	0.2173	24°	0.1942
	26°	1.2080	34°	1.6956	28°	1.6499
	30°	1.6144	-	-	-	-
tri - sodium orthophosphate	50°	0.4909	48°	0.4014	55°	0.4015

† Cumulative Weight Displaced. The underlined weight represents the total amount of sample taken.

Sample	Angle of Repose	Weight Displaced (g)	Angle of Repose	Weight Displaced (g)	Angle of Repose	Weight Displaced (g)
Copper oxychloride	47°	0.2366	46°	0.2052	46°	0.2639
	49°	0.9491	63°	0.9057	47°	0.3846
	-	-	-	-	60°	0.9033
Lead chromate	28°	0.6928	41°	0.8665	26°	0.8206
	40°	0.7946	-	-	29°	0.8749
	-	-	-	-	60°	0.9137
2,3 - dichloro - propanoic acid	79°	0.1192	87°	0.1429	40°	0.0015
	-	0.3605	-	0.3777	83°	0.1574
					-	0.3647
Copper ore	40°	0.2504	41°	1.5259	35°	0.6751
	68°	1.5890	62°	1.5358	36°	1.1239
	-	-	-	-	65°	1.2544
Coffee	47°	0.0607	45°	0.0740	58°	0.0638
	57°	0.1082	-	0.1737	-	0.1741
	-	0.2059	-	-	-	-
Magnesium hydroxide	32°	0.2399	32°	0.2816	30°	0.6113
	37°	0.6695	36°	0.5738	33°	0.6255
	-	-	47°	0.5918	45°	0.6327
Dextran	49°	0.0286	42°	0.0042	40°	0.0943
	87°	0.0413	54°	0.0218	88°	0.1046
	-	0.3140	-	0.3221	-	0.2962
Clay (nozzle)	34°	0.0194	38°	0.3190	49°	0.9984
	40°	0.9999	40°	1.0411	-	-
	50°	1.1129	-	-	-	-
Clay (rotary)	22°	0.0273	26°	1.1776	22°	0.0194
	27°	1.1095	-	-	26°	0.9521
	-	-	-	-	30°	0.9611
	-	-	-	-	32°	0.9936
Glucose	47°	0.1414	40°	0.0224	51°	0.1726
	-	0.4356	66°	0.0890	-	0.3737
	-	-	-	0.4325	-	-
Detergent	35°	0.6294	36°	0.5202	40°	0.5482

Sample	Angle of Repose	Weight Displaced (g)	Angle of Repose	Weight Displaced (g)	Angle of Repose	Weight Displaced (g)
Semi - instant skimmed milk	40°	0.0468	39°	0.0290	46°	0.1463
	49°	0.4032	50°	0.3518	53°	0.1984
	-	0.5685	-	0.5270	59°	0.2384
	-	-	-	-	61°	0.5126
Yogurt Powder	65°	0.2041	89°	0.1814	85°	0.1835
	-	0.5781	-	0.5854	-	0.5416
Co - dried egg and skimmed milk	57°	0.0126	64°	0.5861	56°	0.0142
	71°	0.5337	-	-	82°	0.5233
Titanium dioxide (Drytec - A)	39°	0.0289	38°	0.0146	33°	0.0319
	65°	0.0274	56°	0.1650	55°	0.0815
	87°	0.4430	65°	0.2116	59°	0.2663
	-	0.4590	77°	0.2628	72°	0.3174
	-	-	88°	0.3212	84°	0.4290
	-	-	-	0.4344	-	-
Polymer (Drytec - A)	90°	0.0535	83°	0.0549	73°	0.2847
	-	0.3588	-	0.3634	-	0.3381
Instant drink powder	64°	0.0705	37°	0.0001	60°	0.0001
	-	0.2680	69°	0.0850	70°	0.0446
	-	-	-	0.2779	-	0.2546
Encapsulated flavour	55°	0.1049	49°	0.1151	62°	0.1057
	-	0.3510	85°	0.1178	-	0.4287
	-	-	-	0.4102	-	-
Polymer (sodium salt)	35°	0.0043	55°	0.1424	61°	0.1489
	40°	0.0145	-	0.4707	-	0.4595
	55°	0.0363	-	-	-	-
	85°	0.0856	-	-	-	-
	-	0.5031	-	-	-	-
Organic u.v. brightner	56°	0.0054	36°	0.0045	85°	0.0212
	81°	0.0201	43°	0.0089	-	0.2648
	-	0.3097	51°	0.0141	-	-
	-	-	73°	0.0375	-	-
	-	-	-	0.2905	-	-

Sample	Angle of Repose	Weight Displaced (g)	Angle of Repose	Weight Displaced (g)	Angle of Repose	Weight Displaced (g)
Soluble titanium salt (two-fluid nozzle)	52° 81° -	0.0286 0.0696 0.3194	53° - -	0.1049 0.2825 -	56° - -	0.0911 0.2897 -
Soluble titanium salt (pressure)	62° -	0.1402 0.5069	61° -	0.1437 0.4384	66° -	0.1653 0.6011
Soluble titanium salt (rotary)	46° -	0.1149 0.4610	70° -	0.1575 0.4687	56° -	0.1255 0.4599
Polymer (Drytec - B)	50° 70° - -	0.0966 0.4091 0.4211 -	56° 64° 88° -	0.0435 0.2062 0.2179 0.4909	58° - - -	0.1172 0.4805 - -
Calcium stearate	70° - -	0.1771 0.4751 -	77° - -	0.1539 0.4861 -	50° 69° -	0.0182 0.0806 0.4475
Titanium dioxide (Drytec - B)	51° - - -	0.0818 0.6149 - -	56° 78° - -	0.0877 0.1011 0.6176 -	45° 67° 81° -	0.1331 0.5258 0.5437 0.5623
Gum acacia	67° -	0.1285 0.3873	76° -	0.1124 0.4228	66° -	0.1103 0.3994
Skimmed milk (high density powder)	47° 66° 90° -	0.0304 0.1552 0.4733 0.6381	57° - - -	0.2302 0.6562 - -	61° - - -	0.2069 0.4808 - -
Skimmed milk analogue	58° -	0.3375 0.5050	65° -	0.1406 0.4667	58° -	0.1393 0.5318

A 2.1) Flowability of Commercially Spray-Dried Samples at 15 % Relative Humidity (22.7°C) †

Sample	Angle of Repose	Weight Displaced (g)	Angle of Repose	Weight Displaced (g)	Angle of Repose	Weight Displaced (g)
Aluminium silicate	23°	0.0690	21°	0.0184	22°	0.0133
	25°	0.3071	25°	0.3499	24°	0.3560
	32°	0.4206	29°	0.4191	29°	0.4260
Titanium dioxide (Miro)	41°	0.0651	43°	0.0474	40°	0.0404
	49°	0.3582	46°	0.1898	44°	0.0776
	65°	0.4697	55°	0.4167	49°	0.2221
	-	-	-	-	59°	0.4155
Gum acacia	35°	0.0980	60°	0.1629	88°	0.1711
	71°	0.2370	-	0.4257	-	0.4112
	-	0.3637	-	-	-	-

A 2.2) Flowability of Commercially Spray-Dried Samples at 100 % Relative Humidity (21.4°C) †

Sample	Angle of Repose	Weight Displaced (g)	Angle of Repose	Weight Displaced (g)	Angle of Repose	Weight Displaced (g)
Aluminium silicate	23°	0.5159	22°	0.0115	22°	0.0067
	-	-	27°	0.5205	29°	0.4998
Titanium dioxide (Miro)	34°	0.1885	31°	0.0608	30°	0.0468
	49°	0.3751	40°	0.2347	34°	0.1153
	-	-	48°	0.2395	37°	0.1563
	-	-	55°	0.2592	41°	0.1966
	-	-	61°	0.2889	45°	0.3761
	-	-	81°	0.4378	-	-
Gum acacia	45°	0.0281	41°	0.0885	46°	0.0397
	-	0.2616	-	0.2262	-	0.2490

† Cumulative Weight Displaced. The underlined weight represents the total amount of sample taken.

A 3,0) Particle Morphology - General Observations

Aluminium hydroxide

Powder Colour - White.
Particle Shape - Spherical, regular.
Agglomeration - Some degree of agglomeration, i.e.; agglomerates composed of a large number particles. Dust level - low.
Surface Features - No surface deformation, blowholes, cratering, fissures or cracks.
Surface Structure - Porous and granular. Grain size ≈ 1,5 µm to 3 µm in diameter.
Internal Structure - Solid - identical to surface structure. When collapsed, a small number of particles show vacuolation.

Aluminium silicate

Powder Colour - White.
Particle Shape - Spherical, very regular.
Agglomeration - No agglomeration or dust. There are a large number of fragmented particles, i.e.; half and quarter spheres.
Surface Features - No surface deformation. All particles show fissures and cracks. Cratering is evident in a small number of particles.
Surface Structure - Very smooth, polymeric, skin-like.
Internal Structure - Solid - porous and granular with vacuolation. Grain size ≈ 6 µm to 10 µm in diameter. Particle cross sections clearly show the smooth outer surface structure ≈ 9 µm to 13 µm thick.

Dyestuffs

Powder Colour - Red.
Particle Shape - Spherical, irregular.
Agglomeration - Small amount of agglomeration, i.e.; two or three particle agglomerates. No dust.
Surface Features - Large amount of surface deformation - particle shrivelling and inflation, blowholes, cratering, fissures and cracks. Most of the particles show a crystalline deposit on the surface; shown by X-ray to be sodium chloride.
Surface Structure - Polymeric, skin-like.
Internal Structure - Hollow with a thin wall structure, ≈ 25 µm thick.

Tungsten carbide

Powder Colour - Dark grey.
Particle Shape - Spherical, regular - some particles are elongated.
Agglomeration - No agglomeration, Dust level - low.
Surface Features - No surface deformation. A small number of particles have blowholes.
Surface Structure - Porous and granular. Grain size ≈ 1,5 µm to 2 µm in diameter.
Internal Structure - Hollow with a very thick wall structure ≈ 35 µm. The wall structure is identical to the surface, i.e.; porous and granular.

Aluminium oxide

Powder Colour - White.
Particle Shape - Spherical, regular - some particles are elongated.
Agglomeration - No agglomeration or dust.
Surface Features - No surface deformation. Cratering is evident in a number of particles.
Surface Structure - Porous and granular. Grain size ≈ 2 µm to 4 µm in diameter.
Internal Structure - Solid - identical to surface structure. Most of the particles show vacuolation.

Titanium dioxide (Niro)

Powder Colour - Off-white.
Particle Shape - Spherical, regular.
Agglomeration - Mass agglomeration. Dust level - very high. Some particles are fractured into half and quarter spheres.
Surface Features - No surface deformation, blowholes, cratering, fissures or cracks. Particle surfaces are very dusty.
Surface Structure - Porous and granular - very fine. Grain size < 1 µm in diameter.
Internal Structure - Solid - identical to surface structure. Vacuolation not visible.

Ferrite

Powder Colour - Black.
Particle Shape - Spherical, regular.
Agglomeration - Small amount of agglomeration - five or six particle agglomerates. Dust level - low.
Surface Features - No surface deformation, blowholes, cratering, fissures or cracks.
Surface Structure - Porous and granular. Grain size ≈ 0,5 µm to 3 µm in diameter.
Internal Structure - Solid - identical to surface structure. Vacuolation not visible.

Kaolin

Powder Colour - White.
Particle Shape - Spherical, irregular.
Agglomeration - Small amount of agglomeration - two or three particle agglomerates. Dust level - low.
Surface Features - Some surface deformation. Particles show cratering and surfaces are dusty.
Surface Structure - Has a skin-like appearance but also shows a granular texture.
Internal Structure - Solid - identical to surface structure. Vacuolation not visible.

Barium titanate

Powder Colour - Light buff.
Particle Shape - Spherical, regular.
Agglomeration - No agglomeration or dust.
Surface Features - No surface deformation. Particles show some cratering.
Surface Structure - Porous and granular. Grain size ≈ 2 µm to 10 µm in diameter.
Internal Structure - Solid - identical to surface structure. Most particles show vacuolation.

Tri-sodium orthophosphate

Powder Colour - White.
Particle Shape - Spherical, very irregular.
Agglomeration - Some degree of agglomeration - two or three particle agglomerates. Dust level - low. Large number of particles fractured into half and quarter spheres.
Surface Features - Some surface deformation. No blowholes or cratering. Large amount of fissures and cracks.
Surface Structure - Highly crystalline.
Internal Structure - Hollow with a wall thickness of ± 15 µm to 20 µm. Some of the larger particles contain smaller particles.

Copper oxychloride

Powder Colour - Light green.
Particle Shape - Spherical, regular.
Agglomeration - Some agglomeration - two or three particle agglomerates. No dust.
Surface Features - No surface deformation, blowholes, cratering, fissures or cracks.
Surface Structure - Porous and granular. Grain size ± 0,5 µm to 2 µm in diameter.
Internal Structure - Solid - identical to surface structure. Vacuolation not visible.

Lead chromate

Powder Colour - Bright yellow.
Particle Shape - Spherical, regular - some particles are elongated.
Agglomeration - No agglomeration or dust.
Surface Features - No surface deformation. A number of the particles show blowholes.
Surface Structure - Porous and granular. Grain size < 1 µm to 2 µm in diameter.
Internal Structure - Both solid and hollow particles - material identical to surface structure. Most of the particles show vacuolation with some of the larger particles containing smaller particles.

2,3 - dichloropropanoic acid

Powder Colour - Off-white.
Particle Shape - Spherical, very irregular.
Agglomeration - Mass agglomeration. No dust.
Surface Features - Large amount of surface deformation. Particles show a considerable amount of shrivelling. No inflation, blowholes, cracks or fissures. A small number of particles are cratered.
Surface Structure - Polymeric or skin-like.
Internal Structure - Hollow.

Copper ore

Powder Colour - Black.
Particle Shape - Spherical, irregular.
Agglomeration - Some agglomeration - two or three particle agglomerates. Dust level - low.
Surface Features - No surface deformation, blowholes, cratering, fissures or cracks.
Surface Structure - Porous and granular. Grain size ≈ 2 μm to 7 μm in diameter.
Internal Structure - Solid - identical to surface structure. Vacuolation not visible.

Coffee

Powder Colour - Brown.
Particle Shape - Spherical, irregular.
Agglomeration - Mass agglomeration. Dust level - low. Large number of broken shells.
Surface Features - Surface deformation - all particles show inflation with blowholes. Very little shrivelling or cratering. No cracks or fissures.
Surface Structure - Polymeric, skin-like.
Internal Structure - Hollow. Wall structure is very thin ≈ 2 μm thick. Many of the larger particles contain smaller particles.

Magnesium hydroxide

Powder Colour - White.
Particle Shape - Spherical, regular - a number of particles are elongated.
Agglomeration - No agglomeration or dust.
Surface Features - No surface deformation, blowholes, cratering, fissures or cracks.
Surface Structure - Porous and granular. Grain size ≈ 1,5 μm to 3 μm in diameter.
Internal Structure - Solid - identical to surface structure. Vacuolation not visible.

Dextran

Powder Colour - White.
Particle Shape - Spherical, regular.
Agglomeration - Mass agglomeration. No dust.
Surface Features - Surface distortion - both shrivelling and inflation are evident with cratering and blowholes.
Surface Structure - Polymeric, skin-like.
Internal Structure - Hollow with a very thin wall structure ≈ 2 μm to 5 μm thick.

Clay (Nozzle)

Powder Colour - Light brown.
Particle Shape - Spherical, irregular.
Agglomeration - Small amount of agglomeration - five or six particle agglomerates. Dust level - low.
Surface Features - Surface distortion - some cratering. No blowholes, cracks or fissures. Surface is dusty.
Surface Structure - Has a skin-like appearance but also shows a granular texture.
Internal Structure - Solid - identical to surface structure. Vacuolation not visible.

Clay (Rotary)

Powder Colour - Light brown.
Particle Shape - Spherical, very regular.
Agglomeration - No agglomeration or dust.
Surface Features - No surface distortion - very smooth. Most of the particles show cratering. No blowholes, cracks or fissures.
Surface Structure - Has a skin-like appearance but also shows a granular texture.
Internal Structure - Most of the particles are hollow with a very thick wall structure.

Glucose

Powder Colour - White.
Particle Shape - Spherical, very irregular. There is considerable ligament formation due to incomplete atomization.
Agglomeration - Mass agglomeration. Dust level - low.
Surface Features - Large amount of surface distortion - both shrivelling and particle inflation are evident with cratering and blowholes.
Surface Structure - Polymeric, skin-like.
Internal Structure - Hollow with a very thin wall structure.

Detergent

Powder Colour - White.
Particle Shape - Spherical, very irregular. There is considerable short ligament formation due to incomplete atomization.
Agglomeration - Some agglomeration - four or five particle agglomerates. No dust.
Surface Features - Large amount of surface distortion - blowholes with cracks and fissures. No cratering or shrivelling. Most of the particles are covered with small pores ≈ 1,5 µm to 4,5 µm in diameter.
Surface Structure - Polymeric, skin-like, but also shows a crystalline texture.
Internal Structure - Hollow with a thick, porous wall structure ≈ 50 µm thick. A small number appear solid with a large amount of vacuolation.

Semi-instant skimmed milk

Powder Colour - Pale yellow.
Particle Shape - Spherical, regular.
Agglomeration - Mass agglomeration. No dust.
Surface Features - Surface deformation - shrivelling, particle inflation and cratering are all evident. There are very few blowholes, no cracks or fissures.
Surface Structure - Polymeric, skin-like.
Internal Structure - Hollow with a very thick wall structure. The wall structure shows a large amount of vacuolation.

Yogurt Powder

Powder Colour - Pale orange.
Particle Shape - Spherical, very regular.
Agglomeration - Mass agglomeration. No dust.
Surface Features - No surface deformation, shrivelling or cratering. A number of the particles show blowholes, cracks and fissures.
Surface Structure - Polymeric, skin-like.
Internal Structure - Hollow with a thin wall structure.

Co-dried egg and skimmed milk

Powder Colour - Pale orange,
Particle Shape - Spherical, regular,
Agglomeration - Mass agglomeration, No dust,
Surface Features - Surface deformation - shrivelling, particle inflation and cratering are all evident, There are very few blowholes, no cracks or fissures,
Surface Structure - Polymeric, skin-like,
Internal Structure - Hollow with a thin wall structure ≈ 2 - 3 µm thick,

Titanium dioxide (Drytec - A)

Powder Colour - White,
Particle Shape - Spherical, very regular,
Agglomeration - Mass agglomeration, No dust,
Surface Features - No surface deformation, blowholes cratering, fissures or cracks, Surface is very clean, i.e.; no dust,
Surface Structure - Porous and granular - very fine, Grain size < 1 µm in diameter,
Internal Structure - Solid - identical to surface structure, Vacuolation not visible,

Polymer (Drytec - A)

Powder Colour - White,
Particle Shape - Spherical, very regular,
Agglomeration - Mass agglomeration, No dust,
Surface Features - No surface deformation, cracks, fissures or cratering, There is some degree of particle inflation and a number of the particles show blowholes,
Surface Structure - Polymeric, skin-like,
Internal Structure - Solid - identical to surface structure, Most of the particles show vacuolation,

Instant drink powder

Powder Colour - Off-white,
Particle Shape - Spherical, very regular,
Agglomeration - Mass agglomeration, Dust level - low,
Surface Features - No surface deformation, cracks, fissures or cratering, There is some degree of particle inflation and a number of the particles show blowholes,
Surface Structure - Polymeric, skin-like,
Internal Structure - Hollow,

Encapsulated flavour

Powder Colour - Light Buff.
Particle Shape - Spherical, irregular.
Agglomeration - Some agglomeration. Dust level - low.
Surface Features - Surface deformation - large amount of shrivelling. No blowholes, cratering, cracks or fissures. Very little particle inflation.
Surface Structure - Polymeric, skin-like.
Internal Structure - Hollow with a thin wall structure ≈ 2µm to 3 µm thick.

Polymer (sodium salt)

Powder Colour - White.
Particle Shape - Spherical, regular.
Agglomeration - Mass agglomeration. No dust.
Surface Features - No surface deformation, cracks, fissures or cratering. There is some degree of particle inflation and a number of the particles show blowholes.
Surface Structure - Polymeric, skin-like.
Internal Structure - Hollow.

Organic u.v. brightner

Powder Colour - Pale yellow.
Particle Shape - Spherical, regular - some particle are elongation.
Agglomeration - Mass agglomeration. Dust level - high. Large amount of needle shaped crystals.
Surface Features - No surface deformation, blowholes cratering or particle inflation. Many of the particles show cracks and fissures.
Surface Structure - Highly crystalline.
Internal Structure - Solid - similar to surface structure but crystal structure finer. Some vacuolation.

Soluble titanium salt (Two-fluid nozzle)

Powder Colour - Off-White.
Particle Shape - Spherical, regular.
Agglomeration - Mass agglomeration. Dust level - very high. Large number of broken shells.
Surface Features - No surface deformation, blowholes cratering, fissures or cracks.
Surface Structure - Polymeric, skin-like.
Internal Structure - Hollow.

Soluble titanium salt (Pressure nozzle)

Powder Colour - Off-white.
Particle Shape - Spherical, regular. Particle-size is greater than Titanium salt (2FN).
Agglomeration - Mass agglomeration. Dust level - high (less than Titanium salt (2FN)).
Surface Features - Identical to Titanium salt (2FN).
Surface Structure - Identical to Titanium salt (2FN).
Internal Structure - Identical to Titanium salt (2FN).

Soluble titanium salt (Rotary)

Powder Colour - Off-white.
Particle Shape - Spherical, regular. Particle-size is greater than both Titanium salt (2FN) and (PN).
Agglomeration - Mass agglomeration. Dust level - high (less than Titanium salt (2FN) and (PN).
Surface Features - Identical to Titanium salt (2FN).
Surface Structure - Identical to Titanium salt (2FN).
Internal Structure - Identical to Titanium salt (2FN).

Polymer (Drytec - B)

Powder Colour - White.
Particle Shape - Spherical, regular - larger particles show some degree of distortion.
Agglomeration - Mass agglomeration. Dust level - low. Large number of broken shells.
Surface Features - No surface deformation, cracks, fissures or cratering. There is some degree of particle inflation and a number of the particles show blowholes.
Surface Structure - Polymeric, skin-like.
Internal Structure - Hollow.

Calcium stearate

Powder Colour - Off-white.
Particle Shape - Spherical, regular.
Agglomeration - Mass agglomeration. No dust.
Surface Features - Some surface deformation - blistering. No blowholes or particle inflation. A small number show cratering, cracks and fissures.
Surface Structure - Polymeric, skin-like.
Internal Structure - Hollow with a very thick wall structure.

Titanium dioxide (Drytec - B)

Powder Colour - White.
Particle Shape - Spherical, regular.
Agglomeration - Mass agglomeration. Dust level - very high.
Surface Features - No surface deformation, blowholes cratering, cracks or fissures. Surface is very dusty.
Surface Structure - Porous and granular - very fine. Grain size < 1 µm in diameter.
Internal Structure - Solid - identical to surface structure. Vacuolation not visible.

Gum acacia

Powder Colour - White.
Particle Shape - Spherical, irregular.
Agglomeration - Mass agglomeration. No dust.
Surface Features - Surface deformation - large amount of shrivelling. No blowholes, cratering, cracks fissures or particle inflation.
Surface Structure - Polymeric, skin-like.
Internal Structure - Hollow.

Skinned milk (High density powder)

Powder Colour - Pale yellow.
Particle Shape - Spherical, regular.
Agglomeration - Mass agglomeration. No dust.
Surface Features - Some surface deformation - shrivelling cratering, blowholes and particle inflation are evident. No cracks or fissures.
Surface Structure - Polymeric, skin-like.
Internal Structure - Solid - identical to surface structure. There is a large amount of vacuolation.

Skinned milk analogue

Powder Colour - Pale yellow.
Particle Shape - Spherical, regular.
Agglomeration - Mass agglomeration. No dust.
Surface Features - Some surface deformation - shrivelling cratering, blowholes and particle inflation are evident. No cracks or fissures.
Surface Structure - Polymeric, skin-like.
Internal Structure - Hollow with a very thick wall structure. There is a large amount of vacuolation within the wall structure.

A 4.0) The Evaporation of Pure Liqiud Droplets

Table 1

Run Number = W1
Sample Liquid = Water
Air Temperature (Dry Bulb) = 50.0°C
Air Temperature (Wet Bulb) = 26.3°C
Air Humidity = 0.01249 kg/kg
Air Velocity = 1.0 m/s
Reynolds Number = 1128

Time (s)	Drop Diameter (a x 10^{-3})	Drop Mass (kg x 10^{-6})	Reynolds No. Re_D	Sherwood No. Sh	Nusselt No. Nu	$Re^{0.50}\ Pr^{0.33}$	$Re^{0.50}\ Sc^{0.33}$
15	1,69	2,42	95,57	97,57	115,99	8,71	8,12
30	1,64	2,31	93,62	47,79	55,30	8,61	8,02
45	1,65	2,20	91,92	30,91	35,55	8,53	7,95
60	1,60	2,10	89,67	22,68	25,37	8,43	7,85
75	1,53	1,99	87,98	17,50	19,53	8,35	7,78
90	1,53	1,88	85,72	14,17	15,45	8,24	7,68
105	1,49	1,77	84,03	11,69	12,73	8,16	7,60
120	1,47	1,67	81,77	9,88	10,55	8,05	7,50
135	1,40	1,56	80,08	8,42	8,99	7,96	7,42
150	1,38	1,45	77,83	7,24	7,65	7,85	7,31
165	1,34	1,35	76,13	6,26	6,65	7,77	7,23
180	1,33	1,24	73,88	5,43	5,74	7,65	7,13
195	1,31	1,13	72,19	4,67	5,06	7,56	7,04
210	1,25	1,03	70,49	4,04	4,48	7,47	6,96
225	1,22	0,92	68,24	3,49	3,92	7,35	6,85
240	1,18	0,81	66,55	2,97	3,49	7,26	6,76
255	1,14	0,71	64,29	2,53	3,07	7,14	6,65
270	1,07	0,60	62,60	2,04	2,75	7,04	6,56

Correlating Equations

$$Sh = 8.9784\ e^{-6} \cdot 10\ \hat{}\ (\ 0.81473\ Re^{0.50}\ Sc^{0.33}\ )$$

correlation coefficient = 0.956

$$Nu = 1.3531\ e^{-5} \cdot 10\ \hat{}\ (\ 0.74325\ Re^{0.50}\ Pr^{0.33}\ )$$

correlation coefficient = 0.940

Table 2

Run Number = W2
Sample Liquid = Water
Air Temperature (Dry Bulb) = 50.0°C
Air Temperature (Wet Bulb) = 26.3°C
Air Humidity = 0.01249 kg/kg
Air Velocity = 1.0 m/s
Reynolds Number = 1128

Time (s)	Drop Diameter (m x 10^{-3})	Drop Mass (kg x 10^{-6})	Reynolds No, Re_D	Sherwood No, Sh	Nusselt No, Nu	$Re^{0.50}\ Pr^{0.33}$	$Re^{0.50}\ Sc^{0.33}$
15	1,56	1,89	87,98	83,22	97,67	8,35	7,78
30	1,53	1,81	86,29	40,61	46,98	8,27	7,70
45	1,49	1,73	84,59	26,38	30,10	8,19	7,62
60	1,44	1,65	82,90	19,27	21,68	8,10	7,55
75	1,43	1,57	81,21	14,95	16,65	8,02	7,47
90	1,41	1,49	79,52	12,13	13,30	7,94	7,39
105	1,41	1,41	77,83	10,00	10,92	7,85	7,31
120	1,36	1,33	76,13	8,47	9,15	7,77	7,23
135	1,34	1,25	74,44	7,26	7,77	7,68	7,15
150	1,31	1,17	72,75	6,23	6,68	7,59	7,07
165	1,26	1,10	71,06	5,48	5,79	7,50	6,99
180	1,23	1,02	69,37	4,77	5,06	7,41	6,90
195	1,19	0,94	67,67	4,12	4,45	7,32	6,82
210	1,17	0,86	65,98	3,61	3,93	7,23	6,73
225	1,14	0,78	64,29	3,16	3,48	7,14	6,65
240	1,12	0,70	63,16	2,67	3,15	7,07	6,59
255	1,07	0,62	61,47	2,27	2,81	6,98	6,50
270	1,06	0,54	59,78	1,94	2,51	6,88	6,41

Correlating Equations

$$Sh = 1.7540\ e^{-6} \cdot 10\ \hat{}\ (\ 0.93467\ Re^{0.50}\ Sc^{0.33}\ )$$

correlation coefficient = 0.962

$$Nu = 6.3271\ e^{-6} \cdot 10\ \hat{}\ (\ 0.80519\ Re^{0.50}\ Pr^{0.33}\ )$$

correlation coefficient = 0.923

Table 3

Run Number = W3
Sample Liquid = Water
Air Temperature (Dry Bulb) = 50.0°C
Air Temperature (Wet Bulb) = 26.2°C
Air Humidity = 0.01249
Air Velocity = 1.0 m/s
Reynolds Number = 1128

Time (s)	Drop Diameter (a x 10^{-3})	Drop Mass (kg x 10^{-6})	Reynolds No. Re_D	Sherwood No. Sh	Nusselt No. Nu	$Re^{0.50}\ Pr^{0.33}$	$Re^{0.50}\ Sc^{0.33}$
15	1,93	3,77	109,97	132,62	152,61	9,33	8,69
30	1,91	3,63	108,28	64,93	73,98	9,26	8,63
45	1,89	3,50	106,59	42,41	47,79	9,19	8,56
60	1,87	3,36	104,90	31,02	34,71	9,12	8,49
75	1,83	3,23	103,20	24,27	26,88	9,04	8,42
90	1,82	3,09	101,51	19,63	21,67	8,97	8,35
105	1,80	2,96	99,82	16,41	17,96	8,89	8,28
120	1,74	2,82	98,13	13,91	15,19	8,82	8,21
135	1,71	2,69	96,44	11,99	13,04	8,74	8,14
150	1,69	2,55	94,74	10,43	11,33	8,66	8,07
165	1,65	2,42	93,05	9,18	9,93	8,59	8,00
180	1,64	2,28	91,36	8,08	8,78	8,51	7,92
195	1,60	2,15	89,67	7,13	7,81	8,43	7,85
210	1,58	2,02	87,98	6,34	6,98	8,35	7,78
225	1,53	1,88	86,85	5,62	6,35	8,29	7,73
240	1,49	1,75	84,59	5,01	5,65	8,19	7,62
255	1,45	1,61	82,90	4,42	5,10	8,10	7,55
270	1,44	1,48	81,21	3,94	4,63	8,02	7,47

Correlating Equations

$$Sh = 1.7249\ e^{-7} \cdot 10\ \hat{}\ (\ 0.97140\ Re^{0.50}\ Sc^{0.33}\ )$$

correlation coefficient = 0.949

$$Nu = 2.6623\ e^{-7} \cdot 10\ \hat{}\ (\ 0.88894\ Re^{0.50}\ Pr^{0.33}\ )$$

correlation coefficient = 0.930

Table 4

Run Number = W4
Sample Liquid = Water
Air Temperature (Dry Bulb) = 100.0°C
Air Temperature (Wet Bulb) = 39.4°C
Air Humidity = 0.02436 kg/kg
Air Velocity = 1.0 m/s
Reynolds Number = 877

Time (s)	Drop Diameter (a x 10-3)	Drop Mass (kg x 10-6)	Reynolds No. Re_o	Sherwood No. Sh	Nusselt No. Nu	$Re^{0.50} Pr^{0.33}$	$Re^{0.50} Sc^{0.33}$
5	1,67	2,23	73,27	88,54	117,54	7,59	6,91
10	1,64	2,16	71,95	43,67	56,68	7,52	6,85
15	1,62	2,08	71,07	28,45	36,87	7,48	6,80
20	1,58	2,01	69,76	21,06	26,64	7,41	6,74
25	1,56	1,94	68,88	16,39	20,78	7,36	6,70
30	1,53	1,87	67,56	13,41	16,66	7,29	6,63
35	1,53	1,79	66,69	11,15	13,91	7,24	6,59
40	1,51	1,72	65,37	9,57	11,69	7,17	6,52
45	1,47	1,65	64,49	8,28	10,12	7,12	6,48
50	1,44	1,58	63,18	7,28	8,74	7,05	6,41
55	1,38	1,50	62,30	6,37	7,73	7,00	6,37
60	1,40	1,43	60,98	5,68	6,79	6,93	6,30
65	1,34	1,36	60,10	5,06	6,09	6,88	6,26
70	1,34	1,28	58,79	4,53	5,41	6,80	6,19
75	1,33	1,21	57,91	4,04	4,89	6,75	6,14
80	1,27	1,14	56,59	3,68	4,39	6,67	6,07
85	1,30	1,07	55,72	3,29	4,00	6,62	6,02
90	1,27	0,99	54,40	2,94	3,60	6,54	5,95
95	1,20	0,92	53,52	2,64	3,30	6,49	5,90
100	1,18	0,85	52,21	2,37	2,99	6,41	5,83

Correlating Equations

$$Sh = 6.1973\ e^{-7} \cdot 10^{\wedge} (1.1143\ Re^{0.50}\ Sc^{0.33})$$

correlation coefficient = 0.940

$$Nu = 4.2371\ e^{-7} \cdot 10^{\wedge} (1.0493\ Re^{0.50}\ Pr^{0.33})$$

correlation coefficient = 0.926

Table 5

Run Number = W5
Sample Liquid = Water
Air Temperature (Dry Bulb) = 100.0°C
Air Temperature (Wet Bulb) = 39.2°C
Air Humidity = 0.02436 kg/kg
Air Velocity = 1.0 m/s
Reynolds Number = 877

Time (s)	Drop Diameter (m x 10^{-3})	Drop Mass (kg x 10^{-6})	Reynolds No. Re_D	Sherwood No. Sh	Nusselt No. Nu	$Re^{0.50} Pr^{0.33}$	$Re^{0.50} Sc^{0.33}$
5	1,67	2,36	73,27	93,71	117,54	7,59	6,91
10	1,65	2,28	72,39	45,81	57,37	7,55	6,87
15	1,64	2,20	71,51	29,90	37,33	7,50	6,82
20	1,60	2,12	70,19	21,96	26,97	7,43	6,76
25	1,56	2,05	69,32	17,21	21,04	7,39	6,72
30	1,56	1,97	68,00	14,05	16,87	7,31	6,65
35	1,54	1,89	67,12	11,70	14,09	7,27	6,61
40	1,51	1,81	66,25	9,95	12,01	7,22	6,57
45	1,47	1,73	64,93	8,60	10,26	7,15	6,50
50	1,44	1,65	64,05	7,49	8,99	7,10	6,46
55	1,44	1,57	62,74	6,63	7,83	7,03	6,39
60	1,40	1,50	61,86	5,88	6,98	6,98	6,35
65	1,40	1,42	60,98	5,22	6,27	6,93	6,30
70	1,36	1,37	59,67	4,78	5,57	6,85	6,23
75	1,34	1,26	58,79	4,16	5,05	6,80	6,19
80	1,31	1,18	57,47	3,75	4,52	6,72	6,12
85	1,29	1,10	56,59	3,32	4,13	6,67	6,07
90	1,25	1,02	55,72	2,95	3,77	6,62	6,02
95	1,25	0,94	54,40	2,65	3,41	6,54	5,95
100	1,22	0,87	53,52	2,36	3,13	6,49	5,90

Correlating Equations

$$Sh = 1.6836\ e^{-7} \cdot 10^{\wedge} (1.1982\ Re^{0.50}\ Sc^{0.33})$$

correlation coefficient = 0.950

$$Nu = 2.5407\ e^{-7} \cdot 10^{\wedge} (1.0761\ Re^{0.50}\ Pr^{0.33})$$

correlation coefficient = 0.932

Table 6

Run Number = W6
Sample Liquid = Water
Air Temperature (Dry Bulb) = 100.0°C
Air Temperature (Wet Bulb) = 39.2°C
Air Humidity = 0.02436 kg/kg
Air Velocity = 1.0 m/s
Reynolds Number = 877

Time (s)	Drop Diameter (a x 10^{-3})	Drop Mass (kg x 10^{-6})	Reynolds No, Re_o	Sherwood No, Sh	Nusselt No, Nu	$Re^{0.50}\ Pr^{0.33}$	$Re^{0.50}\ Sc^{0.33}$
5	1,60	2,07	70,20	85,79	107,89	7,43	6,76
10	1,56	1,99	69,32	41,76	52,61	7,39	6,72
15	1,58	1,92	68,00	27,38	33,75	7,31	6,65
20	1,53	1,84	67,12	19,94	24,67	7,27	6,61
25	1,49	1,77	65,81	15,65	18,97	7,20	6,55
30	1,49	1,70	64,93	12,70	15,39	7,15	6,50
35	1,47	1,62	63,61	10,59	12,66	7,07	6,44
40	1,42	1,55	62,74	9,00	10,77	7,03	6,39
45	1,40	1,47	61,42	7,74	9,18	6,95	6,32
50	1,36	1,40	60,54	6,73	8,03	6,90	6,28
55	1,34	1,33	59,23	5,94	6,98	6,83	6,21
60	1,31	1,25	57,91	5,22	6,12	6,75	6,14
65	1,31	1,18	57,03	4,64	5,48	6,70	6,09
70	1,29	1,10	55,72	4,10	4,85	6,62	6,02
75	1,25	1,03	54,84	3,63	4,39	6,57	5,98
80	1,20	0,95	53,52	3,23	3,92	6,49	5,90
85	1,20	0,88	52,65	2,87	3,57	6,44	5,86
90	1,16	0,81	51,33	2,55	3,21	6,35	5,78
95	1,16	0,73	50,45	2,21	2,93	6,30	5,73

Correlating Equations

$$Sh = 5.0552\ e^{-7} \cdot 10^{\wedge} (1.1493\ Re^{0.50}\ Sc^{0.33})$$

correlation coefficient = 0.947

$$Nu = 5.8733\ e^{-7} \cdot 10^{\wedge} (1.0473\ Re^{0.50}\ Pr^{0.33})$$

correlation coefficient = 0.928

Table 7

Run Number = W7
Sample Liquid = Water
Air Temperature (Dry Bulb) = 150.0°C
Air Temperature (Wet Bulb) = 50.1°C
Air Humidity = 0.0516 kg/kg
Air Velocity = 1.0 m/s
Reynolds Number = 704

Time (s)	Drop Diameter (m x 10^{-3})	Drop Mass (kg x 10^{-6})	Reynolds No, Re_D	Sherwood No, Sh	Nusselt No, Nu	$Re^{0.50}\ Pr^{0.33}$	$Re^{0.50}\ Sc^{0.33}$
5	1,53	1,89	54,18	43,56	54,91	6,50	5,79
10	1,51	1,78	53,12	20,92	26,40	6,44	5,74
15	1,47	1,67	51,71	13,40	16,68	6,35	5,66
20	1,44	1,56	50,31	9,68	11,84	6,26	5,58
25	1,40	1,45	49,25	7,35	9,08	6,20	5,52
30	1,36	1,34	47,84	5,83	7,14	6,11	5,44
35	1,33	1,23	46,79	4,68	5,85	6,04	5,38
40	1,29	1,12	45,38	3,85	4,82	5,95	5,30
45	1,25	1,01	44,33	3,16	4,09	5,88	5,24
50	1,22	0,90	42,92	2,62	3,45	5,78	5,16

Correlating Equations

$$Sh = 1.1225\ e^{-7} \cdot 10^{\wedge}\ (\ 1.4261\ Re^{0.50}\ Sc^{0.33}\ )$$

correlation coefficient = 0.964

$$Nu = 2.1777\ e^{-7} \cdot 10^{\wedge}\ (\ 1.2396\ Re^{0.50}\ Sc^{0.33}\ )$$

correlation coefficient = 0.942

Table 8

Run Number = W8
Sample Liquid = Water
Air Temperature (Dry Bulb) = 150.0°C
Air Temperature (Wet Bulb) = 50.4°C
Air Humidity = 0.0516 kg/kg
Air Velocity = 1.0 m/s
Reynolds Number = 704

Time (s)	Drop Diameter (a x 10^{-3})	Drop Mass (kg x 10^{-6})	Reynolds No. Re_D	Sherwood No. Sh	Nusselt No. Nu	$Re^{0.50} Pr^{0.33}$	$Re^{0.50} Sc^{0.33}$
5	1,53	1,67	52,77	39,52	52,10	6,41	5,72
10	1,47	1,57	51,71	18,96	25,02	6,35	5,66
15	1,38	1,47	50,31	12,16	15,79	6,26	5,58
20	1,40	1,37	48,90	8,75	11,19	6,17	5,50
25	1,34	1,28	47,49	6,73	8,44	6,09	5,42
30	1,31	1,18	46,09	5,32	6,62	5,99	5,34
35	1,27	1,08	44,68	4,32	5,33	5,90	5,26
40	1,24	0,99	43,27	3,58	4,67	5,81	5,18
45	1,20	0,89	42,22	2,93	3,71	5,74	5,11
50	1,16	0,79	40,81	2,42	3,11	5,64	5,03

Correlating Equations

$$Sh = 1.9546\ e^{-7} \cdot 10\ \hat{}\ (\ 1.3991\ Re^{0.50}\ Sc^{0.33}\ )$$

correlation coefficient = 0.977

$$Nu = 5.8353\ e^{-7} \cdot 10\ \hat{}\ (\ 1.1871\ Re^{0.50}\ Sc^{0.33}\ )$$

correlation coefficient = 0.966

Table 9

Run Number = W9
Sample Liquid = Water
Air Temperature (Dry Bulb) = 150.0°C
Air Temperature (Wet Bulb) = 50.3°C
Air Humidity = 0.0516 kg/kg
Air Velocity = 1.0 m/s
Reynolds Number = 704

Time (s)	Drop Diameter (a x 10^{-3})	Drop Mass (kg x 10^{-6})	Reynolds No. Re_D	Sherwood No. Sh	Nusselt No. Nu	$Re^{0.50} Pr^{0.33}$	$Re^{0.50} Sc^{0.33}$
5	1.56	1.96	55.23	44.32	57.08	6.56	5.85
10	1.53	1.84	53.82	21.34	27.10	6.48	5.77
15	1.51	1.72	52.42	13.70	17.13	6.39	5.70
20	1.44	1.59	51.01	9.73	12.17	6.31	5.62
25	1.42	1.47	49.60	7.40	9.21	6.22	5.54
30	1.34	1.35	48.20	5.83	7.25	6.13	5.46
35	1.31	1.22	46.44	4.69	5.77	6.02	5.36
40	1.27	1.10	45.03	3.81	4.74	5.93	5.28
45	1.25	0.98	43.62	3.12	3.95	5.83	5.20
50	1.22	0.85	42.22	2.51	3.33	5.74	5.11

Correlating Equations

$$Sh = 1.1944\ e^{-6} \cdot 10^{\wedge}\ (\ 1.2375\ Re^{0.50}\ Sc^{0.33}\ )$$

correlation coefficient = 0.948

$$Nu = 4.8702\ e^{-7} \cdot 10^{\wedge}\ (\ 1.1791\ Re^{0.50}\ Sc^{0.33}\ )$$

correlation coefficient = 0.967

Table 10

Run Number = W10
Sample Liquid = Water
Air Temperature (Dry Bulb) = 200.0°C
Air Temperature (Wet Bulb) = 58.2°C
Air Humidity = 0.08799 kg/kg
Air Velocity = 1.0 m/s
Reynolds Number = 581

Time (s)	Drop Diameter (m x 10^{-3})	Drop Mass (kg x 10^{-6})	Reynolds No. Re_D	Sherwood No. Sh	Nusselt No. Nu	$Re^{0.50} Pr^{0.33}$	$Re^{0.50} Sc^{0.33}$
4	1,58	2,07	45,62	37,93	45,57	5,95	5,20
8	1,56	1,93	44,46	18,11	21,64	5,87	5,13
12	1,45	1,79	43,29	11,50	13,68	5,80	5,07
16	1,45	1,66	42,13	8,24	9,72	5,72	5,00
20	1,38	1,52	40,97	6,20	7,35	5,64	4,93
24	1,38	1,39	39,81	4,86	5,78	5,56	4,86
28	1,34	1,25	38,64	3,85	4,67	5,48	4,79
32	1,31	1,11	37,48	3,09	3,85	5,39	4,71
36	1,24	0,98	36,32	2,50	3,21	5,31	4,64
40	1,20	0,84	35,16	2,00	2,71	5,22	4,57

Correlating Equations

$$Sh = 1.7282\ e^{-7} \cdot 10^{\wedge} (1.5438\ Re^{0.50}\ Sc^{0.33})$$

correlation coefficient = 0.962

$$Nu = 6.2702\ e^{-7} \cdot 10^{\wedge} (1.2641\ Re^{0.50}\ Sc^{0.33})$$

correlation coefficient = 0.942

Table 11

Run Number = W11
Sample Liquid = Water
Air Temperature (Dry Bulb) = 200.0°C
Air Temperature (Wet Bulb) = 58.2°C
Air Humidity = 0.08799 kg/kg
Air Velocity = 1.0 m/s
Reynolds Number = 581

Time (s)	Drop Diameter (m x 10^{-3})	Drop Mass (kg x 10^{-6})	Reynolds No. Re	Sherwood No. Sh	Nusselt No. Nu	$Re^{0.50}\ Pr^{0.33}$	$Re^{0.50}\ Sc^{0.33}$
4	1,64	2,18	46,78	38,91	47,92	6,03	5,27
8	1,53	2,03	45,62	18,60	22,79	5,95	5,20
12	1,53	1,88	44,17	11,87	14,24	5,86	5,12
16	1,47	1,73	43,00	8,39	10,13	5,78	5,05
20	1,40	1,58	41,84	6,31	7,67	5,70	4,98
24	1,40	1,43	40,39	4,93	5,95	5,60	4,89
28	1,38	1,28	39,23	3,89	4,81	5,52	4,82
32	1,31	1,14	38,06	3,12	3,97	5,44	4,75
36	1,27	0,99	36,61	2,51	3,26	5,33	4,66

Correlating Equations

$$Sh = 4.1053\ e^{-7} \cdot 10^{\wedge} (1.4552\ Re^{0.50}\ Sc^{0.33})$$

correlation coefficient = 0.939

$$Nu = 1.6424\ e^{-7} \cdot 10^{\wedge} (1.3555\ Re^{0.50}\ Sc^{0.33})$$

correlation coefficient = 0.978

Table 12

Run Number = W12
Sample Liquid = Water
Air Temperature (Dry Bulb) = 200.0°C
Air Temperature (Wet Bulb) = 58.2°C
Air Humidity = 0.08799 kg/kg
Air Velocity = 1.0 m/s
Reynolds Number = 581

Time (s)	Drop Diameter (m x 10^{-3})	Drop Mass (kg x 10^{-6})	Reynolds No. Re_D	Sherwood No. Sh	Nusselt No. Nu	$Re^{0.50} Pr^{0.33}$	$Re^{0.50} Sc^{0.33}$
4	1,67	2,29	47,36	40,41	49,12	6,06	5,30
8	1,56	2,15	46,49	19,33	23,67	6,01	5,25
12	1,56	2,01	45,33	12,38	15,00	5,93	5,18
16	1,53	1,88	44,46	8,87	10,82	5,87	5,13
20	1,45	1,74	43,29	6,71	8,21	5,80	5,07
24	1,47	1,61	42,42	5,28	6,57	5,74	5,02
28	1,44	1,47	41,26	4,25	5,33	5,66	4,95
32	1,38	1,33	40,39	3,44	4,47	5,60	4,89
36	1,38	1,20	39,52	2,81	3,80	5,54	4,84
40	1,31	1,06	38,35	2,31	3,22	5,46	4,77

Correlating Equations

$$Sh = 1.2595\ e^{-9} \cdot 10^{\wedge}\ (\ 1.9277\ Re^{0.50}\ Sc^{0.33}\ )$$

correlation coefficient = 0.987

$$Nu = 1.3980\ e^{-8} \cdot 10^{\wedge}\ (\ 1.5225\ Re^{0.50}\ Sc^{0.33}\ )$$

correlation coefficient = 0.973

Table 13

Run Number = BuOH1
Sample Liquid = Butan-1-ol
Air Temperature (Dry Bulb) = 50.0°C
Air Temperature (Wet Bulb) = 26.1°C
Wet Bulb (Butan-1-ol) = 34.0°C
Air Humidity = 0.01249 kg/kg
Air Velocity = 1.0 m/s
Reynolds Number = 1128

Time (s)	Drop Diameter (m x 10^{-3})	Drop Mass (kg x 10^{-6})	Reynolds No. Re_o	Sherwood No. Sh	Nusselt No. Nu	$Re^{0.50}\ Pr^{0.33}$	$Re^{0.50}\ Sc^{0.33}$
10	1,42	1,17	80,65	48,22	32,80	7,99	9,53
20	1,38	1,09	77,83	23,27	15,27	7,85	9,36
30	1,33	1,00	75,01	14,76	9,46	7,71	9,19
40	1,31	0,91	72,19	10,50	6,57	7,56	9,02
50	1,24	0,82	69,93	7,79	4,93	7,44	8,88
60	1,16	0,73	67,11	6,04	3,79	7,29	8,70
70	1,14	0,65	64,29	4,81	2,98	7,14	8,51
80	1,09	0,56	61,47	3,78	2,38	6,98	8,32
90	1,05	0,47	59,22	2,92	1,97	6,85	8,17

Correlating Equations

$$Sh = 4.7928\ e^{-6} \cdot 10\ \hat{}\ (\ 0.70697\ Re^{0.50}\ Sc^{0.33}\ )$$

correlation coefficient = 0.981

$$Nu = 1.8545\ e^{-6} \cdot 10\ \hat{}\ (\ 0.87235\ Re^{0.50}\ Sc^{0.33}\ )$$

correlation coefficient = 0.979

Table 14

Run Number = BuOH2
Sample Liquid = Butan-1-ol
Air Temperature (Dry Bulb) = 50.0°C
Air Temperature (Wet Bulb) = 26.1°C
Wet Bulb (Butan-1-ol) = 34.0°C
Air Humidity = 0.01249 kg/kg
Air Velocity = 1.0 m/s
Reynolds Number = 1128

Time (s)	Drop Diameter (m x 10^{-3})	Drop Mass (kg x 10^{-6})	Reynolds No. Re_D	Sherwood No. Sh	Nusselt No. Nu	$Re^{0.50}\ Pr^{0.33}$	$Re^{0.50}\ Sc^{0.33}$
10	1,40	1,11	78,95	46,73	31,44	7,91	9,43
20	1,34	1,01	76,13	22,05	14,61	7,77	9,26
30	1,29	0,91	72,75	13,84	8,90	7,59	9,05
40	1,24	0,81	69,93	9,65	6,17	7,44	8,88
50	1,18	0,71	66,55	7,09	4,47	7,26	8,66
60	1,13	0,60	63,16	5,26	3,35	7,07	8,44
70	1,07	0,50	60,34	3,91	2,63	6,91	8,25
80	1,02	0,40	56,96	2,92	2,05	6,72	8,01
90	0,94	0,30	54,14	2,03	1,64	6,55	7,81

Correlating Equations

$$Sh = 8.9546\ e^{-6} \cdot 10^{\wedge}\ (\ 0.68456\ Re^{0.50}\ Sc^{0.33}\ )$$

correlation coefficient = 0.991

$$Nu = 5.8534\ e^{-6} \cdot 10^{\wedge}\ (\ 0.68431\ Re^{0.50}\ Sc^{0.33}\ )$$

correlation coefficient = 0.962

Table 15

Run Number = BuOH3
Sample Liquid = Butan-1-ol
Air Temperature (Dry Bulb) = 50.0°C
Air Temperature (Wet Bulb) = 26.1°C
Wet Bulb (Butan-1-ol) = 34.0°C
Air Humidity = 0.01249 kg/kg
Air Velocity = 1.0 m/s
Reynold Number = 1128

Time (s)	Drop Diameter (a x 10^{-3})	Drop Mass (kg x 10^{-6})	Reynolds No. Re_D	Sherwood No. Sh	Nusselt No. Nu	$Re^{0.50} Pr^{0.33}$	$Re^{0.50} Sc^{0.33}$
10	1,42	1,18	81,21	48,33	33,26	8,02	9,57
20	1,38	1,08	77,83	23,08	15,27	7,85	9,36
30	1,34	0,98	75,01	14,50	9,46	7,71	9,19
40	1,27	0,88	72,19	10,14	6,57	7,56	9,02
50	1,24	0,78	68,80	7,54	4,77	7,38	8,80
60	1,16	0,68	65,98	5,70	3,66	7,23	8,62
70	1,14	0,58	63,16	4,37	2,87	7,07	8,44
80	1,07	0,48	59,78	3,34	2,25	6,88	8,21
90	1,00	0,38	56,96	2,45	1,82	6,72	8,01

Correlating Equations

$$Sh = 1.3665\ e^{-5} \cdot 10^{\wedge} (0.65672\ Re^{0.50}\ Sc^{0.33})$$

correlation coefficient = 0.961

$$Nu = 1.2287\ e^{-5} \cdot 10^{\wedge} (0.76619\ Re^{0.50}\ Sc^{0.33})$$

correlation coefficient = 0.974

Table 16

Run Number = EtOH1
Sample Liquid = Ethanol
Air Temperature (Dry Bulb) = 50.0°C
Air Temperature (Wet Bulb) = 26.1°C
Wet Bulb (Ethanol) = 19.3°C
Air Humidity = 0.01249 kg/kg
Air Velocity = 1.0 m/s
Reynold Number = 1128

Time (s)	Drop Diameter (a x 10^{-3})	Drop Mass (kg x 10^{-6})	Reynolds No, Re_D	Sherwood No, Sh	Nusselt No, Nu	$Re^{0.50}\ Pr^{0.33}$	$Re^{0.50}\ Sc^{0.33}$
10	1,78	-	100,38	-	40,23	9,03	-
20	1,70	-	95,87	-	18,35	8,82	-
30	1,54	-	86,85	-	10,04	8,40	-
40	1,45	-	81,77	-	5,34	8,15	-
50	1,29	-	72,75	-	4,23	7,68	-

Correlating Equation

$$Nu = 8.7901\ e^{-5} \cdot 10^{\wedge} (0.59850\ Re^{0.50}\ Sc^{0.33})$$

correlation coefficient = 0.922

Table 17

Run Number = EtOH2
Sample Liquid = Ethanol
Air Temperature (Dry Bulb) = 50.0°C
Air Temperature (Wet Bulb) = 26.2°C
Wet Bulb (Ethanol) = 19.3°C
Air Humidity = 0.01249 kg/kg
Air Velocity = 1.0 m/s
Reynold Number = 1128

Time (s)	Drop Diameter (a x 10^{-3})	Drop Mass (kg x 10^{-6})	Reynolds No. Re_D	Sherwood No. Sh	Nusselt No. Nu	$Re^{0.50}\ Pr^{0.33}$	$Re^{0.50}\ Sc^{0.33}$
10	1,62	-	91,36	-	33,33	8,61	-
20	1,46	-	82,34	-	13,53	8,18	-
30	1,30	-	73,31	-	7,15	7,71	-
40	1,14	-	64,29	-	4,13	7,22	-
50	-	-	-	-	-	-	-

Correlating Equation

$$Nu = 3.1807\ e^{-4} \cdot 10^{\wedge} (0.56624\ Re^{0.50}\ Sc^{0.33})$$

correlation coefficient = 0.995

Table 18

Run Number = EtOH3
Sample Liquid = Ethanol
Air Temperature (Dry Bulb) = 50.0°C
Air Temperature (Wet Bulb) = 26.1°C
Wet Bulb (Ethanol) = 19.4°C
Air Humidity = 0.01249 kg/kg
Air Velocity = 1.0 m/s
Reynold Number = 1128

Time (s)	Drop Diameter (m x 10^{-3})	Drop Mass (kg x 10^{-6})	Reynolds No. Re_D	Sherwood No. Sh	Nusselt No. Nu	$Re^{0.50} Pr^{0.33}$	$Re^{0.50} Sc^{0.33}$
10	1,75	-	98,69	-	38,89	8,95	-
20	1,61	-	90,80	-	16,46	8,59	-
30	1,41	-	79,52	-	8,41	8,03	-
40	1,29	-	72,75	-	5,28	7,68	-
50	1,18	-	66,55	-	3,53	7,35	-
60	1,00	-	56,40	-	2,11	6,77	-

Correlating Equation

$$Nu = 5.5397\ e^{-4} \cdot 10^{\ (\ 0.52008\ Re^{0.50}\ Sc^{0.33}\ )}$$

correlation coefficient = 0.985

Table 19

Run Number = PhOH1
Sample Liquid = Phenol
Air Temperature (Dry Bulb) = 100.0°C
Air Temperature (Wet Bulb) = 39.1°C
Wet Bulb (Phenol) = 85°C
Air Humidity = 0.02436 kg/kg
Air Velocity = 1.0 m/s
Reynold Number = 877

Time (s)	Drop Diameter (a x 10^{-3})	Drop Mass (kg x 10^{-6})	Reynolds No. Re_o	Sherwood No. Sh	Nusselt No. Nu	$Re^{0.50} Pr^{0.33}$	$Re^{0.50} Sc^{0.33}$
15	1.64	-	71.95	-	29.53	7.64	-
30	1.60	-	70.19	-	14.05	7.55	-
45	1.50	-	65.81	-	8.23	7.31	-
60	1.42	-	62.30	-	5.53	7.11	-
75	1.31	-	57.47	-	3.77	6.83	-
90	1.23	-	53.96	-	2.77	6.62	-
105	1.13	-	49.58	-	2.00	6.34	-
120	1.03	-	45.19	-	1.45	6.06	-

Correlating Equation

$$Nu = 6.9619\ e^{-4} \cdot 10\ \hat{}\ (\ 0.55813\ Re^{0.50}\ Sc^{0.33}\ )$$

correlation coefficient = 0.953

Table 20

Run Number = PhOH2
Sample Liquid = Phenol
Air Temperature (Dry Bulb) = 100.0°C
Air Temperature (Wet Bulb) = 39.1°C
Wet Bulb (Phenol) = 85°C
Air Humidity = 0.02436 kg/kg
Air Velocity = 1.0 m/s
Reynold Number = 877

Time (s)	Drop Diameter (m x 10^{-3})	Drop Mass (kg x 10^{-6})	Reynolds No, Re_D	Sherwood No, Sh	Nusselt No, Nu	$Re^{0.50} Pr^{0.33}$	$Re^{0.50} Sc^{0.33}$
15	2,02	-	88,62	-	44,81	8,48	-
30	1,94	-	85,11	-	20,66	8,31	-
45	1,88	-	82,48	-	12,93	8,18	-
60	1,80	-	78,97	-	8,89	8,01	-
75	1,74	-	76,34	-	6,65	7,87	-
90	1,70	-	74,58	-	5,29	7,78	-
105	1,60	-	70,19	-	4,01	7,55	-
120	1,50	-	65,81	-	3,09	7,31	-

Correlating Equation

$$Nu = 2.2408\ e^{-6} \cdot 10^{\wedge} (0.82823\ Re^{0.50}\ Sc^{0.33})$$

correlation coefficient = 0.955

Table 21

Run Number = PhOH3
Sample Liquid = Phenol
Air Temperature (Dry Bulb) = 100.0°C
Air Temperature (Wet Bulb) = 39.4°C
Wet Bulb (Phenol) = 85°C
Air Humidity = 0.02436 kg/kg
Air Velocity = 1.0 m/s
Reynold Number = 877

Time (s)	Drop Diameter (m x 10^{-3})	Drop Mass (kg x 10^{-6})	Reynolds No. Re_D	Sherwood No. Sh	Nusselt No. Nu	$Re^{0.50} Pr^{0.33}$	$Re^{0.50} Sc^{0.33}$
15	1,90	-	83,36	-	34,05	8,23	-
30	1,84	-	80,72	-	18,59	8,10	-
45	1,76	-	77,21	-	11,34	7,92	-
60	1,68	-	73,70	-	7,75	7,74	-
75	1,62	-	71,07	-	5,76	7,60	-
90	1,54	-	67,56	-	4,34	7,41	-
105	1,46	-	64,05	-	3,35	7,21	-
120	1,41	-	61,86	-	2,73	7,09	-

Correlating Equation

$$Nu = 6.0670\ e^{-6} \cdot 10\ \hat{}\ (\ 0.79334\ Re^{0.50}\ Sc^{0.33}\ )$$

correlation coefficient = 0.964

A 4.1) Mathematical Models for the Evaporation of Pure Liquid Droplets under Forced Convection

The following models were developed by Audu (106) and Cheong (194) to calculate the average mass and heat transfer coefficients of the gaseous film surrounding a single droplet under forced convection.

Calculation of the Sherwood Number

i.) The Rate of Mass Transfer

By monitoring the humidity of air flowing over a suspended droplet, Audu determined the amount of water evaporated per unit weight of air by,

$$Ho - Hi = \Delta H \quad \ldots\ldots\ldots\ldots\ldots\ldots\ldots\ldots (1)$$

where Ho = outlet humidity
Hi = inlet humidity

Consequently, the rate of evaporation, N_A, is the product of the dry air mass flowrate, G, and ΔH,

$$N_A = \frac{G\ \Delta H}{A} \quad \ldots\ldots\ldots\ldots\ldots\ldots\ldots\ldots (2)$$

In the present investigation, direct measurements of droplet dimensions were preferred; the rate of mass transfer can be expressed as,

$$N_A = \frac{dm}{dt} \cdot \frac{1}{Ae} \quad \ldots\ldots\ldots\ldots\ldots\ldots\ldots\ldots (3)$$

where $Ae = \pi\ De^2$ and $De = (2Dx + Dy) / 3$, see Figure 79.
An instantaneous value of dm / dt can be obtained from a plot of droplet mass versus time, i.e.; $m = (\pi\ D^3\ \rho_D) / 6$.

ii.) The Mass Transfer Coefficient

The rate of mass transfer is proportional to the driving force and a constant of proportionality denoted k'. In Audu's experiments, the driving force was the humidity driving force,

$$\Delta H = Hs - Hi \quad \ldots\ldots\ldots\ldots\ldots\ldots\ldots\ldots (4)$$

where Hs is the saturation humidity at the droplet temperature Td, thus the rate of mass transfer can be expressed as,

$$N_A = k_H (Hs - Hi) \quad \ldots\ldots\ldots\ldots\ldots\ldots\ldots\ldots (5)$$

where k_H is the mass transfer coefficient.

Equation 4 can be transformed to yield the pressure driving force, ΔP, by converting the humidities to pressure analogues (198). Therefore, assuming ideal gas behaviour,

$$H = (M_w p_A) / (M_a (P - p_A) \quad \ldots\ldots(6)$$

where H = absolute humidity
M_w = molecular weight of water
M_a = molecular weight of air
P = total pressure

and,

$$p_A = \frac{H P}{(M_w / M_a) + H}$$

The rate of evaporation is proportional to the pressure driving force (198),

$$N_A = k_P (p_s - p_A) \quad \ldots\ldots(7)$$

The mass transfer coefficient can be obtained from equation 7 by substituting for N_A from equations 2 or 3, i.e.;

$$k_P = \frac{G \Delta H}{A (p_s - p_A)} \quad \ldots\ldots(8)$$

where kp has units of kg m^2/s/atm.

Alternatively, equation 8 can be modified to give,

$$k = \frac{G \Delta H}{A (p_s - p_A)} \cdot \frac{Rc\ Ta}{M_w} \quad \ldots\ldots(9)$$

where k has units of m/s.

Similarly, here the mass transfer coefficient can be expressed as,

$$k = \frac{dm}{dt} \cdot \frac{1}{Ae} \cdot \frac{Rc\ Ta}{M_w (p_s - p_A)} \quad \ldots\ldots(10)$$

if the Sherwood number is defined as,

$$Sh = (k\ De) / Dv \quad \ldots\ldots(11)$$

then, sustituting equation 10 into equation 11 gives,

$$Sh = \frac{dm}{dt} \cdot \frac{1}{Ae} \cdot \frac{Rc\ Ta}{M_w (p_s - p_A)} \cdot \frac{De}{Dv} \quad \ldots\ldots(12)$$

Calculation of the Nusselt Number

In determining the experimental value of the Nusselt number Cheong (194) assumed that,

i.) The droplet is spherical and of constant density.
ii.) The temperature driving force remains constant.
iii.) The temperature at the surface of the droplet is equal to the wet bulb temperature.
iv.) The latent heat of vaporisation and the thermal conductivity are evaluated at the mean temperature between the air and the droplet.

The rate of mass transfer from a spherical droplet can be expressed as,

$$-\frac{dm}{dt} = \frac{(dQ/dt)}{\lambda} \quad \ldots\ldots\ldots\ldots\ldots\ldots\ldots\ldots (13)$$

and the amount of heat transferred to a droplet by,

$$\frac{dQ}{dt} = h_T A \Delta T \quad \ldots\ldots\ldots\ldots\ldots\ldots\ldots\ldots (14)$$

if equation 14 is substituted into equation 13 then,

$$-\frac{dm}{dt} = \frac{h_T A \Delta T}{\lambda} \quad \ldots\ldots\ldots\ldots\ldots\ldots\ldots\ldots (15)$$

Since in the present investigation $m = (\pi De^3 \rho_D) / 6$, to obtain h_T, equation 15 now becomes,

$$h_T = -\frac{\lambda \rho_D}{6 \Delta T De^2} \cdot \frac{d(De^3)}{dt} \quad \ldots\ldots\ldots\ldots\ldots\ldots\ldots\ldots (16)$$

if the Nusselt number is defined as,

$$Nu = \frac{h_T De}{Kd} \quad \ldots\ldots\ldots\ldots\ldots\ldots\ldots\ldots (17)$$

substitution of equation 16 into 17 gives,

$$Nu = -\frac{\lambda \rho_D}{6 Kd \Delta T De} \cdot \frac{d(De^3)}{dt} \quad \ldots\ldots\ldots\ldots\ldots\ldots\ldots\ldots (18)$$

or,

$$Nu = - \frac{\lambda \rho_D}{4 Kd \Delta T} \cdot \frac{d(De^2)}{dt} \quad \ldots\ldots\ldots\ldots\ldots\ldots (19)$$

An instantaneous value of $d(De^2) / dt$ can be obtained from a plot of De^2 versus t.

Heat Transferred to the Droplet by Radiation and Conduction

In addition to heat transferred by forced convection, the droplet may also receive heat by radiation from the experimental apparatus and by conduction through the support filament. The contribution from radiant heat transfer, Qr, can be expressed as,

$$Qr = \sigma A Fa e (Ta^4 - Td^4) \quad \ldots\ldots\ldots\ldots\ldots\ldots (20)$$

where σ = Stefan-Boltzman constant
Fa = a geometry factor assumed to be unity, i.e.; the droplet is surrounded by the drying chamber
e = droplet emissivity

Cheong derived an expression to account for heat transfer to the droplet by conduction through a glass support filament. The assumptions are,

i.) Heat is transferred to the filament from the surroundings by radiation and convection.
ii.) The temperature around the filament is constant and equal to the air temperature.
iii.) There is no radial temperature gradient.
iv.) The length of the filament is much greater than the diameter.

If the filament is considered to be a cylinder of infinite length, then the amount of heat transferred, Qf, can be expressed as,

$$Qf = \frac{\pi}{2} \left(\frac{Kg D_F^3}{5} \left[2\sigma e_A (Td^5 - Ta^5) - 10\sigma e_A Ta^4 \right. \right.$$

$$\left. \left. + (Td - Ta) + 5h_a (Td - Ta)^2 \right] \right)^{0.5} \quad \ldots\ldots\ldots\ldots\ldots (21)$$

where Kg = thermal conductivity of the glass
D_F = diameter of filament
e_A = emissivity of air
h_a = heat transfer coefficient of glass, i.e.;
$h_a = Cp_a Re_F^{0.47} Pr^{0.33} (Kd / D_F)$
Cp_a = specific heat capacity of the glass
Re_F = Reynolds number of filament

In the present investigation, calculation of both Qr and Qf (see Table A 4.1) has shown that the amount of heat transferred to the droplet by radiation and conduction is almost negligible, e.g.; at 200°C the amount of heat transferred to the droplet by convection, Qc, is seventy to eighty times greater than Qr + Qf.

Table A 4.1. Heat Transfer to Droplet by Convection, Conduction and Radiation

Temperature	Qc	Qf	Qr	Qc/Qf+Qr
°C	W	W	W	
50	0.483 - 0.934	0.001	0.001 - 0.002	242 - 311
100	1.536 - 1.747	0.004	0.004 - 0.005	192 - 194
150	1.342 - 1.422	0.006	0.008 - 0.009	95 - 96
200	1.774 - 2.021	0.008	0.016 - 0.018	74 - 78

A 5.0) The Retention of Volatiles - G.L.C Results

Sample	Drying Time (s)	Droplet Diameter (mm) 1	2	3	4	Total Vol (mm^3)	Average Peak Area	% EtOH
sodium chloride	0	1.4	1.5	1.4	1.3	5.8	258526	100.0
- 15 % w/w	20	1.6	1.6	1.6	1.5	7.4	4503	1.4
- 120°C	40	1.5	1.4	1.6	1.4	6.7	3712	1.2
	60	1.3	1.5	1.5	1.5	6.6	2148	0.7
	80	1.4	1.5	1.5	1.5	6.8	1975	0.7
	100	1.3	1.4	1.4	1.5	5.8	1583	0.6
silica	0	1.8	1.8	1.7	1.8	11.9	634242	100.0
- 15 % w/w	20	1.9	1.9	1.9	1.9	14.4	280764	36.6
- 120°C	40	1.9	1.9	1.7	1.8	12.9	180753	26.3
	60	1.8	1.8	1.8	1.8	12.4	49625	7.5
	80	2.0	1.8	1.9	1.9	14.5	16249	2.1
	100	1.7	1.9	1.7	1.7	11.4	4587	0.8
semi - instant	0	1.7	1.6	1.6	1.6	8.9	668603	100.0
skimmed milk	20	1.6	1.6	1.6	1.7	8.9	327821	49.0
- 15 % w/w	40	1.6	1.7	1.6	1.6	8.9	268715	40.2
- 120°C	60	1.7	1.6	1.6	1.5	8.6	274527	42.5
	80	1.6	1.7	1.6	1.6	8.9	280813	42.0
	100	1.6	1.6	1.7	1.7	9.4	281650	39.9
semi - instant	0	1.6	1.7	2.1	1.7	12.1	874336	100.0
skimmed milk	20	1.8	1.7	1.6	1.5	9.6	580076	83.6
- 15 % w/w	40	1.6	1.7	1.7	1.6	9.4	414721	61.1
- 150°C	60	1.6	1.6	1.7	1.6	8.9	329145	51.2
	80	1.6	1.6	1.6	1.7	8.9	340046	52.9
	100	1.6	1.6	1.7	1.7	9.4	322637	47.5
semi - instant	0	1.6	1.7	2.1	1.7	12.1	1124529	100.0
skimmed milk	20	1.6	1.7	1.7	1.8	10.4	622102	64.4
- 15 % w/w	40	1.7	1.7	1.9	1.6	10.9	550835	54.4
- 200°C	60	1.8	1.7	1.7	1.6	10.4	268718	27.8
	80	1.8	1.8	1.6	1.5	10.1	126484	13.5
	100	2.0	1.5	1.7	1.7	11.2	188924	18.2
semi - instant	0	1.7	1.8	1.8	1.7	11.4	1114906	100.0
skimmed milk	20	1.8	1.8	1.8	1.8	12.4	415211	34.2
- 1 % w/w	40	1.7	1.7	1.7	1.7	10.4	137818	13.6
- 120°C	60	1.7	1.7	1.7	1.7	10.4	73101	7.2
	80	1.9	1.7	1.7	1.7	11.4	7886	7.1
	100	1.7	1.8	1.7	1.9	11.9	1744	0.1

Sample	Drying Time (s)	Droplet Diameter (mm) 1	2	3	4	Total Vol (mm^3)	Average Peak Area	% EtOH
semi - instant	0	1.8	1.6	1.7	1.7	10.4	678018	100.0
skimmed milk	20	1.6	1.7	1.7	1.8	10.4	647507	95.5
- 25 % w/w	40	1.6	1.7	1.7	1.6	9.4	540422	88.2
- 120°C	60	1.7	1.6	1.6	1.7	9.4	521528	85.1
	80	1.8	1.7	1.8	1.8	11.9	602104	77.6
	100	1.8	1.6	1.5	1.7	9.4	419363	68.4
water	0	1.7	1.7	1.7	1.7	10.4	532342	100.0
-	20	1.7	1.6	1.6	1.4	8.2	97298	23.2
- 120°C	40	1.6	1.5	1.5	1.5	7.5	12671	3.3
	60	1.6	1.6	1.6	1.6	8.4	5969	1.4
	80	1.5	1.6	1.8	1.6	9.1	3336	0.7
	100	-	-	-	-	-	--	-

A 6.0) Publications

i.) The Evaluation of Drying Behaviour by Single Droplet Studies, with F.Riera and C.J.Mumford, Paper Presented at the 23rd Annual Meeting of the Spanish Chemical Society, Salemanca, Sept. (1990).

ii.) A Study of the Morphology of Spray-Dried Particles, with C.J.Mumford, I.Chem.E. Research Event, University of Manchester Institute of Science and Technology, Jan. (1992).

iii.) Enhanced Heat and Mass Transfer of Oscillating Droplets under Forced Convection, with G.Oteng-Attakora and C.J.Mumford, I.Chem.E. Research Event, University College London. Jan. (1994).

iv.) Spray-Dried Particles : the Variation of Morphology with Drying Conditions, with C.J.Mumford, I.Chem.E. Research Event, University of Edinburgh, Jan. (1995).

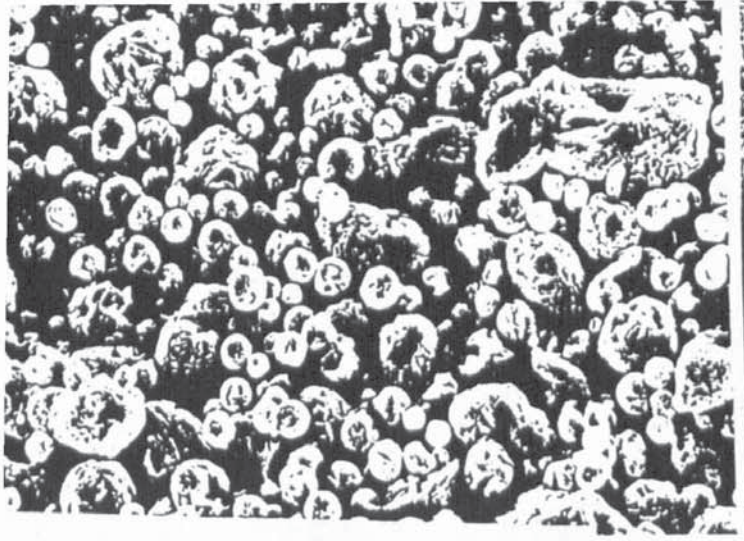

a) Sodium acetate. 150°C (S)

b) Sodium acetate. 150°C (SD)

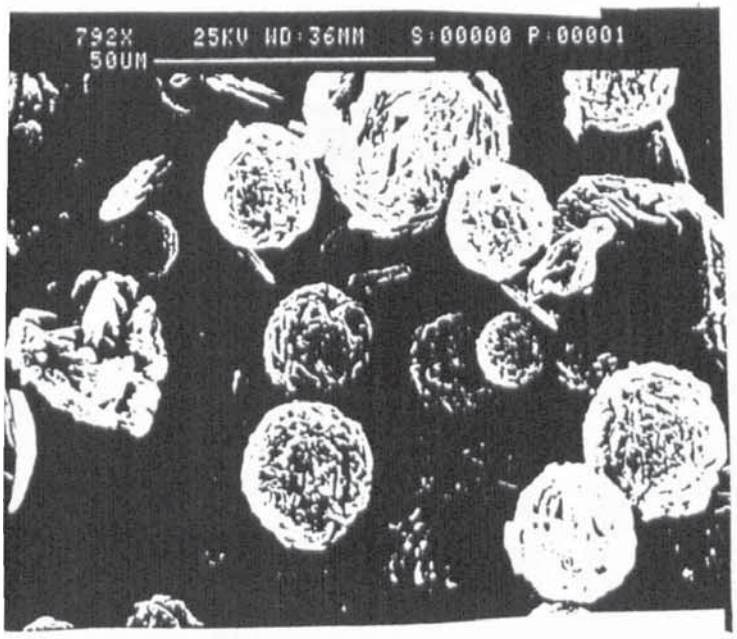

c) Sodium sulfate. 150°C. Aeration (S)

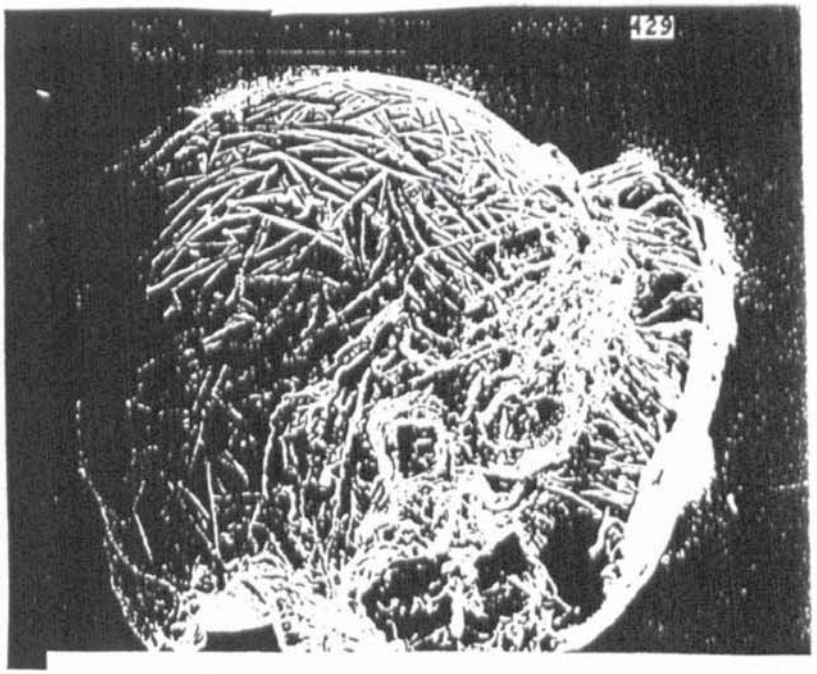

d) Sodium sulfate. 150°C. Aeration. (SD)

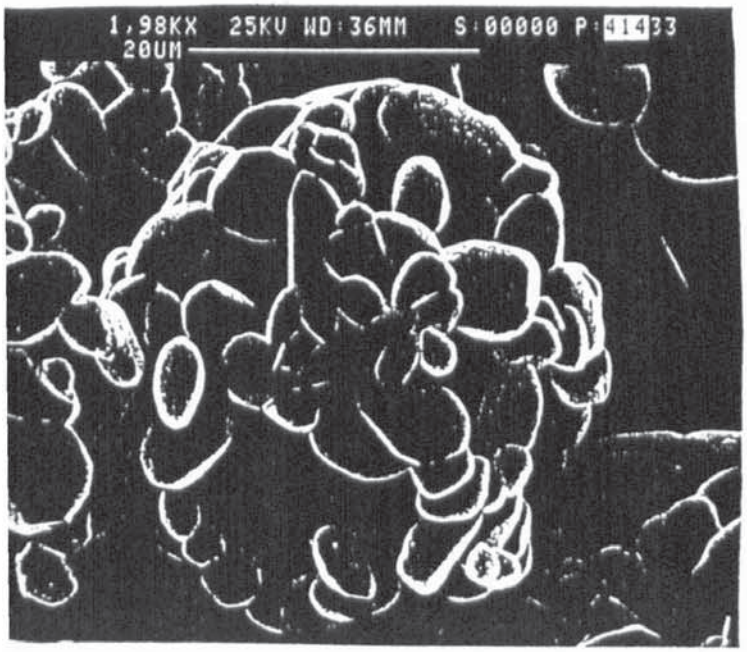

e) Hydrated sodium sulfate. 150°C. (S)

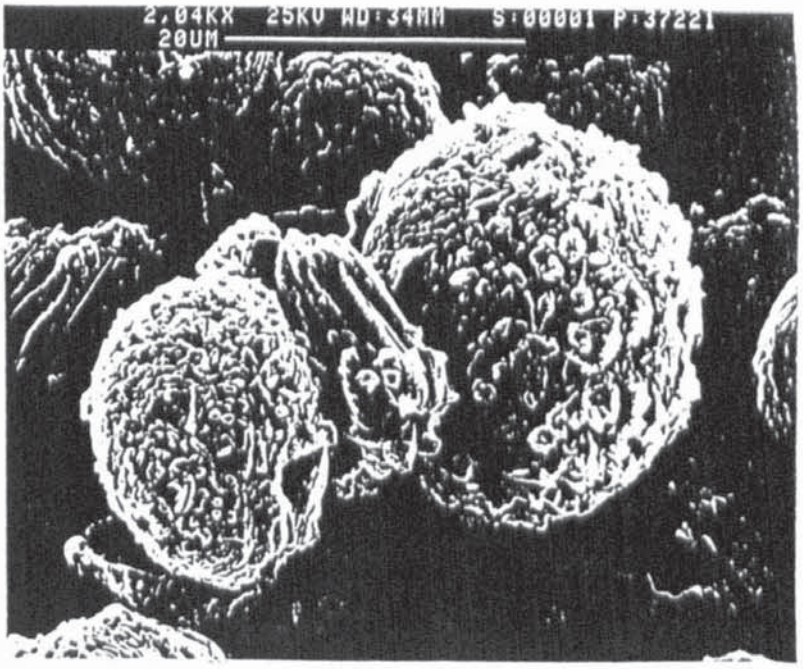

f) Sodium sulfate. 300°C. Aeration (S)

Figure 1. Dried particles from Spray (S) and single drops drying (SD)

TEXT BOUND
INTO
THE SPINE

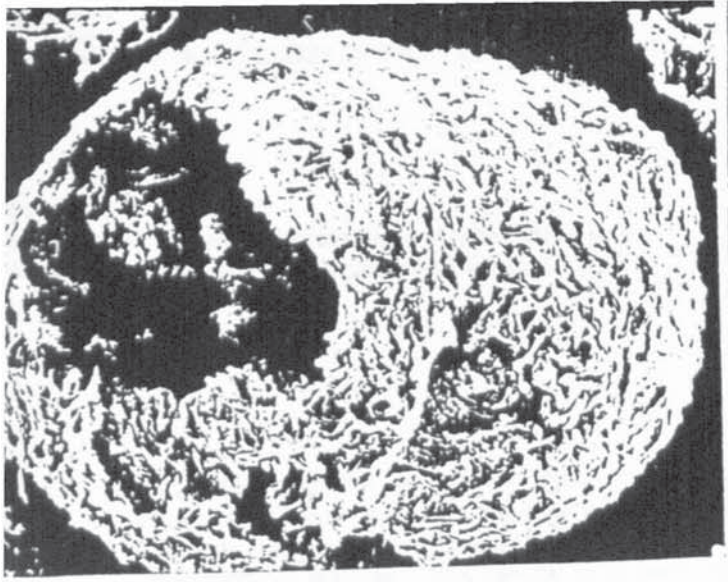

3. Copper Ore (c)

2. Sodium Orthophosphate (c)

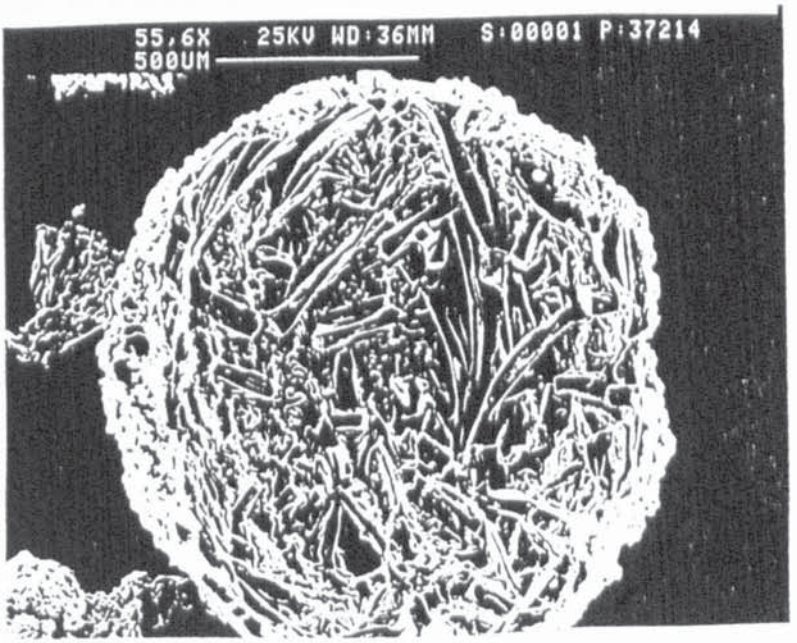

4. Dextran (c)

5. Sodium Carbonate (15% w/w)
Dried at 70°C. (SD)

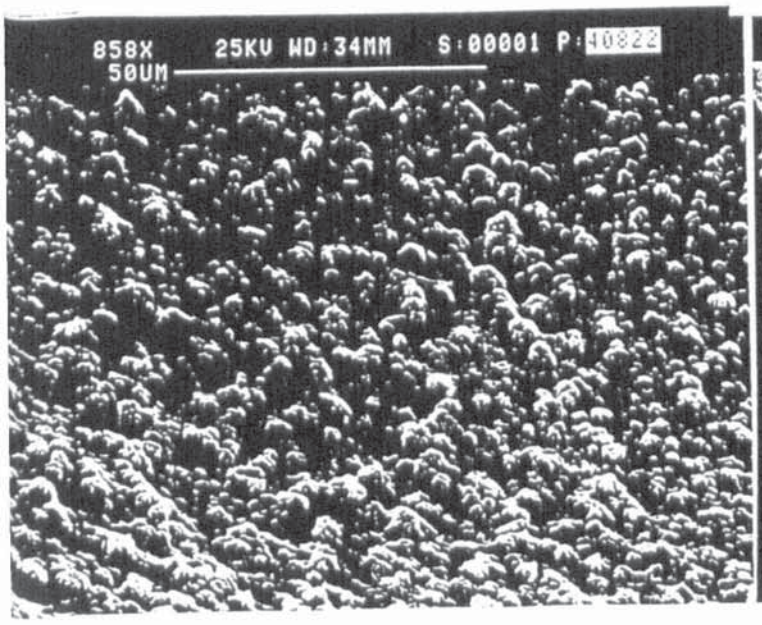

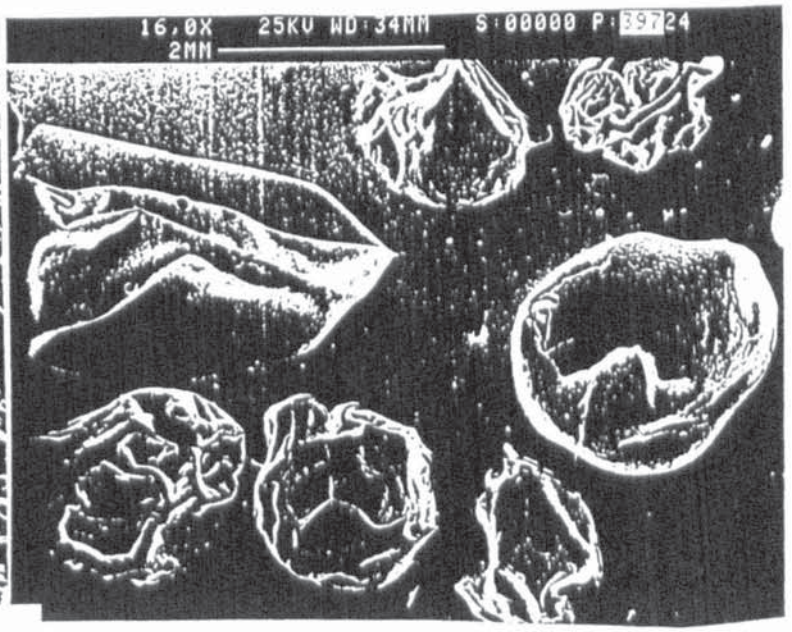

6. Colloidal Carbon
Dried at 210°C. (SD)

7. Skimmed Milk (15% w/w)
Dried at 210°C. (SD)

Figures 2 to 7. Commercially spray-dried (c) and single drop dried (SD) particles

TEXT BOUND
INTO
THE SPINE

NOMENCLATURE

A = transfer surface area .....m^2

coefficient used in equations 62 and 83

Ae = equivalent transfer area .....m^2

As = surface area of droplet .....m^2

a = exponent used in equation 83

B = transfer number, $Cp(\Delta T/\lambda)$

coefficient used in equations 62 and 84

B' = Spalding transfer number, $Cp\Delta T/(\lambda - Qr/w)$

Bo = Bond number, $(\rho_c - \rho_M)D^2g/\sigma_L$

Cb = vapour concentration in the bulk-gas / air .....kg/m^3

Cd = drag coefficient

Ci = vapour concentration at the boundary interface ....kg/m^3

Cp = specific heat capacity of the gas phase .....J/kg/K

Cp_o = specific heat capacity of the droplet .....J/kg/K

Cp_s = specific heat capacity of glass .....J/kg/K

C_∞ = vapour concentration at an infinite distance .....kg/m^3

D = droplet diameter .....m

De = equivalent diameter of droplet .....m

Df = filament diameter .....m

Dh = maximum horizontal diameter of droplet .....m

Di = initial rupture diameter .....m

Dm = droplet diameter at the critical moisture content .....m

Do = initial droplet diameter .....m

Dv = diffusivity .....m^2/s

E = $wCp/4\pi Kd$

e = emissivity of droplet

e_A = emissivity of air

Fa = geometry factor

G = mass flowrate .....kg/s

Gr = Grashof number, $D^3\rho_a^2g\beta\Delta T/\mu_a^2$

g = acceleration due to gravity .....m/s^2

H = absolute humidity .....kg/kg

Hi = inlet humidity .....kg/kg

Ho = outlet humidity .....kg/kg

Hs = saturation humidity at the droplet temperature ....kg/kg

h = height of miniscus; vertical diameter of droplet .....m

h_a = heat transfer coefficient for glass

h_T = heat transfer coefficient .....$W/m^2/K$

Kd = thermal conductivity of air .....W/m/K

Kg = thermal conductivity of glass .....W/m/K

Kv = thermal conductivity of a vapour .....W/m/K

k = mass transfer coefficient .....m/s

Le = Lewis number, $Kd/DvCp\rho_a$

M = molarity

coefficient used in equations 68 and 83

Ma = molecular weight of air

Mv = molar diffusivity per unit area

Mw = molecular weight

m = mass of droplet .....kg

metre .....m

coefficient used in equation 13

N = coefficient used in equations 62, 68 and 84

N_A = rate of evaporation .....kg/m²/s

Nu = Nusselt number, $h_T D/Kd$

n = exponent used in equation 13

P = total pressure .....atms

Pr = Prandtl number, $Cp\mu_a/Kd$

p = exponent used in equation 14

p_A = partial pressure of water vapour in air .....atms

p_s = vapour pressure at the droplet surface .....atms

Q = heat transferred .....W

Qc = heat transferred by convection .....W

Qf = heat transferred to filament .....W

Qr = heat transferred by radiation .....W

q = heat transferred per unit area .....W/m²

exponent used in equation 14

Rc = universal gas constant .....m³.atm/mol/K

Re = Reynolds number, Re_D (droplet), Re_a (gas/air)

Re_P (particle), Re_F (filament) : $vD\rho_a/\mu_a$

r = droplet radius .....m

rI = outer radius of gas-film .....m

r_T = radius of tube or rod .....m

Sc = Schmidt number, $\mu_a/Dv\rho_a$

Sh = Sherwood number, kD/Dv

s = seconds .....s

T = temperature .....°C or K

ΔT = Ta - Td temperature difference driving force ....°C or K

Ta = air temperature .....°C or K

Tamb = ambient temperature .....°C or K

T_b = temperature of the bulk-gas .....°C or K

T_d = droplet temperature .....°C or K

T_f = average film temperature .....°C or K

T_i = temperature at the interface .....°C or K

T_u = turbulence intensity

t = time .....s

t_F = drying time for the falling-rate period .....s

t_s = time at which skin formation first appears .....s

t^T = time required for total closure of rupture .....s

V_d = volume of droplet .....m^3

V_f = volume-fraction of gas in a foam

v = velocity .....m/s

v_F = velocity for fold development .....m/s

v_s = velocity for smoothing .....m/s

W = moles of vapour transferred

W_c = critical moisture content .....kg/kg

W_f = final moisture content .....kg/kg

w = rate of evaporation (mass flowrate) .....kg/s

x = falling distance .....m

z = boundary layer thickness .....m

GREEK LETTERS

$\alpha_{1,2}$ = coefficients used in equations 13 and 14

β = coefficient of bulk expansion 1/T

Γ = folding parameter

λ = latent heat of vaporization .....J/kg

λ_M = molar latent heat of vaporization .....J/mol

μ_c = viscosity of continuous phase .....kg/m/s

μ_D = viscosity of dispersed phase .....kg/m/s

μ_a = viscosity of air or the drying medium .....kg/m/s

μ_L = viscosity of liquid .....kg/m/s

ρ_c = density of continuous phase .....kg/m^3

ρ_D = droplet density .....kg/m^3

ρ_a = density of the gas phase or drying medium ..... kg/m^3

ρ_L = density of liquid .....kg/m^3

ρ_M = density of dispersed phase .....kg/m^3

ρ_P = particle density .....kg/m^3

σ = Stefan-Boltzmann constant .....W/m^2/K^4

σ_L = surface tension of liquid .....N/m

ϕ = measure of sphericity, 6Vd/As((Dh+h)/2)